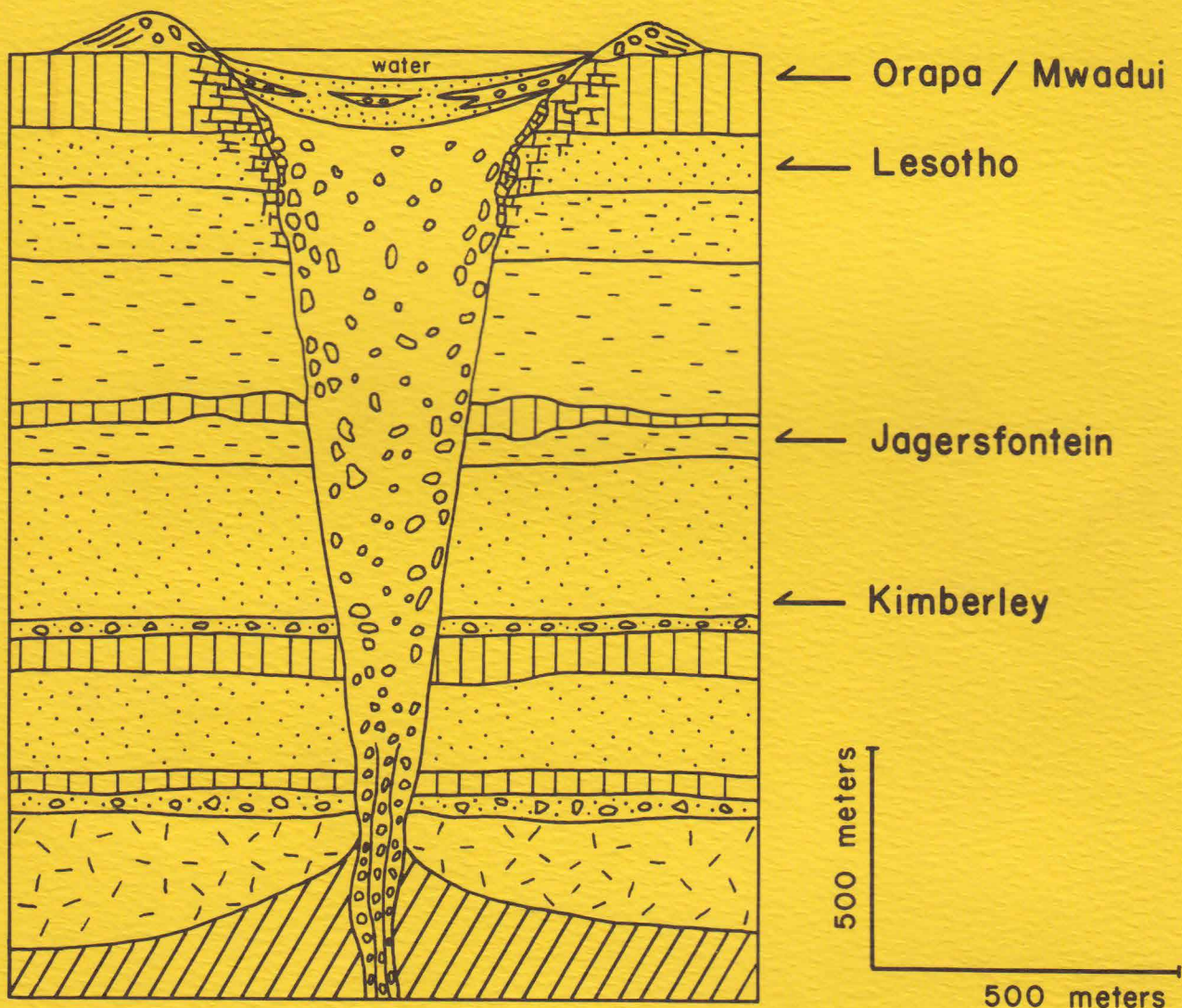


PETROGRAPHY AND MINERAL CHEMISTRY OF ULTRAMAFIC AND RELATED INCLUSIONS FROM THE ORAPA A/K-1 KIMBERLITE PIPE, BOTSWANA

BY RICHARD P. TOLLO



generalized cross-section of a kimberlite pipe
modified after Hawthorne (1975)

CONTRIBUTION NO. 39
DEPARTMENT OF GEOLOGY AND GEOGRAPHY
UNIVERSITY OF MASSACHUSETTS
AMHERST, MASSACHUSETTS

PETROGRAPHY AND MINERAL CHEMISTRY OF
ULTRAMAFIC AND RELATED INCLUSIONS
FROM THE ORAPA A/K-1 KIMBERLITE
PIPE, BOTSWANA

by

RICHARD PAUL TOLLO

Contribution No. 39

Department of Geology and Geography

University of Massachusetts

Amherst, Massachusetts

August, 1982



Richard Paul Tollo
All Rights Reserved

TABLE OF CONTENTS

ACKNOWLEDGEMENT	xi
ABSTRACT	xiii
Chapter	
I. INTRODUCTION	1
The Orapa A/K-1 Kimberlite Pipe	1
Determinative Methods	3
II. OXIDE DISCRETE NODULES	6
Ilmenite	6
Rutile and Ilmenite-Rutile Intergrowths	33
III. SILICATE DISCRETE NODULES	65
Clinopyroxene	65
Ilmenite-Clinopyroxene Intergrowth	79
Garnet	86
Knorringite Garnet-Clinopyroxene-Chromite Intergrowth	101
IV. ECLOGITE NODULES	112
Introduction	112
Petrography	112
Phase Chemistry	121
Geothermometry and Geobarometry	150
V. DISCUSSION	158
VI. SUMMARY AND CONCLUSIONS	177
.
REFERENCES	182
APPENDIX A: LISTING OF THE INDIVIDUAL ELECTRON MICROPROBE ANALYSES USED IN THE CONSTRUCTION OF FIGURE 7	196
APPENDIX B: SUMMARY OF THE EXPERIMENTAL CONDITIONS INVOLVED IN THE ILMENITE-RUTILE SYNTHESIS EXPERIMENTS	202

LIST OF TABLES

Table

1.	Average chemical compositions of individual ilmenite discrete nodules from Orapa - nodule interiors	18
2.	Chemical compositions of coexisting ilmenite and rutile in ilmenite-rutile intergrowth nodules from Orapa and Jagersfontein	42
3.	Calculated bulk compositions for selected coarse lamellar ilmenite-rutile intergrowth nodules from Orapa and Jagersfontein	55
4.	Comparison of X-ray diffraction data for niobian rutile discrete nodule #OR-406 from Orapa and "ilmenorutile" (JCPDS #11-396)	61
5.	Chemical composition of niobian rutile discrete nodule #OR-406 from Orapa compared to lunar rutile	63
6.	Average chemical compositions of individual clinopyroxene discrete nodules from Orapa	66
7.	Average chemical compositions of coexisting clinopyroxene and ilmenite from Orapa nodule #430B	82
8.	Average chemical compositions of individual garnet discrete nodules from Orapa	87
9.	Average chemical compositions of coexisting garnet, clinopyroxene, and chromite from Orapa nodule #431	104
10.	Petrographic data for representative eclogite nodules from Orapa	113
11.	Average chemical compositions of garnet grains in individual eclogite nodules from Orapa	122
12.	Average chemical compositions of clinopyroxene grains in individual eclogite nodules from Orapa	131
13.	Average chemical compositions of rutile grains in individual eclogite nodules from Orapa	143
14.	Average chemical compositions of ilmenite grains in individual eclogite nodules from Orapa	146

Table

15. Representative analyses of individual amphibole grains in Orapa eclogite nodules #105 and #109	148
16. Comparative temperature estimates for garnet discrete nodules containing clinopyroxene inclusions from Orapa	159
17. Comparative temperature estimates for ilmenite-bearing eclogites and ilmenite-clinopyroxene intergrowth nodule #430B from Orapa	162
18. Individual electron microprobe analyses of ilmenite discrete nodule #411A used in the construction of the chemical contour map presented in Figure 7 of the text	198
19. Summary of experimental conditions for individual runs involved in the ilmenite-rutile intergrowth experiments	203

LIST OF ILLUSTRATIONS

Figure

1.	Generalized distribution of kimberlite clusters and major tectonic units in Botswana	2
2a.	Typical inequigranular polycrystalline texture developed in the interior region of an ilmenite nodule	9
2b.	Well-developed, angular-polygonal polycrystalline texture viewed near the periphery of an ilmenite nodule	9
2c.	Polycrystalline texture developed at the periphery of an otherwise homogeneous ilmenite nodule	11
2d.	Prominent twinning lamellae oriented along probable crystallographically equivalent directions in an ilmenite grain at a nodule periphery	11
2e.	Anisotropic shear fabric developed in the interior region of an otherwise homogeneous ilmenite nodule . . .	13
2f.	Heavy surface pitting developed in the interior region of an ilmenite nodule	13
3.	Generalized sequence of events believed to result in the range of textural features observed in the ilmenite discrete nodule suite from Orapa	15
4a.	Compositions of the ilmenite discrete nodule suite from Orapa plotted in the ternary system ilmenite-geikielite-hematite	22
4b.	Compositions of homogeneous and completely polycrystalline discrete nodules plotted in the ternary system ilmenite-geikielite-hematite	22
5.	Plot of MgO and Cr ₂ O ₃ content for the ilmenite discrete nodule suite from Orapa	24
6.	Compositional variation along core-to-periphery microprobe traverses of three ilmenite discrete nodules	26

Figure

7.	Chemical contour map of the MgO content (expressed as weight percent) of ilmenite discrete nodule specimen #411A	28
8.	Plot of MgO versus FeO content for the ilmenite discrete nodule suite from Orapa	31
9.	Plot of Cr versus Ni for the ilmenite discrete nodule suite from Orapa	32
10.	Generalized classification of ilmenite-rutile intergrowth textures	35
11a.	Typical lamellar-type ilmenite lamellae oriented along nearly orthogonal planes within the host rutile	38
11b.	Rim ilmenite situated along the nodule periphery and branching inward to form typical ilmenite lamellae characteristic of the lamellar type of ilmenite-rutile intergrowth nodules at Orapa	38
12.	Compositions of rutiles from kimberlitic nodules, meteorites, lunar surface materials, and terrestrial rocks plotted in terms of atomic percent Ti versus $(\text{Nb}^{5+} + \text{Cr}^{3+} + \text{Ta}^{5+})$	46
13.	Compositions of niobian rutiles from kimberlitic nodules and various alkalic igneous rocks plotted in terms of atomic percent Nb-Fe-Ta	47
14.	Compositions of coarse lamellar, patchy, and atoll-type ilmenite intergrowths within rutile plotted in the ternary system ilmenite-geikielite-hematite	49
15.	Calculated average bulk composition of coarse lamellar ilmenite-rutile nodules from Orapa and Jagersfontein plotted in the hypothetical armalcolite compositional space $\text{Ti}^{4+} - (\text{Fe}^{2+} + \text{Mg}^{2+}) - \text{Cr}^{3+}$, assuming a ± 5 percent relative error inherent in the modal analyses	57
16.	Summary of ilmenite-rutile experimental results plotted in terms of temperature and $-\log f\text{O}_2$	59

Figure

17.	Compositions of the clinopyroxene discrete nodule suite from Orapa plotted in the conventional pyroxene quadrilateral system diopside-enstatite-ferrosilite-hedenbergite	70
18.	Compositions of selected clinopyroxene discrete nodules from Orapa plotted in terms of the "Others" components $VI_{Ti}M_2Na-IVAl$	72
19a.	Compositions of the clinopyroxene discrete nodule suite from Orapa plotted as a function of chrome content versus $Mg/(Mg+Fe)$ ratio	74
19b.	Compositions of the clinopyroxene discrete nodule suite from Orapa plotted as a function of chrome content versus $Ca/(Ca+Mg)$ ratio	74
19c.	Compositions of the clinopyroxene discrete nodule suite from Orapa plotted as a function of chrome content versus Na_2O	75
19d.	Compositions of the clinopyroxene discrete nodule suite from Orapa plotted as a function of chrome content versus Al_2O_3	75
20.	Detailed drawing of a polished section through Orapa nodule #430B comprised of ilmenite intergrown with clinopyroxene and polymineralic alteration products	80
21.	Compositions of the garnet discrete nodule suite from Orapa plotted in terms of mole percent $Ca-Mg-Fe$	94
22.	Compositions of the garnet discrete nodule suite from Orapa plotted as function of chrome content versus $Mg/(Mg+Fe)$ ratio	96
23.	Plot of $Mg/(Mg+Fe)$ ratio versus TiO_2 content for the garnet discrete nodule suite from Orapa	97
24.	Detailed drawing of a thin section through Orapa nodule #431 comprised of green garnet intergrown with clinopyroxene and chromite	102

Figure

25.	Summary plot of (CaO + MgO) content versus Cr ₂ O ₃ content for kimberlitic green garnets, garnet inclusions in diamonds, garnets from peridotite xenoliths in kimberlite, and low-chrome garnet discrete nodules	107
26.	Summary plot of garnet compositions taken from the literature for eclogitic inclusions in kimberlites	129
27.	Summary plot of clinopyroxene compositions taken from the literature for eclogitic inclusions in kimberlites	138
28.	Average compositions of garnets and clinopyroxenes coexisting in eclogite xenoliths from Orapa plotted in terms of Ca-Mg-Fe components	140
29a.	Compositions of garnet discrete nodules and garnets in eclogites from Orapa plotted in terms of MgO/(MgO+FeO) ratio and Cr ₂ O ₃ content	141
29b.	Compositions of clinopyroxene discrete nodules and clinopyroxenes in eclogites from Orapa plotted in terms of MgO/(MgO+FeO) ratio and Cr ₂ O ₃ content	141
30.	Temperature-pressure plot of individual eclogite nodules from Orapa using the Boyd (1973) geotherm for Lesotho as reference	154
31.	Comparative geothermometry of five nodule groups from Orapa	167
32.	Index map showing the location and number of each microprobe analysis used in the construction of the chemical contour map presented in Figure 7	197

ACKNOWLEDGEMENT

The author would like to thank Professor S.E. Haggerty for making the Orapa nodule suite available for study. Reviews of the manuscript by S.E. Haggerty, S.A. Morse, J.M. Rhodes, R.M. Barnes, and J.R. Beckett have contributed significantly to this work and are greatly appreciated. The author also wishes to gratefully acknowledge financial support as a research assistant at the University of Massachusetts Analytical Geochemistry Facility funded through National Science Foundation grant EAR78-19892 to J.M. Rhodes, S.E. Haggerty, and S.A. Morse. This research was directly supported by National Science Foundation grants EAR76-23787 and EAR76-02539 to S.E. Haggerty. In closing, the author would like to express his gratitude for the constant support of S.J. Kreitman, to whom this contribution is dedicated.

ABSTRACT

The Orapa A/K-1 kimberlite pipe occurs within a cluster of more than thirty pipes in east-central Botswana and is noted for preserving a nearly complete stratigraphic section of the original diatreme. Deep-seated nodules from the Orapa pipe include 1) an oxide suite comprised of ilmenite, rutile, and ilmenite-rutile intergrowths, 2) a silicate suite comprised of garnet, clinopyroxene, and various silicate-oxide intergrowths, and 3) a lithic suite comprised primarily of eclogites and various crustal rocks. The compositions of individual ilmenite nodules are typical of those in kimberlites with MgO values varying between 7 and 15 wt. % and Cr_2O_3 contents averaging approximately 2.5 wt. %. Marked peripheral zoning in magnesium content is probably indicative of reaction with the transporting kimberlitic magma. Discrete nodules of rutile and rutile host containing ilmenite lamellae recovered from this pipe are the first reported in the literature and are characterized by rutile with up to 13.5 wt. % Nb_2O_5 and 8 wt. % Cr_2O_3 . Results from experiments involving controlled conditions of temperature and oxygen fugacity (1 atm) suggest the importance of Ti^{3+} -bearing chromian armalcolite as a possible high pressure precursor to the ilmenite-rutile intergrowths. The clinopyroxene and garnet discrete nodules are diopsidic and pyropic, respectively, in composition. Large differences in corresponding Cr_2O_3 contents indicate that these discrete nodules did not originate by disaggregation of the associated eclogites. The eclogites from Orapa include foliated and non-foliated textural types and have been reported to contain both diamond and graphite. Compositions

of the garnet and clinopyroxene coexisting in these eclogites suggest temperatures of equilibration consistent with upper mantle conditions when plotted on model geotherms determined for neighboring areas in southern Africa. The petrographic and mineral chemical data presented in this study demonstrate an overall close similarity between the Orapa nodule suite and those representative of other, more thoroughly investigated districts in Africa, Siberia, and the United States. The Orapa suite is distinctive, however, in its wide variety of oxide discrete nodules, the presence of certain complex silicate/oxide intergrowths, and the previously reported coexistence of diamond and graphite in eclogite.

CHAPTER I

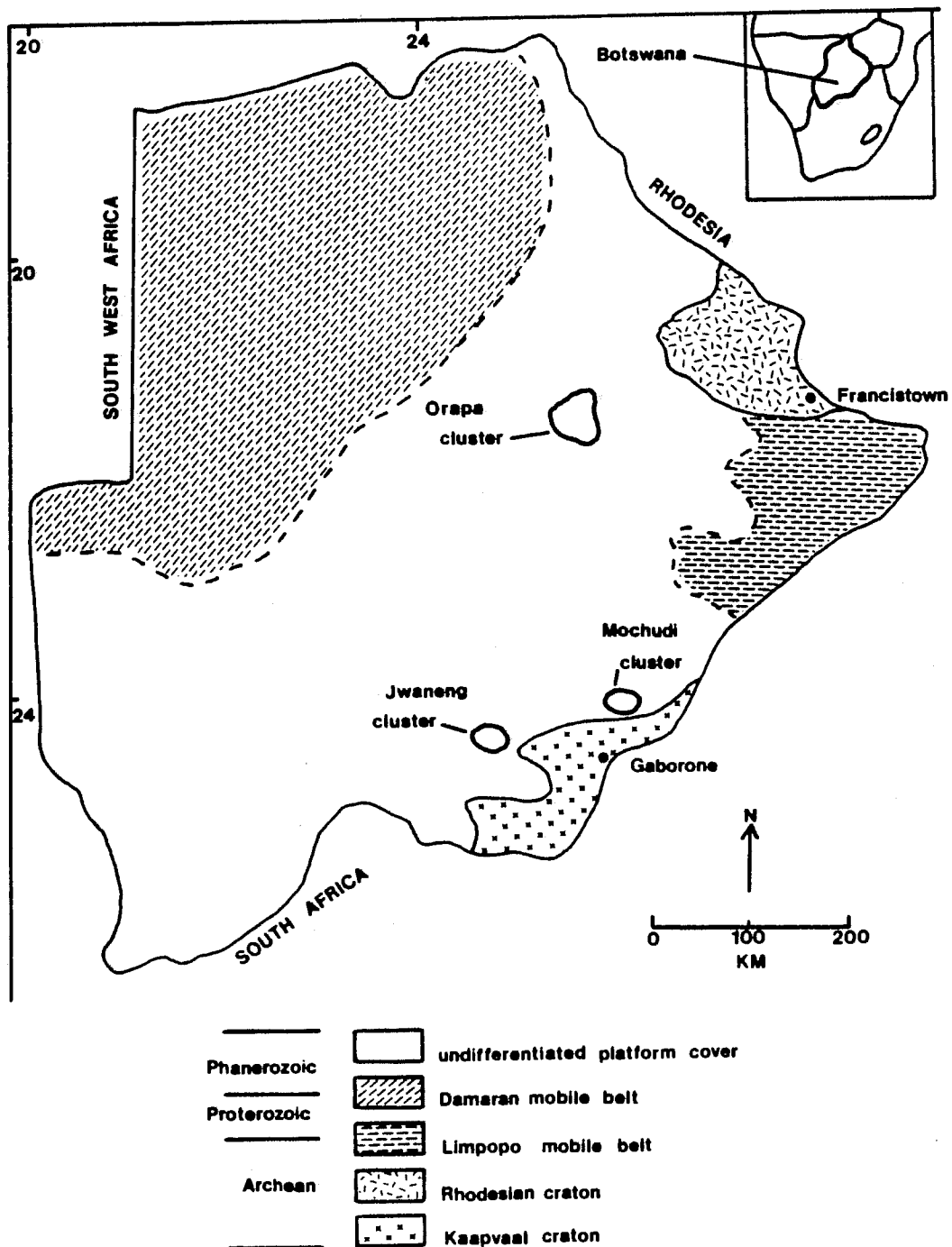
INTRODUCTION

The Orapa A/K-1 Kimberlite Pipe

The Orapa A/K-1 kimberlite pipe was initially located by DeBeers exploration parties in 1967 and has since been shown to be the most noteworthy of a cluster of at least 30 individual pipes situated approximately 250 km west of Francistown in east-central Botswana (Figure 1). The A/K-1 locality is presently the site of an extensive mining and processing facility producing an average of 4.5 million carats of primarily industrial quality diamonds each year (Green, 1981). Zircon age dates obtained from the kimberlite (Davis, 1977; Raber, 1978) indicate an upper Cretaceous time of emplacement for the main Orapa pipe which is consistent with its observed intrusion into rocks of the upper Jurassic Karroo Supergroup. The lithology of the uppermost levels of the mine consists predominantly of intercalated fine-grained sediments and locally epiclastic kimberlite and has been interpreted by Hawthorne (1975) to represent the typical near-surface facies of such diatremes. The surface area of approximately 1.1 km² at Orapa is second only to that of the Mwadui kimberlite in Tanzania and supports the contention that this large pipe has undergone only slight erosion since emplacement. Two other smaller clusters of pipes are located approximately 400 km to the south, but neither contains diatremes comparable to the main Orapa pipe in size or diamond production (Baldock et al., 1976).

The only petrographic and geochemical investigation of the kimberlites in the Orapa area undertaken to date is the reconnaissance survey

Figure 1: Generalized distribution of kimberlite clusters and major tectonic units in Botswana (modified from Baldock et al., 1976).



of Shee (1978) in which a variety of eclogite nodules from the A/K-1 pipe and, to a lesser extent, peridotite nodules from two neighboring pipes were examined, with the eclogites from the A/K-1 pipe described and subdivided on the basis of textural and mineral chemical criteria. A limited number of other types of nodules from the A/K-1 pipe were also analyzed as part of Shee's study; however, some of these data are of only limited value because they were purposely obtained from fragments of individual nodules and thus were not sensitive to chemical variations characteristic of each nodule as a whole.

This study was undertaken in an attempt to build upon the previous data base for the region by analyzing samples from all of the nodule groups known to be present at Orapa. The combination of petrographic, geochemical, and limited experimental work was planned with the intention of establishing a firm foundation for comparison between this pipe and some of those occurring in more thoroughly researched districts.

Determinative Methods

The kimberlitic nodule suite examined in this study was collected at the Orapa A/K-1 mine site by S.E. Haggerty in 1977. This study was begun by washing and cataloguing the individual nodules by hand in order to separate the likely deep-seated specimens from those which were of obvious crustal derivation or too weathered for meaningful analysis. Approximately 125 relatively unweathered nodules, representing about one-third of the original collection, were selected for detailed examination and analysis. These included representatives of each nodule type catalogued during the initial visual classification of the entire suite.

All specimens described in this study have been examined in either polished or thin sections, or both. Individual nodules were generally cut in half, with one piece used for thin section preparation according to conventional methods and the other half used for further analysis or catalogued for reference. Transmitted light and high resolution oil immersion microscopy were performed on all specimens using standard techniques. X-ray diffraction determinations were made on duplicate powder subsplits of selected samples using a 57.3 mm diameter camera with Ni-filtered copper K α radiation ($\lambda=1.54050 \text{ \AA}$) and film mounted according to the Straumanis method (see Zussman, 1977).

All electron microprobe analyses presented in this study were performed on the ETEC Autoprobe at the University of Massachusetts. Full automation of this instrument is achieved through an on-line Interdata computer using a quantitative analysis program developed jointly by the University of Massachusetts and the ETEC Corporation. Matrix corrections were employed according to the procedures of Bence and Albee (1968) and Albee and Ray (1970). Operating conditions generally included an accelerating voltage of 15 kilovolts, an aperture current of 0.3 microamperes, 15 second counting intervals for each element, and an average beam diameter of approximately 4 microns. Ferric iron contents were calculated for the oxide phases using a correction procedure modified from the program FERRIC written by J. Berg and W. Kelley and which assumes 1) perfect stoichiometry, 2) iron is the only element in multiple valence states, and 3) a perfect analysis of the other elements present. These calculations were made using the uncertainty restrictions of Finger (1972). Geochemical standards used for analysis included a variety of

both natural and synthetic silicate and oxide materials from the University of Massachusetts Analytical Geochemistry Facility collection.

The ilmenite-rutile experiments were performed using modified Deltech DT-31 gas mixing furnaces in the Phase Equilibria Laboratory at the University of Massachusetts. Whole sample fragments were suspended using platinum wire in a regulated and mixed flow of ultra-pure hydrogen and carbon dioxide circulating within the furnace environment. Rapid quenching was attained by fusing the platinum wire through the passage of an electric current, resulting in the free fall of the sample into a water bath. Experience has demonstrated that this is an effective quenching technique which does not result in any observable reaction. The oxygen fugacity was measured at a point directly adjacent to the sample position by monitoring the electrical potential established across an yttria-stabilized ZrO_2 ceramic electrolyte cell containing ultra-pure oxygen reference gas in a method similar to that outlined by Sato (1971). Temperatures were measured using a calibrated Pt-Pt₉₀Rh₁₀ thermocouple placed within the closed end of the oxygen sensor.

C H A P T E R I I
O X I D E D I S C R E T E N O D U L E S

Ilmenite

In hand specimen, discrete nodules of ilmenite from the Orapa A/K-1 kimberlite pipe in Botswana are typically dull dark-gray to black in color with local, lighter gray patches of leucoxene alteration present along peripheries and cracks. Individual nodules are typically smooth and somewhat rounded to ovoid in external morphology and locally show numerous closely-spaced fractures. Nodule size consistently averages about 1 centimeter throughout the suite. The overall appearance of these nodules in hand specimen is similar to that described for ilmenites from a variety of other African pipes (for example: Frick, 1973; Mitchell, 1973) and is almost certainly a result of the fluidization and particle abrasion thought to be characteristic of kimberlite diatreme emplacement (Lorenz, 1975; Woolsey et al., 1975).

Viewed in polished section, individual nodules may include only a single homogeneous ilmenite grain or comprise an aggregate of numerous, closely intergrown grains commonly distinguishable by markedly different reflection anisotropies. Such polycrystalline varieties are clearly more abundant and are generally characterized by a range of distinct inequigranular granoblastic-polygonal textures (Spry, 1969) which, in many specimens, do not entirely encompass individual nodules. Intergranular boundaries are typically curved, although straight boundaries with near equal-angle (120°) triple point junctions are locally present in some specimens. A complete gradation from entirely homogeneous to completely

polycrystalline nodules has been characterized. Photomicrographs of representative textural features are shown in Figure 2a-f. Partially polycrystalline specimens typically show development of the polygranular texture only in areas at or near nodule peripheries and probably represent an intermediate stage in the recrystallization of originally homogeneous nodules. Homogeneous and partially polycrystalline nodules characterized by locally anomalous, elongate zones of undulatory extinction indicate that individual nodules must have been first subjected to intense shear stress at some point before temperature-pressure conditions became appropriate for initiation of internal recrystallization. Evidence that such shearing continued during at least the initial stages of the high temperature recrystallization episode is preserved in those polycrystalline and partially polycrystalline nodules which show fine-scale twinning within individual ilmenite grains located near the nodule peripheries. Similar nodules which contain bands of finely-granular ilmenite situated between coarser individuals and polygranular fabrics characterized by irregular to curved self-boundaries indicate that the recrystallization process either resulted in an equilibrium texture that was not maintained (Stanton, 1972) or, perhaps more likely, was quenched before an equilibrium texture could be attained. In summary, it is proposed that the ilmenite nodule suite from Orapa comprises a full range of textures bearing on the transport of originally homogeneous ilmenite through the temperature and pressure regimes encountered by kimberlite magma emanating from a source region in the upper mantle. This textural sequence is shown diagrammatically in Figure 3 and is consistent with the generalized scheme outlined by Mitchell (1973) on the basis of much less complete

Figure 2a: Typical inequigranular polycrystalline texture developed in the interior region of an ilmenite nodule. Note that the self-boundaries between individual grains are delineated by both surface pitting and differences in reflection anisotropy.
(air, 80 X, horizontal dimension equals 2 mm, specimen #OR-417)

Figure 2b: Well-developed, angular-polygonal polycrystalline texture viewed near the periphery of an ilmenite nodule. Note that relatively few boundaries are marked by surface pitting.
(air, 80 X, horizontal dimension equals 2 mm, specimen #OR-427A)

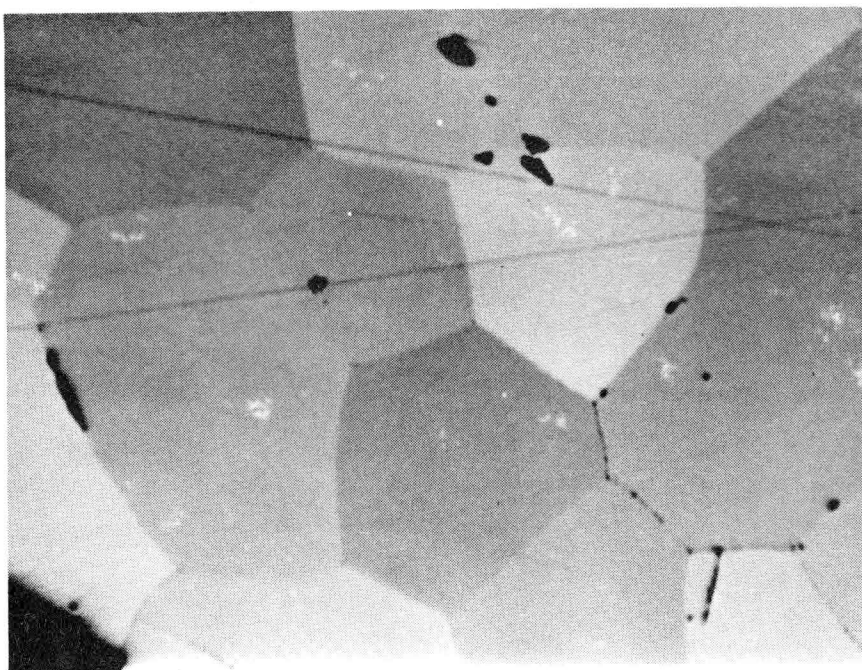
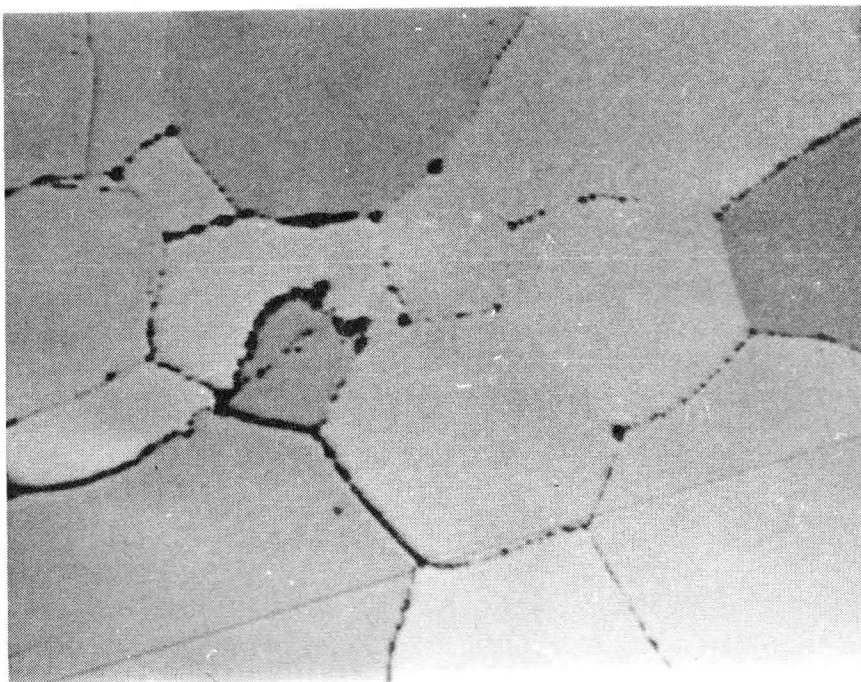


Figure 2c: Polycrystalline texture developed at the periphery of an otherwise homogeneous ilmenite nodule. Note the heavy pitting along self-boundaries, lack of consistency in the degree of pitting between adjacent individuals, and the overall non-equilibrium texture.
(air, 80 X, horizontal dimension equals 2 mm, specimen #OR-407B)

Figure 2d: Prominent twinning lamellae oriented along probable crystallographically equivalent directions in an ilmenite grain at a nodule periphery. Note that one set of lamellae terminate at a polycrystalline self-boundary and are not present in the adjacent grain.
(air, 80 X, horizontal dimension equals 2 mm, specimen #OR-417)

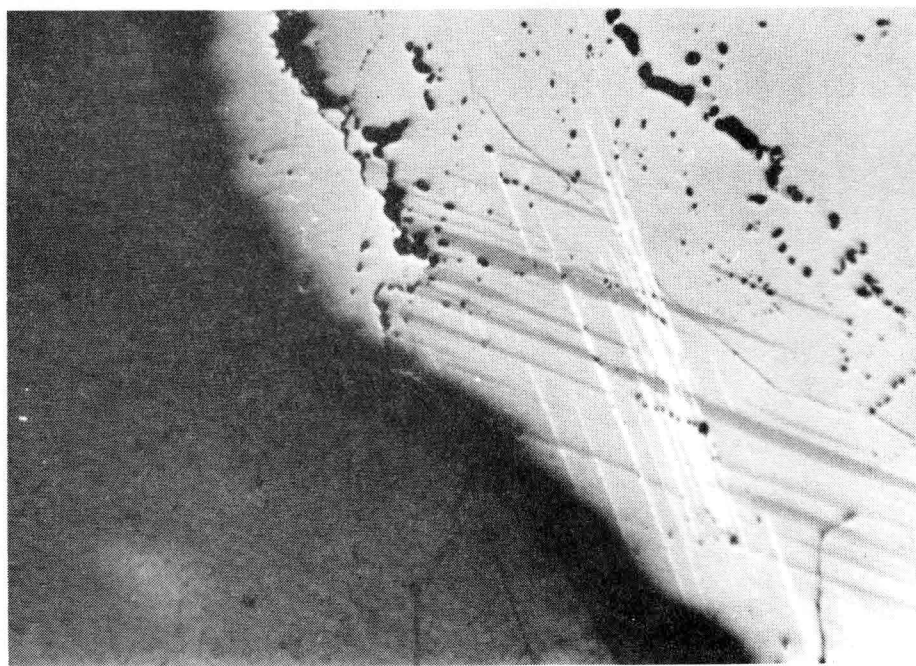
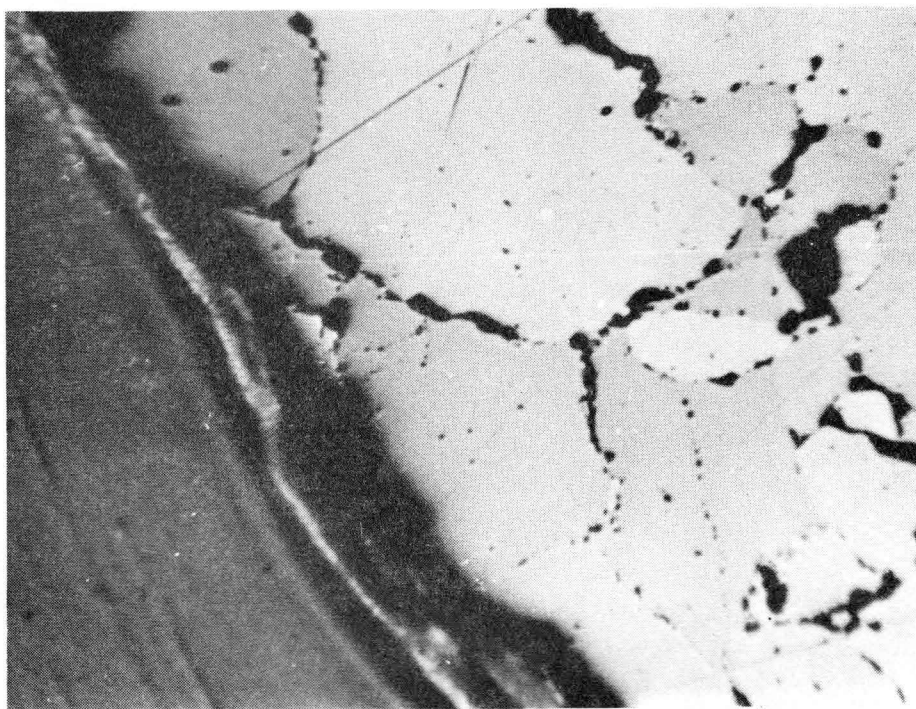
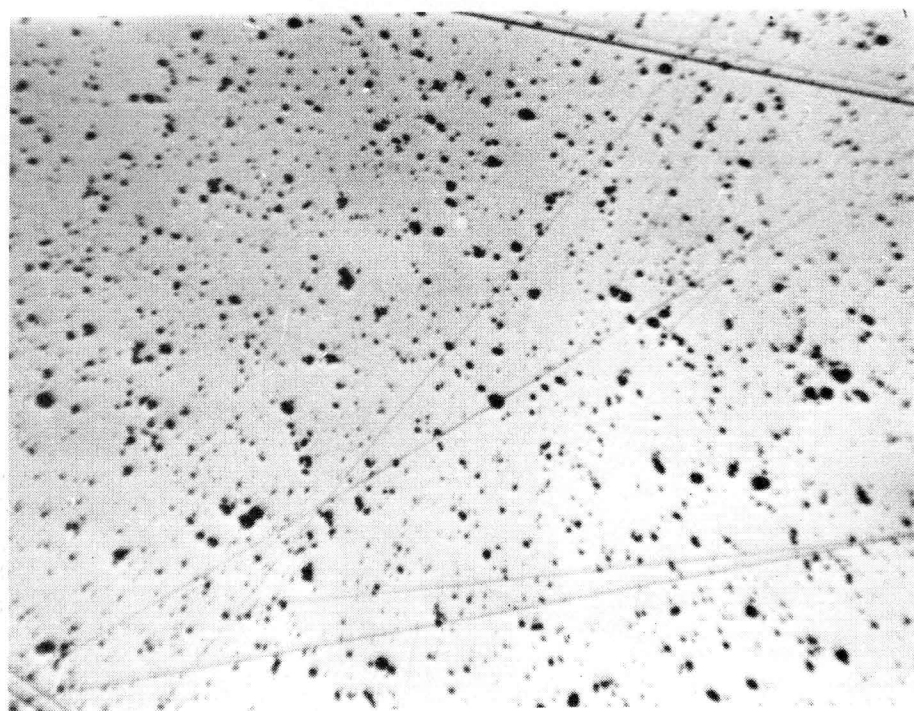
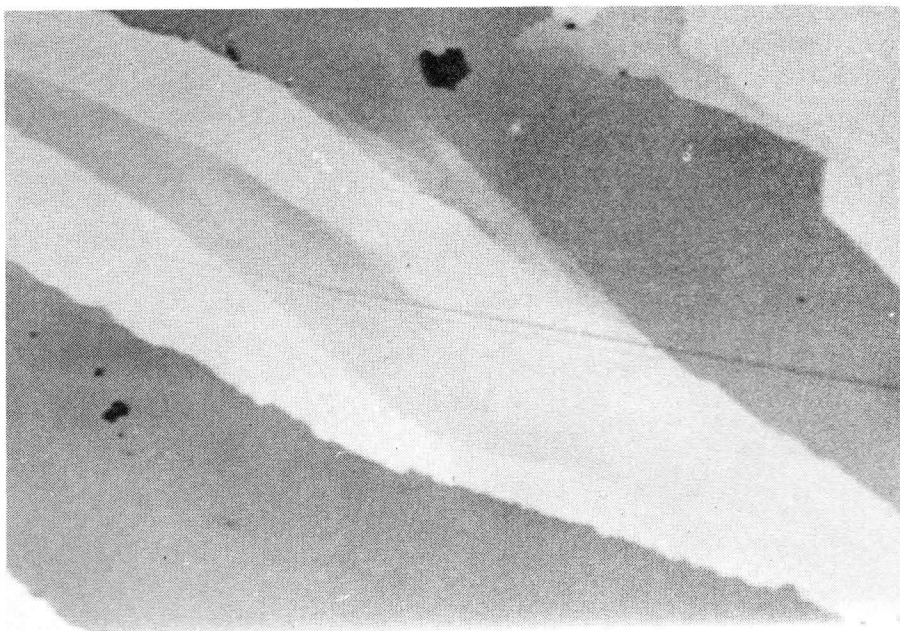


Figure 2e: Anisotropic shear fabric developed in the interior region of an otherwise homogeneous ilmenite nodule. Such fabric is generally not outlined by surface pitting.
(air, 80 X, horizontal dimension equals 2 mm, specimen #OR-405A)

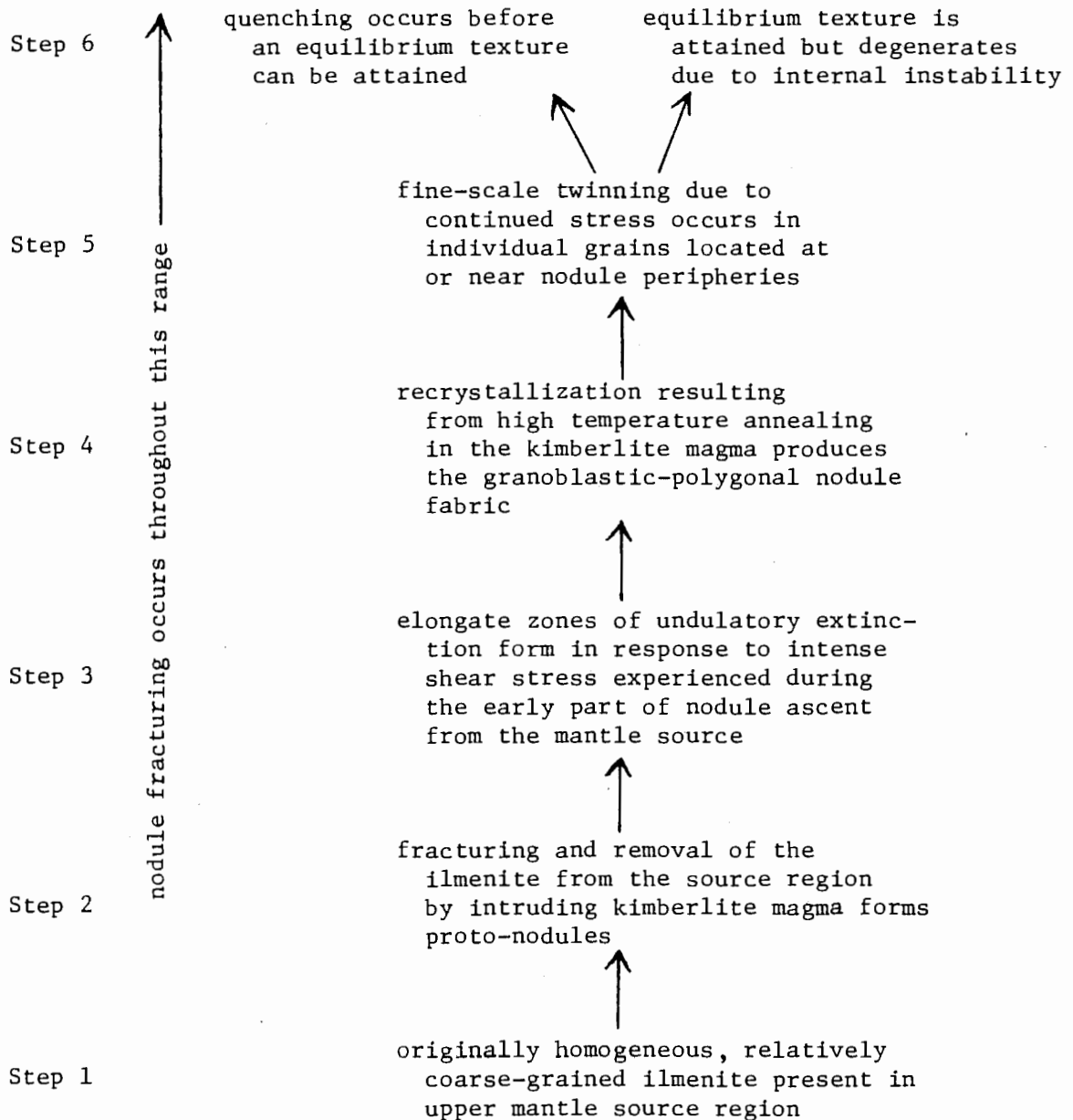
Figure 2f: Heavy surface pitting developed in the interior design of an ilmenite nodule. Such pitting can be locally widespread and usually bears no obvious relation to polycrystalline boundaries which may be present.
(air, 80 X, horizontal dimension equals 2 mm, specimen #OR-407A)



textural evidence.

In the interpretation outlined above and in Figure 3, the ilmenite is envisaged as originating in a deep, probably spatially isolated, upper mantle source composed predominantly of relatively coarse, crystalline grains which were fractured and removed by the action of intruding kimberlite magma. Such ilmenite source regions probably only exist below the depths of basaltic magma generation and above the depths of kimberlite magma formation, and may vary in composition from place to place. Microstructural studies of deformed peridotite and associated nodules (Goetze, 1975) indicate that differential stresses acting during kimberlite intrusion may be as high as 1 kb, with deformation most likely occurring at some time prior to eruption, probably during conduit formation (Mercier, 1979). The development of the various textural features described for the Orapa suite is considered to be a function of both residence time and position in the ascending kimberlite magma. According to this interpretation, the range in textures could result from differing local environs of encapsulation (varying liquid/solid ratios, for example) in the kimberlite magma during transport and emplacement, with those nodules encased in environs most susceptible to transmitting shear stress and temperature gradients developing the most "mature" textural characteristics. The development of these typical textural features during ascent in the kimberlite magma is considered to be more likely than the development of a range of characteristic textures formed in the source region because the latter would imply an unlikely range of temperature and pressure gradients established over relatively local areas at such considerable depths. As described in a later section, textural and chemical

Figure 3: Generalized sequence of events believed to result in the range of textural features observed in the ilmenite discrete nodule suite from Orapa.



evidence suggests that nodule fracturing and abrasion continued during most of the kimberlite ascent phase.

Very fine-scale internal pitting is characteristic of the majority of nodules examined in polished section. This pitting is typically only locally developed and, in some specimens, appears to be restricted to certain individual ilmenite grains, resulting in a polygranular texture comprised of both pitted and unpitted, locally adjacent grains. Self-boundaries between adjacent ilmenite grains in pitted nodules are commonly marked by linear bands of surface pitting and, in those specimens characterized by overall widespread and heavy pitting, the self-boundaries are marked by the coarsest pitting. In lightly pitted nodules, the borders of individual ilmenite grains are typically not continuously pitted and are only visible by differences in reflection anisotropy. In such cases, however, pitting does often occur locally at the angular intersections between adjacent grains. In general, the pitting observed in this ilmenite suite is similar to that described by Pasteris et al. (1979) for nodules collected from the Frank Smith kimberlite pipe in South Africa except that the pitting in the Orapa samples does not appear to show any distinct crystallographic orientation and, unlike similar specimens described by Dawson (1962) from a variety of localities in Lesotho, is not generally visible macroscopically on exterior nodular surfaces. Repeated examination using standard oil-immersion techniques and the electron microprobe has shown no consistent physical or chemical differences between unpitted and pitted ilmenite grains. Concentration of the pitting along individual grain boundaries suggests that it is ultimately a product of alteration which may subsequently become enhanced

during the process of manufacturing the polished sections.

Representative chemical compositions obtained by electron microprobe analysis of individual nodules are presented in Table 1. The compositions are distinctly kimberlitic according to the criteria of Haggerty (1975) with MgO contents varying from approximately 6.6 to 15 wt. %, Fe_2O_3 values ranging from approximately 6 to 16 wt. %, and Cr_2O_3 averaging nearly 2.5 wt. %. Compositions of the core regions of individual nodules are plotted in terms of the ternary solid solution end members FeTiO_3 - MgTiO_3 - Fe_2O_3 (mole percent ilmenite-geikielite-hematite) in Figure 4a and define a relatively tight cluster approximately centered at Ilm-58%, Geik-30%, Hem-12%. This is in broad agreement with ilmenite data previously published by other authors from a variety of southern and west African kimberlite localities (for example: Haggerty, 1975; Mitchell, 1977), although a general decrease in hematite component with increasing geikielite component is not apparent. These data are interpreted to indicate that the ilmenite crystallized under relatively low conditions of oxygen fugacity. Values of MgO for this suite range from 6.63 to 15.04 wt. % and support Mitchell's (1973) proposal that individual kimberlite pipes contain ilmenite suites of varying magnesium content. The range in MgO characterizing the Orapa suite is considerable, exceeding, for example, those reported for the Kao, Sekameng, and Monastery pipes (Mitchell, 1977), but remains less than those characterizing the Frank Smith and Wesselton localities (Mitchell, 1977 and 1973, respectively).

Figure 4b is a ternary plot of compositions from the interior regions of nodules observed to be either nearly completely homogeneous or

Table 1: Average chemical compositions of individual ilmenite discrete nodules from Orapa - nodule interiors.

Specimen:	<u>405A</u>	<u>407A</u>	<u>407B</u>	<u>408A</u>	<u>408B</u>	<u>408C</u>	<u>409A</u>	<u>410A</u>	<u>410B</u>
TiO ₂	47.09	47.70	47.95	47.61	47.16	47.96	48.40	53.84	47.00
Cr ₂ O ₃	1.78	1.75	2.36	1.71	1.45	1.70	1.38	1.85	2.43
Al ₂ O ₃	0.13	0.19	0.18	0.27	0.37	0.27	0.24	0.56	0.17
'Fe ₂ O ₃	13.38	13.36	11.10	12.71	16.16	12.71	11.99	6.12	12.27
FeO	29.26	28.01	29.23	28.10	26.36	28.67	29.96	22.70	29.19
MgO	7.29	8.37	7.83	8.16	8.84	7.85	7.41	14.19	7.23
MnO	0.33	0.21	0.30	0.28	0.24	0.31	0.26	0.31	0.35
ZrO ₂	0.15	0.13	0.32	0.06	0.12	0.02	0.05	0.08	0.32
Nb ₂ O ₅	0.24	0.30	0.27	0.19	0.12	0.00	0.00	0.08	0.09
NiO	0.10	0.13	0.08	0.11	0.04	0.15	0.12	0.23	0.11
Total	<u>99.75</u>	<u>100.15</u>	<u>99.62</u>	<u>99.20</u>	<u>100.86</u>	<u>99.64</u>	<u>99.81</u>	<u>99.96</u>	<u>99.16</u>

Cations based on three (3) oxygens

Ti	0.854	0.855	0.867	0.861	0.836	0.865	0.874	0.921	0.857
Cr	0.034	0.033	0.045	0.032	0.027	0.032	0.026	0.033	0.047
Al	0.004	0.005	0.005	0.008	0.010	0.008	0.007	0.015	0.005
'Fe ³⁺	0.243	0.240	0.201	0.230	0.287	0.229	0.217	0.105	0.224
Fe ²⁺	0.590	0.558	0.588	0.565	0.520	0.575	0.602	0.432	0.592
Mg	0.262	0.297	0.281	0.293	0.311	0.281	0.265	0.482	0.261
Mn	0.007	0.004	0.006	0.006	0.005	0.006	0.005	0.006	0.007
Zr	0.002	0.002	0.004	0.001	0.001	0.000	0.001	0.001	0.004
Nb	0.003	0.003	0.003	0.002	0.001	0.000	0.000	0.001	0.001
Ni	0.002	0.003	0.002	0.002	0.000	0.003	0.002	0.004	0.002
Total	<u>2.001</u>	<u>2.000</u>	<u>2.002</u>	<u>2.000</u>	<u>1.998</u>	<u>1.999</u>	<u>1.999</u>	<u>2.000</u>	<u>2.000</u>
Mg/(Mg+Fe ²⁺) n	0.308 4	0.347 4	0.323 5	0.341 4	0.374 9	0.328 5	0.306 4	0.527 2	0.306 4

' calculated

Table 1 (con't)

Specimen:	<u>411A</u>	<u>411B</u>	<u>412A</u>	<u>412B</u>	<u>413A</u>	<u>414A</u>	<u>414B</u>	<u>415A</u>	<u>415B</u>
TiO ₂	47.38	51.93	47.16	53.67	48.68	48.02	47.69	49.41	47.16
Cr ₂ O ₃	3.63	4.57	3.59	1.66	3.96	4.11	1.39	3.82	3.08
Al ₂ O ₃	0.23	0.13	0.12	0.43	0.22	0.09	0.26	0.03	0.00
'Fe ₂ O ₃	11.33	6.12	12.78	7.45	10.95	12.12	12.55	8.70	13.08
FeO	27.99	23.51	26.06	21.16	25.82	25.58	29.03	26.71	27.03
MgO	8.25	12.72	9.36	15.04	10.15	9.87	7.75	9.94	8.67
MnO	0.18	0.36	0.21	0.24	0.20	0.24	0.27	0.37	0.25
ZrO ₂	0.46	0.00	0.55	0.15	0.31	0.29	0.30	0.16	0.45
Nb ₂ O ₅	0.18	0.16	0.43	0.15	0.41	0.26	0.19	0.41	0.16
NiO	0.18	0.33	0.15	0.23	0.20	0.15	0.04	0.15	0.09
Total	<u>99.81</u>	<u>99.83</u>	<u>100.41</u>	<u>100.18</u>	<u>100.90</u>	<u>100.73</u>	<u>99.47</u>	<u>99.70</u>	<u>99.97</u>

Cations based on three (3) oxygens

Ti	0.852	0.901	0.838	0.912	0.854	0.846	0.863	0.878	0.846
Cr	0.069	0.083	0.067	0.030	0.073	0.076	0.026	0.071	0.058
Al	0.006	0.004	0.003	0.011	0.006	0.003	0.007	0.001	0.000
'Fe ³⁺	0.204	0.106	0.227	0.127	0.192	0.214	0.227	0.155	0.235
Fe ²⁺	0.560	0.454	0.515	0.400	0.504	0.501	0.584	0.528	0.539
Mg	0.294	0.437	0.330	0.507	0.353	0.345	0.278	0.350	0.308
Mn	0.004	0.007	0.004	0.005	0.004	0.005	0.005	0.007	0.005
Zr	0.005	0.000	0.006	0.002	0.003	0.003	0.004	0.002	0.005
Nb	0.002	0.002	0.005	0.002	0.004	0.003	0.002	0.004	0.002
Ni	0.003	0.006	0.003	0.004	0.004	0.003	0.001	0.003	0.002
Total	<u>1.999</u>	<u>2.000</u>	<u>1.998</u>	<u>2.000</u>	<u>1.997</u>	<u>1.999</u>	<u>1.997</u>	<u>1.999</u>	<u>2.000</u>
Mg(Mg+Fe ²⁺)	0.344	0.490	0.391	0.559	0.412	0.408	0.322	0.399	0.364
n	5	5	7	12	13	7	8	4	4

' calculated

Table 1 (con't)

Specimen:	<u>416A</u>	<u>416B</u>	<u>417A</u>	<u>418A</u>	<u>418B</u>	<u>419A</u>	<u>420A</u>	<u>420B</u>	<u>421A</u>
TiO ₂	47.18	47.02	48.37	47.83	47.90	47.09	47.89	48.99	48.08
Cr ₂ O ₃	1.98	1.98	1.69	1.93	1.68	3.79	2.01	1.83	3.37
Al ₂ O ₃	0.25	0.18	0.30	0.26	0.23	0.04	0.11	0.15	0.23
'Fe ₂ O ₃	14.06	15.38	12.76	12.77	12.89	12.16	10.97	10.14	11.53
FeO	26.45	27.20	27.68	29.30	29.47	27.69	31.20	31.52	27.45
MgO	8.94	8.45	8.85	7.55	7.46	8.27	6.63	6.84	8.61
MnO	0.23	0.25	0.20	0.27	0.33	0.37	0.32	0.36	0.28
ZrO ₂	0.15	0.14	0.17	0.25	0.18	0.20	0.17	0.23	0.13
Nb ₂ O ₅	0.17	0.25	0.26	0.02	0.08	0.47	0.24	0.00	0.00
NiO	0.08	0.11	0.20	0.15	0.16	0.15	0.06	0.10	0.22
Total	<u>99.49</u>	<u>100.96</u>	<u>100.48</u>	<u>100.33</u>	<u>100.38</u>	<u>100.23</u>	<u>99.60</u>	<u>100.16</u>	<u>99.90</u>

Cations based on three (3) oxygens

Ti	0.847	0.836	0.860	0.860	0.861	0.845	0.873	0.886	0.860
Cr	0.037	0.037	0.032	0.037	0.032	0.071	0.039	0.035	0.063
Al	0.007	0.005	0.008	0.007	0.007	0.001	0.003	0.004	0.006
'Fe ³⁺	0.253	0.274	0.227	0.230	0.232	0.218	0.200	0.184	0.206
Fe ²⁺	0.528	0.538	0.548	0.586	0.590	0.553	0.633	0.634	0.546
Mg	0.318	0.298	0.312	0.269	0.266	0.294	0.240	0.245	0.306
Mn	0.005	0.005	0.004	0.005	0.007	0.008	0.007	0.007	0.006
Zr	0.002	0.002	0.002	0.003	0.002	0.002	0.002	0.003	0.002
Nb	0.002	0.003	0.003	0.000	0.001	0.005	0.003	0.000	0.000
Ni	0.002	0.002	0.004	0.003	0.003	0.003	0.001	0.002	0.004
Total	<u>2.001</u>	<u>2.000</u>	<u>2.000</u>	<u>2.000</u>	<u>2.001</u>	<u>2.000</u>	<u>2.001</u>	<u>2.000</u>	<u>1.999</u>
Mg(Mg+Fe ²⁺) n	0.376 20	0.356 12	0.363 13	0.315 18	0.311 16	0.347 11	0.275 3	0.279 1	0.359 7

' calculated

Table 1 (con't)

Specimen:	<u>421B</u>	<u>423A</u>	<u>426A</u>	<u>427A</u>	<u>427B</u>	<u>428A</u>	<u>428B</u>	<u>429A</u>	<u>434A</u>	<u>434B</u>
TiO ₂	48.27	46.62	46.78	47.20	46.39	47.69	47.25	47.02	47.72	47.73
Cr ₂ O ₃	3.25	3.50	3.70	1.77	2.46	1.98	1.97	2.39	2.30	1.92
Al ₂ O ₃	0.25	0.05	0.05	0.16	0.05	0.17	0.05	0.23	0.17	0.30
'Fe ₂ O ₃	10.61	13.55	12.59	13.98	14.25	13.13	13.36	12.99	13.44	13.89
FeO	28.06	26.88	29.12	28.40	27.94	28.95	28.95	27.32	27.56	26.98
MgO	8.30	8.40	7.22	7.73	7.74	7.79	7.53	8.38	8.42	8.77
MnO	0.34	0.34	0.37	0.33	0.34	0.27	0.28	0.30	0.33	0.31
ZrO ₂	0.01	0.27	0.29	0.26	0.13	0.35	0.23	0.21	0.10	0.17
Nb ₂ O ₅	0.11	0.24	0.24	0.00	0.32	0.13	0.14	0.24	0.06	0.00
NiO	<u>0.33</u>	<u>0.14</u>	<u>0.13</u>	<u>0.07</u>	<u>0.07</u>	<u>0.12</u>	<u>0.12</u>	<u>0.08</u>	<u>0.13</u>	<u>0.09</u>
Total	99.53	99.99	100.49	99.90	99.69	100.58	99.98	99.16	100.23	100.16

Cations based on three (3) oxygens

Ti	0.868	0.837	0.843	0.852	0.840	0.855	0.853	0.850	0.854	0.852
Cr	0.061	0.066	0.070	0.033	0.047	0.037	0.037	0.045	0.043	0.036
Al	0.007	0.001	0.001	0.004	0.001	0.005	0.004	0.007	0.005	0.008
'Fe ³⁺	0.191	0.244	0.227	0.253	0.258	0.236	0.242	0.235	0.241	0.248
Fe ²⁺	0.562	0.537	0.584	0.570	0.563	0.577	0.582	0.549	0.548	0.536
Mg	0.296	0.299	0.258	0.277	0.278	0.277	0.270	0.301	0.299	0.310
Mn	0.007	0.007	0.007	0.007	0.007	0.006	0.006	0.006	0.007	0.006
Zr	0.000	0.003	0.003	0.003	0.002	0.004	0.003	0.002	0.001	0.002
Nb	0.001	0.003	0.003	0.000	0.003	0.001	0.001	0.003	0.001	0.000
Ni	<u>0.006</u>	<u>0.003</u>	<u>0.002</u>	<u>0.001</u>	<u>0.001</u>	<u>0.002</u>	<u>0.002</u>	<u>0.002</u>	<u>0.002</u>	<u>0.002</u>
Total	1.999	2.000	1.998	2.000	2.000	2.000	2.000	2.000	2.000	2.000
Mg(Mg+Fe ²⁺)	0.345	0.358	0.307	0.327	0.331	0.324	0.317	0.354	0.353	0.366
n	5	6	4	5	4	6	4	5	4	6

' calculated

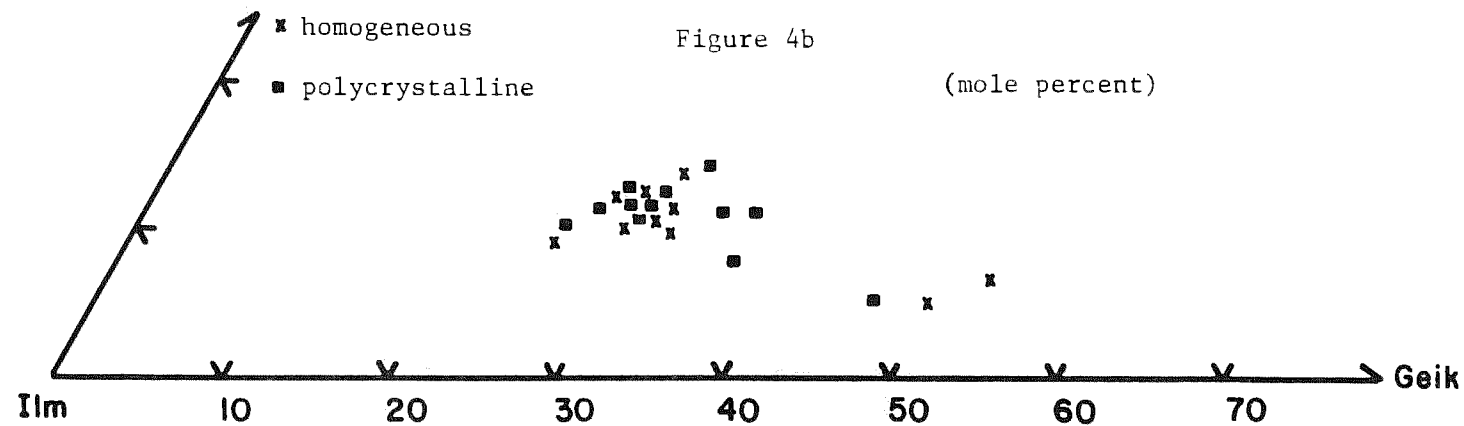
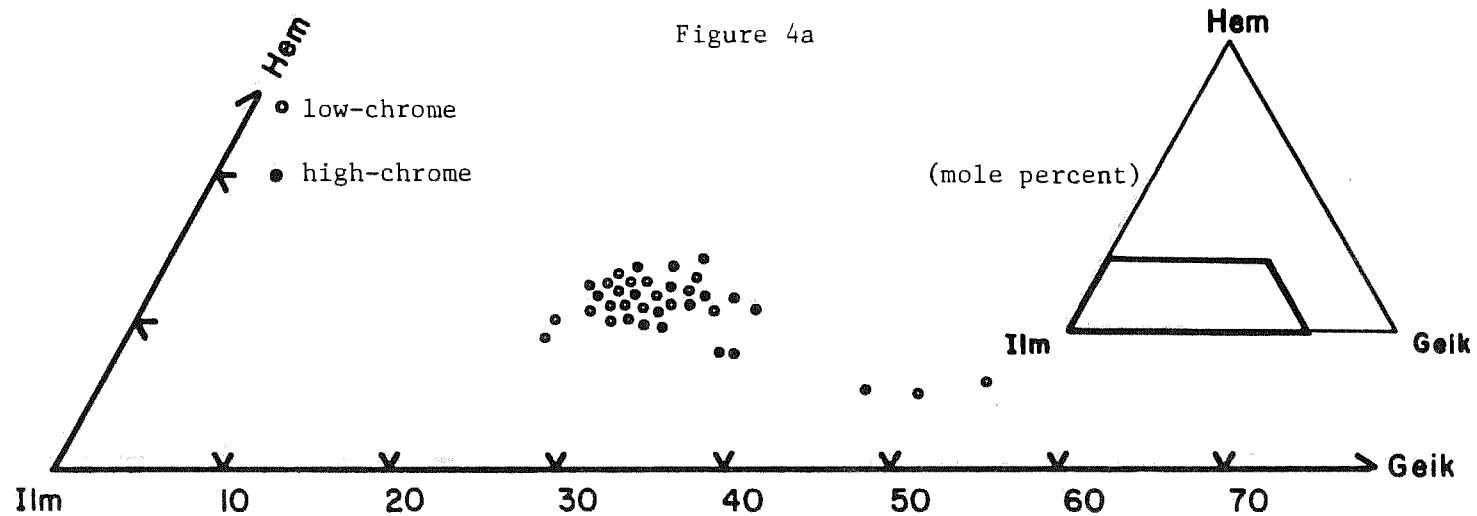


Figure 4 a: Compositions of the ilmenite discrete nodule suite from Orapa plotted in the ternary system ilmenite-geikielite-hematite.

b: Compositions of homogeneous and completely polycrystalline discrete nodules plotted in the ternary system ilmenite-geikielite-hematite.

polycrystalline in texture. The data show considerable overlap and indicate no obvious chemical distinction between the two types. Detailed electron microprobe analyses on opposite sides of intra-nodular polygranular boundaries in polycrystalline varieties also indicate an overall lack of consistent chemical anisotropy. This finding supports earlier work performed by Pasteris et al. (1979) on a similar suite from the Frank Smith kimberlite pipe. The three clearly anomalous points situated to the right of the main cluster refer to samples 411B, 410A, and 412B. These will be discussed specifically elsewhere.

Ilmenite nodules comprising the Orapa suite may be divided into two groups on the basis of Cr_2O_3 content, as shown in Figure 5, with a gap in Cr_2O_3 values extending from approximately 2.60 to 3.10 wt. %. Average Cr_2O_3 content for the high and low groupings is 3.62 and 1.91 wt. % respectively. Plotted in terms of MgO wt. % versus Cr_2O_3 wt. % (Figure 5), the Orapa data define a crudely linear trend situated between the arms of the parabolic curve drawn by Haggerty (1975) to characterize the general relationship between these two variables for a large number of kimberlitic ilmenites from Lesotho and West Africa. A plot of the same parameters for ilmenite discrete nodule cores from the Lihobong kimberlite by Boctor and Boyd (1980) shows a similar two-fold compositional grouping with an apparent Cr_2O_3 hiatus from approximately 1.8 to 2.1 wt. %. These points, however, plot closer to the high magnesium arm of the Haggerty parabola than the Orapa data. Haggerty (pers. comm., 1980) has also recognized a previously unnoted, narrow gap over approximately the same range of Cr_2O_3 values (1.8 to 2.1 wt. %) in the data used in the original compilation of the parabolic relationship. Although

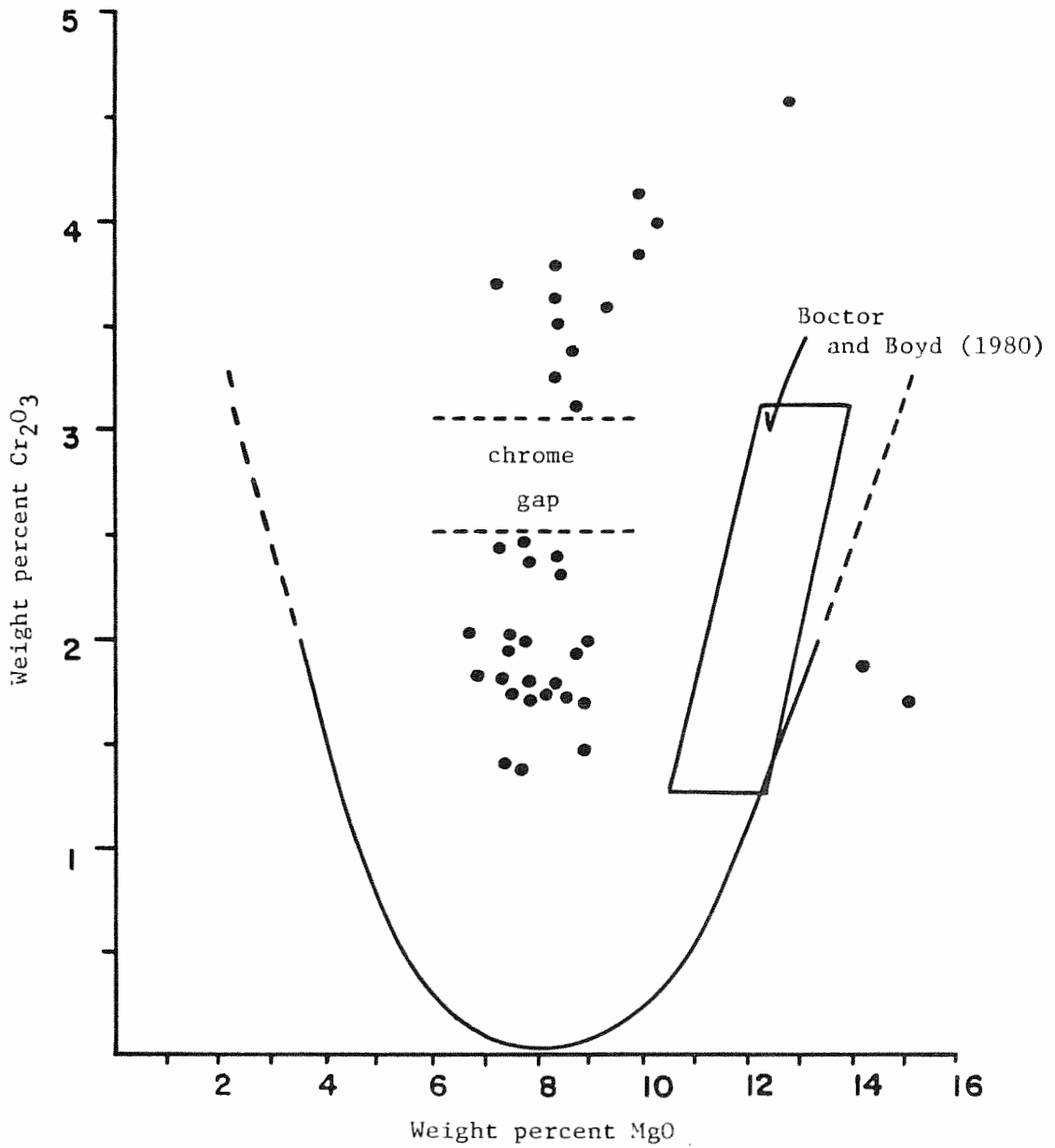


Figure 5: Plot of MgO versus Cr₂O₃ content for the ilmenite discrete nodule suite from Orapa. The parabolic curve is replotted from Haggerty (1975, p. 304). The data of Boctor and Boyd (1980) are contained within the area outlined by the parallelogram.

two groups of nodules are apparent in terms of Cr_2O_3 and MgO at Orapa, it must be stressed that the overall correlation between the two variables is poor ($R^2 = 0.53$). This lack of interdependence is expressed by the nearly constant Cr_2O_3 values throughout individual nodules characterized by marked MgO zoning (Figure 6). The same lack of inter-element correlation within zoned ilmenite has been noted by Boctor and Boyd (1980; discrete nodules) and by Elthon and Ridley (1979; small, disseminated grains in fresh kimberlite).

Chemical zoning of individual ilmenite nodules from kimberlite appears to be relatively common. Haggerty et al. (1979) described two distinct types of zoning in nodules from the Monastery mine including a 1) "magmatic reaction" trend thought to result from reaction with the kimberlite liquid as pressure decreased during emplacement and a 2) "kimberlite reaction" trend believed to be late-stage and related to carbonatite liquid immiscibility. In the magmatic trend, MgO was observed to increase toward nodule peripheries with a concomitant decrease in Fe_2O_3 . The reaction trend, on the other hand, was characterized by increasing FeO from core to rim, decreasing Fe_2O_3 , and overall high (1-5 wt. %) MnO content. Boctor and Boyd (1980) have recently described another, apparently different, core-to-rim MgO enrichment trend in which MgO increases dramatically only in zones 300 to 500 microns from nodule peripheries. They attribute this chemical heterogeneity to reaction with MgO-rich metasomatic fluids. Magnesium zoning in individual nodules from Orapa (Figure 6) appears to most closely resemble the magmatic trend of Haggerty et al. (1979a) with marked increases in MgO content occurring over what is probably a somewhat wider

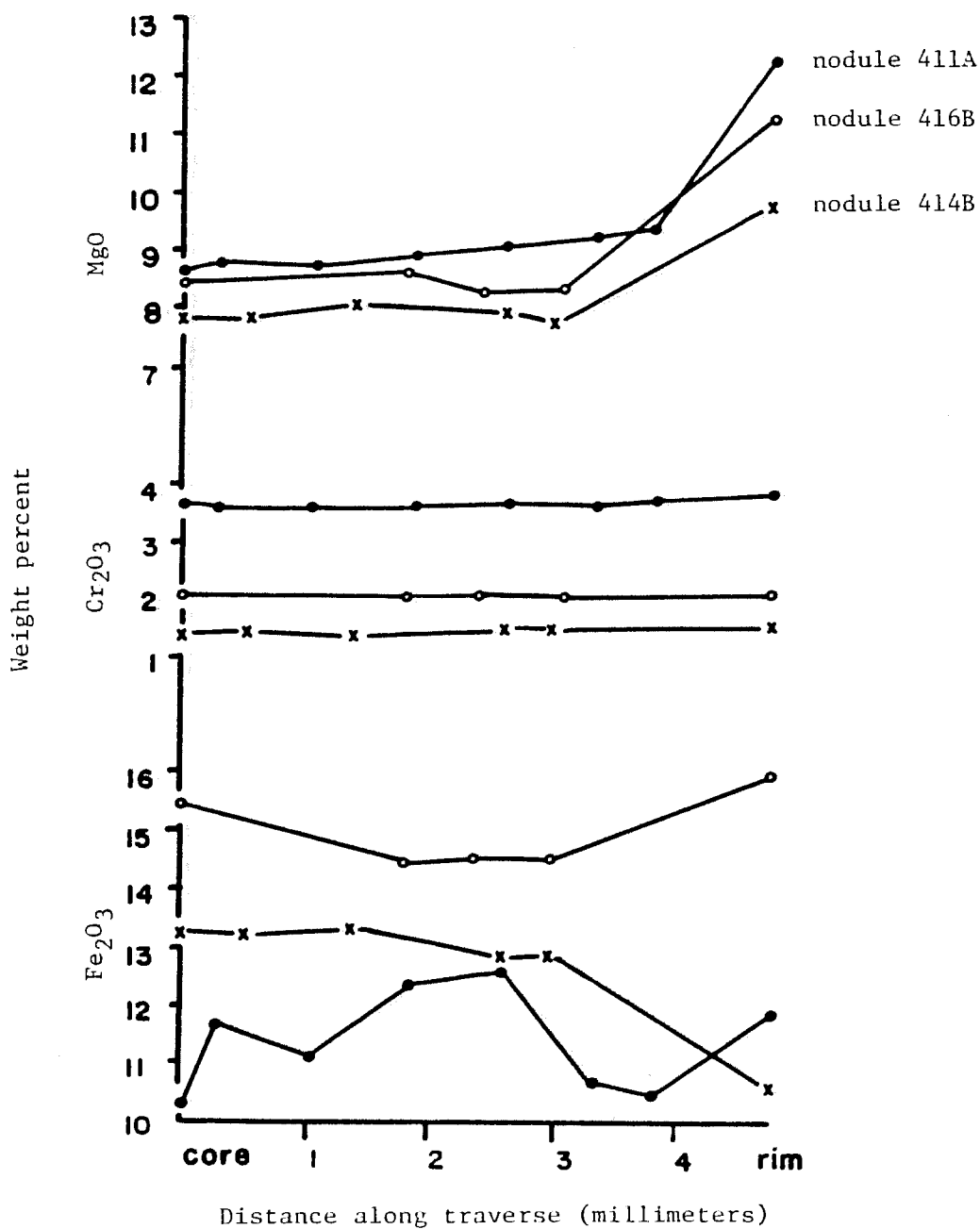


Figure 6: Compositional variation along core-to-periphery microprobe traverses of three ilmenite discrete nodules.

interval at nodule peripheries. Values for Cr_2O_3 are essentially constant throughout such grains and thus show no obvious relation to MgO content. The variation in Fe_2O_3 is, however, quite dramatic in some nodules, showing a tendency to both increase and decrease in core-to-rim traverses. This behavior is, nevertheless, still consistent with the magmatic trend zoning model since Haggerty et al. (1979) observed a steady decrease in Fe_2O_3 content in core-to-rim traverses to be followed in many cases by sudden increase in Fe_2O_3 values at, or very close to, the actual peripheries. Such rapid increases in Fe_2O_3 content at nodule rims is probably the result of a late-stage or even post-emplacement oxidation event perhaps related to weathering. Viewed in these terms, regardless of the mechanism involved, the observed Fe_2O_3 variation in Orapa nodules may simply be a function of the physical environment of encapsulation of the individual nodules in the frozen or near-frozen kimberlite with some Fe_2O_3 -enriched nodules situated where oxidation was pervasive and others situated where it was not. Nodules in which the Fe_2O_3 content is even less systematic may have undergone intense oxidation along fractures, intergranular boundaries, and similar permeable avenues.

When describing such zoning, it is critical that detailed chemical mapping be performed in order to delineate the nature and extent of the chemical heterogeneity and to define the effects of possible nodule fracturing. Figure 7 is a chemical contour map of a representative texturally homogeneous ilmenite nodule from Orapa with weight percent MgO plotted at the location of each of the 35 microprobe analyses presented in Table 18 of Appendix A. The chemical map shows a broad central region

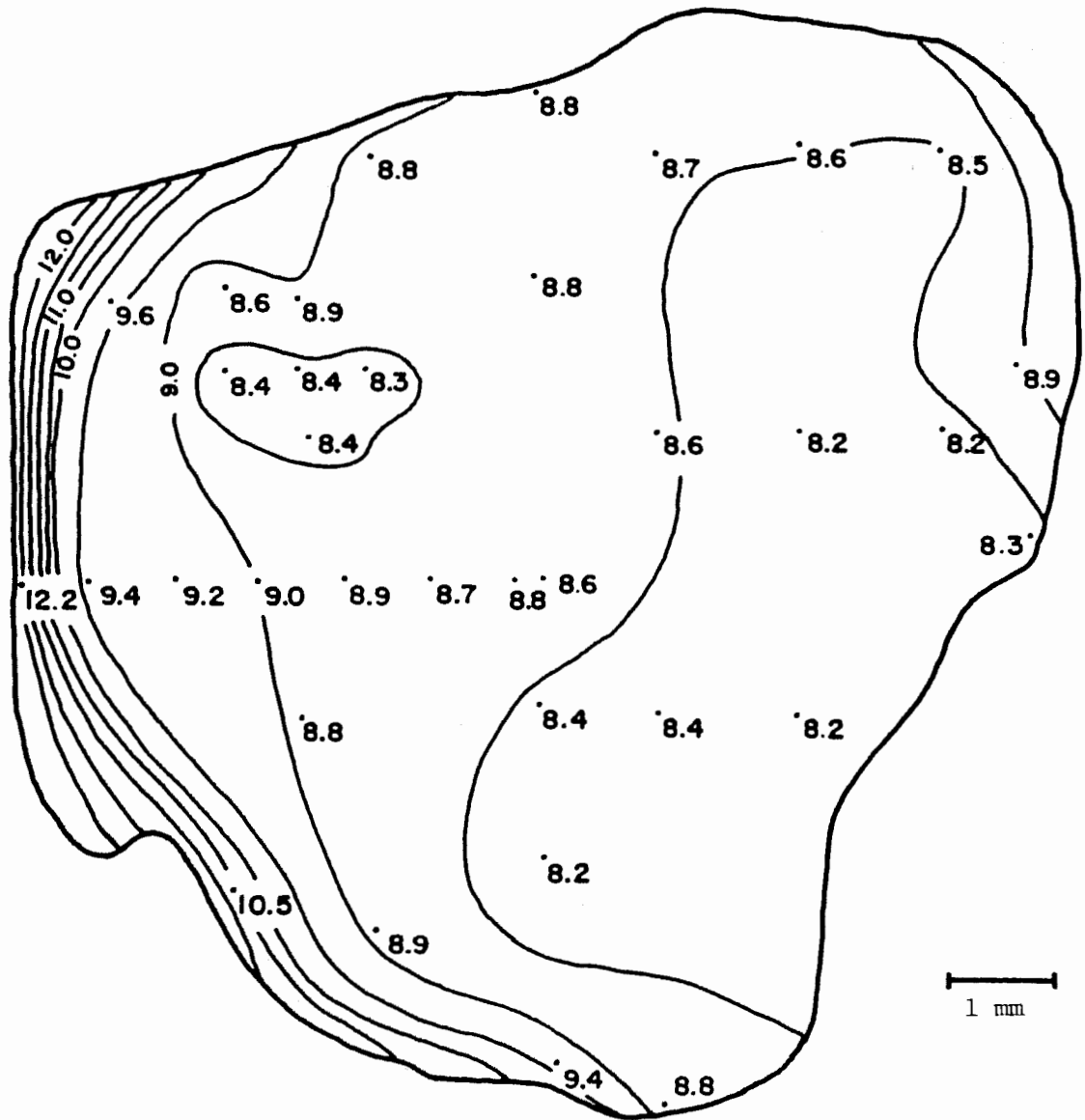


Figure 7: Chemical contour map of the MgO content (expressed in weight percent) of ilmenite discrete nodule specimen #411A. All of the individual analyses used to construct the contours are given, together with an index map for location, in Table 18 and Figure 32, respectively, of Appendix A.

of relatively constant MgO values comprising most of the nodule within the 9.0 wt. % contour and a narrow zone of steep chemical gradient along nearly half of the periphery. This MgO zoning has already been discussed as appearing to be similar to the kimberlite "magmatic reaction" trend of Haggerty et al. (1979a). The most important aspect of the data presented in this figure is, however, the clear indication that the nodule has been fractured at some time after chemical zoning was established. Such fracturing may be relatively common in kimberlite pipes and would be expected to occur along intranodular polycrystalline boundaries or similar planes of weakness. The fact that the fracture planes transect chemical zoning trends considered by Haggerty et al. (1979) to be related to the decreasing pressure of emplacement in the crust clearly suggests that intense shearing and particle abrasion continued to have an effect during even the latest stages of intrusion. The contour pattern in Figure 7 also carries a word of warning for all workers concerned with kimberlitic ilmenite geochemistry in that it would be possible to miss the dramatic zoning of this grain with only cursory microprobe examination of the nodule interior and selected sites on the periphery. Consequently, chemical zoning of ilmenites from kimberlite may be significantly more common than previous studies suggest.

The ultimate origin of ilmenite discrete nodules in kimberlite is as yet unresolved. Present hypotheses invoke origins ranging from primary phenocrysts formed in the kimberlite magma (Mitchell, 1977) to xenocrysts disaggregated by erupting kimberlite from separate crystal-mush magmas located in the low-velocity zone of the mantle (Boyd and Nixon, 1973; Nixon and Boyd, 1973a). Compositional data from the Orapa discrete nodule

suite are, unfortunately, inconclusive with regard to verifying one or the other of these alternatives. The observed range in $Mg/(Mg + Fe^{2+})$ at Orapa, excluding the data from the three samples for which there is evidence of an origin different from that of the discrete nodules, is considerably less than that reported for a similar suite from the Frank Smith mine by Pasteris et al. (1979) and Mitchell (1977), indicating that either the Orapa nodules may have crystallized from liquids of more restricted compositional range, or that the original crystals underwent a compositionally-homogenizing metamorphic or metasomatic event at some upper mantle location prior to incorporation in the kimberlite. The strong negative correlation ($R^2 = 0.95$) between MgO and FeO values for the suite (Figure 8) may be taken as further evidence for an origin by crystallization from a chemically evolving liquid (compare, for example, with Wager, 1960), but gives little indication of the nature of the liquid or of the pressure regime involved. It is clear that some relatively unambiguous chemical parameter indicating the depth of ilmenite nodule crystallization is needed to clarify the dilemma of their origin. High-pressure experiments and expanded geochemical investigation of the characteristic minor and trace element behavior patterns appear to offer the most promising outlooks in this regard. As an example of the latter, a plot of Ni versus Cr for the entire Orapa ilmenite discrete nodule suite is presented in Figure 9 and compared to similar data for ilmenites from a variety of localities in Lesotho (Nixon and Kresten, 1973). It should be noted that the Orapa data were obtained by electron microprobe, while the Lesotho values were the result of detailed atomic absorption spectrophotometry. The Orapa data cluster between 200-3000 ppm Ni and

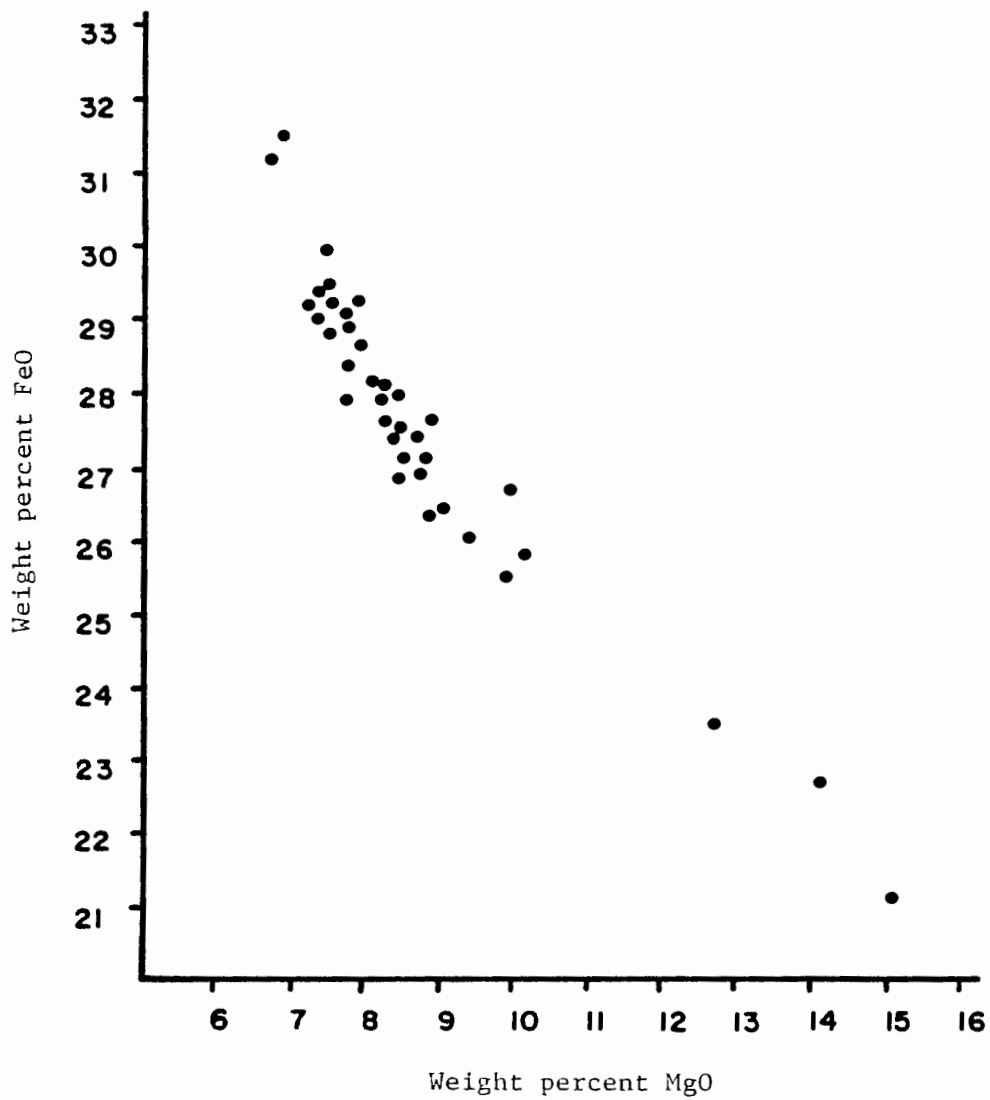


Figure 8: Plot of MgO versus FeO content for the ilmenite discrete nodule suite from Orapa.

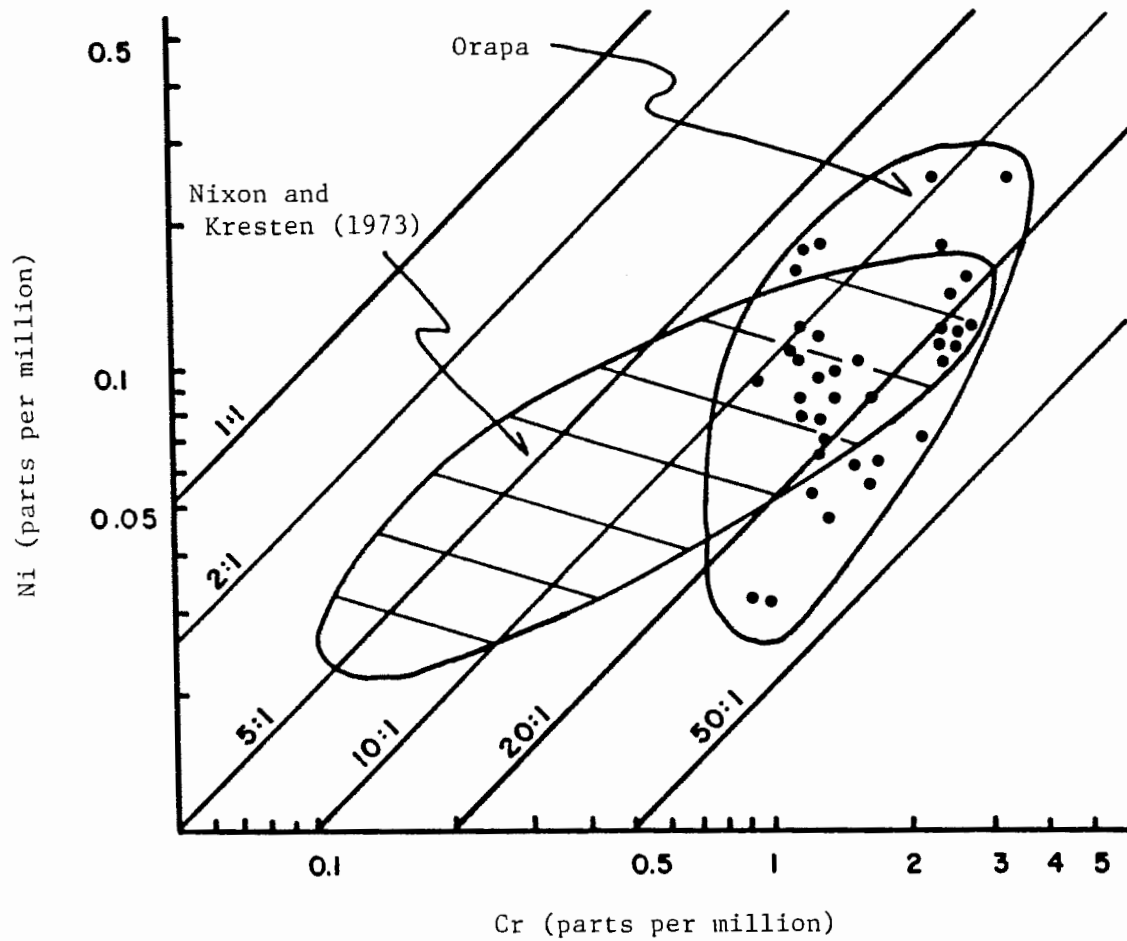


Figure 9: Plot of Ni versus Cr for the ilmenite discrete nodule suite from Orapa. The lined oval area includes the majority of data points for ilmenites from a variety of Lesotho localities given by Nixon and Kresten (1973, p. 236).

9000-31000 ppm Cr and show considerable overlap with the uppermost high-Ni, high-Cr half of the oval field defined by Nixon and Kresten (1973), apparently strengthening their contention that Cr-Ni data plots for ilmenites from different kimberlites tend to cluster at specific values. More data from additional localities are needed to further verify this characteristic and should then be coupled with detailed high-pressure experiments to establish the possible significance of such compositions. In addition, it is also clear that similar minor and trace element data are needed from entire suites of nodules including garnets, pyroxenes, ilmenites, and others from given localities in order to establish a more solid foundation for models concerning the origin of such typical nodules and perhaps the mechanisms involved in the genesis and eruption of kimberlite magma.

Rutile and Ilmenite-Rutile Intergrowths


Although rutile is a relatively uncommon constituent of kimberlite and kimberlitic nodules of presumed mantle origin, it has been reported in a variety of kimberlite-related associations including: 1) kimberlite groundmass (Clarke and Mitchell, 1975; Haggerty, 1975; Elthon and Ridley, 1979), 2) kimberlite autoliths (Ferguson et al., 1973), 3) MARID suite xenoliths in kimberlite (Dawson and Smith, 1977), 4) peridotite xenoliths in kimberlite (Boullier and Nicholas, 1973), 5) grospydite and eclogite xenoliths in kimberlite (Nixon and Boyd, 1973e; Sobolev, 1977), and 6) inclusions in diamonds (Meyer and Tsai, 1976). On the other hand, rutile is typically present as an accessory phase in a wide variety of granulites and related kimberlite xenoliths interpreted to be derived

from portions of the lower crust (Cox et al., 1973; Nixon and Boyd, 1973b).

A suite of four unusual discrete nodules composed of ilmenite intergrown within host rutile has been recovered from Orapa and described in detail. In hand specimen, these nodules are round to ovoid in shape, characteristically smooth in external morphology, and average less than 1 cm in diameter. In addition to recovering these samples from Orapa, Haggerty also collected a second, considerably larger suite of similar nodules from the mine concentrate at the Jagersfontein pipe in South Africa. Although similar in appearance to the Orapa suite, the Jagersfontein nodules are typically smaller, averaging less than 0.5 cm in diameter. Nodules from both localities have been examined and will be described together in detail.

In polished section, a variety of intergrowth textures are apparent and may be categorized as shown in Figure 10. The coarse lamellar texture appears to be more common at Orapa than Jagersfontein and typically consists of numerous distinct ilmenite lamellae situated in an apparently regular geometric orientation within the host rutile. Ramdohr (1969, p. 987) described a morphologically similar, although presumably non-kimberlitic, ilmenite-rutile intergrowth in which he considered the orientation of the ilmenite lamellae to be limited to crystallographically "equivalent" directions within the rutile. The lamellae within the kimberlitic nodules described here are typically lensoidal in form, marked by distinct reflection anisotropy, and range from 0.5 to 2.0 mm in length and from 0.1 to 0.2 mm in width. Such lamellae generally appear to be discontinuous along single planes of growth within the

Figure 10: Generalized classification of ilmenite-rutile intergrowth textures.

Scale:  1 mm

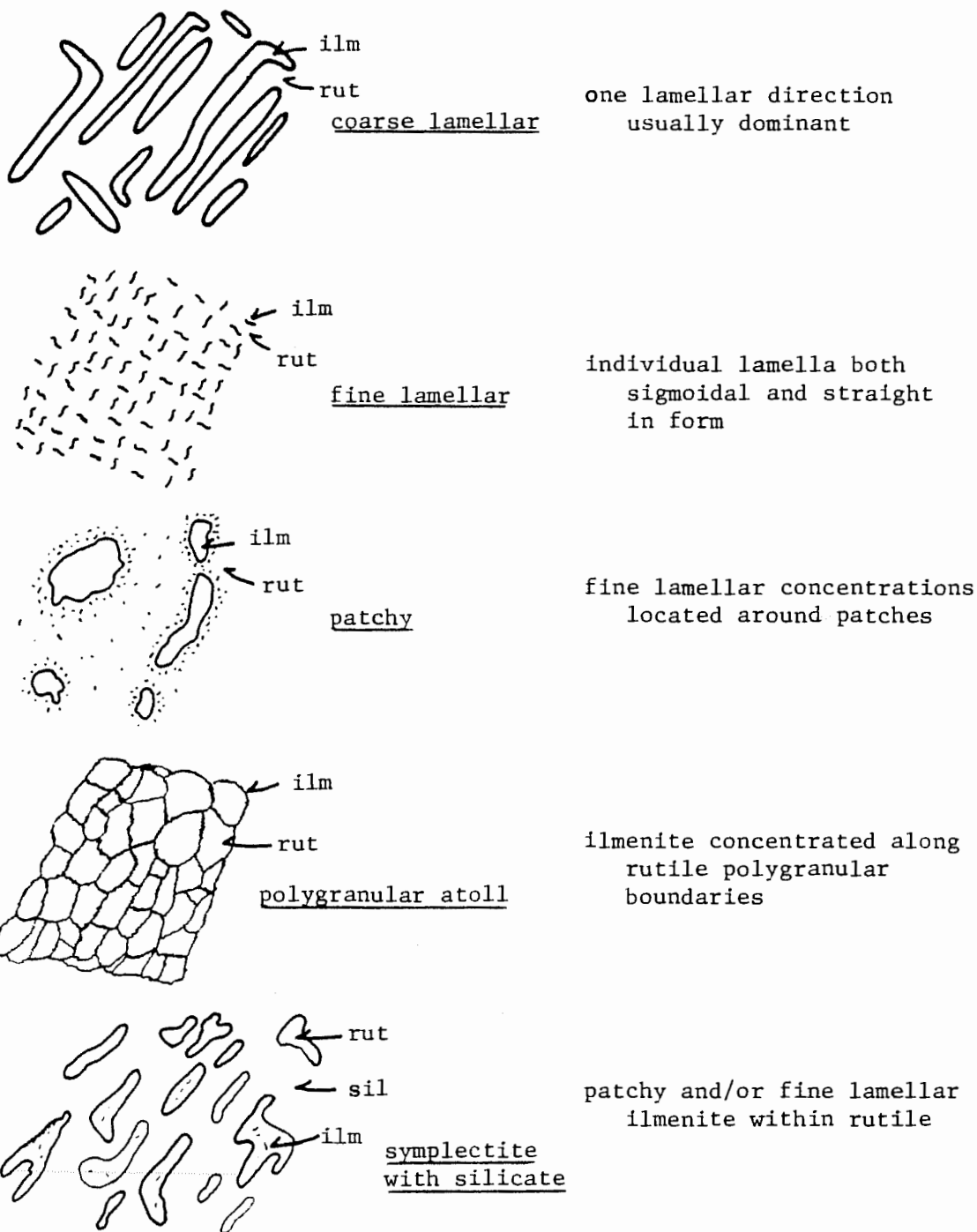
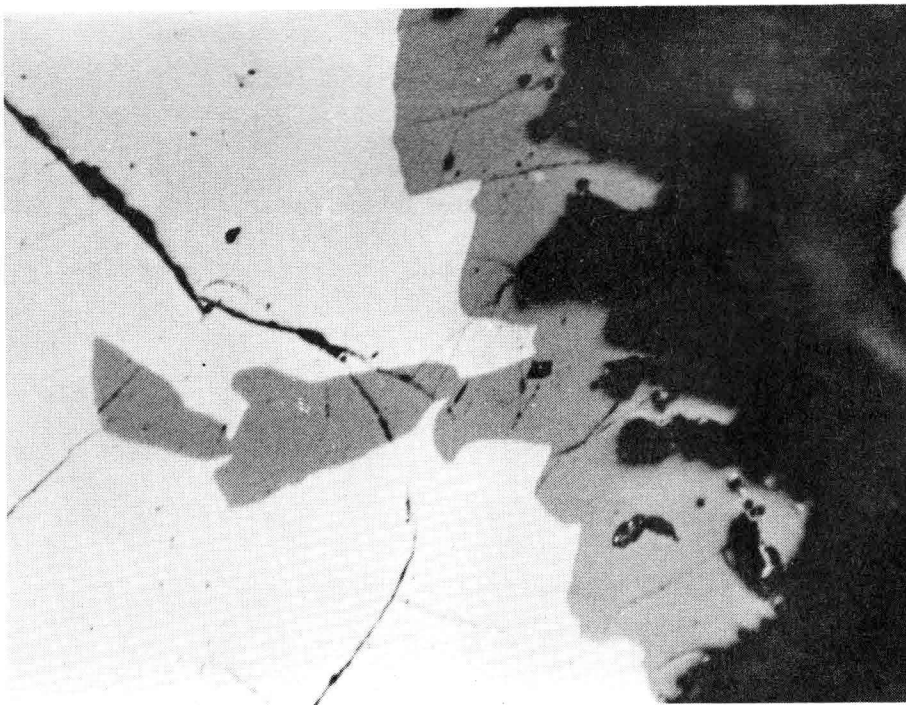
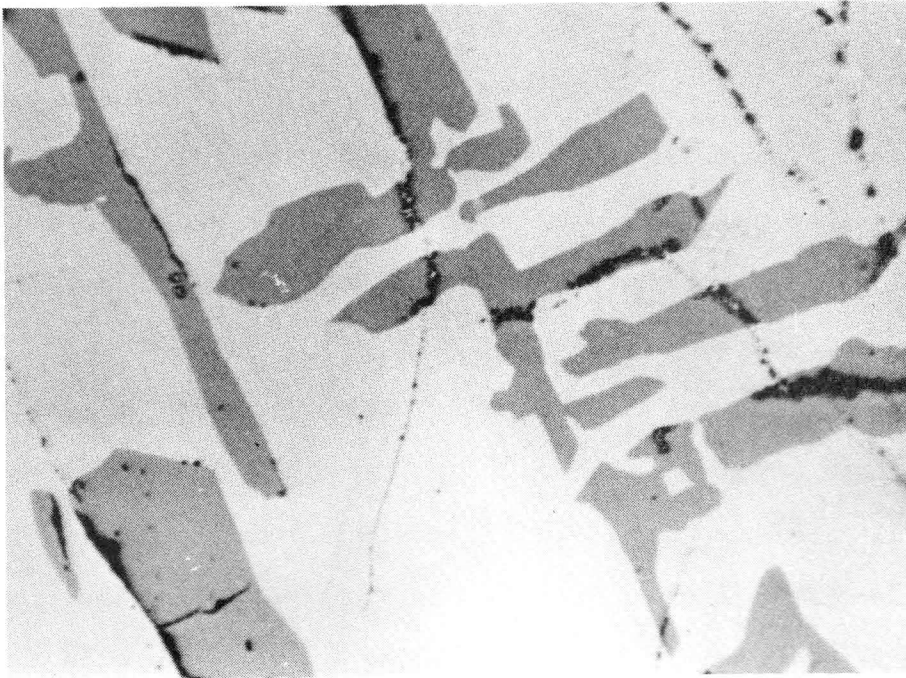


Figure 11a: Typical lamellar-type ilmenite lamellae oriented along two nearly orthogonal planes within the host rutile. Note that lamellar terminations are both tapered and blunt.
(air, 80 X, horizontal dimension equals 2 mm, specimen #OR-405B)

Figure 11b: Rim ilmenite situated along the nodule periphery and branching inward to form typical ilmenite lamellae characteristic of the lamellar type of ilmenite-rutile intergrowth nodules at Orapa and Jagersfontein.
(air, 80 X, horizontal dimension equals 2 mm, specimen #OR-405B)



rutile, with both tapered and blunt ends marking the termination of individual lamellae. The apparent angle of intersection between sets of lamellae is a function of the spatial relationship between the internal crystal geometry and the polished surface, and thus ranges from nearly orthogonal to highly oblique orientations which give rise to apparently branching lamellar patterns.

As shown in Figures 11a and 11b, ilmenite occurs in two distinct modes in these coarse lamellar intergrowths with 1) rim ilmenite situated locally along the periphery of individual nodules and 2) coherent lamellae generally occupying the interior regions. These two types are locally continuous with individual lamellae branching into the interior from the peripheries. Microprobe analyses have illustrated no significant chemical differences between ilmenite situated at the edges and ilmenite forming interior lamellae within individual nodules, suggesting that the rim ilmenite may have formed by subsolidus diffusion of original lamellar ilmenite. Individual lamellae apparently truncated at the periphery of nodule #OR-405B may preserve evidence of nodule fracturing similar to that already described on the basis of asymmetric chemical zoning trends in certain ilmenite discrete nodules (Figure 7). Local development of fine-grained polygranular texture and fine-scale multiple twin lamellae in the ilmenite rimming the periphery of some nodules may indicate that they were subjected to at least some of the same conditions inferred qualitatively on the basis of textural evidence to have affected the ilmenite discrete nodules during transport in the kimberlitic magma at Orapa. Selective pitting of the ilmenite in the intergrowths is locally present and, under high resolution oil immersion microscopy,

appears similar to that described for the ilmenite discrete nodule suite.

The fine lamellar texture consists of numerous very fine ilmenite lamellae oriented within the host rutile in a manner similar to that already described for the coarse lamellar variety. These fine lamellae are typically less than 50 microns in length and may be either straight or sigmoidal in form. Many nodules from Jagersfontein are composed entirely of this texture; however, several coarse lamellar nodules from both pipes show a similar very fine lamellae population oriented parallel to the coarse ilmenite.

Patchy ilmenite within host rutile characterizes several nodules from Jagersfontein and is distinguished from polygranular atoll texture in that the patchy ilmenite is typically oriented in an irregular pattern only locally related to obvious microfractures or cleavage in the host rutile. Numerous very fine ilmenite lamellae characteristically occur in the immediate vicinity surrounding such irregular patches. Polygranular atoll texture, on the other hand, is characterized by irregular ilmenite concentrations along intergranular boundaries in the numerous varieties of polycrystalline host rutile. Morphologically, atoll ilmenite appears similar to the "external granule" texture described for ilmenite-titanomagnetite intergrowths by Buddington and Lindsley (1964) and may in fact have a similar subsolidus diffusion origin. This is supported texturally by the scarcity of fine lamellae within individual polygranular atolls. The patchy ilmenite texture appears less likely to have resulted from the subsolidus diffusion of fine lamellae and may, especially where oriented along microfractures, preserve evidence of

ilmenite formation in situ by some different process. Areas of patchy and polygranular atoll ilmenite coexist with fine lamellae in several polycrystalline nodules from both pipes.

Symplectic intergrowths of rutile and silicate are relatively common in the Jagersfontein nodule suite, typically occurring as part of a nodule otherwise characterized by the fine lamellar, patchy, or polygranular atoll texture. The interface between coexisting silicate and rutile in such symplectites is characteristically sharp in most cases. Very fine scale ilmenite lamellae and patchy intergrowths occur locally within the symplectic rutile in most specimens. The original silicate phase is typically altered beyond recognition; however, green pyroxene has been qualitatively identified in at least one intergrowth.

The host rutile in these nodules appears physically similar to that described in a later section comprising discrete nodule #OR-406. However, texturally the host rutile of the intergrowths varies from single, apparently homogeneous, crystals characteristic of coarse lamellar ilmenite-rutile nodules to several polycrystalline types. The most common of these latter textures has been identified in nodules characterized by abundant polygranular rutile closely resembling the typical fabric already described for the associated ilmenite discrete nodule suite from Orapa. Intergranular rutile boundaries in this case, however, are invariably curved and triple point intersections rarely approach 120 degree dihedral angles. Another relatively common variety of polygranular rutile texture is termed bladed and is comprised of elongate, rectangular individuals, the long axes of which define a strong lineation. This texture appears to be developed along the host cleavage and may have

been tectonically induced during nodule transport. Both types of polycrystalline rutile are characterized by fine lamellar, patchy, and atoll ilmenite intergrowths.

Chemical compositions determined by electron microprobe for coexisting ilmenite and rutile from individual nodules are presented in Table 2. Only the composition of the host rutile is given for the fine lamellar intergrowths because of the probability of microbeam overlap during the analysis of individual fine-scale ilmenite lamellae. The rutile phase in each intergrowth is similar in composition to the single rutile discrete nodule described elsewhere in that Cr_2O_3 , Nb_2O_5 , ZrO_2 , and iron (expressed as Fe_2O_3) are all significant components. The most common diluents are clearly Cr_2O_3 and Nb_2O_5 , ranging from 4.36 to 7.92 wt. % and from 1.93 to 13.38 wt. % respectively. Total iron is expressed as Fe^{3+} in Table 2, although stoichiometric charge balance considerations suggest a portion of the total iron may be present as Fe^{2+} . The actual $\text{Fe}^{2+}/\text{Fe}^{3+}$ ratio cannot be determined from these data because of the valence variability of some of the other cations present in the structure. Although details of the valence considerations were not examined in this study, electron paramagnetic resonance studies (Carter and Okaya, 1960) have indicated that Fe^{3+} and, for appropriate bulk compositions, Cr^{3+} substitute for Ti^{4+} in the rutile structure. Similar studies have not been performed for Fe^{2+} , although the limited data gathered to date (Webster and Bright, 1961) suggest that the $\text{Fe}^{2+}/\text{Fe}^{3+}$ ratio in rutile may be a sensitive indicator of the oxygen fugacity at the time of crystallization. Iron is present as an average 0.022 cation per 2 oxygens in the formulae of the four samples from Orapa (Table 2), a value falling

Table 2: Chemical compositions of coexisting ilmenite and rutile in ilmenite-rutile intergrowth nodules from Orapa and Jagersfontein.

Specimen:	OR-405B		OR-409B		OR-424A		OR-436A	
	rutile	ilmenite	rutile	ilmenite	rutile	ilmenite	rutile	ilmenite
TiO ₂	73.94	52.87	78.81	52.61	85.26	52.58	76.39	51.33
Cr ₂ O ₃	7.75	3.50	6.76	4.83	5.97	2.68	7.92	3.71
Al ₂ O ₃	0.03	0.00	0.08	0.09	0.04	0.01	0.02	0.00
Fe ₂ O ₃	2.39*	5.24'	1.83*	5.98'	1.71*	4.91'	2.38*	5.64'
FeO	-	24.13	-	19.86	-	28.20	-	26.14
MgO	0.24	13.09	0.18	15.71	0.00	10.48	0.10	11.16
MnO	NA	0.51	NA	0.44	NA	0.48	NA	0.49
ZrO ₂	0.95	0.09	0.76	0.21	0.86	0.12	0.81	0.12
Nb ₂ O ₅	13.38	0.57	10.46	0.86	6.94	0.24	12.73	0.52
NiO	NA	0.23	NA	0.03	NA	0.24	NA	0.26
Ta ₂ O ₅	1.50	NA	1.25	NA	0.30	NA	0.42	NA
Total	100.18	100.23	100.13	100.62	101.08	99.94	100.77	99.37

Cations based on two (rutile) and three (ilmenite) oxygens

Ti	0.796	0.913	0.836	0.890	0.881	0.927	0.811	0.906
Cr	0.088	0.064	0.076	0.086	0.065	0.049	0.088	0.069
Al	0.001	0.000	0.001	0.002	0.001	0.000	0.000	0.000
Fe ³⁺	0.026	0.091	0.019	0.101	0.018	0.087	0.025	0.100
Fe ²⁺	-	0.463	-	0.374	-	0.553	-	0.513
Mg	0.005	0.448	0.004	0.527	0.000	0.366	0.002	0.391
Mn	-	0.010	-	0.008	-	0.009	-	0.010
Zr	0.007	0.001	0.005	0.002	0.006	0.001	0.006	0.001
Nb	0.087	0.006	0.067	0.009	0.043	0.003	0.081	0.006
Ni	-	0.004	-	0.001	-	0.005	-	0.005
Ta	0.006	-	0.005	-	0.001	-	0.002	-
Total	1.016	2.000	1.013	2.000	1.015	2.000	1.015	2.001

n	4	9	5	4	1	4	2	4
type:	crs lamellar		fn lam/patchy		crs lamellar		crs lamellar	
modal %	66	34	-	-	79	21	75	25

NA: not analyzed

' calculated

* total iron expressed as Fe₂O₃

Table 2 (con't)

Specimen:	JF-126		JF-115"		JG80-25		JG80-31	
	rutile	ilmenite	rutile	ilmenite	rutile	ilmenite	rutile	ilmenite
TiO ₂	84.74	52.09	82.74	51.36	86.06	52.09	92.88	56.62
Cr ₂ O ₃	6.77	6.84	7.13	7.00	6.51	7.27	4.36	3.20
Al ₂ O ₃	0.13	0.21	0.23	0.22	0.09	0.31	0.01	0.24
Fe ₂ O ₃	0.88*	5.50'	1.08*	6.31'	0.81*	5.54'	0.07*	2.83'
FeO	-	19.15	-	17.54	-	18.78	-	19.39
MgO	0.04	15.37	0.04	16.22	0.00	15.60	0.01	17.44
MnO	NA	0.26	0.00	0.32	NA	0.31	NA	0.38
ZrO ₂	0.92	0.13	1.19	0.36	0.74	0.16	1.08	0.21
Nb ₂ O ₅	6.54	0.12	6.82	0.44	5.49	0.24	2.02	0.05
NiO	NA	0.24	0.10	0.19	NA	0.29	NA	0.21
Ta ₂ O ₅	0.13	NA	0.73	0.15	0.23	NA	0.14	NA
Total	<u>100.15</u>	<u>99.91</u>	<u>100.06</u>	<u>100.11</u>	<u>99.93</u>	<u>100.59</u>	<u>100.57</u>	<u>100.57</u>
Cations based on two (rutile) and three (ilmenite) oxygens								
Ti	0.880	0.885	0.860	0.869	0.892	0.879	0.942	0.942
Cr	0.074	0.122	0.079	0.125	0.071	0.129	0.046	0.056
Al	0.002	0.005	0.004	0.006	0.002	0.008	0.000	0.006
Fe ³⁺	0.009	0.094	0.011	0.107	0.008	0.094	0.001	0.047
Fe ²⁺	-	0.362	-	0.330	-	0.353	-	0.359
Mg	0.001	0.518	0.001	0.544	0.000	0.522	0.000	0.576
Mn	-	0.005	0.000	0.006	-	0.006	-	0.007
Zr	0.006	0.002	0.008	0.004	0.005	0.002	0.007	0.002
Nb	0.041	0.001	0.048	0.004	0.034	0.002	0.012	0.001
Ni	-	0.005	0.001	0.003	-	0.005	-	0.004
Ta	<u>0.001</u>	-	<u>0.003</u>	<u>0.001</u>	<u>0.001</u>	-	<u>0.001</u>	-
Total	1.014	1.999	1.015	1.999	1.013	2.000	1.009	2.000
n	6	5	2	3	5	5	5	5
type:	crs lamellar		crs lamellar		crs lamellar		patchy	
modal %	68	32	NA		NA		-	

" Haggerty - unpublished data

Table 2 (con't)

Specimen:	JG80-33		JG80-34B	JG80-44A	JG80-44C
	rutile	ilmenite	rutile	rutile	rutile
TiO ₂	86.88	52.77	91.56	91.61	91.03
Cr ₂ O ₃	6.49	5.97	4.48	4.85	5.24
Al ₂ O ₃	0.07	0.37	0.02	0.00	0.01
Fe ₂ O ₃	1.01*	5.61'	0.07	0.17	0.10
FeO	-	19.28	-	-	-
MgO	0.00	15.69	0.00	0.00	0.00
MnO	NA	0.31	NA	NA	NA
ZrO ₂	0.75	0.20	1.46	0.99	1.03
Nb ₂ O ₅	4.79	0.21	2.18	1.93	2.70
NiO	NA	0.24	NA	NA	NA
Ta ₂ O ₅	0.34	NA	0.02	0.07	0.01
Total	100.33	100.64	99.79	99.62	100.12
Cations based on two (rutile) and three (ilmenite) oxygens					
Ti	0.897	0.889	0.928	0.928	0.920
Cr	0.071	0.106	0.048	0.052	0.056
Al	0.001	0.010	0.000	0.000	0.000
Fe ³⁺	0.010	0.095	0.001	0.002	0.001
Fe ²⁺	-	0.362	-	-	-
Mg	0.000	0.524	0.000	0.000	0.000
Mn	-	0.006	-	-	-
Zr	0.005	0.002	0.010	0.006	0.007
Nb	0.030	0.002	0.013	0.012	0.016
Ni	-	0.004	-	-	-
Ta	0.001	-	0.000	0.000	0.000
Total	1.015	2.000	1.000	1.000	1.000
n	5	6	3	3	4
type:	crs lamellar		poly atoll/ fn lam	poly atoll/ fn lam/symp	poly atoll/ fn lam
modal %	NA		-	-	-

approximately midway between the iron solubility limits determined by Wittke (1967) for synthetic samples over the temperature range 800 - 1350°C at 1 bar oxygen pressure. Iron substitution is considerably less in the rutiles from Jagersfontein, however. Atomic ratios of Nb/Ta for rutiles from both localities show strong niobium enrichment and indicate that the host phase of these intergrowths should be classified as niobian rutile according to the nomenclature recommendations of Cerny et al. (1964).

Rutile compositions obtained from nodules from both Orapa and Jagersfontein are plotted in Figures 12 and 13. The substitution of $\text{Nb}^{5+} + \text{Cr}^{3+} + \text{Ta}^{5+}$ in natural rutile is shown in Figure 12, with the kimberlitic rutiles from this study defining a narrow compositional field distinct from those of similar rutiles from meteorites (El Goresy, 1971) and a variety of terrestrial alkalic igneous suites (Palache et al., 1944; Cerny et al., 1964; Siivola, 1970) amassed from the literature for comparison. The compositions of two rutiles obtained from lunar surface materials (Marvin, 1971; Hlava et al., 1972) are also plotted and show slight overlap with part of the kimberlitic field. It should be noted that the alkalic igneous field is in fact composed of two slightly overlapping populations including rutiles from granitic pegmatites and related rocks at low TiO_2 values and rutiles from carbonatites and associated intrusives at higher values of TiO_2 . In general, the rutiles from granitic and granitic pegmatite complexes are characterized by lower Nb/Ta ratios and may be contrasted with the relatively Nb-enriched carbonatitic rutiles. The substitution of iron in niobian rutile is considered in Figure 13. The kimberlitic rutiles again plot

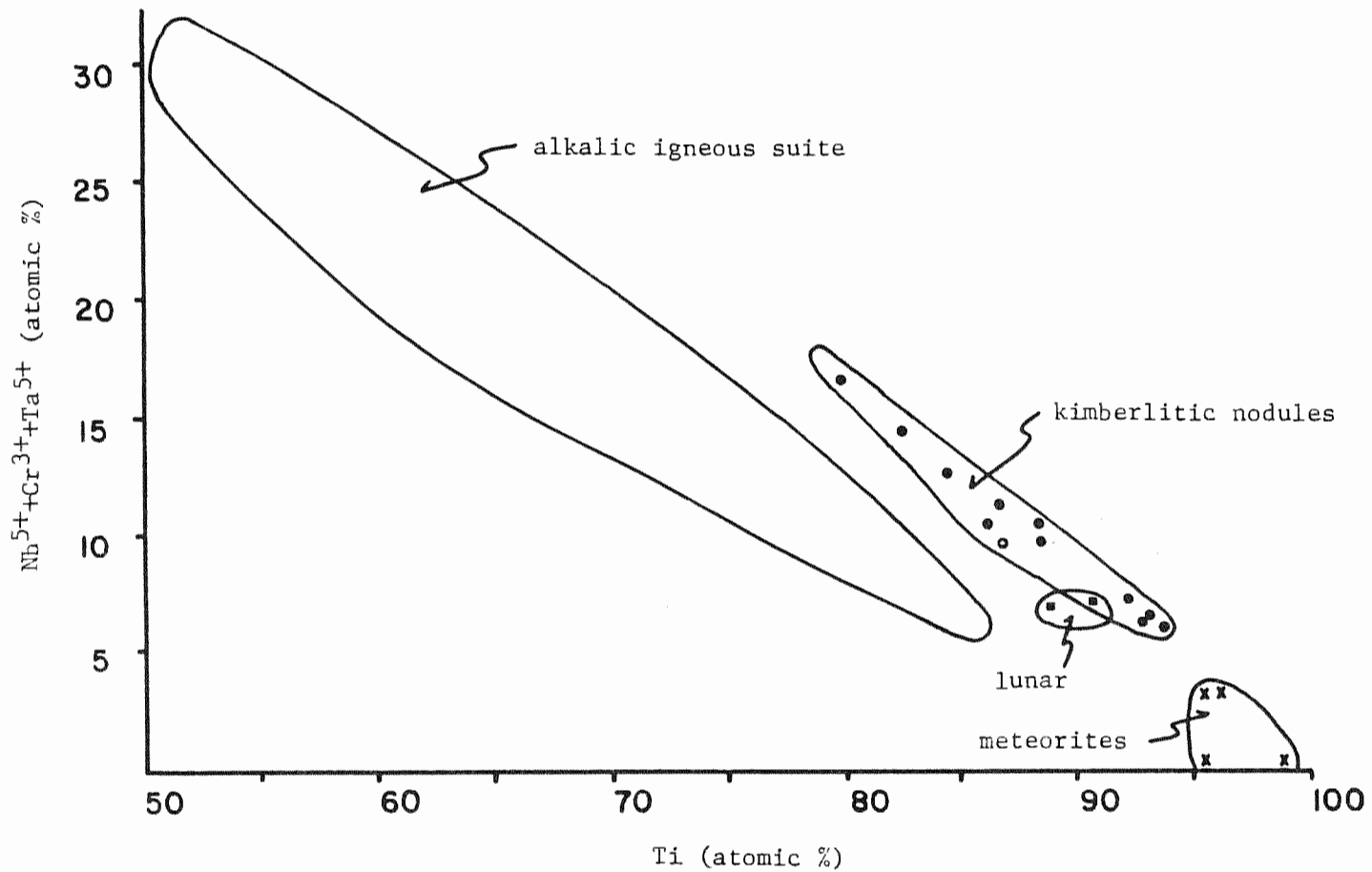


Figure 12: Compositions of rutiles from kimberlitic nodules (•, this study), meteorites (x), lunar surface materials (■), and terrestrial igneous rocks (points not shown for clarity) plotted in terms of atomic percent Ti versus ($\text{Nb}^{5+} + \text{Cr}^{3+} + \text{Ta}^{5+}$). Data for the non-kimberlitic fields are taken from the literature (see the text for specific references). The open circle represents Orapa nodule #OR-406.

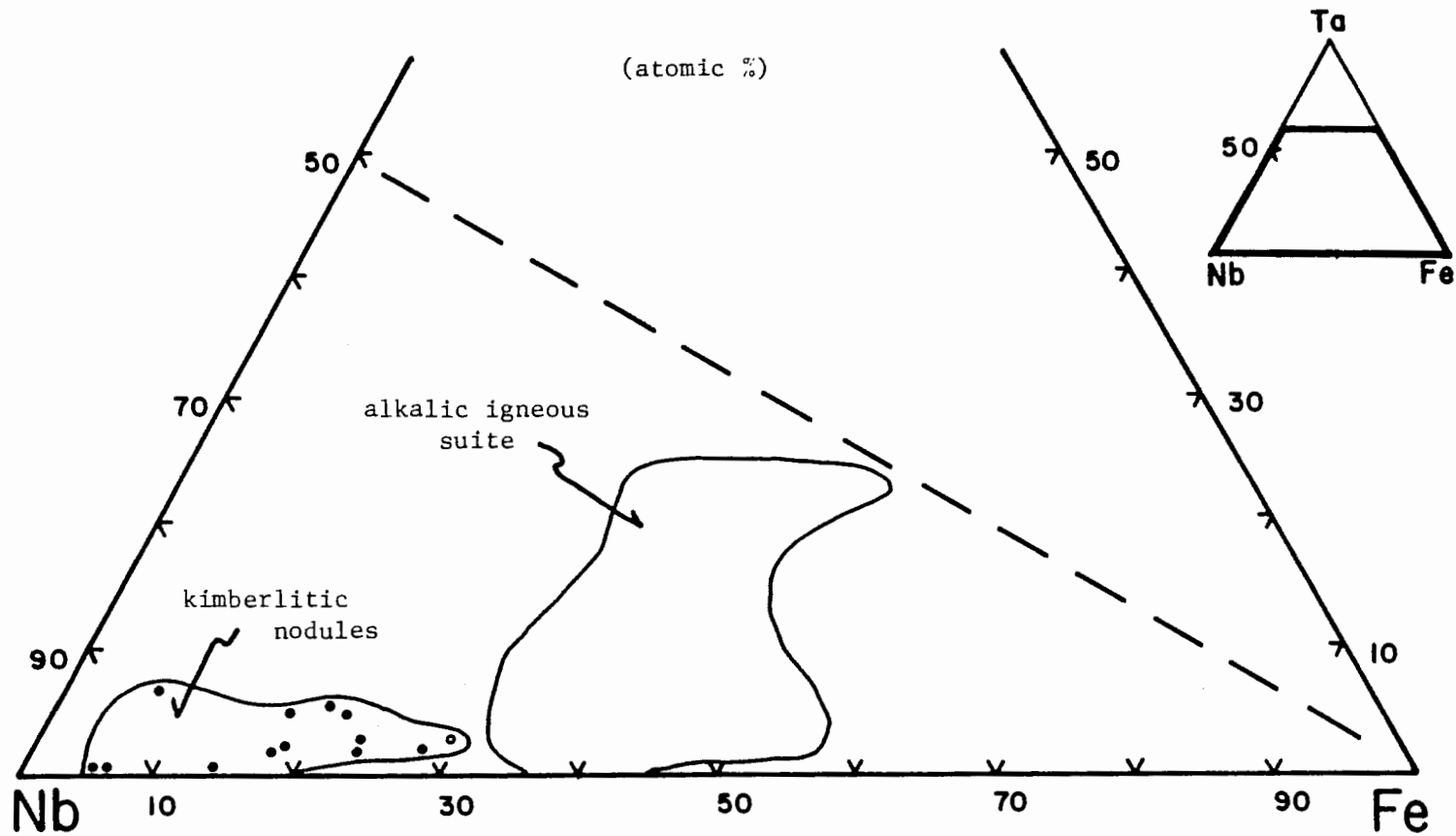


Figure 13: Compositions of niobian rutiles from kimberlitic nodules (this study) and various alkalic igneous rocks (taken from numerous literature sources, see text) plotted in terms of atomic percent Nb-Fe-Ta. The open circle represents nodule #OR-406.

as a distinct, relatively restricted field showing considerable niobium enrichment, limited substitution of iron, and only slight solid solubility toward tantalum. On the other hand, rutiles from terrestrial alkalic igneous suites appear to be characterized by greater substitution of both iron and tantalum, and by lower concentrations of niobium. Within this field, rutiles from carbonatitic complexes tend to cluster closer to the Nb-Fe sideline than rutiles from granitic pegmatites, which characteristically show greater Ta substitution.

Average compositions presented in Table 2 for ilmenite from coarse lamellar, patchy, and polygranular atoll type intergrowths with rutile from both Orapa and Jagersfontein are clearly kimberlitic in character, with MgO and Cr₂O₃ values ranging from 10.48 to 17.44 wt. % and from 2.68 to 7.27 wt. % respectively. The Jagersfontein ilmenite is, on the average, more magnesian and more chromium-rich than the ilmenite from Orapa. Individual compositions are plotted in terms of the ternary solid solution end members FeTiO₃-MgTiO₃-Fe₂O₃ in Figure 14 and define a distinct linear grouping oriented nearly parallel to the ilmenite-geikielite sideline at approximately 5 mole percent hematite component. The main compositional fields of the ilmenite discrete nodules from both Orapa (this study) and Jagersfontein (Haggerty, unpublished data) are also plotted for comparison. The three fields show very little overlap, with the Jagersfontein discrete nodules typically more magnesian than their counterparts from Orapa, thereby mirroring the same relationship shown by the respective lamellae populations. These data suggest that the ilmenite lamellae may have equilibrated under conditions of generally similar, but possibly somewhat lower, oxygen fugacities relative to the

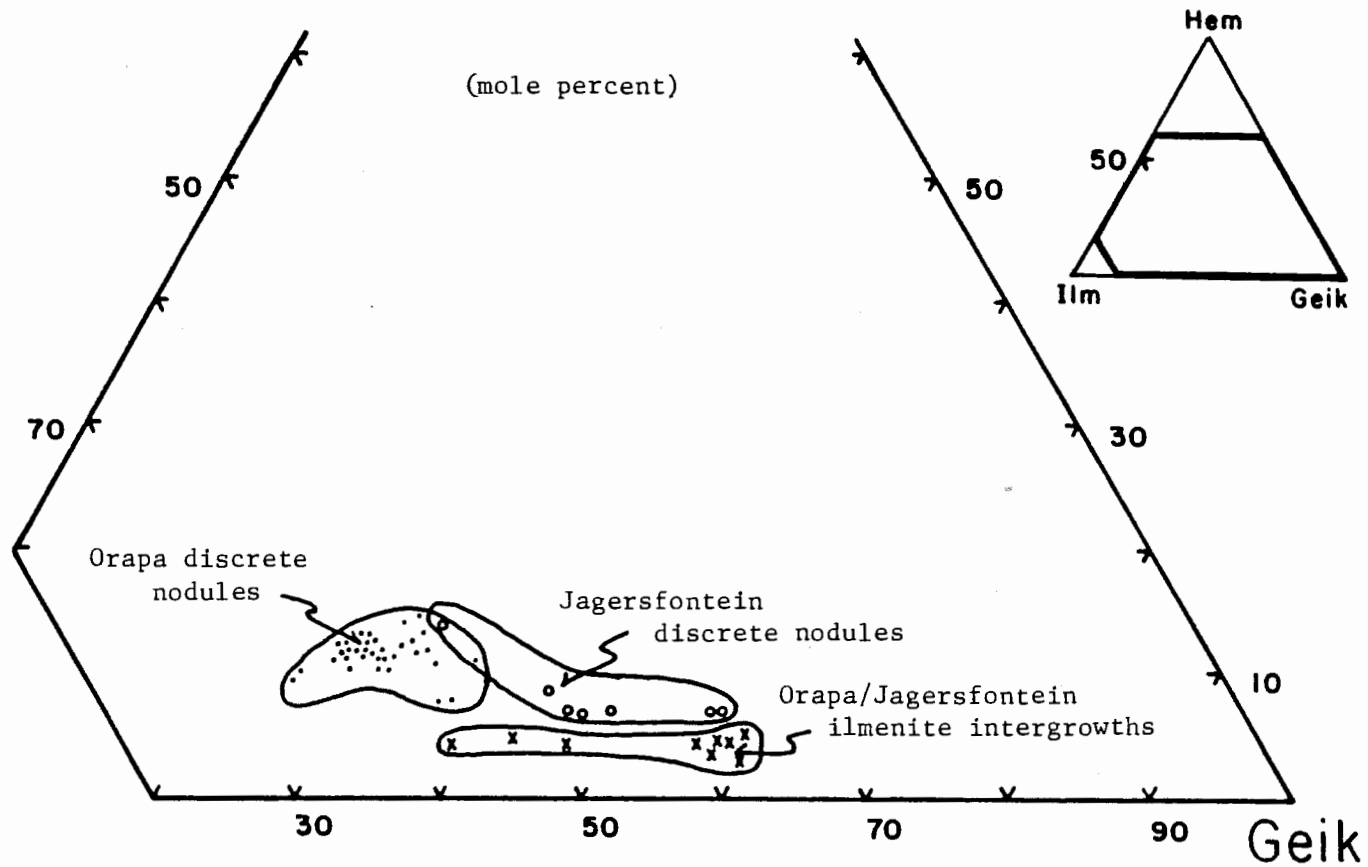


Figure 14: Compositions of coarse lamellar, patchy, and atoll-type ilmenite intergrowths within rutile plotted in the ternary system ilmenite-geikielite-hematite. The compositions of individual ilmenite discrete nodules from Orapa and Jagersfontein have been plotted for comparison.

associated discrete nodules. The lamellae compositions at both pipes are, in general, more chromium-rich than the associated ilmenite discrete nodules, probably reflecting bulk compositional differences resulting from different modes of origin, as will be discussed in a later section. The data presented in Table 2 represent average compositions obtained from multiple analyses of several ilmenite sites within individual intergrowths and it should be noted that detailed microprobe analyses of numerous ilmenite lamellae from individual coarse lamellar intergrowths have demonstrated an apparently typical variability of up to 2 wt. % in MgO values. These data, however, have failed to delineate any consistent spatial patterns characterizing this inhomogeneity within individual lamellae.

It is interesting to note that the points for ilmenite discrete nodules #OR-411B, OR-410A, and OR-412B (not shown), which were clearly distinct from the main group of similar nodules in Figure 3a, plot within the narrow field defined by the ilmenite lamellae in rutile (Figure 14), suggesting a possible relation between the two. However, on the basis of the limited available data, it is believed that these nodules are more closely related to the larger discrete nodule population than to the ilmenite lamellae. The relative deficiency in Fe_2O_3 and enrichment in MgO characterizing these three nodules may be a function of crystallization under conditions of lower oxygen fugacity and by analogy with the "magmatic reaction" trend proposed by Haggerty et al. (1979a), total pressure, relative to the remainder of the suite. There is no petrographic or other textural evidence to indicate that this ilmenite was associated with rutile and, indeed, if these once formed

part of a suite of ilmenite-rutile intergrowths, such intergrowths would certainly have been characterized by extremely coarse grain size.

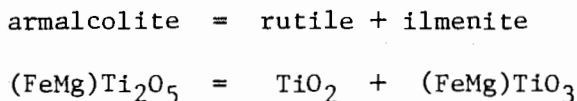
The data in Table 2 serve to illustrate the elemental partitioning observed between coexisting ilmenite and rutile in the intergrowth suites from Orapa and Jagersfontein. Magnesium is almost exclusively incorporated in ilmenite, probably reflecting the strong mutual substitution of Mg^{2+} for Fe^{2+} in octahedrally coordinated lattice positions within the ilmenite structure. Chrome values indicate that Cr^{3+} is present in significant proportions in both minerals. For the Orapa samples, chrome is consistently concentrated in the rutile, with an average relative enrichment factor (wt. % Cr_2O_3 in rutile/wt. % Cr_2O_3 in ilmenite) of approximately 2.0 for the four samples. This factor, however, is quite close to unity for the Jagersfontein ilmenite. The larger cations Zr^{4+} and Nb^{5+} are clearly incorporated preferentially in the rutile from both localities, with average relative enrichment factors of 5.8 and 27.2 respectively. On the basis of ionic radii similarities (Shannon and Prewitt, 1969) and the variety of charge balancing substitutional mechanisms possible, these elemental partitioning effects are not surprising.

A variety of intergrowths composed primarily of ilmenite and rutile have been reported from a number of kimberlitic localities in recent years, occurring as either discrete nodules (Haggerty, 1979b), "xenocrysts" (Shee, 1979), or as part of the kimberlitite groundmass assemblage (Haggerty, 1975; Boctor and Meyer, 1979; Raber and Haggerty, 1979). Boctor and Meyer (1979) described intergrowths composed of ilmenite lamellae in rutile occurring within the kimberlitic groundmass

and as part of complex reaction mantles surrounding ilmenite discrete nodules in kimberlite from Colorado. Although much finer-grained, these intergrowths bear a marked textural similarity to the lamellar varieties found at Orapa and Jagersfontein; but, perhaps significantly, differ in typically having fine-scale lamellae of Cr-bearing spinel present within the ilmenite. Raber and Haggerty (1979) described somewhat similar, although considerably more fine-grained, intergrowths within associated spinel from ilmenite-rutile-zircon assemblages in kimberlite from several southern African localities. Although these latter authors presented limited chemical data for associated ilmenite and described the rutile as nearly "stoichiometric TiO_2 ", neither of these studies contained detailed chemical data characterizing the phases coexisting within the intergrowths. Shee (1979) has briefly described a suite of rutile xenocrysts containing abundant ilmenite lamellae in kimberlite from the Wesselton mine in South Africa, but presented only limited textural information and no chemical data.

The mode of origin most commonly proposed for ilmenite-rutile intergrowths in kimberlite involves the high pressure breakdown of a precursor pseudobrookite-type phase similar to armalcolite in composition (for example, see Haggerty, 1975; Boctor and Meyer, 1979; Raber and Haggerty, 1979). Although armalcolite is relatively abundant as an early liquidus phase in certain high-titanium lunar mare basalts (Haggerty, 1973), terrestrial examples described to date are limited to the kimberlite localities at DuToitspan (Haggerty, 1975) and Mothae (Raber and Haggerty, 1979) in southern Africa and to a suite of lamproite dikes and plugs exposed at Smoky Butte in Montana (Velde, 1975). Haggerty (1975) reported the

armalcolite from DuToitspan as discrete crystals ranging up to 50 microns in diameter and occurring in association with intergrown ilmenite and rutile. Separate intergrowths comprised of ilmenite lamellae in rutile were also found elsewhere in the kimberlite groundmass. The armalcolite described by Raber and Haggerty (1979) from Mothae was found to contain approximately 6 wt. % ZrO_2 , somewhat more than the Zr-armalcolites originally reported from lunar specimens by Haggerty (1973). The close association of such armalcolite with intergrowths of ilmenite and rutile at both Mothae and DuToitspan led these authors to suggest that these latter phases were formed by the reaction:



which is supported by a variety of laboratory evidence. Experimental investigations by Friel and Harker (1977) and Lindsley et al. (1974) have demonstrated that synthetic armalcolite with $Fe/(Fe+Mg)$ ratio equal to 0.5 is stable as a single phase up to 10 kb at 1200°C. With increasing pressure, it breaks down ($dT/dP = 20^\circ\text{C}/\text{kb}$) to a three-phase assemblage consisting of rutile, a more magnesian armalcolite, and ilmenite solid solution which, at 14 kb, in turn breaks down ($dT/dP = 30^\circ\text{C}/\text{kb}$) to a two-phase assemblage of rutile and ilmenite solid solution. This evidence suggests that at least some of the ilmenite-rutile intergrowths described in this study--if the result of decomposition of an armalcolite-type precursor phase--formed at a maximum pressure of approximately 14 kb. Any iron enrichment over $Fe/(Fe+Mg) = 0.5$ would have the effect of lowering this pressure limit somewhat (Lindsley et al., 1974) but, although the effect of Zr has been shown to also decrease the pressure stability

relations (Friel et al., 1977), the effect of other diluents such as Nb is unknown. The effect of the trivalent cations Al^{3+} , Cr^{3+} , and Ti^{3+} has been examined, however, by Kesson and Lindsley (1975) and shown to stabilize the mineral to temperatures lower than those at which the pure synthetic phase is stable and also raise the breakdown temperatures by approximately $35^\circ\text{C}/\text{kb}$.

The chemical data listed in Table 2 were used in an attempt to estimate the composition of possible precursor armalcolite at Orapa and Jagersfontein by combining the compositions of the coexisting ilmenite and rutile from coarse lamellar intergrowths in weighted proportions obtained by modal analysis. Modal analyses were performed on specimens #OR-405B, OR-424A, OR-436A from Orapa and JF-126 from Jagersfontein using standard point-counting techniques (1000-1500 points per specimen, 0.1 mm spacing). This counting was carried out under reflected light on a random plane cut through each intergrowth following the procedure of Chayes (1956) and is considered representative of the volume proportions of the phases present in each sample. The modes presented in Table 2 indicate that rutile is the more abundant phase in each nodule, with the rutile:ilmenite ratio varying between 2:1 and 4:1. The compositions determined for the rutile and ilmenite coexisting in each nodule were combined in the proportions dictated by the relative modal abundances to obtain the calculated bulk compositions presented in Table 3. In an attempt to minimize the variation inherent in the point-counting, an average bulk composition was determined and a mineral formula calculated on the basis of five oxygens for comparison with ideal armalcolite expressed as $\text{R}^{2+}\text{R}_2^{4+}\text{O}_5$. This average bulk composition for several coarse

Table 3: Calculated bulk compositions for selected coarse lamellar ilmenite-rutile intergrowth nodules from Orapa and Jagersfontein.

Specimen:	<u>OR-405B</u>	<u>OR-424A</u>	<u>OR-436A</u>	<u>JF-126</u>	<u>overall average</u>	<u>kimberlitic armalcolite (1)</u>
TiO ₂	66.78	78.40	70.12	74.29	72.40	76.92
Cr ₂ O ₃	6.30	5.28	6.87	6.79	6.31	1.64
Al ₂ O ₃	0.02	0.03	0.01	0.16	0.06	0.02
*FeO	11.23	8.07	9.41	8.25	9.24	13.41
MgO	4.61	2.20	2.87	4.95	3.66	7.08
MnO	0.17	0.10	0.12	0.08	0.12	0.54
ZrO ₂	0.66	0.72	0.64	0.67	0.67	NR
Nb ₂ O ₅	9.02	5.53	9.68	4.49	7.18	NR
NiO	0.08	0.05	0.06	0.08	0.07	NR
Ta ₂ O ₅	<u>0.99</u>	<u>0.24</u>	<u>0.32</u>	<u>0.09</u>	<u>0.41</u>	NR
Total	<u>99.86</u>	<u>100.62</u>	<u>100.10</u>	<u>99.85</u>	<u>100.12</u>	CaO 0.06 SiO ₂ <u>0.28</u> Total <u>100.01</u>

Cations based on five (5) oxygens

Ti ⁴⁺	1.959
Cr ³⁺	0.179
Al ³⁺	0.003
Fe ²⁺	0.278
Mg ²⁺	0.196
Mn ²⁺	0.004
Zr ⁴⁺	0.013
Nb ⁵⁺	0.117
Ni ²⁺	0.002
Ta ⁵⁺	<u>0.004</u>
Total	<u>2.775</u>

* total iron expressed as FeO

NR: not reported

(1): data from Haggerty (1975)

lamellar ilmenite-rutile intergrowths from Orapa and Jagersfontein is somewhat similar to the composition reported by Haggerty (1975) for kimberlitic armalcolite occurring in association with rutile and magnesian ilmenite in the groundmass of the DuToitspan kimberlite, with the calculated data from this study characterized by higher values for Cr_2O_3 and Nb_2O_5 and by lower values for total iron (expressed as Fe_2O_3) and MgO . Both of these compositions are depleted in ZrO_2 and other exotic oxides characterizing the zirconian armalcolite reported from Mothae by Raber and Haggerty (1979). The Orapa/Jagersfontein bulk composition is reconstituted in terms of atomic percent and plotted in the compositional space $\text{Ti}^{4+}-(\text{Fe}^{2+}+\text{Mg}^{2+})-\text{Cr}^{3+}$ in Figure 15, indicating an apparent excess of titanium relative to ideal armalcolite. However, it must be emphasized that, if this bulk composition approximates that of a single-phase precursor to the coarse lamellar ilmenite-rutile intergrowths, then this apparent titanium excess could be due to the presence of trivalent titanium, a cation species which may be present in most lunar armalcolites crystallized under conditions of relatively low oxygen fugacity (Wechsler et al., 1976).

A series of synthesis experiments employing controlled conditions of T and $f\text{O}_2$ were undertaken in order to further explore the significance of the calculated bulk composition discussed above and to attempt to model the paragenesis of such ilmenite-rutile nodules. The experiments were performed using the equipment and techniques described in the determinative methods section and involved run conditions that are summarized in Appendix B. The starting materials for all runs included whole fragments of a slice of nodule #JF-126 from Jagersfontein. This nodule was chosen

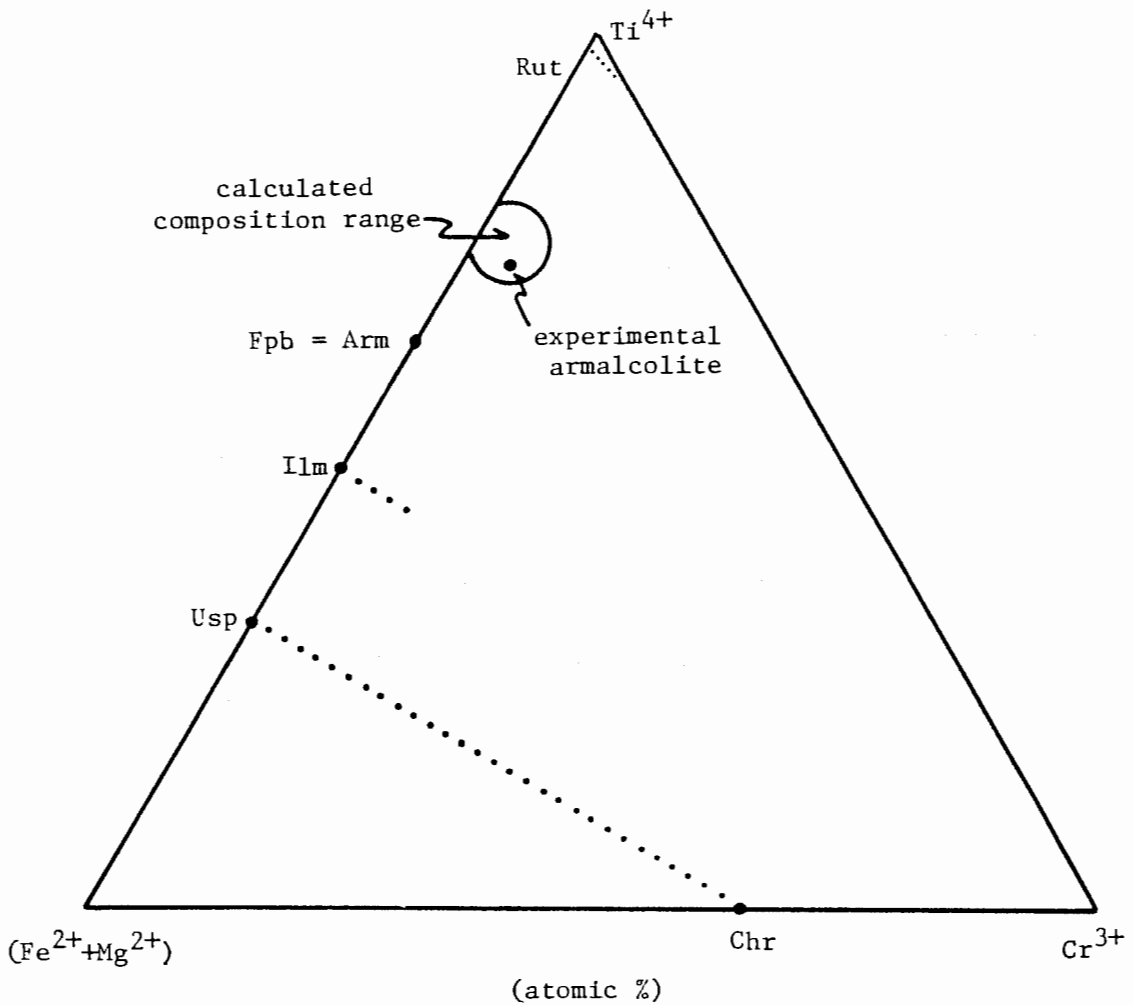


Figure 15: Calculated average bulk composition of coarse lamellar ilmenite-rutile nodules from Orapa and Jagersfontein plotted in the hypothetical armalcolite composition space $Ti^{4+}-(Fe^{2+}+Mg^{2+})-Cr^{3+}$, assuming a ± 5 percent relative error inherent in the modal analyses. The single point represents the composition determined by electron microprobe for the armalcolite phase produced in experimental run #23 using starting material from the coarse lamellar nodule #JF-126.

because of its well defined coarse lamellar texture and relatively large nodular size. Individual run times varied from approximately 20 to 70 hours. The experimental results are summarized in Figure 16. The assemblage armalcolite_{SS} + rutile is stable over a wide range of T and fO_2 conditions at or below the fayalite-magnetite-quartz (FMQ) buffer curve. The armalcolite produced throughout this stability field may be best described as chromian armalcolite containing up to 10 wt. % Cr_2O_3 . A typical analysis is presented in Figure 16. Under these conditions, rutile remained in excess and, in all cases, not more than 50 percent of the original intergrowth was recrystallized. The assemblage ilmenite + rutile remained stable below approximately 1030°C. Approximately 90 percent of the original intergrowth was recrystallized and a radically different, apparently stable armalcolite_{SS} + rutile assemblage was obtained when gas mixing limitations were stretched to attain conditions close to the iron-wustite buffer curve at 1305°C. Microprobe analyses and stoichiometric charge balance calculations indicate that the armalcolite_{SS} phase is in this case a chromian armalcolite containing trivalent titanium with a Ti^{3+}/Ti^{4+} ratio of approximately 0.25, assuming total iron as Fe^{2+} and chromium as Cr^{3+} . Plotting this composition in terms of $Ti^{4+}-(Fe^{2+}+Mg^{2+})-Cr^{3+}$ (Figure 15) shows that it falls within the range predicted from the calculated bulk compositions given in Table 3. The apparent titanium excess is a consequence of the assumption that all of the titanium was quadrivalent. The presence of considerable Ti^{3+} has the effect of lowering both the experimental point and the calculated bulk composition field into coincidence with the projection of the ferrosuedobrookite-karrooite join (which includes

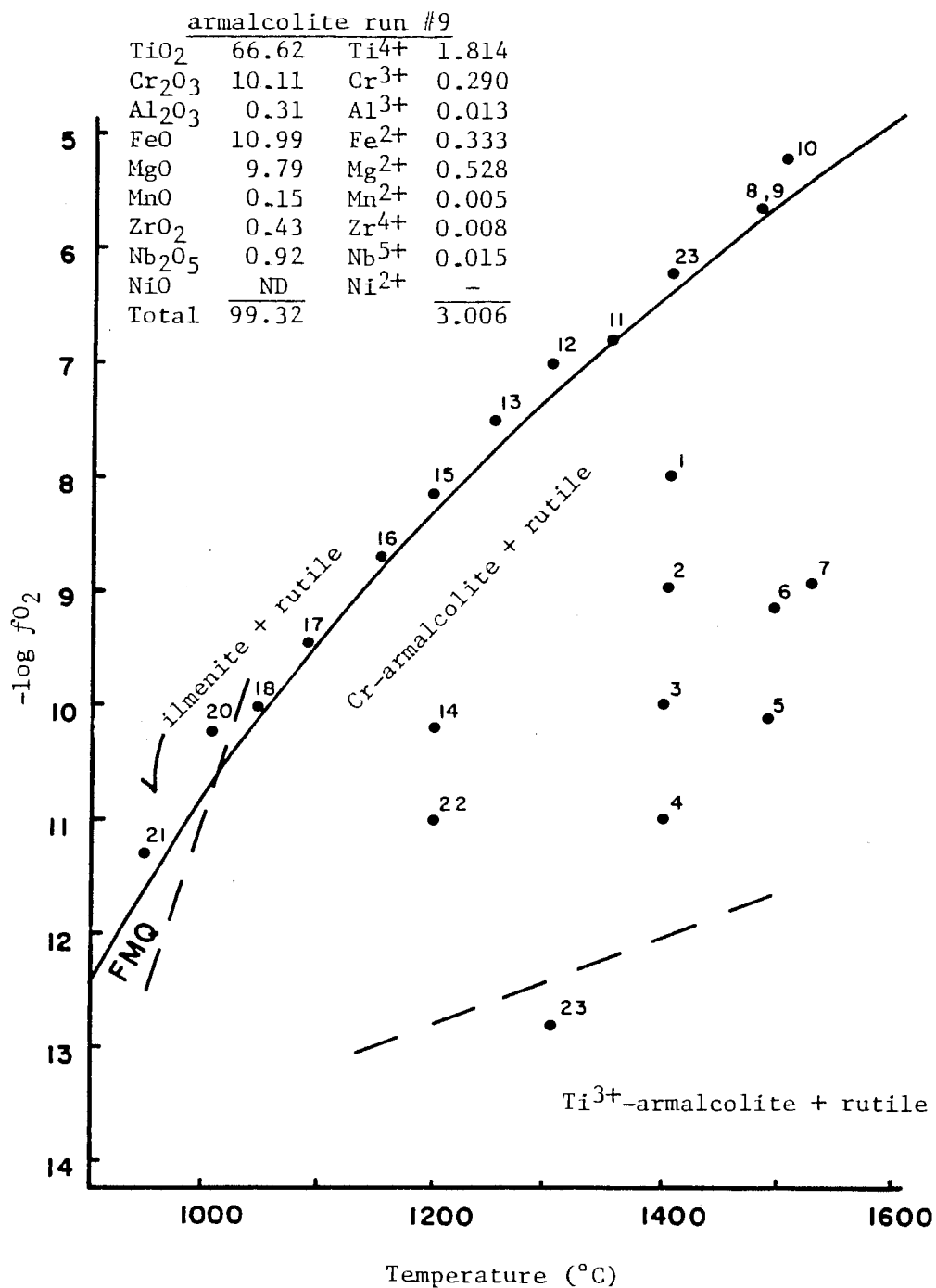


Figure 16: Summary of ilmenite-rutile experimental results plotted in terms of temperature and $-\log f_{O_2}$. The numbered points represent individual experimental runs.

armalcolite) in the figure.

These results strongly suggest that trivalent titanium-bearing chromian armalcolite may be the precursor phase to at least the coarse lamellar variety of ilmenite-rutile intergrowths recovered from Orapa and Jagersfontein. Although the mechanism of such armalcolite decomposition remains speculative and accurate kinetic data are presently unavailable, the coarse texture of the nodules appears to necessitate an extended period of time for the requisite subsolidus diffusion to take place and may indicate that the process is most likely to occur at lower crustal levels prior to incorporation in and eruption of the enclosing kimberlite. Considering the results of Friel and Harker (1977), Lindsley et al. (1974), and this study, it becomes clear that any characterization of possible deep-seated reactions involving armalcolite, ilmenite, and rutile must take into consideration the combined effects of both pressure and oxygen fugacity. In view of the data indicating that increases in both parameters favor the formation of coexisting ilmenite and rutile, future experiments designed to evaluate the relative effects of these variables are clearly needed in order to accurately model the reaction mechanisms involved in the paragenesis of such assemblages.

A single discrete nodule composed solely of rutile has been recovered from the Orapa nodule suite. This particular nodule is ovoid in shape, approximately 1 cm in elliptical diameter, and characterized by an overall smooth exterior surface and dark reddish-black color. Examined under high resolution oil immersion microscopy, this rutile nodule displays characteristic red-orange internal reflections which are

Table 4: Comparison of X-ray diffraction data for niobian rutile discrete nodule #OR-406 from Orapa and "ilmenorutile" (JCPDS #11-396).

<u>I*</u>	<u>calculated d-spacings (Å)</u>		
	<u>OR-406'</u>	<u>JCPDS #11-396</u>	<u>HKL</u>
100	3.245	3.23	110
75	1.686	1.687	211
30	2.482	2.48	101
15	1.625	1.627	220
10	2.183	2.190	111
10	1.360	1.361	301
5	1.347	1.348	112
5	2.050	2.051	210
5	1.480	1.481	002
5	1.452	1.454	310

* estimated visually

' d-spacing data reported as the mean of four individual determinations

Cu K α radiation ($\lambda = 1.54050$), Ni filter

typically visible along prominent cleavages. Although microprobe analysis has indicated an atomic ratio Nb/Ta of approximately 20:1, detailed microscopy has failed to delineate fine scale Nb-rich exsolution lamellae similar to those identified by Cerny et al. (1964) in rutiles from a variety of worldwide non-kimberlitic locations. Mineralogic alteration and apparent reaction relations similar to those described for groundmass rutiles in kimberlite by Elthon and Ridley (1979) are also not visible in polished section.

X-ray diffraction analysis has been performed on two sets of duplicate powder subsplits from this nodule using a 57.3 mm diameter camera with Ni-filtered copper K α radiation ($\lambda = 1.54050 \text{ \AA}$). The mean d-spacings corresponding to the ten most prominent reflections are presented in Table 4 and compared to those reported (Berry, 1974) for "ilmenorutile" (ideal formula of $\text{Fe}_x(\text{Nb,Ta})_{2x}\text{Ti}_{1-x}\text{O}_2$) from north Malaya. The X-ray data indicate a close similarity between these two niobium-bearing rutiles and suggest only slight deviation from the parameters characterizing pure rutile (JCPDS #21-1276). It should be added that the powder diffraction pattern obtained from the Orapa rutile contains no lines attributable to columbite which Cerny et al. (1964) have shown to be a relatively common phase intergrown within niobium-bearing rutiles which may otherwise be homogeneous.

The chemical composition of this rutile nodule, as obtained by electron microprobe analysis, is presented in Table 5 and indicates that chromium and niobium are the major diluents in the structure, with Cr_2O_3 and Nb_2O_5 present as 5.23 and 6.48 wt. % respectively. This composition is without precedent for homogeneous rutile in the kimberlitic

Table 5: Chemical composition of niobian rutile discrete nodule #OR-406 from Orapa compared to lunar rutile.

	<u>OR-406</u>	<u>lunar rutile</u> <u>(Marvin, 1971)</u>
TiO ₂	84.63	87.9
Cr ₂ O ₃	5.23	3.2
Al ₂ O ₃	0.31	NR
*Fe ₂ O ₃	1.87	NR
MgO	0.22	NR
ZrO ₂	0.93	NR
Nb ₂ O ₅	6.49	6.4
Ta ₂ O ₅	0.53	0.2
Total	<u>100.21</u>	
		V ₂ O ₃ 0.4
		Ce ₂ O ₃ 0.8
		La ₂ O ₃ <u>0.4</u>
		Total <u>99.3</u>

Cations based on two (2) oxygens

Ti	0.882	0.915
Cr	0.057	0.035
Al	0.005	-
Fe ³⁺	0.019	-
Mg	0.004	-
Zr	0.006	-
Nb	0.041	0.040
Ta	<u>0.002</u>	0.001
Total	<u>1.016</u>	
		V 0.004
		Ce 0.004
		La <u>0.002</u>
		Total <u>1.001</u>
n	5	

* total iron expressed as Fe₂O₃

NR: not reported or reported only in trace quantities

literature, although it bears a strong similarity to that reported by Marvin (1971) for rutile of unknown origin recovered from lunar surface breccia materials (Table 5). As shown in Figure 12, the composition of this discrete nodule falls within the range defined by the host rutile from the ilmenite-rutile intergrowths in terms of $(\text{Nb}^{5+} + \text{Cr}^{3+} + \text{Ta}^{5+})$ substitution. However, from Figure 13, it is clear that the nodule is slightly richer in total iron than the other kimberlitic rutiles examined in this study. With an atomic ratio Nb/Ta greater than unity, this single homogeneous Orapa nodule is classified as niobian rutile according to the nomenclature recommendations of Cerny et al. (1964).

C H A P T E R I I I
S I L I C A T E D I S C R E T E N O D U L E S

Clinopyroxene

A total of 22 individual clinopyroxene discrete nodules have been recovered from the Orapa suite and examined in detail. In hand specimen, these nodules are typically dull to bright green in color with local areas of dull grey-green, mostly cryptocrystalline, alteration developed along microfractures. Individual nodules are characteristically ovoid in shape, average approximately 1 cm in diameter, and typically have smooth exterior surfaces. Such clinopyroxene nodules are distinctly less abundant in the Orapa mine concentrate than either ilmenite or garnet (S.E. Haggerty, pers. comm., 1978).

Examined in both thin and polished section, individual nodules appear to be homogeneous with no evidence of exsolution lamellae or mineral intergrowths other than the selective alteration already described. Where resolvable under the microscope, this alteration appears to be a polycrystalline assemblage comprised mostly of chlorite, serpentine, and calcite. Average chemical compositions obtained by electron microprobe analysis of individual nodules are presented in Table 6. On the basis of multiple analyses, all nodules have been found to be homogeneous in major element composition within the analytical limits of the microprobe. Classified according to the mineral chemical cluster analysis criteria developed for kimberlitic pyroxenes by Stephens and Dawson (1977), these clinopyroxene compositions correspond to the groupings designated as diopside (10 nodules), subcalcic diopside (7 nodules),

Table 6: Average chemical compositions of individual clinopyroxene discrete nodules from Orapa.

Specimen:	<u>801</u>	<u>802</u>	<u>803</u>	<u>804A</u>	<u>804B</u>	<u>804C</u>	<u>804D</u>	<u>805A</u>	<u>805B</u>
SiO ₂	55.17	54.95	54.03	56.19	55.90	55.19	55.77	55.17	55.26
TiO ₂	0.35	0.31	0.33	0.16	0.28	0.43	0.11	0.18	0.26
Cr ₂ O ₃	0.76	0.60	1.44	0.50	0.14	0.21	0.48	0.46	0.59
Al ₂ O ₃	2.03	1.89	2.44	3.02	6.38	6.86	2.85	2.67	2.31
*FeO	3.62	3.35	4.90	4.97	4.34	4.28	4.90	5.14	5.11
MgO	17.53	17.06	16.39	20.48	13.12	12.63	20.22	20.68	19.23
MnO	0.05	0.12	0.10	0.14	0.05	0.04	0.09	0.10	0.16
CaO	19.28	19.52	17.78	13.61	16.61	16.60	13.42	13.73	15.77
Na ₂ O	2.00	1.86	2.83	2.07	3.98	4.85	2.12	1.83	1.73
Total	<u>100.79</u>	<u>99.66</u>	<u>100.24</u>	<u>101.14</u>	<u>100.80</u>	<u>101.09</u>	<u>99.96</u>	<u>99.96</u>	<u>100.42</u>

Cations based on six (6) oxygens

Si	1.980	1.992	1.964	1.983	1.990	1.967	1.991	1.975	1.981
IVAl	0.020	0.008	0.036	0.017	0.010	0.033	0.009	0.025	0.019
VIAl	0.066	0.073	0.069	0.109	0.258	0.255	0.111	0.088	0.079
Ti	0.010	0.008	0.009	0.004	0.007	0.012	0.003	0.005	0.007
Cr	0.022	0.017	0.041	0.014	0.004	0.006	0.013	0.013	0.017
Fe	0.109	0.102	0.149	0.147	0.129	0.128	0.146	0.154	0.153
Mg	0.938	0.922	0.889	1.078	0.696	0.672	1.076	1.104	1.028
Mn	0.001	0.004	0.003	0.004	0.001	0.001	0.003	0.003	0.005
Ca	0.742	0.759	0.693	0.515	0.634	0.634	0.514	0.527	0.606
Na	0.139	0.131	0.200	0.142	0.275	0.335	0.147	0.127	0.120
Total	<u>4.027</u>	<u>4.016</u>	<u>4.053</u>	<u>4.013</u>	<u>4.004</u>	<u>4.043</u>	<u>4.013</u>	<u>4.021</u>	<u>4.015</u>
Ca/(Ca+Mg)	0.442	0.452	0.438	0.323	0.477	0.484	0.323	0.323	0.371
Mg/(Mg+Fe)	0.896	0.900	0.856	0.880	0.844	0.840	0.881	0.878	0.870
n	4	3	4	4	6	7	3	4	3

* total iron expressed as FeO

Table 6 (con't)

Specimen:	<u>805C</u>	<u>805D</u>	<u>806A</u>	<u>806B</u>	<u>806C</u>	<u>806D</u>	<u>807A</u>	<u>807B</u>	<u>807C</u>
SiO ₂	54.29	54.05	53.96	53.94	53.59	53.91	54.69	54.70	54.36
TiO ₂	0.36	0.38	0.34	0.35	0.31	0.39	0.38	0.37	0.32
Cr ₂ O ₃	0.32	0.74	2.35	1.18	0.67	0.85	0.55	0.52	0.56
Al ₂ O ₃	8.25	2.20	2.51	2.22	2.81	2.24	2.31	2.59	2.32
*FeO	4.93	3.38	2.97	3.06	6.15	3.37	3.61	5.19	3.55
MgO	11.77	18.01	16.04	17.00	15.71	17.38	17.78	19.33	17.73
MnO	0.03	0.02	0.05	0.10	0.16	0.09	0.05	0.11	0.16
CaO	15.29	20.07	18.87	19.90	17.85	19.67	19.33	15.96	19.72
Na ₂ O	5.36	1.85	2.94	1.90	2.66	1.95	1.87	1.98	1.92
Total	<u>100.60</u>	<u>100.70</u>	<u>100.03</u>	<u>99.65</u>	<u>99.91</u>	<u>99.85</u>	<u>100.57</u>	<u>100.75</u>	<u>100.64</u>

Cations based on six (6) oxygens

Si	1.946	1.948	1.960	1.962	1.963	1.958	1.967	1.960	1.959
IVAl	0.054	0.052	0.040	0.038	0.037	0.042	0.033	0.040	0.041
VIAl	0.295	0.041	0.068	0.057	0.084	0.054	0.065	0.069	0.058
Ti	0.010	0.010	0.009	0.010	0.009	0.011	0.010	0.010	0.009
Cr	0.009	0.021	0.068	0.034	0.019	0.024	0.016	0.015	0.016
Fe	0.148	0.102	0.090	0.093	0.188	0.102	0.109	0.156	0.107
Mg	0.629	0.968	0.869	0.923	0.858	0.942	0.954	1.033	0.953
Mn	0.001	0.001	0.002	0.003	0.005	0.003	0.002	0.002	0.005
Ca	0.588	0.776	0.735	0.776	0.701	0.766	0.746	0.613	0.762
Na	0.373	0.129	0.207	0.134	0.189	0.137	0.130	0.138	0.134
Total	<u>4.053</u>	<u>4.048</u>	<u>4.048</u>	<u>4.030</u>	<u>4.053</u>	<u>4.039</u>	<u>4.032</u>	<u>4.036</u>	<u>4.044</u>
Ca/(Ca+Mg)	0.483	0.445	0.458	0.457	0.450	0.448	0.439	0.372	0.444
Mg/(Mg+Fe)	0.810	0.905	0.906	0.908	0.820	0.902	0.897	0.869	0.899
n	1	8	5	3	4	4	3	4	4

* total iron expressed as FeO

Table 6 (con't)

Specimen:	<u>807D</u>	<u>808A</u>	<u>808B</u>	<u>808C</u>
SiO ₂	54.15	54.09	54.31	54.92
TiO ₂	0.34	0.32	0.37	0.23
Cr ₂ O ₃	0.48	0.58	0.65	0.42
Al ₂ O ₃	2.35	2.38	2.29	2.80
*FeO	3.56	4.99	3.29	5.36
MgO	17.76	19.68	17.82	21.18
MnO	0.03	0.13	0.05	0.11
CaO	19.40	15.79	19.71	13.86
Na ₂ O	<u>1.97</u>	<u>1.78</u>	<u>1.85</u>	<u>1.90</u>
Total	<u>100.04</u>	<u>99.74</u>	<u>100.34</u>	<u>100.78</u>

Cations based on six (6) oxygens

Si	1.960	1.957	1.959	1.956
IVAl	0.040	0.043	0.041	0.044
VIAl	0.060	0.058	0.057	0.074
Ti	0.009	0.009	0.010	0.006
Cr	0.014	0.017	0.019	0.012
Fe	0.108	0.151	0.099	0.160
Mg	0.959	1.062	0.959	1.125
Mn	0.001	0.004	0.001	0.003
Ca	0.753	0.612	0.762	0.529
Na	<u>0.138</u>	<u>0.125</u>	<u>0.130</u>	<u>0.131</u>
Total	4.042	4.038	4.037	4.040
Ca/(Ca+Mg)	0.440	0.366	0.443	0.319
Mg/(Mg+Fe)	0.899	0.876	0.906	0.875
n	4	4	4	1

* total iron expressed as FeO

jadeitic diopside (3 nodules), and chrome diopside (2 nodules). By definition, the diopside nodules at Orapa are characterized by higher values of CaO, ranging from 17.78 to 20.07 wt. %, compared to the associated subcalcic diopsides which range from 13.42 to 15.96 wt. %. The three jadeitic diopside nodules are characterized by CaO values ranging from 15.29 to 16.61 wt. % and, by definition, higher Al₂O₃ and Na₂O contents, averaging 7.16 and 4.73 wt. % respectively. The two nodules assigned to the chrome diopside group average approximately 1.70 wt. % Cr₂O₃, with values for CaO, (MgO+FeO), and Al₂O₃ similar to the associated calcic diopside group.

Plotted solely in terms of the conventional pyroxene quadrilateral system end members CaMgSi₂O₆ - CaFeSi₂O₆ - MgMgSi₂O₆ - FeFeSi₂O₆ (mole percent diopside - hedenbergite - enstatite - ferrosilite, respectively) in Figure 17, Orapa clinopyroxene nodules corresponding to the diopside, subcalcic diopside, and chrome diopside groupings of Stephens and Dawson (1977) show a wide range of compositional variation, defining an elongate field oriented subparallel to the enstatite-diopside join. This plot readily shows the distinction between the diopside and subcalcic diopside groups, but is by design relatively insensitive to the substitutional effects of cation species other than Ca²⁺, Mg²⁺, and Fe²⁺. This point is emphasized by the fact that the two chrome diopside nodules plot adjacent to the diopside group in the figure.

The importance of non-quadrilateral cation substitutions is considered in the "Quad" versus "Others" classification of Papike et al. (1974). According to this classification, the Orapa pyroxene nodule compositions are characterized by a minimum of from 12 to 37 %

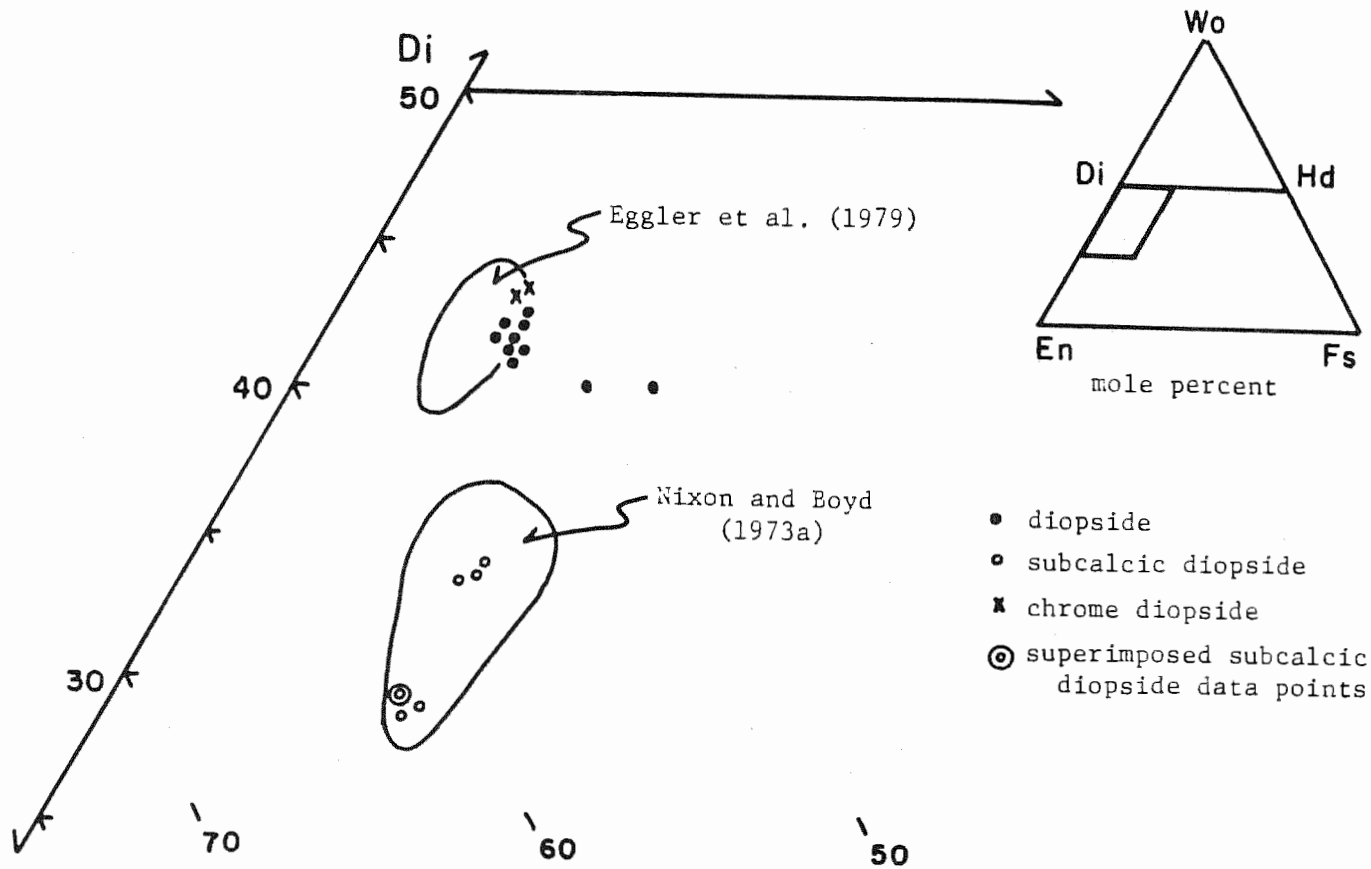
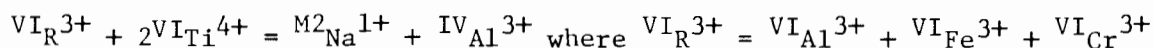


Figure 17: Compositions of the clinopyroxene discrete nodule suite from Orapa plotted in the conventional pyroxene quadrilateral system diopside-enstatite-ferrosilite-hedenbergite. Orapa jadeitic diopsides are not plotted. The compositional fields for similar nodules from other localities are outlined and labelled for comparison. See text for discussion.

substitution by "Others" components, as these are defined by the charge balance equation:



(for discussion, see Cameron and Papike, 1981). Figure 18 is part of a ternary plot involving the three components VI_{Ti}^{4+} , VI_{Na}^{1+} , and IV_{Al}^{3+} .

In this figure, the Orapa pyroxenes define a relatively restricted compositional field close to the VI_{Na}^{1+} apex, parallel to the $VI_{Na}^{1+} - IV_{Al}^{3+}$ sideline, demonstrating the importance of Na^{1+} substitution for Ca^{2+} in the M2 structural site. This entrance of sodium into the pyroxene structure is most likely accompanied by charge-balancing trivalent ion substitution for $(Mg,Fe)^{2+}$ in the M1 site (Cameron and Papike, 1981). On the basis of bulk composition (Table 6), comparison with numerous previously reported analyses of kimberlitic clinopyroxenes (for example, Stephens and Dawson, 1977; Egglar et al., 1979; Gurney et al., 1979), and known crystal chemical cation behavior (Cameron and Papike, 1980, 1981; Robinson, 1980), most of this trivalent ion substitution is believed to involve Al^{3+} and Cr^{3+} , with Fe^{3+} and the couple $(Fe^{2+}Ti^{4+})_{1/2}$ present in only minor amounts.

With regard to these latter two components, it should be noted that the total iron data is reported in Table 6 as FeO, even though minor amounts of ferric iron may be present. This has been done in order to make these analyses more readily comparable to pyroxene data previously reported in the kimberlitic literature and because ferric iron values calculated according to recently proposed schemes (Papike et al., 1974; Robinson, 1980) can be shown to be extremely sensitive to analytical error in the values determined for other components--most notably

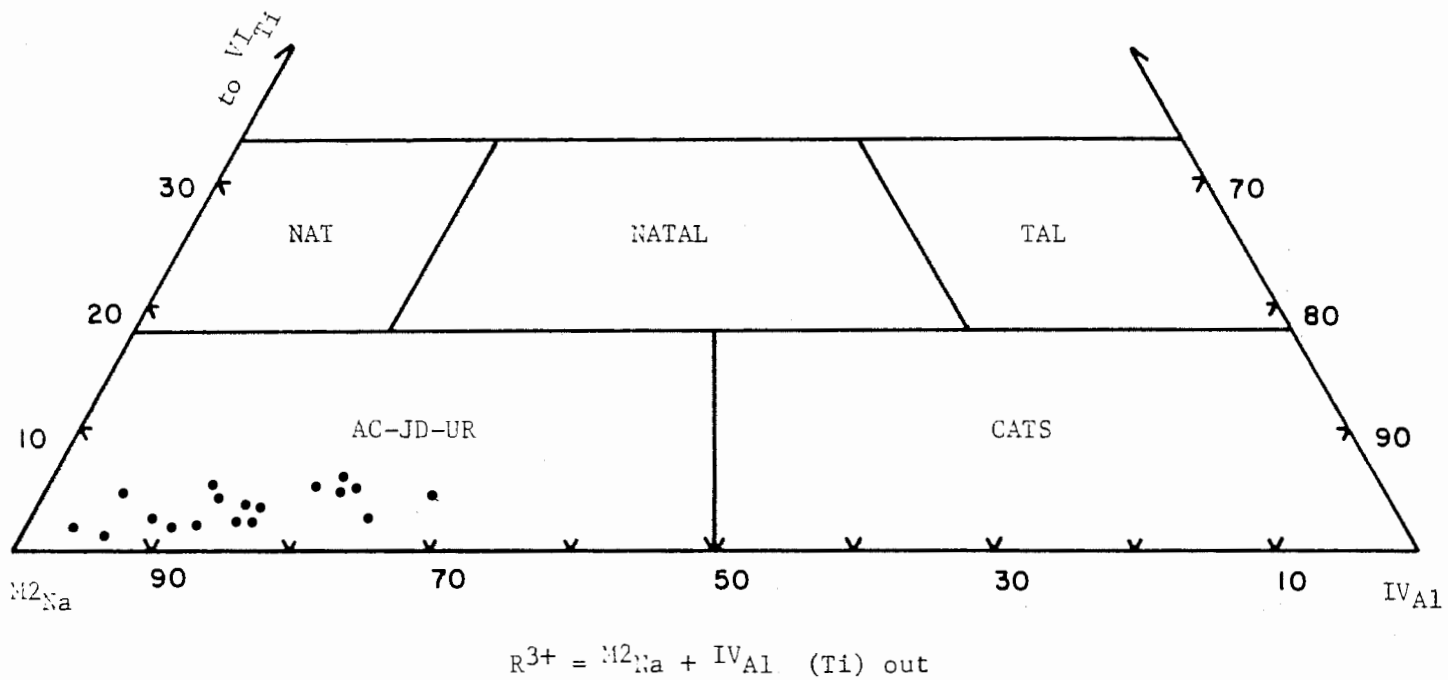


Figure 18: Compositions of selected clinopyroxene discrete nodules from Orapa plotted in terms of the "Others" components ^{VI}Ti - $M2_{Na}$ - $IVAl$ (after Cameron and Papike, 1981).

silica--through microprobe analysis.

A variety of geochemical parameters characterizing the Orapa clinopyroxene discrete nodule suite are compared with those of similar suites from other major worldwide localities in Figures 19a-19d. The data for nodules from the Colorado-Wyoming stateline and Iron Mountain, Wyoming districts (combined and labelled simply "Colorado-Wyoming" in Figures 19a-19d) are taken from Egger et al. (1979) who sampled a number of dikes and pipe clusters in the area. For comparison purposes, data for clinopyroxene suites from the Monastery kimberlite pipe in South Africa (Whitelock, 1973; Gurney et al., 1979) and several localities in neighboring Lesotho (Bloomer and Nixon, 1973; Nixon and Boyd, 1973a) have been combined and treated as a single broad district.

Egger et al. (1979) divided nodules from the Colorado-Wyoming area into relatively chrome-rich and chrome-poor suites with olivine, orthopyroxene, clinopyroxene, and garnet nodules common to both. Based on similarities in the observed ranges of Cr_2O_3 , TiO_2 , and Al_2O_3 values and $\text{Mg}/(\text{Mg}+\text{Fe})$ ratios, all nodules comprising the Orapa clinopyroxene suite should be assigned to the chrome-poor category, although several nodules have Cr_2O_3 contents which are alone comparable to the chrome-rich variety from Colorado-Wyoming. All nodules plotted in the South Africa-Lesotho group are, in general, compositionally similar to the chrome-poor variety of Egger et al. (1979).

Clinopyroxene nodules from both the Colorado-Wyoming and South Africa-Lesotho areas show a general increase in Cr_2O_3 content with $\text{Mg}/(\text{Mg}+\text{Fe})$ ratio (Figure 19a). The data from Orapa also illustrate this relationship and are characterized by considerable overlap with the

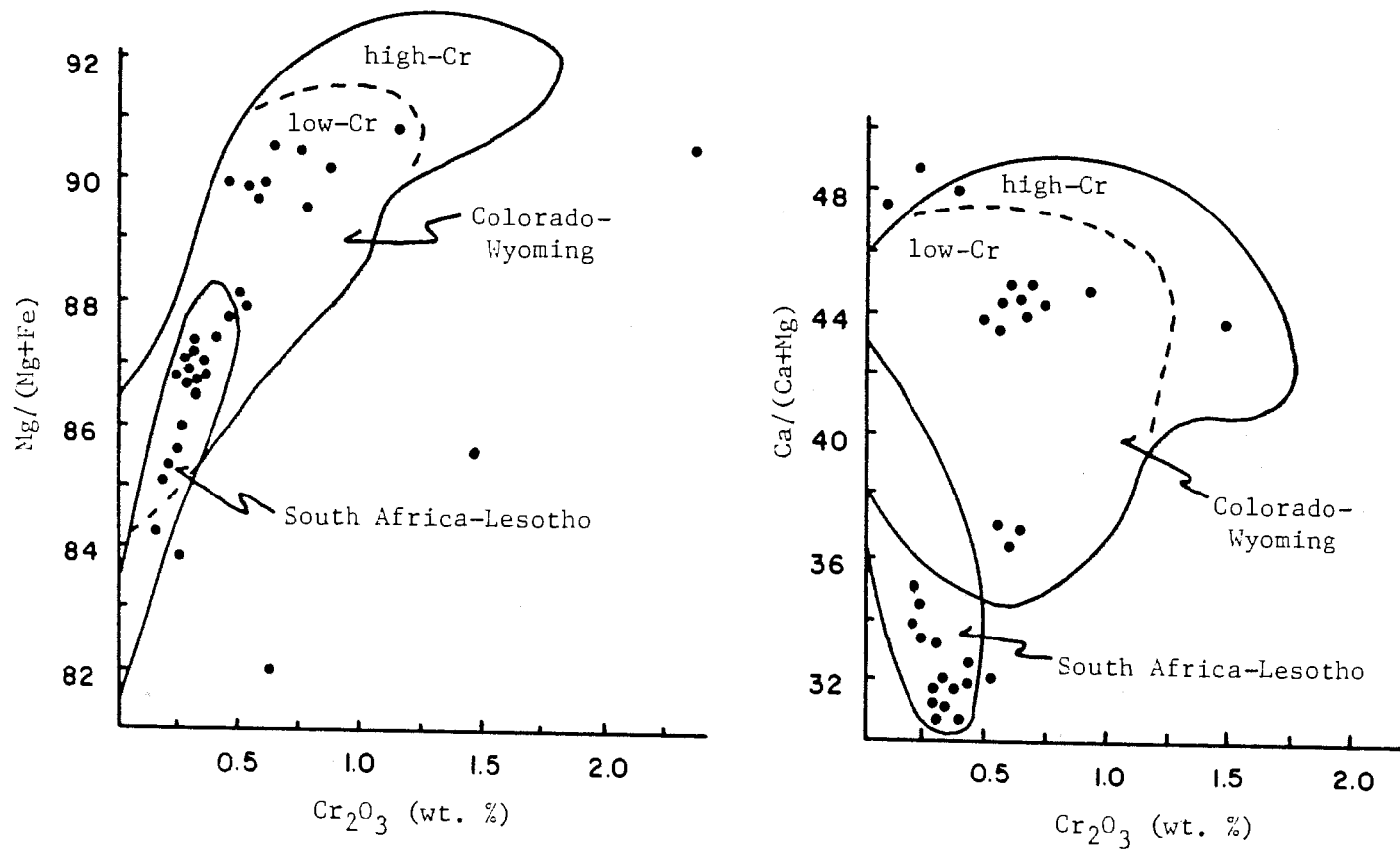


Figure 19a (left) and 19b (right): Compositions of the clinopyroxene discrete nodule suite from Orapa (solid circles) plotted as a function of chrome content versus $\text{Mg}/(\text{Mg}+\text{Fe})$ ratio (19a) and $\text{Ca}/(\text{Ca}+\text{Mg})$ ratio (19b). The compositional fields for similar nodules from South Africa-Lesotho and Colorado-Wyoming (points not shown for clarity) are outlined and labelled for comparison. See text for references and discussion.

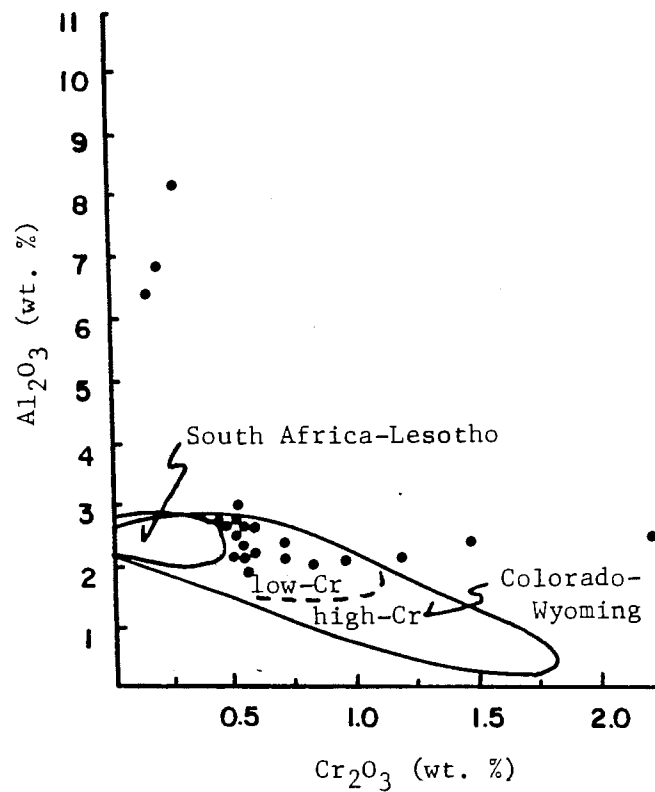
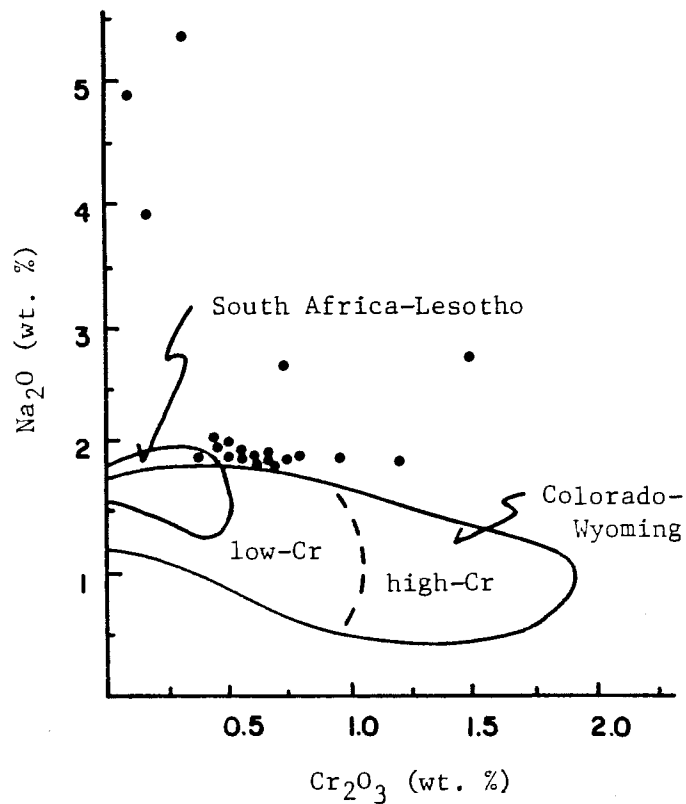


Figure 19c (left) and 19d (right): Compositions of the clinopyroxene discrete nodule suite from Orapa plotted as a function of chrome content versus Na_2O (19c) and Al_2O_3 (19d) values. Symbols are the same as in Figures 19a and 19b.

chrome-poor field from Colorado-Wyoming. In general, data points from all three areas fall along the same trend, with nodules from South Africa-Lesotho characterized by the lowest values. In Figure 19b, the Orapa data show a broad range of $\text{Ca}/(\text{Ca}+\text{Mg})$ ratio as a function of Cr_2O_3 content, with points overlapping both the chrome-rich and chrome-poor fields from Colorado-Wyoming. Nodules from South Africa-Lesotho are characterized by a narrow range of generally low values of both parameters. Nodules from both South Africa-Lesotho and Colorado-Wyoming show considerable overlap in Na_2O content at low Cr_2O_3 values in Figure 19c. However, both suites are generally lower in Na_2O than clinopyroxenes from Orapa throughout the full range of chrome contents, and this difference in Na_2O is apparently the most consistent chemical difference between the majority of the Orapa nodules and the chrome-poor suite from Colorado-Wyoming. In terms of Al_2O_3 content (Figure 19d), all of the nodules comprising the South Africa-Lesotho suite and most of those from Orapa are similar to the chrome-poor suite from Colorado-Wyoming.

It is apparent from the data presented in Figures 19a-19d that most of the Orapa clinopyroxene nodules are compositionally similar to the chrome-poor suite from Colorado-Wyoming except that Na_2O values are consistently lower in the latter. On the other hand, the Orapa nodules are overall chemically distinct from the South Africa-Lesotho suite which is predominantly subcalcic in composition and which, in turn, is otherwise generally similar to the Colorado-Wyoming suite at low Cr_2O_3 values. In most cases, nodules from all three suites appear to define continuous chemical trends which appear to support the use of Cr_2O_3 content as a

basis for nodule comparison. In most of the graphs in Figures 19a-19d, Orapa nodules #803, 804B, 804C, 805C, 806A and 806C plot away from the main Orapa grouping and off of the trends defined by the Orapa, South Africa-Lesotho, and Colorado-Wyoming suites. In general, these Orapa nodules are characterized by lower $Mg/(Mg+Fe)$ ratios and by higher values of Cr_2O_3 , Na_2O , and Al_2O_3 than the nodules falling on the main compositional trends.

Approximate temperatures of equilibration for the Orapa clinopyroxene nodules with relatively low R_2O_3 contents may be obtained by use of the pyroxene solvi of either Davis and Boyd (1966) or Lindsley and Dixon (1976). Temperatures calculated using these geothermometers are clearly only estimations and are most useful solely for comparative purposes because of the still mostly uncalibrated effect of substitutions by even minor amounts of sodium and certain trivalent cations. Such estimations must also be viewed with caution because there is no direct evidence that these clinopyroxenes are saturated with respect to an enstatite component at the time of equilibration. Nevertheless, the $Ca/(Ca+Mg)$ ratios of the two small clusters of subcalcic diopsides from Orapa (Figure 17) indicate equilibration temperatures in the ranges 1380-1360°C and 1280-1265°C when plotted on the 30 kb $MgSiO_3$ -saturated diopside solvus of Davis and Boyd (1966), with the corresponding temperatures slightly higher when plotted on the modified solvus of Lindsley and Dixon (1976). This overall high temperature range agrees quite closely with ranges determined for similar nodules from the Monastery pipe in South Africa (Gurney et al., 1979) and from a variety of pipes in Lesotho (Nixon and Boyd, 1973a). The compositions of the relatively Ca-rich

diopside nodules from Orapa indicate a lower temperature range of approximately 1020-920°C (using Davis and Boyd, 1966). Although the absolute values of these numbers must be regarded with caution due to the known insensitivity of the solvus geothermometer at low temperatures (MacGregor and Basu, 1976; Mori and Green, 1976), such a range appears to be comparable with those characterizing the entire chrome-rich suite and relatively calcic members of the chrome-poor suite from Colorado-Wyoming (Eggler et al., 1979, Figure 3).

The available geochemical data and calculated temperatures of equilibration obtained in this study of the Orapa clinopyroxene discrete nodule suite are inconclusive with regard to models of petrogenesis. The coarse grain size and the occurrence, although rare, of mineral intergrowths (to be described) suggest that these nodules may have at one time grown in the presence of liquid and the observed correspondance between Mg/(Mg+Fe) ratio and Cr₂O₃ content (Figure 19a) appears to be consistent with trends expected in such proposed fractionating crystal/liquid systems. However, the lack of agreement between the Ca/(Ca+Mg) ratio, representing temperature, and Mg/(Mg+Fe), used as an indicator of igneous fractionation, stands in contradiction to these nodules representing a single, well-defined fractionation sequence.

As presently characterized by a variety of geochemical parameters, the Orapa clinopyroxene suite appears to be composed of at least two groups. The numerically larger group includes the diopside and subcalcic diopside nodules with less than 2.50 wt. % Na₂O and which, in most cases, is compositionally similar to the chrome-poor suite from Colorado-Wyoming. These Orapa nodules generally follow chemical trends defined by the more

numerous combined suites from Colorado-Wyoming and South Africa-Lesotho, but the bimodal variation in $\text{Ca}/(\text{Ca}+\text{Mg})$ ratios, and hence inferred temperature of equilibration, characterizing these nodules may indicate that they comprise two distinct subgroups with different parageneses. The other group of nodules from Orapa is composed of the six samples mentioned previously as continually plotting off of the main compositional trends in Figures 19a-19d. These nodules vary considerably in chemical composition, but all are characterized by Na_2O contents greater than 2.50 wt. %, and several individual nodules have $\text{Ca}/(\text{Ca}+\text{Mg})$ ratios and Al_2O_3 contents much higher than the average values characterizing the Orapa group as a whole. Although this small group of six nodules shows a trend of increasing Cr_2O_3 content with increasing $\text{Mg}/(\text{Mg}+\text{Fe})$ ratio (Figure 19a) similar to that defined by the larger Orapa group and by nodules from Colorado-Wyoming and South Africa-Lesotho, the overall chemical variability of these nodules may indicate that they are less likely to represent a single coherent sampling episode at some point along the intrusional pathway of the Orapa kimberlite.

Ilmenite-Clinopyroxene Intergrowth

A single discrete nodule composed primarily of ilmenite formerly intergrown with clinopyroxene has been recovered from the Orapa suite and examined in detail. In hand specimen, this nodule is characterized by an overall irregular external form and generally dull dark-grey color. The nodule is approximately 5 mm in diameter and is coated by a very fine-grained, light-grey to locally orange alteration product on one flat exterior surface which may represent a nodule fracture plane.

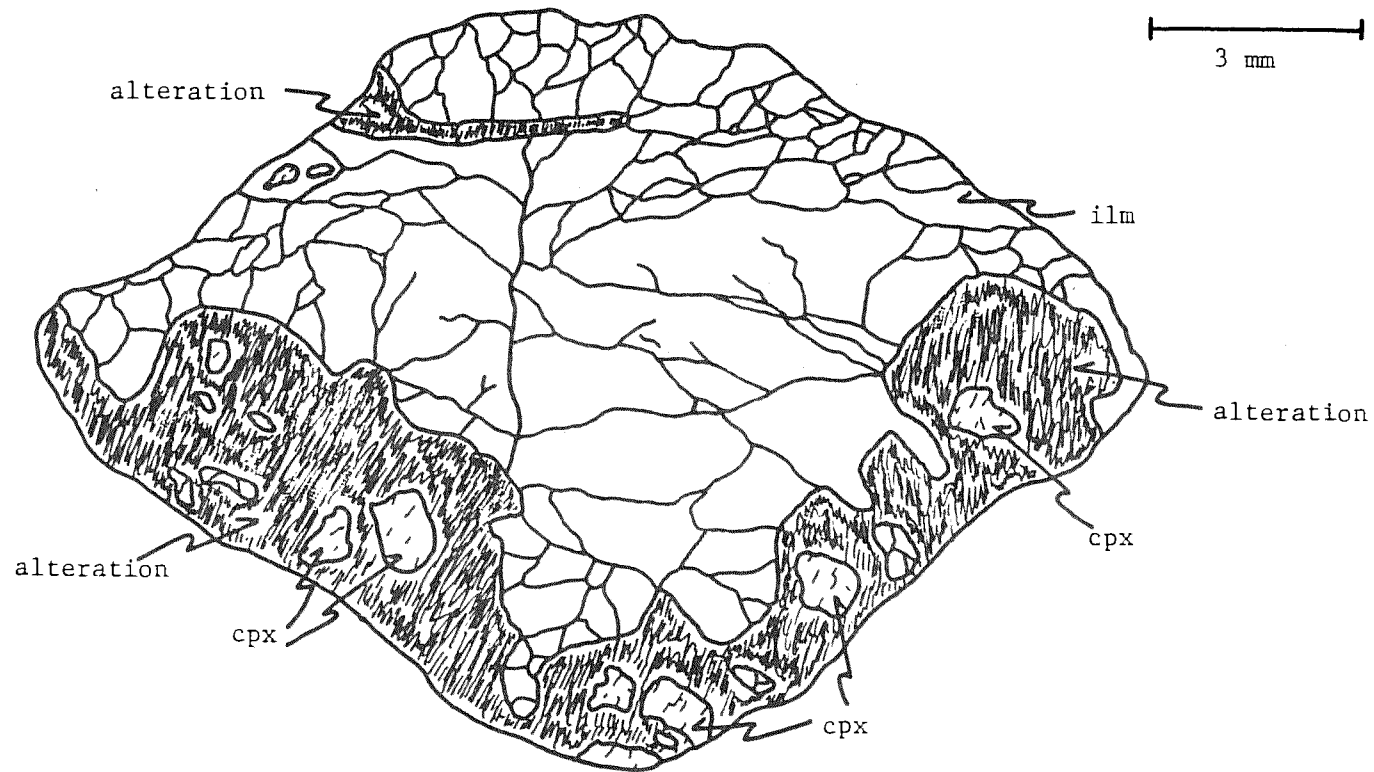


Figure 20: Detailed drawing of a polished section through Orapa nodule #430B composed of ilmenite intergrown with clinopyroxene and polymineralic alteration products.

In polished section (Figure 20), the ilmenite is characterized by an overall polygranular texture in which individual grains are marked by subtle differences in reflection anisotropy. Except for such differences in optical properties, most polygranular individuals have boundaries which are unmarked by surface features. Where such features exist, however, these are typically very fine microfractures or localized, relatively coarse pitting which is generally limited to polygranular triple point junctions. Prominent twin lamellae, similar to those already described for some of the ilmenite discrete nodules, are present in the ilmenite at several locations along the nodule periphery. The clinopyroxene of this intergrowth is highly altered to a creamy-white, extremely fine-grained secondary phase which cannot be unambiguously identified by either optical or electron microprobe techniques, but which may be a polymineralic assemblage dominated by serpentine, chlorite, and calcite. Relatively fresh, green clinopyroxene remnants are present locally along most of the nodule periphery and are typically surrounded by the more abundant alteration product. Although the ilmenite and clinopyroxene are nowhere in direct contact, the distribution of the polymineralic alteration suggests that the original intergrowth was characterized by clinopyroxene forming an irregular mantle around at least a portion of the polygranular ilmenite core. Assuming, as microscope studies suggest, that the observed mineralogic alteration can be ascribed nearly entirely to the pyroxene, the original ilmenite: clinopyroxene modal ratio is approximately 70:30.

Both phases are relatively homogeneous in composition throughout the nodule (Table 7). The ilmenite contains an average 1.81 wt. %

Table 7: Average chemical compositions of coexisting clinopyroxene and ilmenite from Orapa nodule #430B.

	<u>ilmenite</u>	<u>clinopyroxene</u>
SiO ₂	-	53.30
TiO ₂	54.26	0.40
Cr ₂ O ₃	1.81	0.74
Al ₂ O ₃	0.55	2.10
Fe ₂ O ₃	6.31'	-
FeO	21.72	3.41*
MgO	14.90	17.84
MnO	0.27	0.07
CaO	NA	20.22
Na ₂ O	NA	1.89
ZrO ₂	0.13	NA
Nb ₂ O ₅	0.02	NA
NiO	0.35	NA
Total	<u>100.32</u>	<u>99.97</u>

Cations based on three (ilmenite)
and six (clinopyroxene) oxygens

Si	-	1.940
Ti	0.921	0.011
Cr	0.032	0.022
Al	0.015	0.090
'Fe ³⁺	0.107	-
Fe ²⁺	0.410	0.104
Mg	0.501	0.969
Mn	0.005	0.002
Ca	-	0.789
Na	-	0.133
Zr	0.001	-
Nb	0.000	-
Ni	0.007	-
Total	<u>1.999</u>	<u>4.060</u>
Ca/(Ca+Mg)	-	0.449
Mg/(Mg+Fe)	0.550	0.903
n	5	4

NA: not analyzed

* total iron expressed as FeO

' calculated

Cr_2O_3 , a value coinciding with the mode of the lower chrome ilmenite subgroup of discrete nodules at Orapa (Figure 4). The ilmenite of this intergrowth is, however, considerably more magnesian than most of the core compositions of associated discrete nodules and thus plots off of the main compositional trends defined by this population. This enrichment in MgO for ilmenite in association with clinopyroxene relative to associated ilmenite discrete nodules is consistent with the compositional relationship observed by Haggerty et al. (1979) for discrete nodules and lamellar intergrowths from the Monastery pipe in South Africa. In terms of most major components, the clinopyroxene of this intergrowth is quite similar in composition to the diopside subgroup of the associated discrete nodules.

Nodular ilmenite-pyroxene intergrowths have been shown in the last decade to be a relatively common constituent of kimberlitic nodule suites from such diverse localities as Yakutia in the U.S.S.R. (Ilupin et al., 1973), Iron Mountain, Wyoming (Smith et al., 1976), and a variety of pipes in South Africa and Lesotho (Boyd and Nixon, 1973; Gurney et al., 1973; Haggerty et al., 1979a; Rawlinson and Dawson, 1979). Such nodules are typically comprised of micro-ilmenite intergrown with either clinopyroxene or, more rarely, orthopyroxene. In these intergrowths, the oxide phase is generally present as uniformly-oriented, optically continuous lamellae which, in many examples, define a characteristic graphic texture similar to that typical of some quartz-feldspar intergrowths in certain granites. Irregular intergrowth textures do occur in some ilmenite-pyroxene nodules, however, and appear to be more common in the orthopyroxene-bearing assemblages (Boyd and Nixon, 1973).

Models for the origin of nodular intergrowths comprised primarily of ilmenite and pyroxene have evolved over the past decade as the worldwide data base and analytical/experimental techniques have improved. Dawson and Reid (1970) used textural and bulk chemical evidence to infer the existence of a high pressure, TiO_2 -rich "ilmenite-structured pyroxene" which, by means of decompression-stimulated exsolution, could generate typical nodules of lamellar ilmenite in pyroxene. Noting the stoichiometric similarity between the reconstituted formulae of certain garnets and the theoretical combination of a pyroxenoid and an ilmenite-type molecule, Ringwood and Lovering (1970) synthesized a titanium-rich garnet from a fused portion of an intergrowth at 1000°C and a minimum pressure of 105 kb. An apparently stable two-phase assemblage of ilmenite + pyroxene was produced at a series of temperatures and pressures below 1000°C and 105 kb, but the overall results are generally judged as inconclusive because the garnet-producing reaction was never reversed. In any case, the applicability of both models appears to be contradicted by subsequent experimental studies which have shown that the solubility of TiO_2 at 30 kb is too limited in both clinopyroxene (Akella and Boyd, 1972) and garnet (Green and Sobolev, 1975) to suggest that either of these phases serves as a high pressure precursor to the intergrowths. Gurney et al. (1973) also challenged these models on the basis of a variety of geochemical parameters which seemed to imply that the intergrowths were the result of eutectic crystallization at depths in the upper mantle consistent with proposed kimberlite magma formation. This latter viewpoint is supported by the detailed experimental studies of Wyatt (1977) in which intergrowths of ilmenite and clinopyroxene

shown to be texturally, crystallographically, and chemically similar to natural examples were produced from crushed natural starting materials by controlled cooling of the melt over a range of pressures.

The Orapa intergrowth appears to be texturally most similar to the granular type described by Boyd and Nixon (1973). The spatial segregation and relative modal proportions characteristic of this specimen are unlikely to be the result of subsolidus decomposition of any single precursor phase but, instead, are much more suggestive of possibly simultaneous crystallization of the two phases. Unfortunately, the relative order of crystallization for these two minerals cannot be satisfactorily determined on a textural basis for the Orapa intergrowth because of the small size and probable fractured nature of this particular specimen. Other studies (Boyd and Nixon, 1973; Wyatt, 1977) have shown, however, that clinopyroxene is typically the initial liquidus phase, followed at some lower temperature by precipitation of ilmenite. The similarity in chemical composition between the clinopyroxene of the intergrowth and the diopside subgroup of the associated pyroxene discrete nodules is consistent with the data characterizing similar, although predominantly lamellar, suites from Iron Mountain, Wyoming (Smith et al., 1976) and South Africa-Lesotho (Boyd and Nixon, 1973). This compositional relationship suggests that these two types of pyroxenes may be paragenetically related, although the available data are insufficient to support Wyatt's (1977) contention that a large proportion of the clinopyroxene discrete nodules in a particular kimberlite pipe may be related to associated ilmenite-clinopyroxene intergrowths by fractional crystallization.

Garnet

A total of 46 garnet discrete nodules have been recovered from the Orapa suite and examined in detail. In hand specimen, these nodules are typically ellipsoidal in shape with characteristically smooth exterior surfaces. The range in individual size varies from approximately 1 to 2.5 cm and is generally coarser than that characteristic of the associated clinopyroxene discrete nodule suite. Closely-spaced fractures are common and, in several specimens, are bent in a manner suggestive of stress-induced deformation. The garnet nodules vary in color from various shades of pink and red to red-purple and appear similar to some of the low-chrome varieties described from the Kao kimberlite locality in Lesotho by Hornung and Nixon (1973). Mineralogic alteration is apparent along microfractures in many nodules, but is characteristically extremely fine-grained and difficult to identify accurately. Although such alteration may be locally pervasive, nodules examined in either thin or polished section appear to be otherwise homogeneous, except for the small number of nodules containing relatively coarse clinopyroxene inclusions or, in one case to be described in a later section, a coarse intergrowth with clinopyroxene and chromite.

The average chemical compositions of individual garnet nodules from Orapa, as determined by electron microprobe analysis, are presented in Table 8. Multiple analyses performed at a variety of locations within individual garnets indicate that these nodules are homogeneous in major element composition within the analytical limits of the microprobe. The compositions of the individual nodules have been classified according to

Table 8: Average chemical compositions of individual garnet discrete nodules from Orapa.

Specimen:	<u>202</u>	<u>203</u>	<u>204</u>	<u>205</u>	<u>206A</u>	<u>206B</u>	<u>206C</u>	<u>206D</u>	<u>207A</u>
SiO ₂	42.27	41.99	42.65	42.21	41.52	41.97	42.69	42.45	41.47
TiO ₂	0.96	1.04	0.36	0.42	0.92	1.00	0.37	0.87	0.89
Cr ₂ O ₃	1.87	1.86	2.40	0.36	1.88	1.79	2.74	1.11	1.18
Al ₂ O ₃	20.82	20.82	21.58	23.04	20.85	20.96	21.01	20.78	22.38
*FeO	8.90	9.13	6.95	9.61	9.23	9.36	6.93	8.85	10.45
MgO	20.92	20.85	21.96	21.09	20.63	20.46	21.31	21.06	18.09
MnO	0.34	0.32	0.29	0.34	0.32	0.33	0.34	0.24	0.43
CaO	4.54	4.67	4.57	3.76	4.63	4.66	4.35	4.26	4.70
Na ₂ O	0.16	0.13	0.09	0.21	0.11	0.14	0.03	0.10	0.17
Total	<u>100.78</u>	<u>100.81</u>	<u>100.85</u>	<u>101.04</u>	<u>100.09</u>	<u>100.67</u>	<u>99.77</u>	<u>99.72</u>	<u>99.76</u>

Cations based on twenty-four (24) oxygens

Si	6.003	5.973	5.998	5.950	5.959	5.982	6.066	6.066	5.976
Ti	0.102	0.111	0.038	0.045	0.100	0.107	0.040	0.093	0.096
Cr	0.210	0.209	0.267	0.040	0.214	0.201	0.308	0.125	0.134
Al	3.487	3.493	3.579	3.830	3.529	3.524	3.520	3.501	3.803
Fe	1.057	1.086	0.818	1.133	1.109	1.116	0.824	1.059	1.260
Mg	4.432	4.423	4.604	4.434	4.392	4.348	4.515	4.488	3.887
Mn	0.041	0.038	0.035	0.041	0.040	0.039	0.041	0.029	0.053
Ca	0.692	0.713	0.690	0.568	0.713	0.711	0.662	0.652	0.727
Na	0.044	0.036	0.025	0.058	0.031	0.037	0.009	0.027	0.046
Total	<u>16.068</u>	<u>16.082</u>	<u>16.054</u>	<u>16.099</u>	<u>16.087</u>	<u>16.065</u>	<u>15.985</u>	<u>16.040</u>	<u>15.982</u>
Ca/(Ca+Mg)	0.135	0.139	0.130	0.113	0.140	0.140	0.128	0.127	0.158
Mg/(Mg+Fe)	0.807	0.803	0.849	0.796	0.798	0.796	0.846	0.809	0.755
n	1	1	2	2	2	4	4	5	5

* total iron expressed as FeO

Table 8 (con't)

Specimen:	<u>207B</u>	<u>207C</u>	<u>208A</u>	<u>208B</u>	<u>208C</u>	<u>209A</u>	<u>209B</u>	<u>209C</u>	<u>210A</u>
SiO ₂	41.76	41.27	41.53	42.15	42.12	42.10	42.16	42.27	41.48
TiO ₂	0.48	0.88	1.10	1.01	1.17	1.04	0.96	0.84	0.92
Cr ₂ O ₃	3.40	1.12	0.44	1.54	2.04	1.66	1.19	1.22	0.89
Al ₂ O ₃	20.60	21.48	21.09	20.93	20.72	21.22	21.51	21.28	21.57
*FeO	7.81	9.23	12.09	9.29	9.43	9.66	9.02	8.58	10.34
MgO	20.35	20.35	18.33	20.44	19.59	19.86	21.20	21.66	19.97
MnO	0.31	0.33	0.39	0.33	0.31	0.37	0.28	0.33	0.45
CaO	4.60	4.36	4.54	4.35	4.38	4.40	4.38	4.30	4.51
Na ₂ O	0.03	0.09	0.17	0.18	0.12	0.09	0.04	0.14	0.08
Total	<u>99.34</u>	<u>99.11</u>	<u>99.68</u>	<u>100.22</u>	<u>99.88</u>	<u>100.40</u>	<u>100.74</u>	<u>100.62</u>	<u>100.21</u>

Cations based on twenty-four (24) oxygens

Si	6.007	5.956	6.027	6.020	6.044	6.011	5.974	5.988	5.951
Ti	0.052	0.095	0.121	0.109	0.126	0.112	0.103	0.089	0.099
Cr	0.387	0.128	0.050	0.173	0.231	0.188	0.134	0.137	0.101
Al	3.495	3.656	3.610	3.525	3.507	3.573	3.595	3.556	3.650
Fe	0.940	1.115	1.468	1.110	1.132	1.154	1.069	1.017	1.241
Mg	4.367	4.380	3.967	4.353	4.193	4.229	4.480	4.576	4.273
Mn	0.037	0.041	0.048	0.040	0.038	0.045	0.033	0.040	0.055
Ca	0.710	0.674	0.707	0.666	0.673	0.674	0.666	0.653	0.693
Na	0.007	0.024	0.047	0.051	0.032	0.026	0.012	0.039	0.022
Total	<u>16.002</u>	<u>16.069</u>	<u>16.045</u>	<u>16.047</u>	<u>15.976</u>	<u>16.012</u>	<u>16.066</u>	<u>16.095</u>	<u>16.085</u>
Ca/(Ca+Mg)	0.140	0.133	0.151	0.133	0.138	0.137	0.129	0.125	0.140
Mg/(Mg+Fe)	0.823	0.797	0.730	0.797	0.787	0.786	0.807	0.818	0.775
n	1	1	3	2	2	3	2	1	3

* total iron expressed as FeO

Table 8 (con't)

Specimen:	<u>210B</u>	<u>210C</u>	<u>211A</u>	<u>211B</u>	<u>211C</u>	<u>212A</u>	<u>212C</u>	<u>214A</u>	<u>214B</u>
SiO ₂	41.60	40.99	41.80	42.06	41.91	42.41	42.33	42.34	41.68
TiO ₂	1.03	0.80	0.90	0.98	1.14	1.25	0.98	1.16	1.05
Cr ₂ O ₃	1.93	4.07	1.21	0.48	1.79	1.66	1.82	1.63	1.96
Al ₂ O ₃	20.56	19.28	21.22	21.52	20.73	21.24	20.83	21.03	20.83
*FeO	9.33	11.33	8.85	11.34	9.90	10.10	9.44	9.60	9.39
MgO	20.67	18.34	19.96	19.34	20.39	18.98	20.24	20.07	19.39
MnO	0.38	0.52	0.41	0.42	0.40	0.41	0.40	0.35	0.45
CaO	4.55	5.19	5.17	4.37	4.70	4.63	4.62	4.45	4.81
Na ₂ O	0.08	0.15	0.09	0.14	0.12	0.10	0.17	0.17	0.09
Total	<u>100.13</u>	<u>100.67</u>	<u>99.61</u>	<u>100.65</u>	<u>101.08</u>	<u>100.78</u>	<u>100.83</u>	<u>100.80</u>	<u>99.65</u>

Cations based on twenty four (24) oxygens

Si	5.967	5.959	6.004	6.018	5.969	6.044	6.023	6.021	6.008
Ti	0.111	0.088	0.097	0.105	0.122	0.134	0.105	0.125	0.114
Cr	0.219	0.468	0.138	0.054	0.202	0.187	0.205	0.184	0.223
Al	3.478	3.304	3.595	3.632	3.482	3.570	3.495	3.527	3.540
Fe	1.119	1.378	1.064	1.357	1.180	1.205	1.124	1.142	1.133
Mg	4.422	3.977	4.275	4.126	4.331	4.034	4.295	4.257	4.167
Mn	0.046	0.064	0.050	0.051	0.048	0.050	0.048	0.042	0.055
Ca	0.700	0.809	0.797	0.671	0.717	0.707	0.705	0.678	0.743
Na	0.023	0.042	0.026	0.040	0.032	0.027	0.047	0.048	0.025
Total	<u>16.085</u>	<u>16.089</u>	<u>16.046</u>	<u>16.054</u>	<u>16.083</u>	<u>15.958</u>	<u>16.047</u>	<u>16.024</u>	<u>16.008</u>
Ca/(Ca+Mg)	0.137	0.169	0.157	0.140	0.142	0.149	0.141	0.137	0.151
Mg/(Mg+Fe)	0.798	0.743	0.801	0.753	0.786	0.770	0.793	0.788	0.786
n	3	4	3	2	3	3	1	3	1

* total iron expressed as FeO

Table 8 (con't)

Specimen:	<u>214C</u>	<u>215A</u>	<u>215B</u>	<u>215C</u>	<u>215D</u>	<u>216A</u>	<u>216B</u>	<u>216C</u>
SiO ₂	42.23	41.54	41.49	41.31	41.99	41.97	41.98	41.92
TiO ₂	0.97	1.14	0.97	1.00	1.09	1.05	0.96	1.03
Cr ₂ O ₃	1.14	2.11	1.42	3.66	2.02	1.35	1.19	1.42
Al ₂ O ₃	21.51	20.59	21.18	19.45	20.99	21.51	21.83	21.26
*FeO	10.32	9.27	9.95	8.45	9.21	10.42	9.48	10.29
MgO	19.66	19.44	20.06	19.25	19.60	19.01	19.94	18.62
MnO	0.43	0.32	0.40	0.42	0.28	0.40	0.36	0.40
CaO	4.63	4.55	4.55	5.20	4.67	4.65	4.45	4.74
Na ₂ O	0.14	0.16	0.13	0.08	0.10	0.08	0.15	0.10
Total	<u>101.03</u>	<u>99.12</u>	<u>100.15</u>	<u>98.82</u>	<u>99.95</u>	<u>100.44</u>	<u>100.34</u>	<u>99.78</u>

Cations based on twenty-four (24) oxygens

Si	6.006	6.014	5.958	6.021	6.019	6.008	5.986	6.040
Ti	0.104	0.124	0.105	0.110	0.117	0.113	0.103	0.112
Cr	0.128	0.241	0.162	0.422	0.229	0.153	0.134	0.162
Al	3.608	3.516	3.585	3.343	3.549	3.632	3.670	3.612
Fe	1.229	1.123	1.195	1.030	1.105	1.248	1.131	1.241
Mg	4.169	4.198	4.295	4.184	4.190	4.059	4.241	4.001
Mn	0.052	0.039	0.049	0.052	0.034	0.048	0.043	0.048
Ca	0.706	0.706	0.701	0.812	0.718	0.713	0.680	0.732
Na	0.038	0.044	0.035	0.023	0.027	0.023	0.041	0.028
Total	<u>16.041</u>	<u>16.005</u>	<u>16.085</u>	<u>15.997</u>	<u>15.998</u>	<u>15.997</u>	<u>16.029</u>	<u>15.976</u>
Ca/(Ca+Mg)	0.145	0.144	0.140	0.163	0.146	0.149	0.138	0.155
Mg/(Mg+Fe)	0.772	0.789	0.782	0.802	0.791	0.765	0.789	0.763
n	4	4	2	4	4	1	3	3

* total iron expressed as FeO

Table 8 (con't)

Specimen:	<u>217A</u>	<u>217B</u>	<u>217C</u>	<u>220A</u>	<u>220B</u>	<u>220C</u>	<u>221A</u>	<u>221C</u>
SiO ₂	40.45	42.54	41.67	41.70	41.56	41.83	41.60	41.91
TiO ₂	0.53	0.92	1.02	0.95	0.94	0.95	0.97	0.99
Cr ₂ O ₃	0.06	0.56	1.77	1.70	2.09	1.79	2.96	1.85
Al ₂ O ₃	23.06	22.06	20.95	21.21	20.74	20.98	20.14	20.66
*FeO	13.88	8.61	9.50	9.60	8.95	9.72	8.71	9.97
MgO	11.95	21.91	20.06	20.08	20.49	20.16	19.78	19.35
MnO	0.29	0.31	0.36	0.36	0.29	0.32	0.42	0.33
CaO	10.16	4.22	4.59	4.54	4.42	4.48	4.95	4.52
Na ₂ O	0.12	0.06	0.11	0.16	0.09	0.11	0.09	0.12
Total	<u>100.50</u>	<u>101.19</u>	<u>100.03</u>	<u>100.30</u>	<u>99.57</u>	<u>100.34</u>	<u>99.62</u>	<u>99.70</u>

Cations based on twenty-four (24) oxygens

Si	5.946	5.974	5.980	5.969	5.979	5.985	6.002	6.041
Ti	0.059	0.097	0.110	0.102	0.102	0.103	0.105	0.107
Cr	0.007	0.063	0.200	0.193	0.238	0.202	0.337	0.211
Al	3.998	3.654	3.546	3.581	3.519	3.541	3.427	3.512
Fe	1.708	1.012	1.140	1.149	1.078	1.164	1.052	1.203
Mg	2.621	4.590	4.294	4.287	4.397	4.302	4.257	4.161
Mn	0.036	0.036	0.044	0.043	0.036	0.039	0.051	0.040
Ca	1.601	0.636	0.706	0.697	0.682	0.687	0.765	0.698
Na	0.034	0.015	0.032	0.045	0.024	0.030	0.027	0.033
Total	<u>16.010</u>	<u>16.077</u>	<u>16.052</u>	<u>16.066</u>	<u>16.055</u>	<u>16.053</u>	<u>16.023</u>	<u>16.006</u>
Ca/(Ca+Mg)	0.379	0.122	0.141	0.140	0.134	0.138	0.152	0.144
Mg/(Mg+Fe)	0.605	0.819	0.790	0.789	0.803	0.787	0.802	0.776
n	2	1	4	3	4	3	1	1

* total iron expressed as FeO

Table 8 (con't) - compositions of garnet nodules and clinopyroxene inclusions

Specimen:	<u>225C</u>		<u>226A</u>		<u>226D</u>	
	cpx	gnt	cpx	gnt	cpx	gnt
SiO ₂	54.17	41.73	54.36	42.19	54.61	41.85
TiO ₂	0.14	0.35	0.26	0.42	0.14	0.38
Cr ₂ O ₃	1.42	4.13	1.70	3.76	0.86	2.40
Al ₂ O ₃	2.06	21.28	2.61	21.45	2.29	21.56
*FeO	2.83	7.24	2.92	7.14	2.65	7.19
MgO	18.42	20.33	17.75	21.02	18.67	21.52
MnO	0.08	0.40	0.08	0.36	0.07	0.40
CaO	18.85	4.80	18.11	4.33	19.64	4.43
Na ₂ O	1.74	0.02	2.55	0.03	1.76	0.09
Total	<u>99.71</u>	<u>100.28</u>	<u>100.34</u>	<u>100.70</u>	<u>100.69</u>	<u>99.82</u>

Cations based on six (clinopyroxene) and
twenty-four (garnet) oxygens

Si	1.962	5.947	1.957	5.966	1.958	5.959
Ti	0.004	0.037	0.007	0.044	0.004	0.041
Cr	0.041	0.466	0.048	0.421	0.024	0.270
Al	0.088	3.577	0.111	3.577	0.097	3.620
Fe	0.086	0.864	0.088	0.845	0.079	0.857
Mg	0.995	4.321	0.953	4.433	0.998	4.571
Mn	0.003	0.048	0.003	0.043	0.002	0.048
Ca	0.732	0.733	0.699	0.657	0.755	0.676
Na	<u>0.122</u>	<u>0.005</u>	<u>0.178</u>	<u>0.008</u>	<u>0.122</u>	<u>0.025</u>
Total	<u>4.033</u>	<u>15.998</u>	<u>4.044</u>	<u>15.994</u>	<u>4.039</u>	<u>16.067</u>
Ca/(Ca+Mg)	0.424	0.145	0.423	0.129	0.431	0.129
Mg/(Mg+Fe)	0.920	0.833	0.915	0.840	0.927	0.842
n	3	3	4	6	1	3

* total iron expressed as FeO

the mineral chemical cluster analysis criteria developed for kimberlitic garnets by Dawson and Stephens (1975) and correspond to their groups #1 (5 nodules), 2 (32 nodules), 3 (1 nodule), and 9 (8 nodules) designated as titanian pyrope, high-titanium pyrope, calcic pyrope-almandine, and chrome pyrope respectively (see Dawson and Stephens, 1976). Excluding nodule #217A which plots alone in group #3 of the Dawson and Stephens (1975, 1976) classification, most of the Orapa garnets are remarkably similar in chemical composition, with MgO and Al₂O₃ varying throughout the suite from 18.09 to 21.96 wt. % and from 19.28 to 22.38 wt. % respectively. Total iron (expressed as FeO) and CaO are the next most abundant components, averaging 9.39 and 4.68 wt. % respectively. Values of Cr₂O₃ range from 0.36 to 4.13 wt. % and, considered together with the other suggested parameters TiO₂ content, CaO content, and atomic ratio Mg/(Mg+Fe), indicate an overall close compositional similarity between these Orapa nodules and the chrome-poor garnet nodule suite from Colorado-Wyoming (Eggler et al., 1979).

Average compositions for individual Orapa garnet nodules are plotted in terms of the major A-site components Ca-Mg-Fe in Figure 21, defining an elongate field oriented parallel to the Mg-Fe sideline at approximately 12% Ca component. This compositional field is quite similar to those characterizing garnet nodule suites from the widely separated localities of Colorado-Wyoming (Eggler et al., 1979), the Monastery mine in South Africa (Gurney et al., 1979), a number of widely scattered pipes in South Africa and Lesotho (Nixon and Boyd, 1973a), and the Artur De Paiva kimberlite pipe in Angola (Boyd and Danchin, 1974).

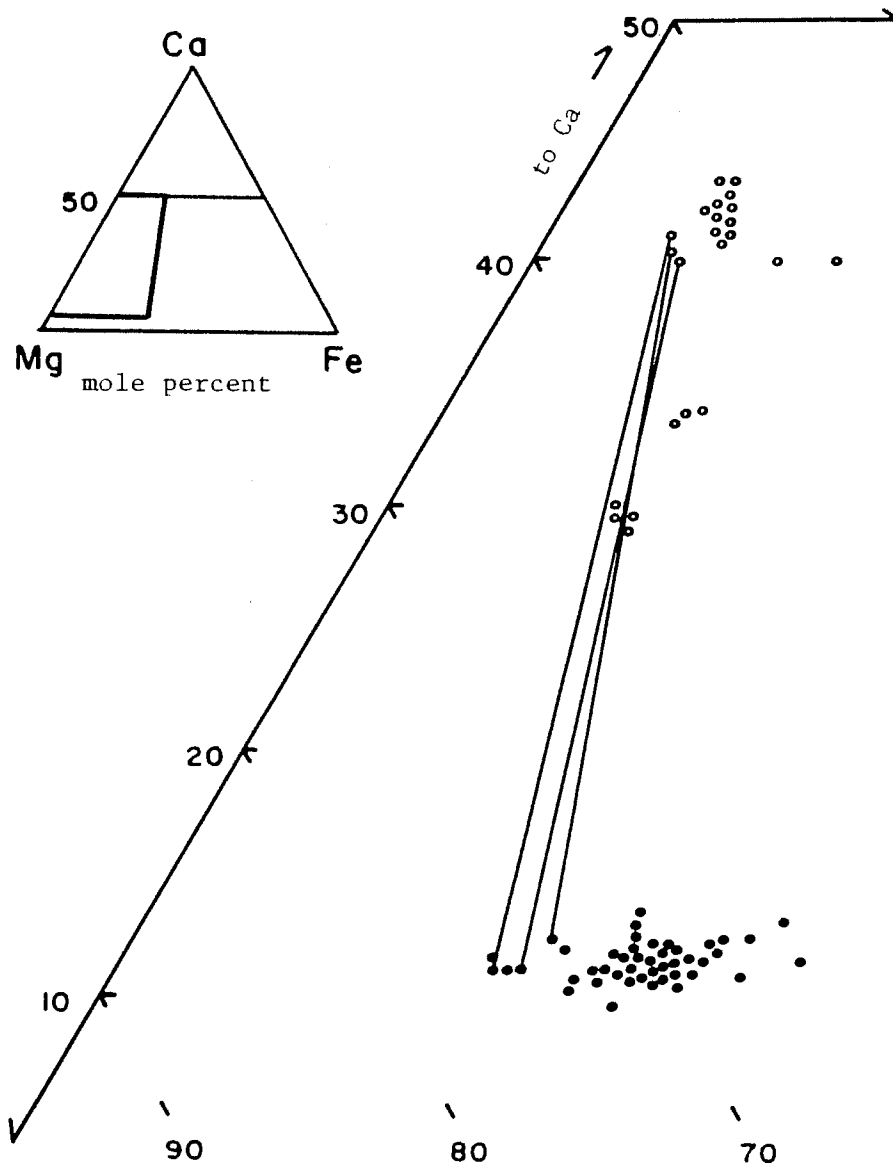


Figure 21: Compositions of garnet discrete nodule suite from Orapa (solid circles) plotted in terms of mole percent Ca-Mg-Fe. The compositions of selected clinopyroxene discrete nodules from Orapa (open circles) have been plotted for comparison. The tie lines connect individual garnet-clinopyroxene inclusion pairs.

The relationship between $Mg/(Mg+Fe)$ ratio and Cr_2O_3 content has been used by several authors (Eggler et al., 1979; Gurney et al., 1979) in order to demonstrate chemical trends characteristic of garnet nodule suites from kimberlites. These data for the Orapa nodules are plotted in Figure 22 and compared to similar data taken from the literature for nodules from Colorado-Wyoming (Eggler et al., 1979) and a variety of localities in South Africa and Lesotho (Nixon and Boyd, 1973a, 1973c; Gurney et al., 1979). The Orapa data show considerable overlap with both suites in this plot and are characterized by the same general increase in Cr_2O_3 content with increasing $Mg/(Mg+Fe)$ ratio. Titanium, on the other hand, demonstrates the opposite behavior (Figure 23), increasing with decreasing $Mg/(Mg+Fe)$ ratio in the Orapa garnets which again overlap considerably with the South Africa-Lesotho compositional field. Similar data are not available for the Colorado-Wyoming nodule suite, however. Considering the known geochemical behavior of these elements in magmatic systems, both trends appear to be compatible with garnet interaction with fractionating liquids prior to incorporation in the enclosing kimberlite.

Orapa garnet nodules #225C, 226A, and 226D each contain a prominent light-green clinopyroxene inclusion near the center. Average chemical compositions of the coexisting phases in these nodules are presented at the end of Table 8. The three garnets bearing these inclusions are generally similar in chemical composition but, as a group, are somewhat distinct from the majority of the garnet suite, plotting at the magnesian end of the compositional trend in Figure 21 and at the inferred high temperature ends of the Cr_2O_3 vs $Mg/(Mg+Fe)$ and TiO_2 vs $Mg/(Mg+Fe)$

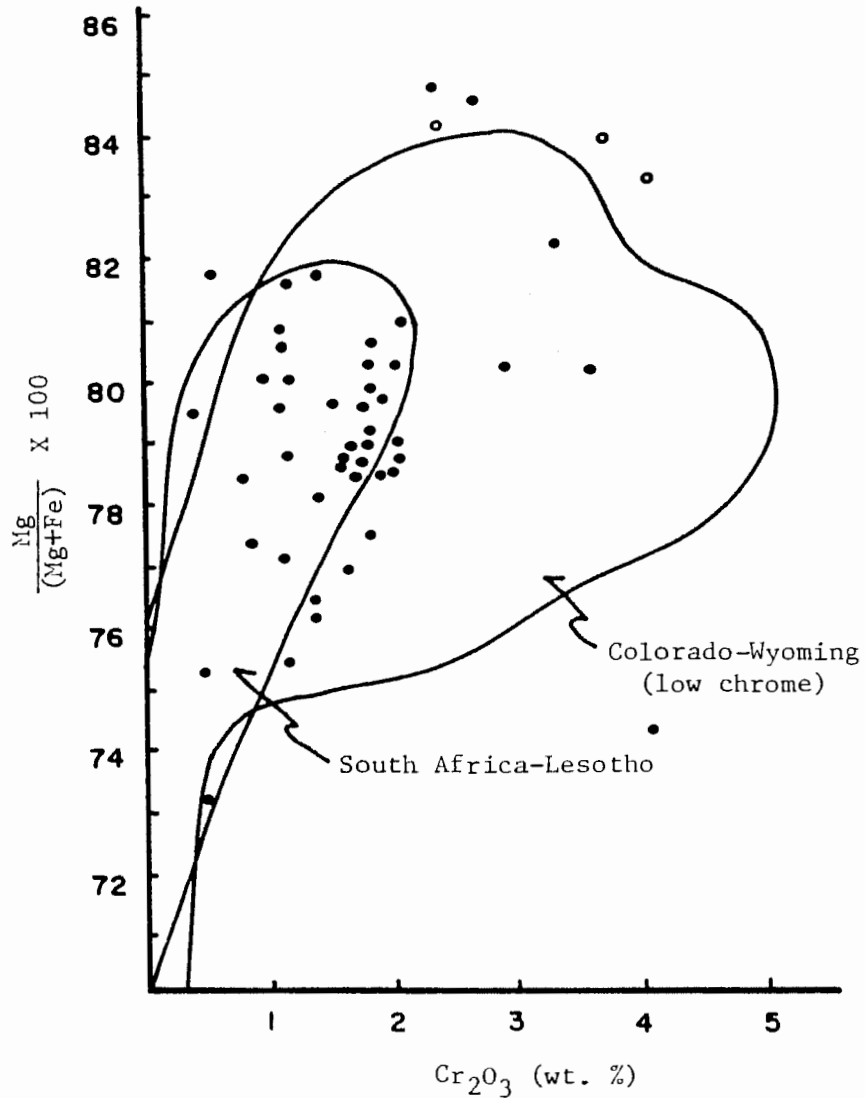


Figure 22: Compositions of the garnet discrete nodule suite from Orapa (solid circles) plotted as a function of chrome content versus Mg/(Mg+Fe) ratio. The large open circles represent garnet nodules from Orapa with clinopyroxene inclusions. The compositional field for similar garnet discrete nodules from South Africa-Lesotho and Colorado-Wyoming (points not shown for clarity) are outlined and labelled for comparison. See text for references and discussion.

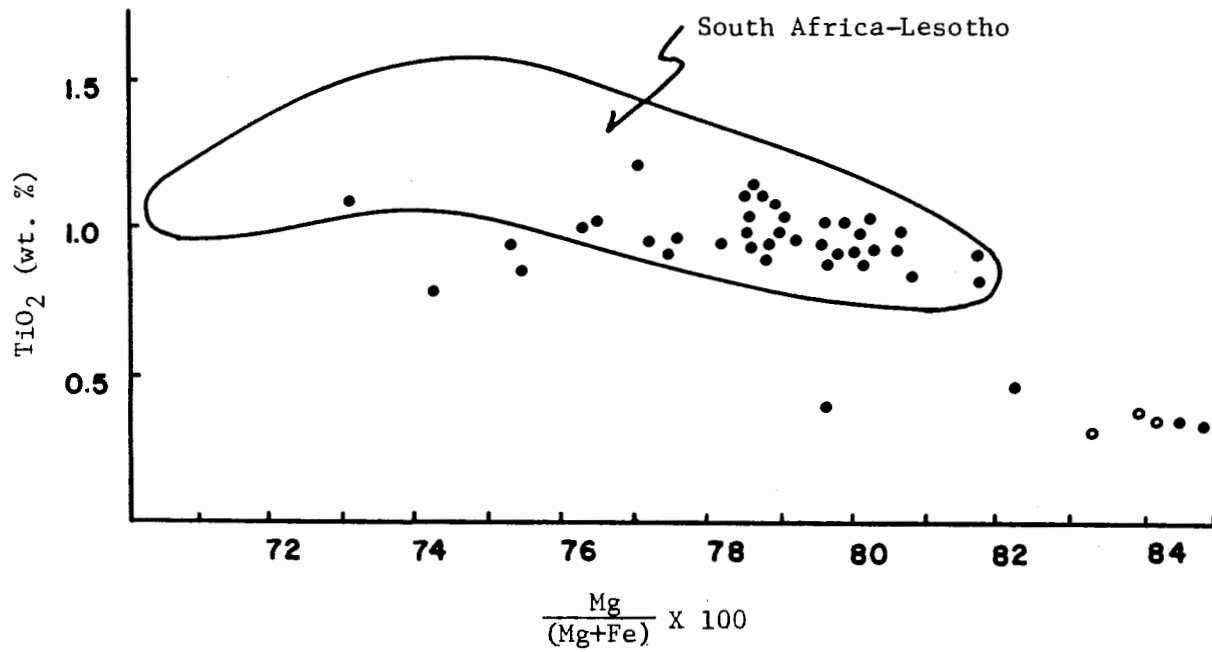


Figure 23: Plot of Mg/(Mg+Fe) ratio versus TiO₂ content for the garnet discrete nodule suite from Orapa (solid circles). The large open circles represent garnet nodules from Orapa with clinopyroxene inclusions. The compositional field for garnet nodules from South Africa-Lesotho is outlined and labelled for comparison. See text for references and discussion.

trends in Figures 22 and 23 respectively. The clinopyroxene inclusions may be classified as diopsides according to the chemical criteria of Stephens and Dawson (1977) and correspondingly plot adjacent to the relatively Ca-rich group of Orapa pyroxene nodules in Figure 21. These inclusions are similar to their garnet hosts in that they are also characterized by relatively high Mg/(Mg+Fe) ratios, and by higher values of Cr₂O₃ and lower values of TiO₂ than their corresponding group of inclusion-free monomineralic nodules.

Although garnet nodules containing pyroxene inclusions are probably not uncommon in kimberlites, published data regarding such occurrences are relatively scarce. Gurney et al. (1979) briefly described two such nodules from the Monastery pipe, but did not present detailed geochemical data. Other occurrences for which geochemical data are available include at least two discrete nodules from Lesotho (Kresten, 1973; Nixon and Boyd, 1973a) and at least one other from Colorado-Wyoming (Smith et al., 1976). In general, the three Orapa intergrowths are chemically quite distinct from those reported from South Africa and Lesotho. Both the garnet and clinopyroxene from Orapa are two to four times richer in Cr₂O₃. The garnet from Orapa is characterized by higher Mg/(Mg+Fe) ratios and lower TiO₂ values than the host garnets from the other localities and the Orapa clinopyroxenes are typically higher in both Mg/(Mg+Fe) ratios and Na₂O contents than the corresponding inclusions. Coexisting garnet and clinopyroxene from Colorado-Wyoming are typically intermediate in composition between those from Orapa and South Africa-Lesotho except that the Colorado-Wyoming garnet is almost identical to the Orapa garnet in Mg/(Mg+Fe) ratio and the Colorado-Wyoming pyroxene contains

less Na_2O than any from the other localities.

Temperatures of equilibration for such intergrowths may be estimated from the $\text{Ca}/(\text{Ca}+\text{Mg})$ ratio of the clinopyroxene (Davis and Boyd, 1966; Lindsley and Dixon, 1976) and by use of the MgO/FeO distribution coefficient calculated for the coexisting garnet and clinopyroxene phases (Akella and Boyd, 1974). Temperatures determined for four nodules from South Africa and Lesotho, using data from Gurney et al. (1979, p. 237), Nixon and Boyd (1973a, p. 68), and Kresten (1973, p. 162) are remarkably consistent between localities, varying from 1315 to 1375°C using the 30 kb pyroxene solvus of Davis and Boyd (1966) and from 1280 to 1366°C using the K_D method of Akella and Boyd (1974). Data for an intergrowth from Colorado-Wyoming (Smith et al., 1976, p. 543) indicate a diopside solvus temperature of 1270°C and an estimate of approximately 1300°C using garnet-clinopyroxene partitioning data. Temperatures calculated for the Orapa nodules are consistently lower, but still show reasonable agreement between the two methods with ranges of 1115-1130°C (pyroxene solvus) and 1156-1215°C (MgO/FeO K_D). Although internally consistent, these relatively low temperatures calculated from the Orapa data are somewhat surprising in view of the relatively unevolved nature of any magmatic liquids which might be inferred to have been in equilibrium with these garnet nodules on the basis of their characteristically high $\text{Mg}/(\text{Mg}+\text{Fe})$ ratios, high Cr_2O_3 contents, and low TiO_2 values. It should be emphasized that all of the temperature estimates calculated for these nodules using the Akella and Boyd (1974) geothermometer assume $\text{Fe}^{2+} = \text{Fe}_{\text{total}}$ and as such probably represent maximum values.

Unlike the associated clinopyroxene nodules, the garnet nodule suite from Orapa appears to define a single geochemical group with specific compositional limits. In terms of the characteristic parameters $Mg/(Mg+Fe)$ ratio and Cr_2O_3 and TiO_2 content, the Orapa suite is quite similar to garnet nodules from South Africa (Gurney et al., 1979), Lesotho (Kresten, 1973; Nixon and Boyd, 1973a, 1973c), and Colorado-Wyoming (Eggler et al., 1979) and in general reflects the same compositional trends typical of garnet nodules from these localities. Only Orapa nodule #217A is clearly divergent from these trends and appears, on the basis of compositional parameters such as Cr_2O_3 , FeO, and MgO contents (Table 8), to be paragenetically distinct from the remainder of the Orapa garnet nodule suite. It may be possible, however, that the remainder of the garnet suite is linked petrogenetically to the diopside subgroup of the pyroxene nodule suite on the basis of the compositional similarity between the pyroxene inclusions in garnet and that group of pyroxene nodules. If this is so, then it would appear that the closest approximation to a possible equilibrium temperature range characteristic of these garnet and clinopyroxene nodules prior to incorporation in the kimberlite is that calculated from the garnet-clinopyroxene-inclusion pairs and not that obtained from the pyroxene nodules, which may have themselves undergone a subsequent temperature re-equilibration from which the pyroxene inclusions were thermally insulated. The problems inherent in such an interpretation can be far-reaching in that it is implied that the Orapa kimberlite may have incorporated clinopyroxene crystals at a minimum of two, and possibly three, different levels of intrusion, at only one of which garnets were included. Also inherent

is the dilemma of why apparently only the diopside nodule subgroup shows the effects of probable temperature re-equilibration in a system inferred to contain at least several groups of other temperature-sensitive coexisting phases.

Knorringite Garnet-Clinopyroxene-Chromite
Intergrowth

A single discrete nodule composed primarily of highly fractured green garnet with locally irregular patches of intergrowth chromium-bearing diopside and chromite has been recovered and examined in detail. This smooth-surfaced, slightly ovoid nodule is approximately 1 cm in average cross-sectional diameter and characterized by a dark green to nearly black color in hand specimen. The irregular pattern and distribution of the intergrown phases is apparent in Figure 24, a detailed drawing of a thin section through the nodule. Mineralogic alteration is developed locally throughout the nodule, occurring both as fine-grained, possibly kelephytic intergrowths along fractures and selected areas of the nodule periphery, and as light-colored, extremely fine-grained patches spatially related to intergrown clinopyroxene and chromite. The extremely fine-grained, irregular texture and possibly polymineralic composition of this latter type of alteration make petrographic and geochemical characterization imprecise, especially in view of the limited amount of material present.

Viewed in thin section under plane-polarized light, the nodule is characterized by the strong light green coloration of the host garnet which, when examined under crossed polars, displays a slight

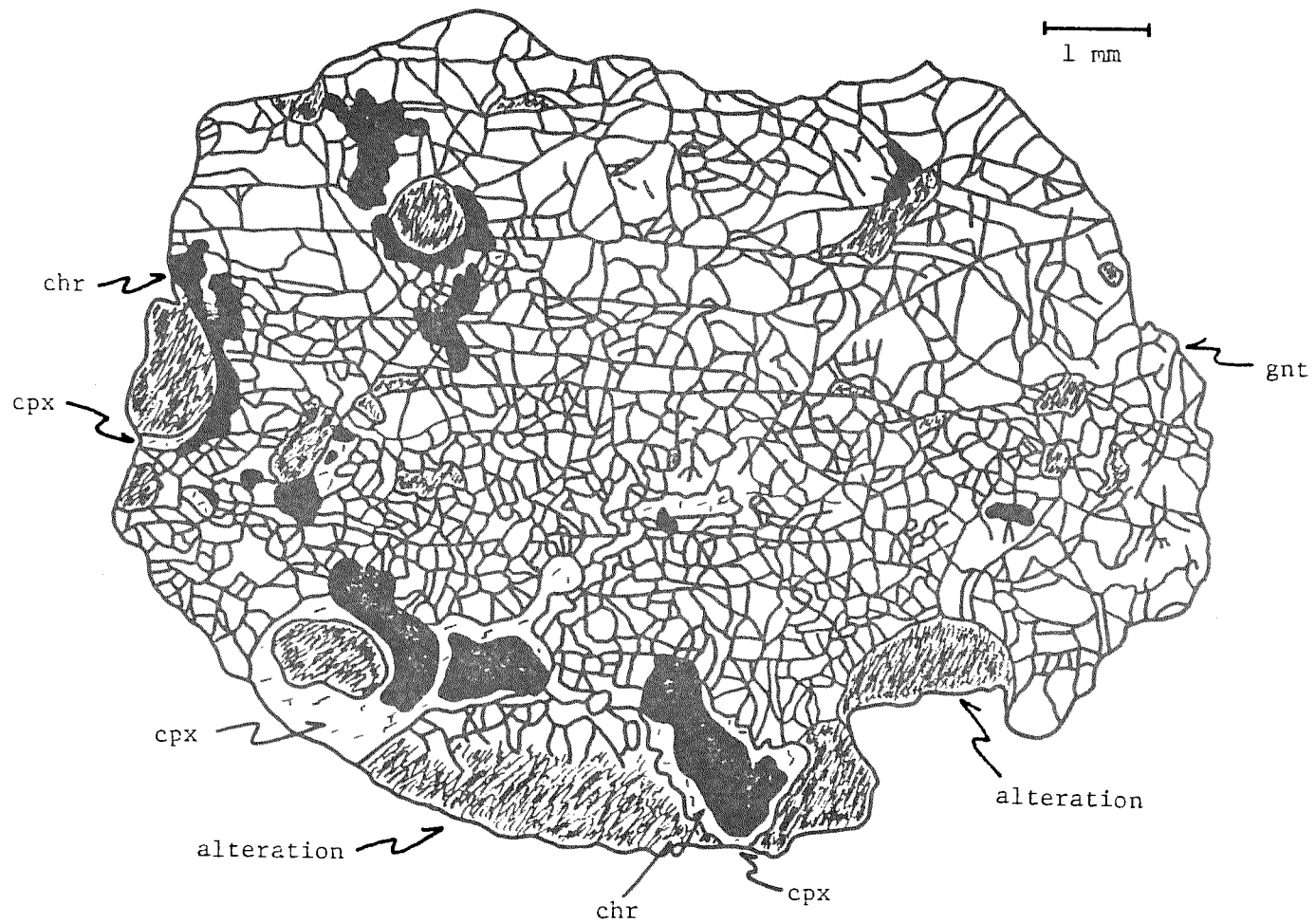


Figure 24: Detailed drawing of a thin section through Orapa nodule #431 composed of green garnet intergrown with clinopyroxene and chromite.

birefringence as the stage is rotated. As stated above, the clinopyroxene and chromite are irregular in both texture and distribution within the garnet, with the size of the individual polymineralic intergrowth patches averaging 1-2 mm in cross-section. Clinopyroxene and chromite are typically present together in isolated intergrowths with the silicate most commonly surrounding the oxide. Throughout the nodule, however, both phases can be observed to be in local contact with the garnet and, in several locations, either clinopyroxene or chromite may be isolated singly within the green garnet host. Rounded patches of the light-colored alteration occur locally within the cores of several isolated intergrowths, surrounded by either clinopyroxene or chromite, or both.

Average chemical compositions determined by electron microprobe analyses of the garnet, clinopyroxene, and chromite coexisting in this nodule are presented in Table 9. The oxide phase, containing an average of 57.46 wt. % Cr_2O_3 , is a chromium spinel with a composition which plots near the base of the modified multicomponent spinel prism (see Haggerty, 1976, p. Hg-105) close to the MgCr_2O_4 - FeCr_2O_4 join, indicating that it may be best described as a slightly aluminous picrochromite solid solution. Although characterized by rather high values of both Cr_2O_3 and MgO , this composition is not without precedent in the kimberlitic literature, falling near the chromium- and magnesium-rich ends of cation compositional plots compiled by Haggerty (1979a) for spinels from a variety of xenoliths in kimberlite.

The clinopyroxene from this intergrowth is a relatively chromium-rich variety which corresponds in overall composition to cluster #6,

Table 9: Average chemical compositions of coexisting garnet, clinopyroxene, and chromite from Orapa nodule #431.

	<u>garnet</u>	<u>pyroxene</u>	<u>chromite</u>
SiO ₂	39.42	54.64	NA
TiO ₂	0.25	0.09	1.27
Cr ₂ O ₃	15.93	4.89	57.46
Al ₂ O ₃	12.22	1.90	6.71
Fe ₂ O ₃	-	-	6.96'
FeO	6.56*	2.60*	13.64
MgO	16.89	16.04	12.94
MnO	0.57	0.10	0.48
CaO	8.91	16.19	NA
Na ₂ O	0.02	3.25	NA
NiO	NA	NA	0.13
Total	<u>100.77</u>	<u>99.70</u>	<u>99.59</u>
Cations based on () oxygens			
	(24)	(6)	(32)
Si	5.896	1.984	-
Ti	0.028	0.002	0.253
Cr	1.884	0.140	12.018
Al	2.155	0.081	2.094
*Fe ³⁺	-	-	1.382
Fe ²⁺	0.821	0.079	3.020
Mg	3.769	0.869	5.098
Mn	0.072	0.003	0.108
Ca	1.428	0.630	-
Na	0.005	0.229	-
Ni	-	-	0.027
Total	<u>16.058</u>	<u>4.017</u>	<u>24.000</u>
Ca/(Ca+Mg)	0.275	0.420	-
Mg/(Mg+Fe)	0.821	0.917	0.628
n	2	4	3

NA: not analyzed

* total iron expressed as FeO

' calculated

designated as ureyitic diopside in the mineral chemical classification developed by Stephens and Dawson (1977) for kimberlitic pyroxenes. This phase is similar in many compositional parameters to the majority of the clinopyroxene discrete nodules already described from Orapa, South Africa-Lesotho, and Colorado-Wyoming except for relatively high values of Na_2O and Cr_2O_3 . This pyroxene composition again indicates a substantial presence of "Others" components (Papike et al., 1974) in the monoclinic structure which stoichiometric calculations (Table 9) suggest may be dominated by the $\text{Na}^{1+}\text{Cr}^{3+}$ cation couple.

The green garnet comprising the bulk of this intergrowth is perhaps the most noteworthy phase in terms of composition. It is characterized by average values for Cr_2O_3 and CaO of 15.93 and 8.91 wt. % respectively, corresponding to cluster #12, designated as knorringitic uvarovite-pyrope in the mineral chemical classification developed for kimberlitic garnets by Dawson and Stephens (1975; 1976). This suggested nomenclature is verified by stoichiometric calculations (Table 9) which clearly indicate the importance of $\text{Cr}^{3+}\text{-Al}^{3+}$ mutual substitution in the octahedrally-coordinated B garnet sites, accompanied by substitution of Mg^{2+} , Ca^{2+} , and relatively minor amounts of Fe^{2+} in the larger A cation sites of the structure. The significance of this particular chemical composition is underscored by end member calculations based on the relative proportions of the grossular, uvarovite, pyrope, and knorringite molecules and which indicate that the $\text{Mg}^{2+}\text{Cr}^{3+}$ (knorringite) couple is present as a minimum of 23 mole %. The importance of this substitution is further supported by the remarkable similarity between the chemical composition of this Orapa specimen and that of the bluish-green garnet from the Kao

kimberlite pipe which was cited by Nixon and Hornung (1968) in their original description of a natural occurrence containing a substantial amount of this substitutional couple.

Green garnets are extremely rare in kimberlites and kimberlite-related intrusions, with Orapa marking only the fifth locality in the world from which they have been reported. This Orapa specimen is, however, the first unequivocal occurrence of green garnet comprising most of a recognizable discrete nodule. Figure 25 is a summary plot of Cr_2O_3 wt. % vs $(\text{CaO}+\text{MgO})$ wt. % for garnets from the most common kimberlite-related xenolithic and xenocrystic parageneses: low-chrome discrete nodules (Nixon and Boyd, 1973a, 1973b; Boyd and Danchin, 1974; Egger et al., 1979; Gurney et al., 1979; this study) peridotite nodules (Nixon and Boyd, 1973d; Carswell et al., 1979; MacGregor, 1979), and diamond inclusions (Sobolev et al., 1969; Meyer and Boyd, 1972). The compositional field for green garnets from Orapa (this study), the Kao kimberlite pipe in Lesotho (Nixon and Hornung, 1968; Hornung and Nixon, 1973), and the Newlands (Clarke and Carswell, 1977) and Premier (Scott and Skinner, 1979) pipes in South Africa defines a broad region characterized by consistently high chrome contents and generally variable $(\text{CaO}+\text{MgO})$ values. It is apparent from this plot that such green garnets are compositionally unique in kimberlitic systems and that only the most chrome-rich garnet inclusions in diamonds are characterized by comparable chrome contents. Not shown in Figure 25 are the relatively uncommon chrome-rich garnet discrete nodules from Colorado-Wyoming (Egger et al., 1979) and a suite of variable CaO, generally high Cr_2O_3 garnets recovered from the mine concentrates of several kimberlites in Yakutia (Sobolev

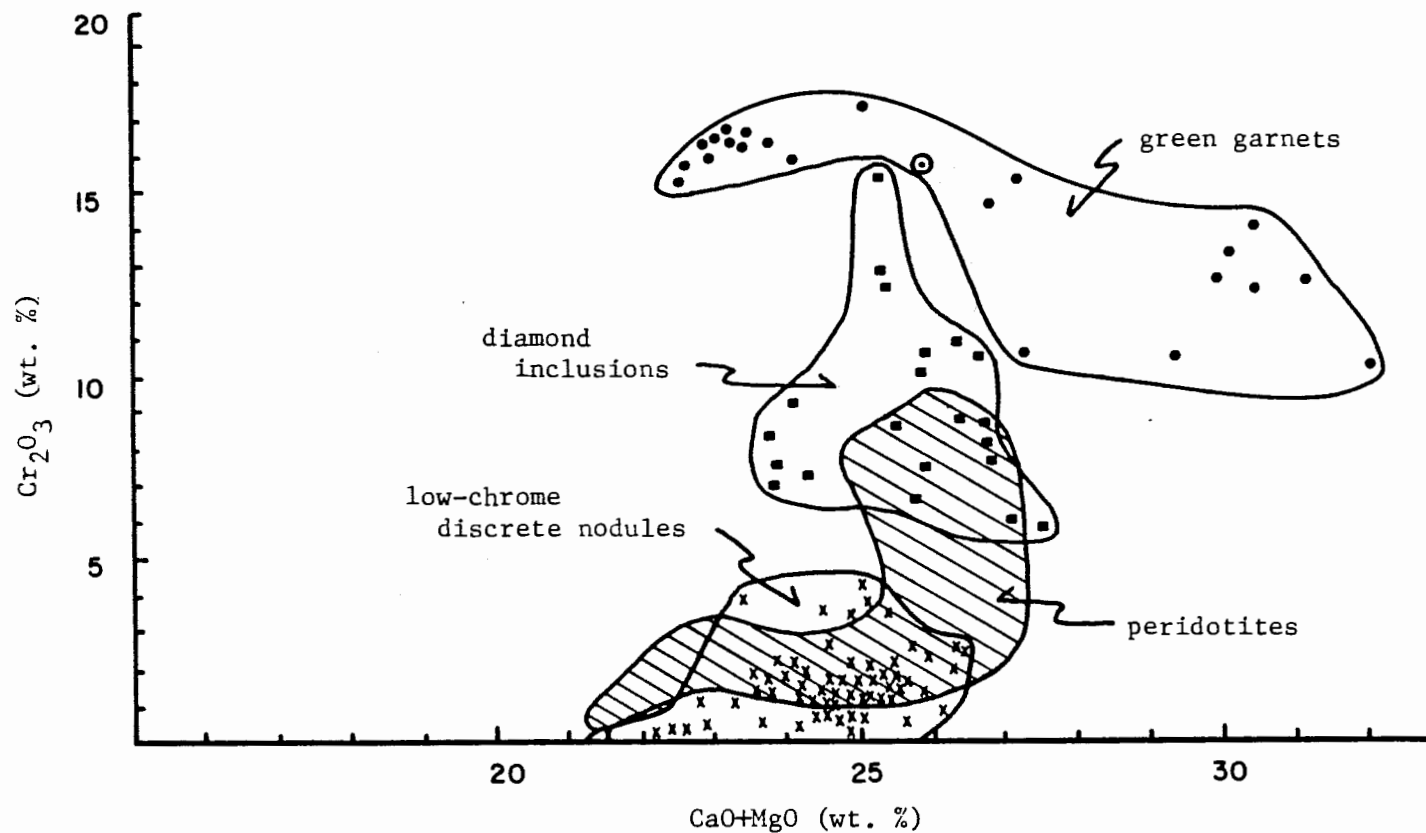


Figure 25: Summary plot of $(\text{CaO}+\text{MgO})$ content versus Cr_2O_3 content for kimberlitic green garnets (solid circles), garnet inclusions in diamonds (squares), garnets from peridotite xenoliths in kimberlite (lined field), and low-chrome garnet discrete nodules (x-shapes). The Orapa green garnet point is circled. See text for references and discussion.

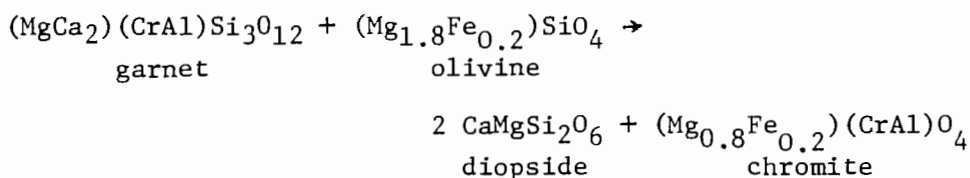
et al., 1973). Although variable in composition, these two suites show considerable overlap with the lower part of the diamond inclusion field and with the more chromium-rich garnets from peridotite xenoliths.

The only previously documented analogue to this chromium-rich, polymineralic intergrowth from Orapa is a single discrete nodule recovered from Letseng-La-Terae and briefly described by Bloomer and Nixon (1973). These authors characterize this nodule as consisting "solely of vivid green chromium diopside with subordinate kelephitized lilac Cr-rich pyrope and chromite" (p. 29), but do not describe any of the textural details. In addition to having a probably much greater clinopyroxene/garnet modal ratio, this assemblage also differs from the Orapa intergrowth in that the individual phases are consistently less rich in chrome, with the garnet, clinopyroxene and chromite characterized by 11.22, 3.71, and 50.36 wt. % Cr_2O_3 , respectively.

Any model for the paragenesis of such intergrowths must take into consideration the detailed textural relations of the nodule, the characteristic chemical compositions of the constituent phases, and the extraordinary bulk composition of the environment of formation implied by these phases. Viewed in these terms, the Orapa intergrowth appears to offer unique evidence of deep-seated petrogenetic processes but, at the same time, is characterized by certain parameters which appear to be nevertheless geologically perplexing. The chromium-rich composition of the garnet in the Orapa specimen is certainly noteworthy and, if modelled in terms of a possible igneous event, may indicate that the host formed as an early liquidus phase, perhaps accompanied by olivine, during the fractional crystallization of an as yet unspecified, but

possibly proto-kimberlitic magma at considerable depth in the mantle. Evidence for such crystalline residua from the mantle is extremely rare, but may be preserved in such xenoliths as the diamondiferous garnet dunitites reported by N.V. Sobolev et al. (1969, 1973) from Yakutia although, in this case, the garnets were not particularly rich in chromium. The depth of such a proposed origin cannot be determined directly from the available data. However, the similarity in chrome content between the green garnet of this intergrowth and garnet inclusions in diamond (Figure 25) suggests that this could have been a deep-seated event possibly occurring within the diamond stability field.

The development of coexisting clinopyroxene and chromite in this intergrowth is interpreted on the basis of textural evidence to post-date formation of the garnet. Such an event may have occurred at somewhat lower pressure and have involved at least partial subsolidus decomposition of the original garnet phase. Calculations indicate that the chemical compositions of the coexisting minerals in this intergrowth necessitate the presence of at least one other phase in order to produce clinopyroxene and chromite and, on the basis of a variety of geochemical and theoretical data (MacGregor, 1970) and the relative abundance of mineral inclusions in diamond (Meyer and Boyd, 1972; Harris and Gurney, 1979), this phase is inferred to have been olivine. Such subsolidus decomposition may have occurred in a manner similar to the following reaction:



in which clinopyroxene and chromium spinel are produced by reaction of a uvarovite-pyrope solid solution and forsteritic olivine. Such a reaction would be similar to the more familiar forsterite + grossular-pyrope = diopside + spinel reaction studied by MacGregor (1970) in the system $\text{CaO-MgO-Al}_2\text{O}_3\text{-SiO}_2$ and inferred on the basis of several types of evidence to define the boundary between the spinel and garnet peridotite stability fields in the upper mantle (Green and Ringwood, 1970; MacGregor, 1970). Whether this nodule preserves such evidence for the mantle beneath Botswana during the Cretaceous is uncertain, especially in view of experimental work (MacGregor, 1970) indicating that, for bulk compositions rich in Cr_2O_3 , the boundary moves to higher pressures and becomes characterized by a broadening five-phase zone of transition involving both clinopyroxene and orthopyroxene. Although not yet studied in sufficient detail, this chromium bulk compositional effect leaves open the possibility that such subsolidus decomposition could also have occurred at pressures compatible with the diamond stability field as, in fact, the close compositional similarity between the clinopyroxene and chromite reaction products at Orapa and similar phases occurring as inclusions in diamonds (Meyer and Boyd, 1972; Harris and Gurney, 1979) would suggest. Nevertheless, regardless of the inferred depth of this subsolidus transformation, it appears texturally that the garnet-consuming reaction was abruptly terminated, possibly because olivine was no longer available for combination or because of fragmentation of the assemblage and transport to the crust in the kimberlite.

This proposed two-step model for the evolution of Orapa nodule #431 is, of course, inherently flawed in that the proposed generalized

reaction for garnet decomposition is not strictly applicable to the compositions determined from the intergrowth. In addition to this, the model also fails to account for the observed rather high Na_2O content of the clinopyroxene. On the other hand, the proposed early liquidus origin of the green garnet is supported by both the rather low TiO_2 content and low $(\text{Fe}+\text{Mn})/(\text{Fe}+\text{Mn}+\text{Mg})$ ratio characterizing the Orapa specimen and, in fact, the latter parameter is nearly identical with those determined for garnets occurring as inclusions in diamonds from Yakutia (Sobolev et al., 1970), one of which was found intergrown with chrome-rich clinopyroxene. The extreme scarcity of such intergrowths and uncommon occurrence of corresponding monomineralic nodules of comparable chrome-rich compositions is significant and may be indicative of, among other factors, the relatively limited occurrence and depth/spatial distribution of garnet/olivine differentiates in the mantle. This evidence may also illustrate a general tendency for chromian garnet decomposition reactions to go to completion so that we observe only the disaggregated high-chrome pyroxene and spinel equivalents at the surface in kimberlite mine concentrates.

C H A P T E R I V

ECLOGITE NODULES

Introduction

Eclogite nodules are the most common type of presumed mantle-derived xenoliths recovered from the Orapa A/K-1 site (Shee, 1978). Although peridotite suite rocks are generally much more common in kimberlites (Dawson, 1980), no olivine-bearing xenoliths have yet been reported from Orapa. Other localities characterized by a predominance of eclogite xenoliths include the Roberts Victor pipe in South Africa (Hatton, 1978) and the Zagadochnaya pipe in Yakutia (Sobolev et al., 1968).

Examined in hand specimen, individual eclogite nodules from Orapa are typically ovoid in shape, range between one and three centimeters in maximum diameter, and are characterized by an overall dull, mottled green and red color. Most of the more than fifty nodules examined contain large amounts of a soft, cream-colored, pyroxene alteration product which, in many nodules, has completely replaced the original clinopyroxene. For this reason, detailed analytical data are reported for only 14 nodules, while the reported textural data represent information from a slightly larger population including a number of nodules in which remnant textures may be discerned.

Petrography

The Orapa eclogite nodules may be divided texturally into foliated and non-foliated, or granular, groups (Table 10). The foliated varieties are comprised of generally anhedral to subhedral, elongate grains of

Table 10: Petrographic data for representative eclogite nodules from Orapa.

Nodule #	Textural Type	Average Grain Size (mm)		Mode (vol. %)							Group*	Remarks
		gnt	cpx	gnt	cpx	rut	ilm	amph	alt	gnt/cpx		
OR-102	foliated	2	2	40	50	<1	-	-	19	0.8	I	contains rutile and a single coarse graphite crystal
OR-102b	foliated	1	1	35	42	<1	-	-	22	0.8	I	contains rutile with sigmoidal ilmenite lamellae
OR-103	foliated	2-3	2-3	31	35	1	-	-	33	0.9	I	contains rutile
OR-103b	granular	2-3	2-3	52	16	<1	-	-	31	3.3	II	contains rutile, garnet with prominent kelyphite rims
OR-103c	granular	2	2	48	20	-	-	-	32	2.4	II	bimineralic
OR-104	granular	1	1	48	47	4	-	-	<1	1.0	I	contains rutile, trace zircon
OR-105	granular	1	1-2	46	27	-	-	<1	26	1.7	I	contains minor amphibole
OR-106	granular	<1	<1	43	47	<1	-	-	<10	0.9	II	contains rutile, overall granular-mosaic texture
OR-107	granular	2-5	2-4	35	32	-	-	-	33	1.1	I	bimineralic; coarse grain size
OR-108	granular	4	1-2	75	13	-	<1	-	<12	5.8	I	contains ilmenite
OR-109	granular	2-3	1	44	34	-	1	<1	20	1.3	I	contains ilmenite and minor amphibole
OR-110	granular	5	4	63	18	<1	-	-	18	3.5	I	contains rutile; small nodule with coarse grain size
OR-111	granular	5	7	40	43	-	2	-	15	0.9	I	contains ilmenite; small nodule with very coarse grain size
OR-114	granular	2-3	9	26	62	-	-	-	12	0.4	I	bimineralic, with very coarse-grained clinopyroxene

* MacGregor and Carter (1970)

pink garnet and green clinopyroxene oriented parallel to the plane of foliation. Although such nodules appear superficially similar to the sheared peridotites from Lesotho described by Boyd (1973), petrographic evidence of cataclasis is not present, and the closest textural analogues appear to be certain eclogites described from the Kao kimberlite pipe in Lesotho by MacGregor (1979). The granular nodules are more common at Orapa and are characterized by generally interlocking fabrics which range from fine-grained hypidiomorphic mosaics to poikilitic intergrowths in which medium-grained garnets are enclosed within coarse matrix pyroxene. The former type is similar to eclogite nodules reported from Kao by MacGregor (1979), while the poikilitic varieties are nearly identical to eclogites described from the Roberts Victor mine in South Africa by MacGregor and Carter (1970). These latter authors proposed a somewhat different textural classification based on their sampling of 48 coarse-grained eclogite nodules from the Roberts Victor mine. According to this classification, end member types include eclogites in which subhedral to rounded grains of garnet are set in an anhedral to interstitial matrix of clinopyroxene (Group I) and eclogites in which generally anhedral grains of garnet and clinopyroxene comprise a tightly interlocking fabric (Group II). In addition, further subdivision was based on large scale mineral segregation and layering observable in these large nodules. Although direct application of this classification scheme to the Orapa eclogites is difficult because of the generally variable grain size and small physical size of the nodules, an attempt has been made and the results are included in Table 10. Classified in this manner, most of the granular and all of the foliated nodules may be assigned

to Group I; however, it is believed that the generalized and descriptive classification proposed in this study will ultimately prove to be of greater value for such small, typically fine-grained nodules.

Examined in thin section, the garnets in the granular eclogites from Orapa are typically pale pink in color, subhedral, and completely isotropic with no hint of birefringence under crossed polars. Garnets from foliated nodules are similar except for their generally elongated form. In most nodules, the garnets are observably fresher than the coexisting pyroxenes; however, where present, the garnet alteration assemblage is characteristic and distinctive. Such alteration is typically fine-grained and limited to the grain peripheries where it is separated from the fresh garnet by a sharp contact oriented parallel to the original grain edge. The assemblage typically consists of fibrous, pale yellow to brown serpentine, pale green chlorite, and relatively minor, extremely fine grains of a pale-colored spinel(?). The serpentine is characteristically developed adjacent and oriented perpendicular to the contact with the fresh garnet, and generally grades rather abruptly into the chlorite which dominates modally at greater distances from the primary mineral. The oxide in this assemblage is never more than a minor phase although, where present, it is generally developed throughout the intergrowth. It should be noted that this alteration assemblage is mineralogically distinct from the microcrystalline "kelephyte" alteration rinds which are typically developed around kimberlitic garnets and which are composed of the assemblage spinel + phlogopite + chlorite + amphibole ± plagioclase (Dawson, 1980).

Observed in thin section, pyroxenes from the granular eclogites are generally subhedral and characterized by an overall pale green color and faint pleochroism. Individual grains appear to be homogeneous with no observable evidence of exsolution lamellae or other types of intergrowths. Pyroxenes in the foliated varieties are similar except for their generally elongated form. The garnet/clinopyroxene modal ratio varies considerably and at least one nodule (#OR-114) is composed primarily of coarse, granular pyroxenes which poikilitically enclose scattered garnets to form a fabric similar to one of the variants included in Group I of the MacGregor and Carter (1970) classification. Pyroxenes in the Orapa eclogites are generally more altered than the coexisting garnets. This alteration typically appears in thin section as a light-colored, extremely fine-grained turbid intergrowth developed on most grain peripheries and locally along cleavage and fracture planes. Although the intergrowths are generally petrographically irresolvable, green chlorite has been identified in some specimens. The extremely fine-grained nature and local predominance of chlorite suggest that this alteration may be similar to that which characterizes most of the clinopyroxene discrete nodules and thus may be either a consequence of chemical reaction with the volatile-rich kimberlite magma or a result of post-emplacement alteration.

Garnet and clinopyroxene grains in several nodules contain abundant, very fine-grained, oriented inclusions. In specimen #OR-106, both of the coexisting silicates contain inclusions while, in two other eclogites, the observed inclusions are limited to either garnet (#OR-109) or pyroxene (#OR-104). The inclusions range from approximately 30 to 100

microns in length and are characteristically highly birefringent with inclined extinction. Individual grains vary in shape from acicular needles to squat prisms and are typically situated along planes oriented at approximately 60° angles to one another within the host phase. Similar inclusions have been reported in garnets from eclogites recovered at a number of African kimberlite localities (for example: Nixon et al., 1963; O'Hara and Yoder, 1967); however, only Griffin et al. (1971) have observed such inclusions in both coexisting garnet and clinopyroxene. Using electron microprobe and X-ray diffraction analysis, Griffin et al. (1971) identified the inclusions in an eclogite from the Bultfontein pipe in South Africa as rutile and attributed the anomalous extinction of this phase to the effects of high pressure exsolution during cooling of relatively Ti-rich silicates. These authors cited as evidence the preliminary experimental work of O'Hara and Yoder (1967) who observed apparent rehomogenization of presumed rutile inclusions and host garnet in a natural eclogite at 30 kb, but noted that the rutiles in that study were characterized by straight extinction. The mineral inclusions in the Orapa eclogites appear to be rutile similar to that described by Griffin et al. (1971). The Orapa samples may, therefore, preserve a record of a similar decompression reaction, but further characterization of the process is limited by the analytical constraints imposed by the extremely fine grain size of the inclusions and by the lack of an accurate pressure indicator in the eclogite assemblage.

Rutile also occurs as the most common accessory phase in the Orapa eclogites. Individual grains are generally characterized by subhedral morphology and range between 0.1 and 1.0 mm in diameter. Where

relatively unaltered, the rutile is characterized by a distinctive straw yellow color when observed in transmitted light, and by prominent red-orange internal reflections when observed in reflected light. Rutile grains typically occur scattered throughout the interstitial fabric of individual nodules, although, in nodule #OR-110, the oxide phase is restricted in occurrence to isolated inclusions within garnet. The rutile in nodule #OR-102b contains extremely fine, sigmoidal lamellae of ilmenite oriented in an orthogonal pattern similar to that already described for the fine lamellar variety of ilmenite-rutile intergrowths observed in rutile discrete nodules from Orapa and Jagersfontein (Figure 10). Individual ilmenite lamellae are generally less than 50 microns in length and occur throughout host rutile grains in this eclogite. Local development of atoll ilmenite occurring along the peripheries of some grains suggests that limited migration of the ilmenite lamellae may have occurred at subsolidus temperatures. Although rutile has been reported as an accessory phase in kimberlitic eclogites from a number of localities (for example: Sobolev and Kuznetsova, 1966; Lappin and Dawson, 1975), similar intergrowths of ilmenite and rutile in eclogite have been confirmed and reported from only the Stockdale kimberlite in Kansas (Meyer and Boctor, 1975).

Ilmenite also occurs as an accessory phase in several Orapa eclogites. However, with the exception of the lamellar intergrowths described above, ilmenite does not coexist with rutile. The ilmenite generally occurs as rounded to subhedral grains ranging from 0.1 to 1.0 mm in size. Examined by oil immersion microscopy, individual grains appear to be homogeneous and characterized by the typical properties of

tan pleochroism and distinct reflection anisotropy. The ilmenite generally occurs as isolated subhedral grains scattered throughout the interstitial fabric, but is also present as very fine-grained, round inclusions in several garnets and pyroxenes in nodule #OR-109. Although ilmenite is not a common accessory mineral in kimberlitic eclogites, its mode of occurrence at Orapa appears to be typical of those described to date (Dawson, 1980).

Eclogite samples #OR-105 and OR-109 each contain isolated grains of light brown amphibole developed in close proximity to the nodule peripheries. In both cases, the fine-grained amphibole is spatially associated with clinopyroxene and appears to occupy interstitial positions within the nodular fabrics. Optical identification of the amphibole is hindered by the presence of an extremely fine-grained alteration product which is closely intergrown throughout individual crystals. Nevertheless, the amphibole in both nodules is pale brown in color with subtle pleochroism, characterized by inclined extinction, and may be possibly optically negative with a 2V angle of approximately 50 degrees. On the basis of this limited petrographic evidence, the amphibole is tentatively identified as a member of the hornblende group (Deer et al., 1963). The presence of amphibole in kimberlitic eclogites has been previously reported from several localities including the Roberts Victor pipe in South Africa (Bishop et al., 1978) and a number of pipes in the Stockdale, Kansas area (Meyer and Brookins, 1971). Although there is limited experimental data indicating that primary amphibole may be generated in the upper mantle (Lambert and Wyllie, 1968), direct evidence from eclogitic inclusions is still lacking. A

review of the literature indicates that the amphiboles in eclogites from the Stockdale area (Meyer and Brookins, 1971) and Orapa (this study) are among the best documented in terms of textural characteristics and chemical composition. The amphiboles from these two localities are similar petrographically in that they 1) occupy less than 1 modal percent of each xenolith examined, 2) are tentatively assigned to the hornblende group, and 3) occur almost exclusively in interstitial positions located along the peripheries of coarser grained silicate minerals. Although certainly not unequivocal, the similarity of these occurrences appears to be more suggestive of a common origin by any of a variety of secondary processes rather than direct evidence of formation of hydrous silicates under upper mantle temperature and pressure conditions. In the eclogites from Orapa, the close association of this amphibole with pyroxene and the presence of isolated pyroxene enclaves within the amphibole suggests that the hydrous phase formed at the expense of primary pyroxene. Hornblende in an intergrowth presumably formed pseudomorphically after primary clinopyroxene in an eclogite nodule described by Berg (1968) from an unknown South African locality may provide independent evidence to support this conclusion.

Individual eclogite nodules containing trace quantities of diamond, graphite, and coexisting diamond and graphite have been reported from the Orapa A/K-1 kimberlite pipe by Robinson (1979). Nevertheless, diamond appears to be absent in the particular nodules examined in this study and confirmed occurrences of graphite are scarce. Graphite is well developed only in nodule #102 where it is present in two distinct modes. A single coarse crystal measuring approximately 4 mm in diameter

has been observed intergrown with garnet and pyroxene on the exterior surface of the nodule. This particular crystal is subhedral in morphology and characterized by the typical dull gray color. Such preservation of relatively fragile graphite imbedded in an exposed surface of a kimberlite nodule is not uncommon (Robinson, 1979), and appears to be due in this case to the nearly perpendicular orientation of the graphite {0001} crystallographic planes and the curved exterior surface of the nodule. Graphite has also been observed (Haggerty, pers. comm., 1978) in this nodule as extremely fine-grained crystalline aggregates locally dispersed throughout the narrow interstices between coarser silicate grains. Such graphite occurs as generally shapeless, unoriented plates averaging approximately 20-30 microns in cross section. Detailed mineralogic studies of graphite occurring in kimberlitic eclogite nodules are scarce and are usually only undertaken in conjunction with work on coexisting diamonds. Nevertheless, relatively coarse graphite has been reported in eclogites from the Orapa, Jagersfontein, and Roberts Victor localities by Robinson (1979), from Roberts Victor by Hatton and Gurney (1979), and from the Mir pipe in Yakutia by Sobolev (1977, p. 49). Extremely fine-grained, disseminated graphite similar to the variety observed in specimen #OR-102, has not previously been reported in the kimberlitic literature.

Phase Chemistry

The average chemical compositions of individual garnets from each of the eclogite nodules analyzed in this study are presented in Table 11. Multiple analyses performed at a variety of locations within individual

Table 11: Average chemical compositions of garnet grains in individual eclogite nodules from Orapa.

Specimen:	<u>102-1g</u>	<u>102-2g</u>	<u>102-3g</u>	<u>102-4g</u>	<u>102-5g</u>	<u>102b-1g</u>	<u>103-1g</u>	<u>103-2g</u>	<u>103-3g</u>
SiO ₂	39.49	39.55	39.35	39.45	39.21	39.15	40.30	40.29	40.28
TiO ₂	0.11	0.10	0.13	0.14	0.13	0.16	0.06	0.04	0.05
Cr ₂ O ₃	0.05	0.04	0.07	0.01	0.06	0.09	0.02	0.00	0.00
Al ₂ O ₃	22.27	22.17	22.75	22.67	22.68	21.83	23.02	22.93	23.13
*FeO	18.58	18.57	18.47	18.44	18.33	18.25	18.01	18.01	17.81
MgO	9.58	9.10	10.00	9.77	10.33	10.61	10.51	10.55	11.12
MnO	0.44	0.46	0.43	0.39	0.39	0.50	0.55	0.52	0.53
CaO	9.04	8.95	8.99	9.12	8.99	8.87	8.20	8.17	7.92
Na ₂ O	0.01	0.00	0.02	0.00	0.00	0.01	0.00	0.02	0.08
Total	<u>99.57</u>	<u>98.94</u>	<u>100.21</u>	<u>99.99</u>	<u>100.12</u>	<u>99.47</u>	<u>100.67</u>	<u>100.53</u>	<u>100.92</u>

Cations based on twenty-four (24) oxygens

Si	5.979	6.022	5.917	5.942	5.899	5.936	5.991	5.997	5.965
Ti	0.012	0.012	0.014	0.016	0.015	0.018	0.007	0.005	0.005
Cr	0.006	0.004	0.008	0.001	0.007	0.010	0.002	0.000	0.000
Al	3.977	3.981	4.035	4.027	4.024	3.903	4.037	4.026	4.041
Fe	2.354	2.367	2.324	2.324	2.308	2.315	2.241	2.243	2.207
Mg	2.164	2.067	2.242	2.194	2.319	2.399	2.330	2.342	2.455
Mn	0.056	0.060	0.055	0.050	0.049	0.064	0.070	0.065	0.066
Ca	1.467	1.462	1.450	1.473	1.450	1.442	1.307	1.304	1.257
Na	0.002	0.000	0.006	0.000	0.000	0.003	0.000	0.005	0.022
Total	<u>16.017</u>	<u>15.975</u>	<u>16.051</u>	<u>16.027</u>	<u>16.071</u>	<u>16.090</u>	<u>15.985</u>	<u>15.987</u>	<u>16.018</u>
Ca/(Ca+Mg)	0.404	0.414	0.393	0.402	0.385	0.375	0.359	0.358	0.339
Mg/(Fe+Mg)	0.479	0.466	0.491	0.486	0.501	0.509	0.510	0.511	0.527
n	11	3	8	3	7	2	3	4	3

* total iron expressed as FeO

Table 11 (con't)

Specimen:	<u>103b-1g</u>	<u>103b-2g</u>	<u>103b-3g</u>	<u>103b-4g</u>	<u>103b-5g</u>	<u>103c-1g</u>	<u>103c-2g</u>	<u>103c-3g</u>	<u>104-1g</u>
SiO ₂	40.22	40.30	40.45	40.01	39.79	39.56	40.00	39.55	39.29
TiO ₂	0.11	0.15	0.14	0.13	0.11	0.10	0.14	0.15	0.04
Cr ₂ O ₃	0.00	0.00	0.00	0.00	0.00	0.03	0.01	0.05	0.09
Al ₂ O ₃	22.89	22.56	22.83	22.47	22.73	23.04	22.90	23.11	21.37
*FeO	17.64	17.59	17.52	17.59	17.72	17.87	17.52	17.78	25.01
MgO	9.81	9.46	9.52	9.19	9.40	9.92	9.98	10.00	9.04
MnO	0.42	0.38	0.38	0.42	0.48	0.43	0.42	0.42	0.51
CaO	9.98	9.87	9.90	9.84	9.78	9.74	9.88	9.74	4.22
Na ₂ O	0.07	0.10	0.08	0.08	0.08	0.02	0.03	0.07	0.04
Total	<u>101.14</u>	<u>100.41</u>	<u>100.82</u>	<u>99.73</u>	<u>100.09</u>	<u>100.71</u>	<u>100.88</u>	<u>100.87</u>	<u>99.61</u>

Cations based on twenty-four (24) oxygens

Si	5.972	6.024	6.016	6.025	5.977	5.911	5.954	5.898	6.047
Ti	0.013	0.017	0.016	0.015	0.013	0.011	0.015	0.016	0.004
Cr	0.000	0.000	0.000	0.000	0.000	0.004	0.002	0.006	0.011
Al	4.010	3.977	4.005	3.990	4.027	4.060	4.020	4.064	3.879
Fe	2.192	2.200	2.180	2.217	2.228	2.234	2.182	2.219	3.221
Mg	2.174	2.109	2.112	2.064	2.106	2.209	2.214	2.225	2.075
Mn	0.052	0.048	0.047	0.053	0.061	0.055	0.053	0.053	0.066
Ca	1.586	1.581	1.578	1.589	1.575	1.560	1.577	1.558	0.696
Na	0.020	0.030	0.024	0.024	0.023	0.006	0.008	0.020	0.011
Total	<u>16.019</u>	<u>15.986</u>	<u>15.978</u>	<u>15.977</u>	<u>16.010</u>	<u>16.050</u>	<u>16.025</u>	<u>16.059</u>	<u>16.010</u>
Ca/(Ca+Mg)	0.422	0.428	0.428	0.435	0.428	0.414	0.416	0.412	0.251
Mg/(Fe+Mg)	0.498	0.489	0.492	0.482	0.486	0.497	0.504	0.501	0.392
n	5	3	4	6	2	3	2	5	5

* total iron expressed as FeO

Table 11 (con't)

Specimen:	<u>104-2g</u>	<u>104-3g</u>	<u>104-4g</u>	<u>104-5g</u>	<u>105-1g</u>	<u>105-2g</u>	<u>105-3g</u>	<u>105-4g</u>	<u>105-5g</u>
SiO ₂	39.29	39.34	38.98	38.92	40.33	40.27	39.77	40.76	40.62
TiO ₂	0.04	0.04	0.04	0.01	0.06	0.06	0.09	0.06	0.10
Cr ₂ O ₃	0.08	0.08	0.11	0.09	0.08	0.07	0.07	0.08	0.09
Al ₂ O ₃	22.47	22.12	21.48	22.11	23.10	23.19	23.17	23.07	23.19
*FeO	24.87	25.10	24.93	24.78	16.33	16.16	16.50	16.22	16.57
MgO	9.12	8.92	9.29	9.29	13.18	13.23	13.15	12.99	13.20
MnO	0.58	0.57	0.56	0.56	0.44	0.40	0.38	0.38	0.40
CaO	4.21	4.17	4.15	4.10	6.10	6.22	6.13	6.20	6.14
Na ₂ O	0.02	0.03	0.02	0.04	0.09	0.05	0.05	0.02	0.01
Total	<u>100.68</u>	<u>100.37</u>	<u>99.56</u>	<u>99.90</u>	<u>99.71</u>	<u>99.65</u>	<u>99.31</u>	<u>99.78</u>	<u>100.32</u>

Cations based on twenty-four (24) oxygens

Si	5.970	6.004	6.004	5.965	5.973	5.964	5.925	6.021	5.981
Ti	0.005	0.005	0.004	0.002	0.007	0.007	0.011	0.007	0.009
Cr	0.010	0.009	0.014	0.011	0.010	0.009	0.008	0.009	0.010
Al	4.028	3.982	3.902	3.996	4.035	4.050	4.070	4.020	4.027
Fe	3.162	3.205	3.214	3.179	2.024	2.003	2.057	2.005	2.042
Mg	2.068	2.030	2.133	2.123	2.913	2.922	2.922	2.862	2.898
Mn	0.075	0.074	0.073	0.072	0.054	0.050	0.048	0.047	0.050
Ca	0.686	0.682	0.686	0.674	0.968	0.988	0.979	0.982	0.969
Na	0.006	0.009	0.005	0.011	0.025	0.015	0.013	0.006	0.002
Total	<u>16.010</u>	<u>16.000</u>	<u>16.035</u>	<u>16.033</u>	<u>16.009</u>	<u>16.008</u>	<u>16.033</u>	<u>15.959</u>	<u>15.988</u>
Ca/(Ca+Mg)	0.249	0.251	0.243	0.241	0.249	0.253	0.251	0.255	0.251
Mg/(Mg+Fe)	0.395	0.388	0.399	0.400	0.590	0.593	0.587	0.588	0.587
n	6	4	4	4	4	5	3	5	5

* total iron expressed as FeO

Table 11 (con't)

Specimen:	<u>105-6g</u>	<u>106-1g</u>	<u>106-2g</u>	<u>106-3g</u>	<u>106-4g</u>	<u>107-1g</u>	<u>107-2g</u>	<u>107-3g</u>	<u>108-1g</u>
SiO ₂	39.89	39.95	40.35	40.35	40.18	40.78	41.26	41.76	41.92
TiO ₂	0.09	0.03	0.01	0.01	0.05	0.46	0.50	0.47	0.12
Cr ₂ O ₃	0.09	0.08	0.09	0.07	0.08	0.09	0.07	0.09	0.01
Al ₂ O ₃	23.22	23.21	22.79	22.92	22.82	22.45	23.22	23.47	24.20
*FeO	16.53	19.81	19.71	19.23	19.59	10.15	10.29	10.08	10.33
MgO	13.06	10.89	11.06	11.33	10.99	13.01	13.54	13.72	18.95
MnO	0.39	0.71	0.71	0.71	0.71	0.30	0.21	0.24	0.35
CaO	6.20	6.27	5.91	6.15	6.09	11.82	10.38	10.97	3.96
Na ₂ O	0.03	0.01	0.00	0.00	0.00	0.15	0.11	0.11	0.00
Total	<u>99.50</u>	<u>100.96</u>	<u>100.63</u>	<u>100.77</u>	<u>100.51</u>	<u>99.21</u>	<u>99.58</u>	<u>100.91</u>	<u>99.84</u>
Cations based on twenty-four (24) oxygens									
Si	5.931	5.945	6.013	5.996	5.996	6.002	6.015	6.008	5.978
Ti	0.010	0.004	0.001	0.001	0.006	0.051	0.055	0.050	0.013
Cr	0.010	0.010	0.011	0.008	0.010	0.011	0.007	0.010	0.001
Al	4.071	4.075	4.005	4.016	4.017	3.897	3.993	3.982	4.070
Fe	2.057	2.467	2.457	2.391	2.446	1.250	1.255	1.214	1.233
Mg	2.897	2.416	2.458	2.511	2.445	2.857	2.944	2.944	4.030
Mn	0.049	0.090	0.089	0.090	0.090	0.037	0.026	0.029	0.042
Ca	0.988	1.001	0.944	0.979	0.975	1.865	1.622	1.692	0.606
Na	0.008	0.002	0.000	0.000	0.000	0.044	0.032	0.030	0.000
Total	<u>16.021</u>	<u>16.010</u>	<u>15.978</u>	<u>15.992</u>	<u>15.985</u>	<u>16.014</u>	<u>15.949</u>	<u>15.959</u>	<u>15.973</u>
Ca/(Ca+Mg)	0.254	0.293	0.277	0.281	0.285	0.395	0.355	0.365	0.131
Mg/(Mg+Fe)	0.585	0.495	0.500	0.512	0.500	0.696	0.701	0.708	0.766
n	3	3	5	4	5	3	2	4	4

* total iron expressed as FeO

Table 11 (con't)

Specimen:	<u>108-2g</u>	<u>108-3g</u>	<u>108-4g</u>	<u>109-1g</u>	<u>109-2g</u>	<u>109-3g</u>	<u>109-4g</u>	<u>110-1g</u>	<u>110-2g</u>
SiO ₂	41.94	42.01	41.74	41.89	40.78	41.54	41.79	40.54	40.41
TiO ₂	0.12	0.10	0.12	0.04	0.06	0.03	0.05	0.13	0.13
Cr ₂ O ₃	0.00	0.02	0.00	0.13	0.12	0.14	0.15	0.04	0.04
Al ₂ O ₃	24.18	23.93	24.14	23.20	23.14	23.33	23.54	22.55	22.60
*FeO	10.49	10.40	10.32	14.12	14.16	13.88	14.02	15.35	15.37
MgO	19.06	19.05	18.86	16.65	16.22	16.55	16.59	12.48	12.29
MnO	0.42	0.40	0.38	0.42	0.41	0.44	0.41	0.24	0.25
CaO	3.78	3.81	3.83	4.33	4.29	4.38	4.40	8.83	8.85
Na ₂ O	0.03	0.02	0.01	0.04	0.05	0.00	0.00	0.00	0.00
Total	<u>100.02</u>	<u>99.74</u>	<u>99.40</u>	<u>100.82</u>	<u>99.23</u>	<u>100.29</u>	<u>100.95</u>	<u>100.16</u>	<u>99.94</u>

Cations based on twenty-four (24) oxygens

Si	5.975	5.998	5.978	6.030	5.976	6.009	6.004	5.993	5.989
Ti	0.012	0.011	0.013	0.004	0.007	0.004	0.006	0.015	0.015
Cr	0.000	0.002	0.000	0.015	0.014	0.015	0.017	0.005	0.005
Al	4.063	4.030	4.078	3.939	3.999	3.979	3.989	3.931	3.950
Fe	1.250	1.242	1.236	1.701	1.737	1.680	1.686	1.899	1.906
Mg	4.050	4.056	4.028	3.575	3.546	3.570	3.556	2.752	2.717
Mn	0.051	0.049	0.047	0.051	0.050	0.054	0.049	0.031	0.031
Ca	0.577	0.583	0.589	0.668	0.674	0.680	0.679	1.400	1.406
Na	0.008	0.006	0.002	0.012	0.014	0.000	0.000	0.000	0.000
Total	<u>15.986</u>	<u>15.977</u>	<u>15.971</u>	<u>15.995</u>	<u>16.017</u>	<u>15.991</u>	<u>15.986</u>	<u>16.026</u>	<u>16.019</u>
Ca/(Ca+Mg)	0.125	0.126	0.128	0.157	0.160	0.160	0.160	0.337	0.341
Mg/(Mg+Fe)	0.764	0.766	0.765	0.678	0.671	0.680	0.678	0.592	0.588
n	6	2	4	4	4	4	5	4	5

* total iron expressed as FeO

Table 11 (con't)

Specimen:	<u>110-3g</u>	<u>111-1g</u>	<u>111-2g</u>	<u>111-3g</u>	<u>114-1g</u>	<u>114-2g</u>	<u>114-3g</u>
SiO ₂	40.51	41.59	41.77	41.61	40.72	40.74	40.59
TiO ₂	0.13	0.08	0.10	0.11	0.15	0.15	0.14
Cr ₂ O ₃	0.05	0.10	0.14	0.15	0.25	0.19	0.19
Al ₂ O ₃	22.52	23.46	23.39	23.28	22.98	22.80	22.79
*FeO	15.37	12.44	12.38	12.31	16.86	16.98	17.04
MgO	12.56	18.89	18.84	18.82	14.18	14.23	14.13
MnO	0.24	0.36	0.37	0.42	0.39	0.42	0.42
CaO	8.86	3.52	3.53	3.65	5.34	5.36	5.34
Na ₂ O	0.01	0.00	0.00	0.00	0.02	0.01	0.01
Total	<u>100.25</u>	<u>100.44</u>	<u>100.52</u>	<u>100.35</u>	<u>100.89</u>	<u>100.88</u>	<u>100.65</u>
Cations based on twenty-four (24) oxygens							
Si	5.986	5.956	5.974	5.967	5.961	5.969	5.963
Ti	0.015	0.009	0.011	0.012	0.017	0.017	0.015
Cr	0.006	0.011	0.016	0.017	0.029	0.022	0.022
Al	3.924	3.963	3.946	3.936	3.967	3.939	3.949
Fe	1.901	1.490	1.482	1.478	2.065	2.082	2.095
Mg	2.767	4.034	4.020	4.025	3.095	3.110	3.097
Mn	0.030	0.044	0.045	0.051	0.049	0.052	0.052
Ca	1.404	0.540	0.541	0.561	0.839	0.842	0.842
Na	0.002	0.000	0.000	0.000	0.005	0.003	0.002
Total	<u>16.035</u>	<u>16.047</u>	<u>16.035</u>	<u>16.047</u>	<u>16.027</u>	<u>16.036</u>	<u>16.037</u>
Ca/(Ca+Mg)	0.337	0.118	0.119	0.122	0.213	0.213	0.214
Mg/(Mg+Fe)	0.593	0.730	0.731	0.731	0.600	0.599	0.596
n	5	4	5	4	4	5	8

* total iron expressed as FeO

garnets indicate that these crystals are characteristically homogeneous in major element composition within the analytical limits of the microprobe. Such compositional homogeneity is characteristic of eclogitic garnets recovered from kimberlite localities throughout the world (Dawson, 1980). The data in Table 11 also indicate that the compositions of coexisting garnets show little variation within individual nodules. Although such intrasample homogeneity appears to characterize most kimberlitic eclogite nodules (Rickwood et al., 1968), wide variation in garnet compositions has been reported in a small number of eclogites from the Roberts Victor pipe (Rickwood et al., 1968; Lappin and Dawson, 1975). The compositions of individual garnets from the Orapa eclogites have been classified according to the mineral chemical cluster analysis criteria developed by Dawson and Stephens (1975) and correspond to their groups #1 (one nodule), 3 (12 nodules), and 5 (one nodule) designated as titanian pyrope, calcic pyrope-almandine, and magnesian almandine respectively (Dawson and Stephens, 1976). Considered in terms of individual chemical components, the Orapa garnets show significant variation only in the values for CaO (3.52-11.82 wt. %), MgO (8.92-19.06 wt. %), and total iron (expressed as FeO, 10.08-25.10 wt. %). Values for Al₂O₃ are relatively constant throughout the suite, ranging from approximately 21.4 to 24.2 wt. %.

Figure 26 is a summary plot of garnet compositions taken from the literature for eclogitic inclusions from a variety of locations in southern Africa (Kushiro and Aoki, 1968; Nixon and Boyd, 1973e; Reid et al., 1976; Smyth and Hatton, 1977; Lappin, 1978) and the Yakutian district of Siberia (Sobolev et al., 1968; Sobolev, 1977). Expressed

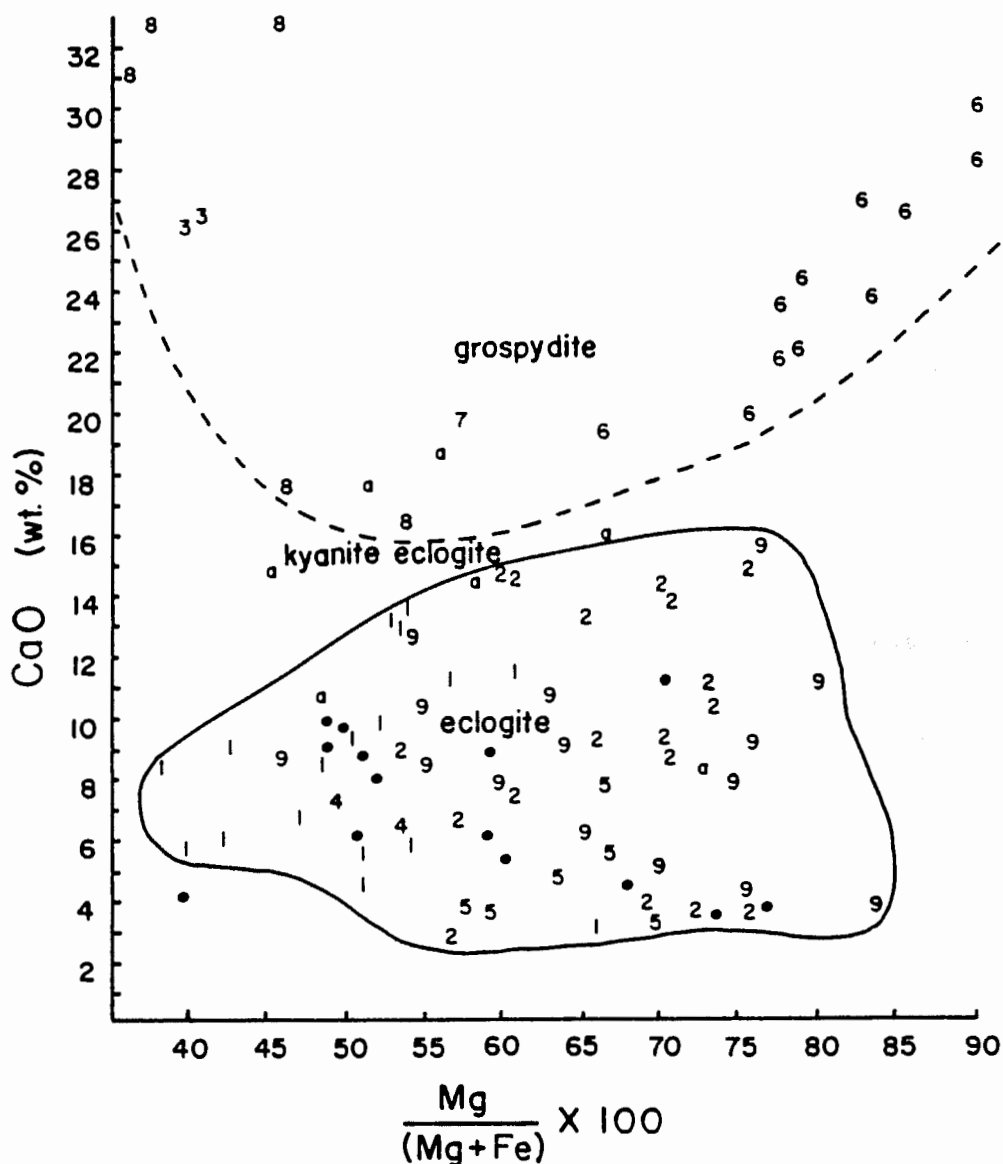


Figure 26: Summary plot of garnet compositions taken from the literature for eclogitic inclusions in kimberlites. Data sources for biminerally eclogites include (1) Sobolev (1977, p. 92-3), (2) Reid et al. (1976), (4) Nixon and Boyd (1973e), (5) Kushiro and Aoki (1968), and (9) Sobolev (1977, p. 48-9). Sources for grospydite data include (3) Lappin (1978), (6) Sobolev et al. (1968), (7) Smyth and Hatton (1977), and Sobolev (1977, p. 48-9). Source for kyanite eclogite data is (a) Sobolev (1977, p. 60-1). Solid circles represent compositional average of garnets from individual Orapa eclogites.

in terms of $Mg/(Mg+Fe)$ ratio and CaO content, garnets from such rocks are characterized by a broad compositional range which is largely a function of mineralogy and bulk chemistry. Garnets from essentially biminerally eclogites are characterized by a broad range of $Mg/(Mg+Fe)$ ratios and by CaO contents which are generally less than 15 wt. %. Such garnets are compositionally distinct from those which occur in relatively rare grosspydite (grossular-rich garnet + pyroxene + disthene [kyanite]) nodules now known to exist in pipes from both the Yakutian and southern African regions in that these latter garnets are by definition relatively enriched in calcium component. Kyanite eclogites, which are distinguished from grosspydites on the basis of garnet compositions with less than 50% grossular component (Sobolev et al., 1968), contain garnets with CaO contents which overlap the adjacent extremes of the grosspydite and biminerally eclogite fields to form a continuum of garnet compositions ranging from approximately 3 wt. % CaO to values in excess of 20 wt. %. Plotted in terms of these variables (Figure 26), the average compositions of garnets from the Orapa eclogites generally fall within the biminerally eclogite field and are characterized by low to moderate CaO values relative to garnets from similar assemblages.

The average chemical compositions of individual clinopyroxene grains from each of the eclogite nodules analyzed in this study are presented in Table 12. Multiple analyses performed at a variety of locations within individual pyroxenes indicate that the grains are characteristically homogeneous in major element composition within the analytical limits of the microprobe. Although similar data regarding eclogitic pyroxenes from other localities are presently not available in

Table 12: Average chemical compositions of clinopyroxene grains in individual eclogite nodules from Orapa.

Specimen:	<u>102-1p</u>	<u>102-2p</u>	<u>102-3p</u>	<u>102-4p</u>	<u>102-5p</u>	<u>102-6p</u>	<u>102b-1p</u>	<u>103-1p</u>	<u>103-2p</u>
SiO ₂	53.84	54.15	54.99	53.94	54.68	53.77	53.45	53.13	53.58
TiO ₂	0.38	0.41	0.37	0.39	0.39	0.38	0.44	0.42	0.40
Cr ₂ O ₃	0.01	0.09	0.05	0.11	0.09	0.09	0.11	0.06	0.06
Al ₂ O ₃	9.38	9.42	9.09	9.42	9.35	9.41	9.06	9.25	9.13
*FeO	3.54	3.70	3.78	3.67	3.73	3.85	3.88	3.76	3.49
MgO	10.75	10.59	10.29	10.76	10.45	10.61	10.99	11.06	10.93
MnO	0.00	0.02	0.00	0.00	0.00	0.00	0.01	0.00	0.01
CaO	16.79	16.75	16.47	16.82	16.74	16.76	16.36	16.10	15.92
Na ₂ O	4.93	4.85	4.86	4.93	4.91	4.78	6.40	6.19	5.88
Total	<u>99.62</u>	<u>99.98</u>	<u>99.90</u>	<u>100.04</u>	<u>100.34</u>	<u>99.65</u>	<u>100.70</u>	<u>99.97</u>	<u>99.40</u>

Cations based on six (6) oxygens

Si	1.939	1.942	1.969	1.936	1.953	1.937	1.919	1.917	1.937
IV Al	0.061	0.058	0.031	0.064	0.047	0.063	0.081	0.083	0.063
VI Al	0.337	0.340	0.353	0.335	0.347	0.337	0.302	0.311	0.327
Ti	0.010	0.011	0.010	0.010	0.010	0.010	0.012	0.011	0.011
Cr	0.000	0.003	0.002	0.003	0.002	0.003	0.003	0.002	0.002
Fe	0.107	0.111	0.113	0.110	0.111	0.116	0.117	0.113	0.106
Mg	0.577	0.567	0.550	0.576	0.557	0.570	0.588	0.596	0.589
Mn	0.000	0.000	0.000	0.000	0.000	0.000	0.000	0.000	0.000
Ca	0.648	0.644	0.632	0.647	0.641	0.647	0.630	0.623	0.617
Na	0.344	0.338	0.338	0.343	0.340	0.334	0.446	0.433	0.413
Total	<u>4.023</u>	<u>4.014</u>	<u>3.998</u>	<u>4.024</u>	<u>4.008</u>	<u>4.017</u>	<u>4.098</u>	<u>4.089</u>	<u>4.065</u>
Ca/(Ca+Mg)	0.529	0.532	0.535	0.529	0.535	0.532	0.517	0.511	0.512
Mg/(Mg+Fe)	0.844	0.836	0.830	0.840	0.834	0.831	0.834	0.841	0.847
n	3	3	3	6	3	3	2	3	3

* total iron expressed as FeO

Table 12 (con't)

Specimen:	<u>103-3p</u>	<u>103-4p</u>	<u>103-5p</u>	<u>103b-1p</u>	<u>103b-2p</u>	<u>103b-3p</u>	<u>103b-4p</u>	<u>103b-5p</u>	<u>103c-1p</u>
SiO ₂	53.52	53.81	54.12	53.94	53.76	54.00	54.15	53.67	53.61
TiO ₂	0.39	0.40	0.41	0.39	0.38	0.38	0.41	0.39	0.36
Cr ₂ O ₃	0.05	0.07	0.07	0.02	0.02	0.02	0.01	0.02	0.08
Al ₂ O ₃	8.94	9.17	9.37	10.20	10.10	10.01	10.10	9.99	9.97
*FeO	3.49	3.70	3.64	3.49	3.49	3.48	3.61	3.48	3.56
MgO	10.97	10.88	11.04	10.24	10.36	10.31	10.23	9.95	9.94
MnO	0.00	0.00	0.01	0.02	0.02	0.08	0.00	0.01	0.03
CaO	16.18	16.11	16.00	15.27	15.11	15.84	16.06	16.11	15.34
Na ₂ O	5.95	6.04	6.34	6.24	6.34	6.36	6.40	6.23	6.52
Total	<u>99.49</u>	<u>100.18</u>	<u>101.00</u>	<u>99.81</u>	<u>99.58</u>	<u>100.48</u>	<u>100.97</u>	<u>99.85</u>	<u>99.41</u>

Cations based on six (6) oxygens

Si	1.936	1.934	1.929	1.936	1.935	1.931	1.928	1.932	1.937
IVAl	0.064	0.066	0.071	0.064	0.065	0.069	0.072	0.068	0.063
VIAl	0.317	0.322	0.323	0.368	0.364	0.353	0.352	0.356	0.362
Ti	0.011	0.011	0.011	0.011	0.010	0.010	0.011	0.011	0.010
Cr	0.001	0.002	0.002	0.001	0.001	0.001	0.000	0.001	0.002
Fe	0.106	0.111	0.109	0.105	0.105	0.104	0.108	0.105	0.108
Mg	0.592	0.583	0.587	0.548	0.556	0.550	0.544	0.534	0.536
Mn	0.000	0.000	0.000	0.001	0.001	0.002	0.000	0.000	0.001
Ca	0.627	0.621	0.611	0.588	0.583	0.607	0.613	0.622	0.594
Na	0.417	0.421	0.438	0.434	0.442	0.441	0.442	0.435	0.457
Total	<u>4.071</u>	<u>4.071</u>	<u>4.081</u>	<u>4.056</u>	<u>4.062</u>	<u>4.068</u>	<u>4.070</u>	<u>4.064</u>	<u>4.070</u>
Ca/(Ca+Mg)	0.514	0.516	0.510	0.518	0.512	0.525	0.538	0.538	0.526
Mg/(Mg+Fe)	0.848	0.840	0.843	0.839	0.841	0.841	0.834	0.836	0.832
n	3	4	4	3	3	6	4	4	4

* total iron expressed as FeO

Table 12 (con't)

Specimen:	<u>103c-2p</u>	<u>103c-3p</u>	<u>103c-4p</u>	<u>103c-5p</u>	<u>103c-1p</u>	<u>104-1p</u>	<u>104-2p</u>	<u>104-3p</u>	<u>104-4p</u>
SiO ₂	53.58	53.61	53.54	53.61	53.47	54.17	53.84	54.14	54.19
TiO ₂	0.40	0.42	0.40	0.41	0.41	0.27	0.22	0.22	0.20
Cr ₂ O ₃	0.06	0.06	0.06	0.07	0.08	0.12	0.15	0.14	0.17
Al ₂ O ₃	9.94	10.03	9.93	9.94	9.95	5.89	5.75	5.77	5.77
*FeO	3.47	3.57	3.50	3.45	3.63	7.04	7.11	7.23	7.20
MgO	9.97	9.90	9.89	10.14	10.02	11.53	11.38	11.51	11.42
MnO	0.03	0.03	0.00	0.02	0.02	0.01	0.03	0.01	0.01
CaO	15.48	15.52	15.26	15.41	15.52	16.45	16.53	16.56	16.31
Na ₂ O	6.29	6.25	6.58	6.10	6.20	5.46	5.30	5.23	5.37
Total	<u>99.29</u>	<u>99.39</u>	<u>99.16</u>	<u>99.15</u>	<u>99.30</u>	<u>100.94</u>	<u>100.31</u>	<u>100.81</u>	<u>100.64</u>

Cations based on six (6) oxygens

Si	1.938	1.936	1.938	1.938	1.934	1.966	1.968	1.968	1.972
IVAl	0.062	0.064	0.062	0.062	0.066	0.034	0.032	0.032	0.028
VIAl	0.362	0.363	0.362	0.362	0.359	0.218	0.216	0.215	0.220
Ti	0.011	0.011	0.011	0.011	0.011	0.007	0.006	0.006	0.006
Cr	0.002	0.002	0.002	0.002	0.002	0.003	0.004	0.004	0.005
Fe	0.105	0.108	0.106	0.104	0.110	0.214	0.217	0.220	0.219
Mg	0.538	0.534	0.534	0.547	0.540	0.624	0.621	0.624	0.620
Mn	0.001	0.001	0.000	0.000	0.000	0.000	0.001	0.000	0.000
Ca	0.601	0.601	0.592	0.597	0.602	0.640	0.648	0.645	0.636
Na	0.441	0.438	0.462	0.428	0.435	0.384	0.376	0.369	0.379
Total	<u>4.061</u>	<u>4.058</u>	<u>4.069</u>	<u>4.051</u>	<u>4.059</u>	<u>4.090</u>	<u>4.089</u>	<u>4.083</u>	<u>4.085</u>
Ca/(Ca+Mg)	0.528	0.530	0.526	0.522	0.527	0.506	0.511	0.508	0.506
Mg/(Mg+Fe)	0.837	0.832	0.834	0.840	0.831	0.745	0.741	0.739	0.739
n	3	2	3	1	2	3	3	4	3

* total iron expressed as FeO

Table 12 (con't)

Specimen:	<u>105-1p</u>	<u>105-2p</u>	<u>105-3p</u>	<u>105-4p</u>	<u>105-5p</u>	<u>105-6p</u>	<u>106-1p</u>	<u>106-2p</u>	<u>106-3p</u>
SiO ₂	53.30	53.47	53.54	53.53	53.45	53.49	52.89	52.45	52.93
TiO ₂	0.28	0.28	0.27	0.28	0.27	0.28	0.49	0.50	0.33
Cr ₂ O ₃	0.10	0.09	0.10	0.10	0.09	0.10	0.11	0.10	0.10
Al ₂ O ₃	4.50	4.64	4.53	4.60	4.52	4.39	5.20	5.55	4.61
*FeO	3.82	3.87	3.91	3.77	3.77	3.87	4.64	4.60	4.67
MgO	14.23	14.50	14.33	14.36	14.40	14.34	13.90	13.93	14.04
MnO	0.02	0.02	0.01	0.03	0.03	0.02	0.07	0.04	0.04
CaO	19.89	20.00	19.81	20.21	20.05	20.00	21.16	21.01	21.38
Na ₂ O	3.29	3.22	3.29	3.34	3.30	3.35	2.37	2.41	2.28
Total	99.43	100.09	99.79	100.22	99.88	99.84	100.83	100.59	100.38

Cations based on six (6) oxygens

Si	1.949	1.943	1.950	1.944	1.947	1.950	1.917	1.906	1.929
^{IV} Al	0.051	0.057	0.050	0.056	0.053	0.050	0.083	0.094	0.071
^{VI} Al	0.143	0.142	0.145	0.141	0.141	0.139	0.139	0.144	0.127
Ti	0.008	0.008	0.007	0.008	0.007	0.008	0.014	0.014	0.009
Cr	0.003	0.003	0.003	0.003	0.003	0.003	0.003	0.003	0.003
Fe	0.117	0.118	0.119	0.114	0.115	0.118	0.141	0.140	0.142
Mg	0.776	0.786	0.779	0.778	0.782	0.779	0.752	0.755	0.763
Mn	0.001	0.001	0.000	0.001	0.001	0.001	0.002	0.001	0.001
Ca	0.780	0.779	0.774	0.787	0.783	0.781	0.823	0.818	0.836
Na	0.233	0.227	0.233	0.235	0.233	0.237	0.166	0.170	0.161
Total	4.061	4.064	4.060	4.067	4.065	4.066	4.040	4.045	4.042
Ca/(Ca+Mg)	0.501	0.498	0.498	0.503	0.500	0.501	0.523	0.520	0.523
Mg/(Mg+Fe)	0.869	0.869	0.867	0.872	0.872	0.868	0.842	0.844	0.843
n	4	4	4	4	5	5	4	4	4

* total iron expressed as FeO

Table 12 (con't)

Specimen:	<u>107-1p</u>	<u>107-2p</u>	<u>108-1p</u>	<u>108-2p</u>	<u>108-3p</u>	<u>109-1p</u>	<u>109-2p</u>	<u>109-3p</u>	<u>110-1p</u>
SiO ₂	54.04	54.68	54.40	54.93	54.82	53.79	53.62	53.74	55.34
TiO ₂	0.27	0.42	0.43	0.41	0.43	0.20	0.20	0.20	0.33
Cr ₂ O ₃	0.04	0.04	0.04	0.03	0.03	0.11	0.12	0.14	0.00
Al ₂ O ₃	9.37	7.93	4.77	4.54	4.74	2.75	2.72	2.69	11.69
*FeO	3.65	3.97	3.03	2.73	2.70	3.36	3.32	3.28	2.51
MgO	11.57	12.46	14.73	14.57	14.79	16.07	15.84	15.94	9.33
MnO	0.03	0.04	0.05	0.05	0.07	0.03	0.07	0.06	0.01
CaO	15.19	15.81	19.09	19.18	19.30	21.92	21.55	21.30	13.85
Na ₂ O	5.85	5.26	3.63	3.55	3.64	2.15	2.08	2.00	7.75
Total	<u>100.01</u>	<u>100.61</u>	<u>100.17</u>	<u>99.99</u>	<u>100.52</u>	<u>100.38</u>	<u>99.52</u>	<u>99.35</u>	<u>100.81</u>

Cations based on six (6) oxygens

Si	1.937	1.952	1.961	1.978	1.966	1.953	1.961	1.966	1.950
IV Al	0.063	0.048	0.039	0.022	0.034	0.047	0.039	0.034	0.050
VI Al	0.333	0.286	0.163	0.171	0.166	0.071	0.078	0.082	0.436
Ti	0.007	0.011	0.012	0.011	0.012	0.005	0.006	0.006	0.009
Cr	0.001	0.001	0.001	0.001	0.001	0.003	0.004	0.004	0.000
Fe	0.110	0.119	0.091	0.082	0.081	0.102	0.102	0.100	0.074
Mg	0.618	0.664	0.792	0.783	0.791	0.870	0.863	0.869	0.490
Mn	0.001	0.001	0.001	0.002	0.002	0.001	0.002	0.002	0.000
Ca	0.584	0.605	0.738	0.741	0.742	0.853	0.845	0.835	0.523
Na	0.407	0.364	0.254	0.248	0.254	0.151	0.147	0.142	0.530
Total	<u>4.061</u>	<u>4.051</u>	<u>4.052</u>	<u>4.039</u>	<u>4.049</u>	<u>4.056</u>	<u>4.047</u>	<u>4.040</u>	<u>4.062</u>
Ca/(Ca+Mg)	0.486	0.477	0.482	0.486	0.484	0.495	0.495	0.490	0.516
Mg/(Mg+Fe)	0.849	0.848	0.897	0.905	0.907	0.895	0.894	0.897	0.869
n	6	6	5	5	5	5	7	3	6

* total iron expressed as FeO

Table 12 (con't)

Specimen:	<u>110-2p</u>	<u>111-1p</u>	<u>111-2p</u>	<u>114-1p</u>	<u>114-2p</u>
SiO ₂	53.90	53.82	54.20	53.90	54.03
TiO ₂	0.49	0.41	0.39	0.33	0.33
Cr ₂ O ₃	0.06	0.14	0.20	0.20	0.19
Al ₂ O ₃	9.58	4.97	4.65	5.78	6.32
*FeO	4.23	3.29	3.63	4.46	4.51
MgO	11.25	14.29	14.27	12.77	12.84
MnO	0.08	0.06	0.08	0.04	0.05
CaO	15.24	18.66	18.74	17.24	17.26
Na ₂ O	<u>5.89</u>	<u>3.59</u>	<u>3.46</u>	<u>4.95</u>	<u>4.79</u>
Total	<u>100.72</u>	<u>99.23</u>	<u>99.62</u>	<u>99.67</u>	<u>100.32</u>

Cations based on six (6) oxygens

Si	1.925	1.959	1.968	1.962	1.952
IVAl	0.075	0.041	0.032	0.038	0.038
VIAl	0.328	0.172	0.167	0.210	0.231
Ti	0.013	0.012	0.011	0.009	0.009
Cr	0.002	0.004	0.006	0.006	0.006
Fe	0.126	0.100	0.110	0.136	0.136
Mg	0.599	0.776	0.772	0.693	0.692
Mn	0.002	0.002	0.003	0.001	0.001
Ca	0.584	0.728	0.729	0.673	0.668
Na	<u>0.408</u>	<u>0.254</u>	<u>0.243</u>	<u>0.350</u>	<u>0.335</u>
Total	<u>4.062</u>	<u>4.048</u>	<u>4.041</u>	<u>4.078</u>	<u>4.068</u>
Ca/(Ca+Mg)	0.494	0.484	0.486	0.493	0.491
Mg/(Mg+Fe)	0.826	0.886	0.875	0.836	0.836
n	4	4	4	4	12

* total iron expressed as FeO

the literature, such intragrain homogeneity is probably typical of this xenolith type, based on the restricted compositional variation already documented for coexisting garnets in eclogites from several localities (Dawson, 1980). The data in Table 12 also indicate that the compositions of coexisting clinopyroxenes show little variation within individual nodules. The compositions of individual pyroxenes from the Orapa eclogites have been classified according to the mineral chemical cluster analysis criteria developed by Stephens and Dawson (1977) and correspond to their groups #2 (four nodules), 4 (one nodule), 8 (three nodules), and 9 (six nodules) designated as diopside, low chrome diopside, jadeitic diopside, and omphacite respectively. Pyroxenes assigned to the latter two groups are characterized by slightly higher Na_2O and Al_2O_3 contents although, in general, compositional variation throughout the suite is not large.

Figure 27 is a summary plot of pyroxene compositions taken from the literature for eclogitic inclusions from a variety of locations in southern Africa (Kushiro and Aoki, 1968; Nixon and Boyd, 1973e; Reid et al., 1976; Smyth and Hatton, 1977; Lappin, 1978) and Yakutia (Sobolev et al., 1968; Sobolev, 1977). Considered in terms of $\text{Ca}/(\text{Ca}+\text{Mg})$ ratio and Al_2O_3 content, pyroxenes from these rocks exhibit a well-defined compositional trend characterized by mutually increasing calcium and aluminum. Pyroxenes from bimineralic eclogites cluster at low $\text{Ca}/(\text{Ca}+\text{Mg})$ values, but show considerable variation in Al_2O_3 content. Pyroxenes from grospydrite and kyanite eclogite nodules overlap a portion of the bimineralic eclogite field and are generally characterized by high $\text{Ca}/(\text{Ca}+\text{Mg})$ and Al_2O_3 values. Plotted in terms of these

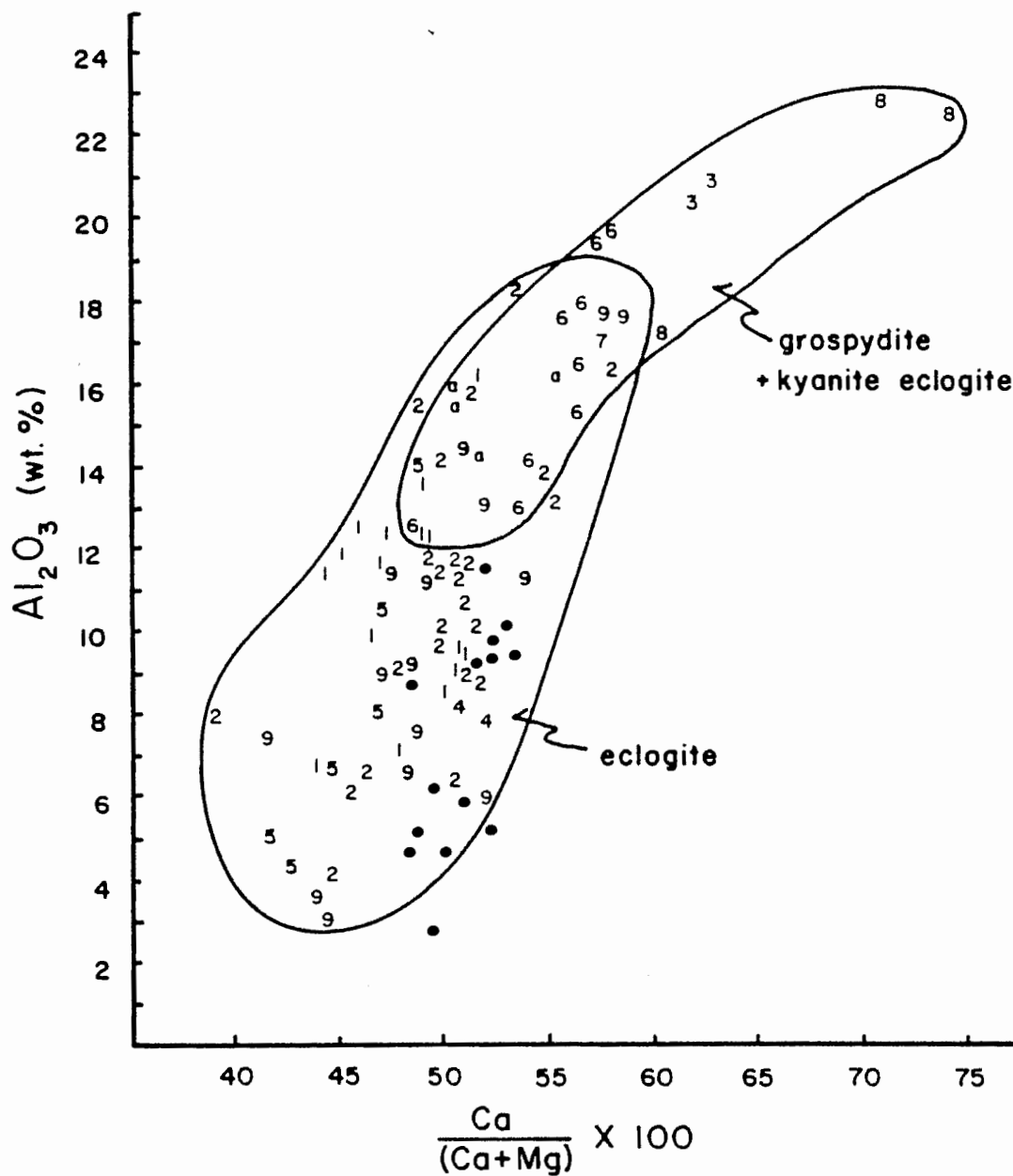


Figure 27: Summary plot of clinopyroxene compositions of Orapa samples (solid circles) compared with those taken from the literature for eclogitic inclusions in kimberlites. Data sources and symbols are the same as given in Figure 26.

variables, the average compositions of pyroxenes from individual Orapa eclogites plot mostly within the bimineral field and are characterized by a relatively restricted range in Ca/(Ca+Mg) ratios and by generally low to moderate Al₂O₃ contents.

The average compositions of coexisting garnets and clinopyroxenes from each of the individual eclogite nodules examined in this study are plotted in a Ca-Mg-Fe ternary diagram in Figure 28. Pyroxenes from these rocks show a relatively tight clustering near the diopside compositional end member and typically contain less than 10 mole % Fe substitution. The coexisting garnets, on the other hand, are characterized by a broad range of compositions involving substantial variation in the relative proportions of all three components. A similar pattern of compositional variation characterizes coexisting clinopyroxenes and garnets in eclogites from the Roberts Victor pipe in South Africa and has been summarized by Dawson (1980). The data from the Roberts Victor eclogites indicate that the clinopyroxenes coexisting with the most magnesium-rich garnets in eclogites from this locality are characterized by relatively high Cr₂O₃ contents. However, this relationship is not apparent in the data characterizing the coexisting phases from the Orapa eclogites.

Disaggregation of polymineralic nodules during transport has been considered as a possible source for silicate discrete nodules (Nixon and Boyd, 1973a) and diamonds (Robinson, 1979) occurring in associated kimberlite. As shown in Figure 28, the compositions of garnets and clinopyroxenes coexisting in Orapa eclogites show a slight overlap with the fields delineated by the associated discrete nodules and, moreover,

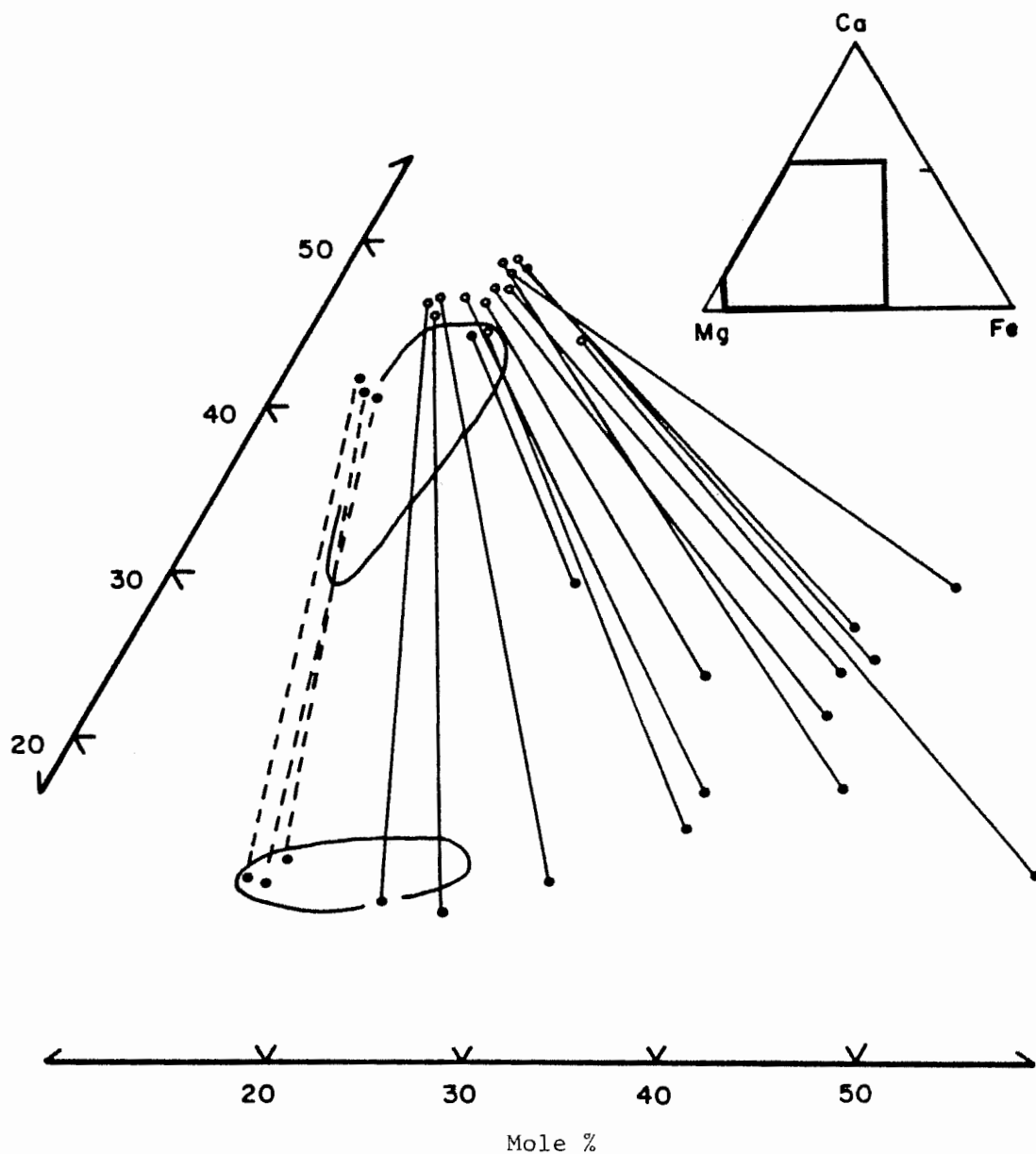


Figure 28: Average compositions of garnets (full circles) and clinopyroxenes (open circles) coexisting in eclogite xenoliths from Orapa plotted in terms of Ca-Mg-Fe components. Enclosed areas represent the compositional fields for garnet and clinopyroxene discrete nodules from Orapa and the dashed tie lines connect the compositions of garnet discrete nodules and associated clinopyroxene inclusions.

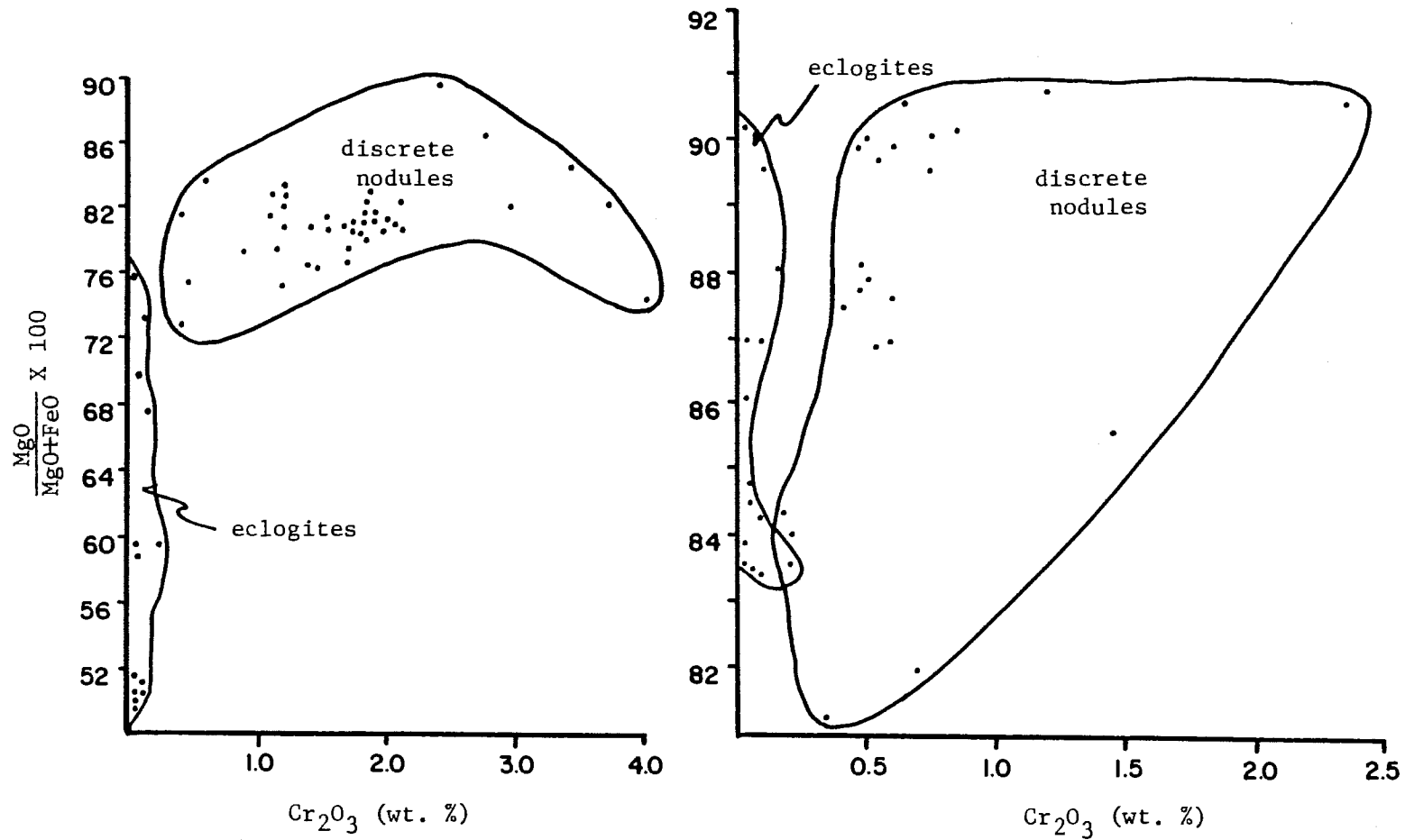


Figure 29a (left): Compositions of garnet discrete nodules and garnets in eclogites from Orapa plotted in terms of MgO/(MgO+FeO) ratio and Cr₂O₃ content.

Figure 29b (right): Compositions of clinopyroxene discrete nodules and clinopyroxenes in eclogites from Orapa plotted in terms of MgO/(MgO+FeO) ratio and Cr₂O₃ content.

appear to continue the compositional trends defined by these suites. However, other compositional parameters strongly suggest that these nodule types are paragenetically unrelated. The compositions of garnet discrete nodules and garnets in eclogite xenoliths from Orapa are plotted in terms of $\text{MgO}/(\text{MgO}+\text{FeO})$ ratio and Cr_2O_3 content in Figure 29a. The broad range in $\text{MgO}/(\text{MgO}+\text{FeO})$ ratio and characteristically low Cr_2O_3 contents typical of the eclogitic garnets contrast sharply with the relatively restricted magnesium/iron ratios and variable chrome contents of the discrete nodules. Chromium content also acts as a discriminant between the clinopyroxenes occurring in the eclogites and as discrete nodules at Orapa (Figure 29b) with the latter characterized by a broader range of typically higher Cr_2O_3 values. In this case, however, both suites are characterized by similar ranges in $\text{MgO}/(\text{MgO}+\text{FeO})$ ratios. The large disparity in grain size between the eclogites and discrete nodules is a further factor suggesting different parageneses for these inclusions at Orapa.

Rutile and ilmenite are the most common accessory phases in the Orapa eclogites. Average compositions for these minerals from individual eclogite nodules are presented in Tables 13 and 14. The rutile shows little compositional variation between nodules and between grains located in the same nodule. Individual grains appear to be homogeneous in major element composition within the analytical limits of the microprobe. The eclogitic rutile is compositionally distinct from that already described in the Orapa discrete nodule suite in that 1) TiO_2 values are consistently high, ranging from 97.0 to 99.9 wt. %, 2) iron (expressed as Fe^{3+}), aluminum, and chromium are the only significant

Table 13: Average chemical compositions of rutile grains in individual eclogite nodules from Orapa.

Specimen:	<u>103b-1R</u>	<u>104-2R</u>	<u>104-3R</u>	<u>106-1R</u>	<u>110-1R</u>	<u>110-2R</u>
TiO ₂	98.93	98.71	98.00	99.88	97.01	98.08
Cr ₂ O ₃	0.11	0.19	0.21	0.28	0.16	0.18
Al ₂ O ₃	0.32	0.13	0.22	0.18	0.63	0.50
*Fe ₂ O ₃	0.36	0.66	1.06	0.13	1.36	0.61
MgO	0.01	0.00	0.01	0.00	0.02	0.00
Total	<u>99.73</u>	<u>99.69</u>	<u>99.50</u>	<u>100.39</u>	<u>99.18</u>	<u>99.38</u>
Cations based on two (2) oxygens						
Ti	0.990	0.989	0.983	0.993	0.974	0.984
Cr	0.001	0.002	0.002	0.003	0.002	0.002
Al	0.005	0.002	0.004	0.003	0.010	0.008
Fe ³⁺	0.004	0.007	0.011	0.001	0.014	0.006
Mg	<u>0.000</u>	<u>0.000</u>	<u>0.000</u>	<u>0.000</u>	<u>0.000</u>	<u>0.000</u>
Total	<u>1.000</u>	<u>1.000</u>	<u>1.000</u>	<u>1.000</u>	<u>1.000</u>	<u>1.000</u>
n	4	2	3	1	3	2

* total iron expressed as Fe₂O₃

substituting cations, and 3) niobium, tantalum and zirconium, if present, occur in amounts below the detection limits of the electron microprobe. Analytical data regarding accessory oxides in kimberlite eclogites are relatively scarce and are at present limited to isolated studies of xenoliths from Yakutia (Sobolev et al., 1972), southern Africa (Smith and Dawson, 1975), and the Stockdale kimberlite in Kansas (Meyer and Boctor, 1975). In addition, Dawson and Smith (1977) have summarized a limited amount of data characterizing rutiles occurring in MARID (mica-amphibole-rutile-ilmenite-diopside) suite xenoliths from several localities in southern Africa and the Siberian province. According to these studies, rutiles from eclogite xenoliths are characterized by total iron values (expressed as Fe_2O_3) which are generally less than 2 wt. % and are distinct from the relative chrome-rich rutiles in MARID suite and peridotite inclusions in containing less than 0.5 wt. % Cr_2O_3 . Considered in these terms, the rutiles from the Orapa eclogites are typical. Dawson and Smith (1977) reported extremely fine-grained lamellae and microprobe analyses indicating relatively Fe-rich and -poor regions in rutiles from MARID suite rocks. Although these authors tentatively ascribed this to the presence of spinel intergrowths, it is possible that they were dealing with fine-scale ilmenite-rutile intergrowths similar to that previously described in Orapa specimen #102b. In fact, compositional data for this intergrowth are not reported in Tables 13 and 14 because of the variability observed in point analyses which apparently involved varying proportions of the two intergrown phases. The Orapa intergrowth is quite similar morphologically to those described from eclogites recovered from the

Stockdale kimberlite in Kansas by Meyer and Boctor (1975). The compositions of the host rutile in both cases are nearly identical.

The ilmenite occurring as accessory grains in the Orapa eclogites (Table 14) is characterized by very low chrome contents and MgO values ranging from 9.64 to 11.68 wt. %. The magnesium values differ slightly between xenoliths and between different grains within the same xenolith. Individual grains appear to be homogeneous. This eclogitic ilmenite differs compositionally from the associated ilmenite discrete nodules in that 1) TiO_2 contents are consistently lower, 2) chrome is present in quantities less than 0.2 wt. %, and 3) $\text{Fe}^{3+}/\text{Fe}^{2+}$ ratios (calculated) are significantly lower. Accessory ilmenite in kimberlitic eclogites is relatively rare and the limited data presented in this study represent the most detailed documentation of such an occurrence yet available in the literature. Meyer and Boctor (1975) described rare grains in eclogites recovered from the Stockdale kimberlite in Kansas and presented two representative analyses which bear a strong similarity to the average composition of eclogitic ilmenite from Orapa. It is not clear from the description by these authors whether ilmenite coexists with rutile in the Stockdale nodules, although this should probably not be expected on the basis of bulk chemical considerations and by analogy with the phase relations observed in the Orapa samples. Ilmenite occurring as one of the primary constituents in MARID suite nodules (Dawson and Smith, 1977) is, in general, compositionally similar to the ilmenite in eclogites from Orapa and Stockdale except that the latter are characterized by consistently lower chrome contents.

Table 14: Average chemical compositions of ilmenite grains in individual eclogite nodules from Orapa.

Specimen:	<u>108-1I</u>	<u>108-2I</u>	<u>109-1I</u>	<u>109-2I</u>	<u>109-3I</u>	<u>111-1I</u>	<u>111-2I</u>
TiO ₂	55.14	55.44	53.15	53.52	53.66	53.44	53.59
Cr ₂ O ₃	0.03	0.04	0.14	0.14	0.12	0.17	0.16
Al ₂ O ₃	0.54	0.47	0.31	0.35	0.13	0.45	0.27
'Fe ₂ O ₃	4.54	3.79	6.87	5.72	5.80	6.45	6.65
FeO	28.36	28.99	29.51	30.70	29.93	28.78	27.72
MgO	11.68	11.50	10.10	9.64	10.15	10.66	11.39
MnO	0.39	0.41	0.27	0.34	0.23	0.39	0.23
Nb ₂ O ₅	0.00	0.05	0.00	0.10	0.01	0.12	0.08
Total	<u>100.68</u>	<u>100.69</u>	<u>100.35</u>	<u>100.51</u>	<u>100.03</u>	<u>100.45</u>	<u>100.09</u>

Cations based on three (3) oxygens

Ti	0.953	0.960	0.934	0.942	0.946	0.934	0.936
Cr	0.001	0.001	0.003	0.003	0.002	0.003	0.003
Al	0.015	0.013	0.009	0.010	0.004	0.012	0.007
'Fe ³⁺	0.079	0.066	0.121	0.101	0.102	0.113	0.116
Fe ²⁺	0.545	0.558	0.577	0.601	0.587	0.560	0.538
Mg	0.400	0.395	0.352	0.336	0.355	0.369	0.394
Mn	0.008	0.008	0.005	0.007	0.005	0.008	0.004
Nb	<u>0.000</u>	<u>0.000</u>	<u>0.000</u>	<u>0.001</u>	<u>0.000</u>	<u>0.001</u>	<u>0.001</u>
Total	<u>2.001</u>	<u>2.001</u>	<u>2.001</u>	<u>2.001</u>	<u>2.001</u>	<u>2.000</u>	<u>1.999</u>
Mg/(Mg+Fe ²⁺)	0.423	0.414	0.379	0.359	0.377	0.397	0.423
n	4	2	4	4	4	5	5

' calculated

Representative chemical analyses of individual amphibole grains occurring in Orapa eclogite specimens #105 and 109 are presented in Table 15. Although certainly representative of the actual compositions, these analyses are not considered to have the accuracy and precision that characterizes the data obtained for other minerals in this study because of the highly altered nature of the amphibole grains. Nevertheless, the data are sufficient to characterize the amphiboles and to establish the compositional similarity between grains occurring in the different eclogites. The amphiboles may be classified according to the chemical criteria of Leake (1968) which involve the amounts of Si, Ca+Na+K, and Mg/(total Fe+Mn+Mg) in the calculated half-unit cell. No attempt has been made to estimate the ferric iron content from these analyses because of the uncertain effects of the widespread, closely intergrown alteration. Nevertheless, the Orapa amphiboles plot as edenitic hornblendes according to this classification system and this nomenclature seems appropriate based on the calculated presence of octahedrally coordinated aluminum and substantial substitution of sodium and potassium in the A-sites of the somewhat subcalcic structure. According to the Leake criteria, both of the prefixes sodic and subcalcic apply to these amphiboles with Na and Ca present as 1.249 and 1.480 cations per 24 (O,OH), respectively, in the average calculated formula. As stated in the petrography section, the only other analyzed occurrence of amphibole in kimberlite eclogite includes nodules from the Roberts Victor pipe in South Africa (Bishop et al., 1978) and the Stockdale area of Kansas (Meyer and Brookins, 1971). The amphiboles from these rocks are grossly similar in composition to those from Orapa

Table 15: Representative analyses of individual amphibole grains in Orapa eclogite nodules #105 and #109.

Specimen:	<u>105-1A</u>	<u>105-2A</u>	<u>109-1A</u>	<u>109-2A</u>
SiO ₂	45.08	45.43	47.50	47.44
TiO ₂	1.00	1.00	0.99	1.05
Cr ₂ O ₃	0.09	0.10	0.11	0.07
Al ₂ O ₃	11.98	11.96	11.16	10.94
FeO	6.11	6.19	5.07	5.14
MgO	17.04	16.97	19.08	19.14
MnO	0.03	0.04	0.01	0.06
CaO	9.80	9.60	9.66	9.79
Na ₂ O	4.61	4.60	4.40	4.50
K ₂ O	<u>1.04</u>	<u>1.08</u>	<u>0.95</u>	<u>1.02</u>
Total	96.78	96.97	98.93	99.15

Cations based on twenty-three (23) oxygens

Si	6.515	} 8.000	6.546	} 8.000	6.649	} 8.000	6.640	} 8.000
IVAl	1.485		1.454		1.351		1.360	
VIAl	0.557	} 5.090	0.579	} 5.099	0.492	} 5.188	0.447	} 5.171
Ti	0.109		0.108		0.105		0.111	
Cr	0.010	} 5.090	0.012	} 5.099	0.012	} 5.188	0.008	} 5.171
Fe	0.738		0.747		0.594		0.602	
Mg	3.673	} 5.090	3.648	} 5.099	3.984	} 5.188	3.995	} 5.171
Mn	0.003		0.005		0.001		0.008	
Ca	1.518	} 2.000	1.484	} 2.000	1.450	} 2.000	1.469	} 2.000
Na ^{M4}	0.482		0.516		0.550		0.531	
Na ^A	0.810	} 1.003	0.771	} 0.969	0.644	} 0.814	0.692	} 0.874
K	0.193		0.198		0.170		0.182	
Total	16.093		16.068		16.002		16.045	

except for somewhat lower SiO_2 contents, slightly higher Al_2O_3 values, and differing $\text{Fe}/(\text{Fe}+\text{Mg})$ ratios. Although probably unverifiable on the basis of the limited evidence available, this general similarity in composition may be a function of the likely secondary origin of these amphiboles, with the observed chemical differences representing variations in the primary silicate compositions. Amphiboles occurring in MARID suite xenoliths (Erlank and Finger, 1970; Dawson and Smith, 1977) generally plot as subcalcic potassic richterites or subcalcic potassic sodic richterites in the Leake (1968) classification and may be differentiated from the eclogitic amphiboles on the basis of their characteristic higher SiO_2 , MgO , and Na_2O contents and substantially lower Al_2O_3 values. Such amphiboles are quite similar in composition to potassic richterites occurring in mica-rich peridotite nodules from the Dutoitspan, Wesselton, and Bultfontein localities in South Africa (Aoki, 1974, 1975). There appears at present to be little question regarding the importance of volatile components in the upper mantle (Wyllie, 1979b) and, in view of the experimental evidence for the high pressure stability of potassic richterite in certain bulk chemical compositions (Kushiro and Erlank, 1970), this phase may possibly be an important volatile reservoir. As a result, the origin of apparently deep-seated, richterite-bearing assemblages has been the subject of considerable study and has been to date variously interpreted as due to processes ranging from subsolidus peridotite reaction with K-rich aqueous fluids (Aoki, 1975) to local igneous accumulation with or without associated metasomatism at depths of approximately 50-100 km in the upper mantle (Erlank, 1976; Dawson and Smith, 1977).

Geothermometry and Geobarometry

Extrapolations of data from experimental studies to geochemically more complex natural systems in order to determine possible temperatures and pressures of nodule equilibration is not only presently useful in attempts to characterize the conditions influencing petrogenetic processes in the lower crust and upper mantle, but may in the future result in the ability to predict diamond-producing capabilities of individual kimberlite pipes based on chemical parameters characterizing the relatively abundant, silicate and/or oxide phases. In essence, all such attempts involve utilizing mineral chemical data from coexisting phases in order to derive independent estimates of the temperatures and pressures of assumed equilibration. The landmark study of Boyd (1973) involved phase relations in a large suite of lherzolite nodules and resulted in the determination of a possible geotherm characteristic of the crust and upper mantle beneath Lesotho at the time of kimberlitic emplacement throughout that province. Temperatures for this geotherm were estimated from the $\text{Ca}/(\text{Ca}+\text{Mg})$ ratios of the clinopyroxenes (Davis and Boyd, 1966) and pressures were estimated from the Al_2O_3 content of the associated orthopyroxenes coexisting with pyrope garnet (MacGregor, 1974). Although the Lesotho pyroxene geotherm closely approximated the shield geotherm previously calculated by Clark and Ringwood (1964) at depths above approximately 170 km, the nodule data showed a sharp inflection at greater depths which Boyd ascribed to frictional heating at the base of the southern Africa lithosphere. Geotherms obtained from xenoliths from the Premier kimberlite pipe in South Africa (Danchin and

Boyd, 1976; Danchin, 1979), alkali basalts from Hawaii (MacGregor, 1974), and kimberlites from various locations in South Africa, Lesotho, and Namibia (MacGregor and Basu, 1974) are all characterized by a similar deep-seated inflection. However, geotherms derived from xenolithic peridotites and orthopyroxene discrete nodules from kimberlite pipes in the Colorado-Wyoming district (Eggler et al., 1979) and from garnet peridotite nodules from alkalic intrusions in Montana (Hearn and Boyd, 1975) show no apparent inflection, although it should be noted that the Montana suite consists of relatively few specimens. Although the general similarity in configuration between geotherms determined at different locations appears to substantiate the significance of such curves, Mercier and Carter (1975) have questioned the existence of deep-seated inflection limbs on the basis of a variety of geophysical constraints and Irving (1976) has demonstrated the need for caution in the interpretation of such data.

Determination of a possible Cretaceous geotherm for the lithosphere beneath Botswana cannot be undertaken from the eclogite data alone because the absence of orthopyroxene makes pressure calculations impossible. Nevertheless, an estimation of a possible temperature and pressure range characterizing the Orapa eclogite suite can be attempted by use of independent temperature determinations and certain assumptions regarding the configuration of the appropriate paleogeotherm. Estimation of equilibrium temperatures for the eclogite suite is possible through application of the geothermometers of either Akella and Boyd (1974) or Råheim and Green (1974). The Akella and Boyd (1974) calibration is based on experiments using mechanical mixtures of natural

mineral separates and involves direct calculation of equilibration temperatures from the magnesium-iron partitioning coefficient, expressed as $K_D^{\text{gnt/cpx}} = \frac{(\text{MgO/FeO})_{\text{gnt}}}{(\text{MgO/FeO})_{\text{cpx}}}$, between coexisting garnet and clinopyroxene over the pressure range 31-44 kb. The Råheim and Green (1974) technique involved a series of experimental studies of synthetic glass compositions and demonstrated a direct relationship between $\ln K_D$, expressed as $K_D^{\text{gnt/cpx}} = \frac{(\text{FeO/MgO})_{\text{gnt}}}{(\text{FeO/MgO})_{\text{cpx}}}$, and pressure in the range of 20 to 40 kb at a constant temperature of 1100°C. This relationship may be expressed through the equation $T(^{\circ}\text{K}) = \frac{3686 + 28.35 \times P(\text{kb})}{\ln K_D + 2.33}$, by which it is possible to calculate either the temperature or pressure of equilibration for an eclogite assemblage when one of these two variables and the appropriate partition coefficient are known. It should be emphasized that differences exist between the chemical compositions of average garnets and clinopyroxenes from the Orapa eclogites and the analyzed run products from both studies, indicating that values calculated by either method should be considered as only first-order approximations of the actual equilibrium conditions represented by the nodules.

This limitation notwithstanding, an attempt has been made to estimate the temperature and pressure range of Orapa eclogite equilibration by using the paleogeotherm determined for the Cretaceous lithosphere beneath Lesotho by Boyd (1973) as a basis for calculation. This geotherm was chosen because of 1) the close spatial proximity of the Lesotho and central Botswana cratonic areas, 2) the Cretaceous age of emplacement in the two areas, and 3) the similarity between the Boyd (1973) geotherm and those determined for other areas of kimberlitic intrusion in southern Africa (MacGregor and Basu, 1974; Danchin and

Boyd, 1976; Danchin, 1979). For this first-order estimation of the temperature and pressure range characterizing the Orapa suite, temperatures were calculated according to the Akella and Boyd (1974) geothermometer and plotted on the Lesotho geotherm in order to generate corresponding pressures.

Using average compositions of coexisting garnets and clinopyroxenes to calculate representative K_D values for individual eclogites, the Orapa data indicate a temperature range of approximately 870-1150°C according to the Akella and Boyd (1974) calibration which, when plotted on the Lesotho geotherm (Figure 30), corresponds to a pressure range of approximately 35-56 kb and a possible depth range of approximately 114-183 km. These temperature estimates are not uniformly distributed, however, and may be divided into a well defined cluster of ten relatively low temperature nodules (870-955°C) and a more widely spaced, high temperature grouping of four nodules (1015-1150°C). The pressure range encompassed by the low temperature group is approximately 35-41 kb, corresponding to a possible depth range of 114-136 km, and the pressure range encompassed by the high temperature group is approximately 47-56 kb, corresponding to a possible depth range of 154-183 km. The agreement between the Akella and Boyd (1974) and the Råheim and Green (1974) geothermometers, assuming a pressure of 30 kb for the latter, is excellent ($\Delta T_{ave} = 12^\circ\text{C}$) for nodules in both subgroups. This is not surprising, however, in view of the fact that the two geothermometers were calibrated for what are essentially the same chemical partitioning equilibria. A systematic difference exists between the two methods, nevertheless, and is manifested by the slightly higher ($\Delta T = 5-15^\circ\text{C}$) temperatures

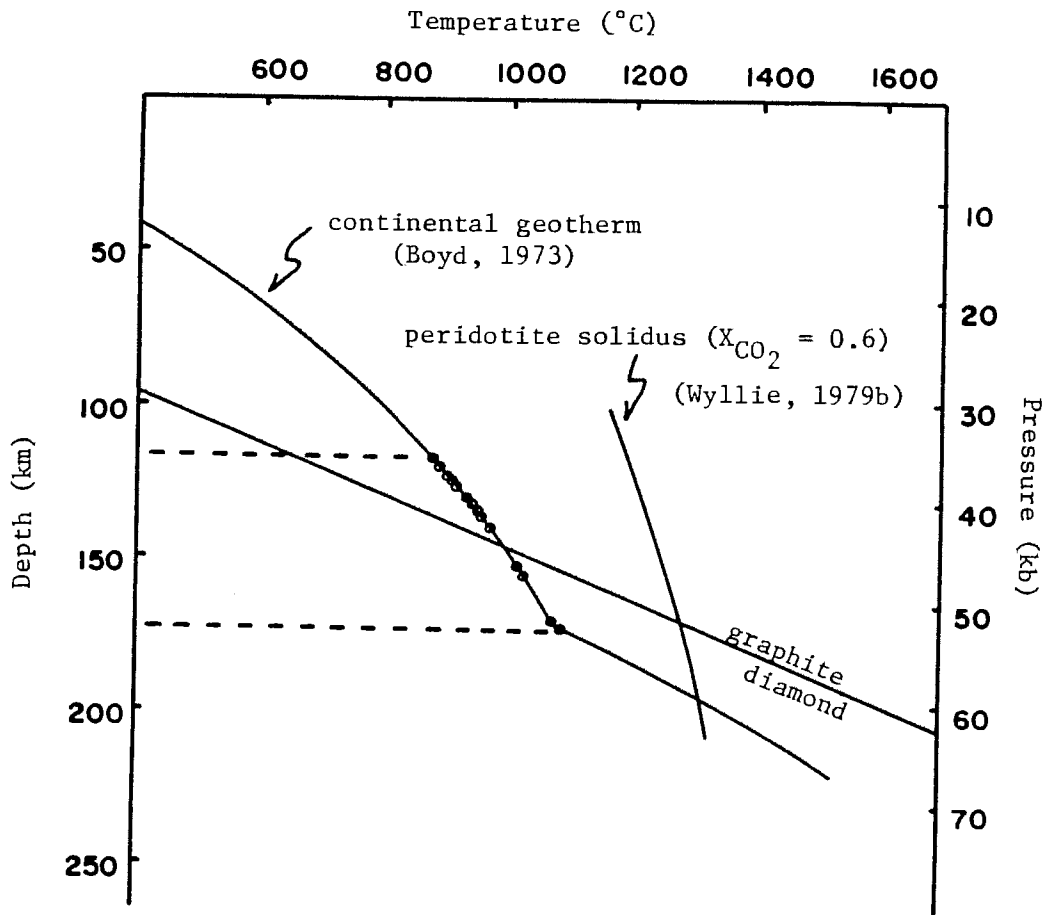


Figure 30: Temperature-pressure plot of individual eclogite nodules from Orapa using the Boyd (1973) continental geotherm for Lesotho as a reference. The diamond-graphite stability curve is plotted using data from Kennedy and Kennedy (1976).

calculated for each nodule using the Akella and Boyd (1974) calibration.

Although the derivation of these temperatures and pressure conditions is rather crude and involves analogy with phase and bulk compositions not strictly coincident with those characterizing the Orapa eclogites, this estimation is believed to approximate the equilibrium conditions represented by the eclogite suite and is supported by several lines of evidence. There is, of course, no indication that the 14 nodules examined in this study comprise a truly representative sampling of the eclogite inclusions in the Orapa kimberlite and thus the temperature and pressure range inferred from these nodules can only be interpreted as a minimum. Nevertheless, the observed intersection (Figure 30) of the geotherm segment encompassed by the Orapa eclogites and the diamond-graphite stability curve of Kennedy and Kennedy (1976) is consistent with the known occurrence of nodules bearing diamond, graphite, and both diamond and graphite at Orapa. The fact that eclogite nodule #OR-102, which contains coarse graphite, plots well within the graphite stability field is also encouraging. It should be noted that the point of intersection between the carbon polymorph stability curve and the geotherm segment occurs within the interval separating the high and low temperature nodule groupings. However, the significance of this intersection cannot be unambiguously interpreted due to the limitations inherent in the data and may in large part represent an artifact of the limited number of samples. Although the poorer agreement between geothermometers for the four high temperature nodules probably indicates a somewhat different configuration of the actual paleogeotherm within the

diamond stability field, the lower limit of the segment occupied by the Orapa eclogite xenoliths should not extend beyond the region of possible kimberlite magma production. Recent experimental work and theoretical considerations (Wyllie and Huang, 1975; Eggler and Wendlandt, 1979; Wyllie, 1979a, 1979b) have suggested that production of kimberlite magma involves the partial melting of mantle peridotite containing minor amounts of H_2O and CO_2 , probably locked within the structures of phlogopite and dolomite respectively. The location of such a melting event can be estimated by the zone of intersection defined by a series of peridotite solidi, characterized by various $CO_2/(CO_2+H_2O)$ ratios (Wyllie, 1979a), and the approximate geotherm. One such intersection is shown in Figure 30, occurring at approximately $1300^\circ C$ and 59 kb for peridotite in equilibrium with a vapor composition of $X_{CO_2} = 0.6$. Although the exact location of such a potential melting zone is a complex function of factors influencing the slope of the geotherm and the peridotite vapor composition, none of which can be constrained by the data in this study, the wide separation between the high temperature nodules and this potential kimberlite source region leaves room for considerable fluctuation in the positioning of these curves and is consistent with the observed xenolithic nature of the eclogites.

These interpretations regarding the eclogite suite, as stated above, represent only first-order approximations but, nevertheless, are consistent with the observed presence of diamond and graphite and, as such, strongly suggest that these xenoliths equilibrated under upper mantle conditions. The nature of such eclogite at high levels of the earth's mantle is still a matter of speculation, but may take the form of

geophysically unresolvable, isolated bodies occurring at depths above more substantial eclogite regions such as the gravitationally stable layer postulated to exist between 220-400 km by Anderson (1979). The configuration of the Boyd (1973) paleogeotherm is probably not strictly applicable to the upper mantle beneath Botswana and the poor agreement between geothermometers for the high temperature nodules may indicate that a slope change occurs close to the diamond-graphite stability curve intersection. Nevertheless, the observations outlined above appear to indicate that the Lesotho curve may serve as a useful approximation of the Cretaceous geotherm beneath Botswana and, in any case, the chain of reasoning used in interpreting these data seems to be at least as justifiable as the previously employed procedures of assuming that entire suites equilibrated along linear extensions of associated ultramafic trends (MacGregor, 1979) or at some unique point along the diamond-graphite stability curve (Shee, 1978). It should be noted that the three Orapa eclogite nodules characterized by foliated textures plot in the highest portion of the geotherm segment occupied by the nodules and, as such, appear to be unrelated to the exclusively deep-seated, sheared peridotites reported from Lesotho by Boyd (1973). The significance of all of these interpretations regarding the Orapa eclogite suite will be considered in conjunction with the data characterizing the other nodules recovered from this pipe in the next section.

CHAPTER V

DISCUSSION

The Orapa nodule suite provides several opportunities to compare temperature estimates calculated by different geothermometers using data from the same mineral assemblages. Although useful for comparative purposes, the results from such an exercise must be interpreted with caution because of the numerous problems inherent in the extrapolation of laboratory data from different sources to more chemically complex natural systems in which equilibrium characteristics may be more difficult to delineate. This limitation notwithstanding, the following discussion is an attempt to develop and evaluate a series of comparative estimates of equilibration temperatures calculated from a variety of Orapa nodule data.

As previously described, temperatures of equilibration may be estimated for the three garnet nodules containing clinopyroxene inclusions by use of Fe/Mg partitioning data (Akella and Boyd, 1974) or by assuming that the compositions of the pyroxenes are constrained to the pyroxene solvus (Davis and Boyd, 1966; Lindsley and Dixon, 1976). Both pyroxene geothermometers yield results close to those obtained by the Akella and Boyd (1974) method (Table 16) with temperatures determined using the Davis and Boyd (1966) solvus (30 kb) consistently lower ($\Delta T_{ave} = -52^{\circ}\text{C}$) and those determined using the Lindsley and Dixon (1976) solvus (20 kb) consistently higher ($\Delta T_{ave} = +46^{\circ}\text{C}$). The agreement between these estimates, involving two different sets of mineral equilibria calibrated over a range of pressures, is encouraging although the 100°C discrepancy

Table 16: Comparative temperature estimates for garnet discrete nodules containing clinopyroxene inclusions from Orapa.

Specimen:	<u>225C</u>	<u>226A</u>	<u>226D</u>
Ca/(Ca+Mg) _{cpx}	0.424	0.423	0.431
K _D = (FeO/MgO) _{gnt/cpx}	2.318	2.065	2.354
<u>geothermometer</u>		<u>temperature</u> (°C)	
Davis and Boyd (1966)	1130	1130	1115
Akella and Boyd (1974)	1162	1214	1156
Lindsley and Dixon (1976)	1230	1230	1210
Råheim and Green (1974) 30 kb	1158	1212	1151
Råheim and Green (1974) 20 kb	1068	1119	1062

between the pyroxene solvus determinations exceeds that which may be expected from analytical error alone. Because Lindsley and Dixon (1976) have demonstrated the existence of a pressure effect on the diopside solvus, the Råheim and Green (1974) geothermometer was utilized as a fourth estimation of possible equilibrium temperatures for these nodules. As shown in Table 16, the agreement between the Akella and Boyd (1974) and the Råheim and Green (1974) estimates, assuming a pressure of 30 kb for the latter, is excellent, while the Råheim and Green (1974) determinations assuming a pressure of 20 kb are even lower than those obtained using the Davis and Boyd (1966) solvus. The results appear to indicate that estimates based on either of the pyroxene solvi alone could be inaccurate for these specimens, and that the use of other independent geothermometers, when available, is a necessary prerequisite to meaningful interpretation.

A similar analysis of comparative geothermometry can be applied to the three ilmenite-bearing eclogite assemblages (#OR-108, 109, and 111) and to the ilmenite-clinopyroxene discrete nodule intergrowth (#OR-430B) from Orapa. Bishop (1980) used a variety of experimental data to calibrate the partitioning behavior of Fe^{2+} and Mg^{2+} between coexisting ilmenite and clinopyroxene as a function of temperature, pressure, and chemical composition. This geothermometer incorporates a strictly regular solution model for the coexisting phases and is based on pyroxene compositions that are restricted to the diopside-hedenbergite join and ilmenites that may be described solely in terms of FeTiO_3 (ilmenite) and MgTiO_3 (geikielite) components. According to this formulation, equilibration temperatures may be calculated for coexisting ilmenite and

clinopyroxene by use of the equation:

$$T (^{\circ}\text{K}) = \frac{748 + 2745\left\{\frac{\text{Mg}}{\text{Mg}+\text{Fe}^{2+}}\right\}_{\text{cpx}} + 817\left\{2\left\{\frac{\text{Fe}^{2+}}{\text{Fe}^{2+}+\text{Mg}}\right\}_{\text{ilm}} - 1\right\} + 0.0106 \cdot P}{\ln K_D}$$

where $K_D = (\text{Mg}/\text{Fe}^{2+})_{\text{cpx}} / (\text{Mg}/\text{Fe}^{2+})_{\text{ilm}}$. It should be noted that there is a misprint in this equation as presented within the abstract of the original Bishop (1980) paper. Temperatures calculated assuming a pressure of 30 kb for the Orapa samples (Table 17) range from approximately 1123 to 1266°C for the three eclogites and suggest equilibration at approximately 1512°C for the ilmenite-clinopyroxene nodular intergrowth. Comparative estimates calculated for the three eclogites using Fe/Mg partitioning data (Akella and Boyd, 1974; Råheim and Green, 1974) and a possible pyroxene solvus analogue (Davis and Boyd, 1966) do not overlap with this calculated temperature range, however, clustering instead at relatively lower temperatures ranging from approximately 930 to 1035°C.

Factors which may possibly contribute to this observed discrepancy include 1) significant differences between the closure temperatures for atomic migration in the ilmenite-clinopyroxene, garnet-clinopyroxene, and orthopyroxene-clinopyroxene systems, 2) inaccuracies in the activity-composition relationships derived from experimental data for coexisting ilmenite and clinopyroxene by Bishop (1980), 3) the presence of ferric iron in any of the participating phases, and 4) the uncalibrated effects of components other than diopside and hedenbergite present in the clinopyroxene. The possible contribution of the first factor cannot at present be rigorously evaluated because of the limited availability of accurate Fe/Mg diffusion data (Freer, 1981) and uncertainties regarding

Table 17: Comparative temperature estimates for ilmenite-bearing eclogites and ilmenite-clinopyroxene intergrowth nodule #OR-430B from Orapa. For estimates involving a pressure term, $P = 30$ kb.

a) calculations based on $Fe^{2+} = Fe_{total}$ in the clinopyroxene:

Specimen:	eclogite			ilm-cpx
	<u>108</u>	<u>109</u>	<u>111</u>	<u>430B</u>
$Ca/(Ca+Mg)^{cpx}$	0.484	0.492	0.485	0.449
$K_D = (FeO/MgO)^{gnt/cpx}$	2.854	4.091	2.711	-
$K_D = (Mg/Fe^{2+})^{cpx/ilm}$	2.559	2.673	2.361	2.031
geothermometer		temperature ($^{\circ}C$)		
Bishop (1980)	1167	1123	1266	1512
Råheim and Green (1974)	1069	940	1090	-
Akella and Boyd (1974)	1078	953	1098	-
Davis and Boyd (1966)	920	900	920	940
Lindsley and Dixon (1976)	-	-	-	1040

b) calculations based on $Fe^{2+} = 0.7 Fe_{total}$ in the clinopyroxene:

$K_D = (FeO/MgO)^{gnt/cpx}$	4.805	5.854	3.875	-
$K_D = (Mg/Fe^{2+})^{cpx/ilm}$	18.205	20.692	15.032	10.863
Bishop (1980) (2 comp)	1019	985	1099	1278
Bishop (1980) (7 comp)	898	907	964	1131
Råheim and Green (1974)	941	834	958	-
Akella and Boyd (1974)	953	849	970	-
Davis and Boyd (1966)	920	900	920	940
Lindsley and Dixon (1976)	-	-	-	1040

the relative effects of various environmental parameters on diffusion-blocking mechanics (Fraser and Lawless, 1978). It should also be noted that this sampling is obviously too small to provide any indication regarding the possibly large difference in blocking temperatures observed for Mg-Fe diffusion between garnet and clinopyroxene relative to Ca-Mg diffusion between clinopyroxene and orthopyroxene coexisting in ilmenite nodules from a variety of kimberlite pipes in southern Africa by Fraser and Lawless (1978).

The magnitude of the coefficients to the mole fraction terms in the Bishop (1980) equation given above demonstrates the necessity of using accurately defined activity-composition data in this estimation of paleo-temperatures calculated from mineral equilibria. This requisite was emphasized by Bishop (1980) and is particularly important in the ilmenite-clinopyroxene model in which both phases are considered non-ideal. The likelihood of a significant contribution to the discrepancy in calculated temperatures from this factor is underscored by the difference (+2.5 kcal) between the $\Delta G_{\text{rxn}}^{\circ}$ determined from the experimental results used to calibrate this geothermometer and the $\Delta G_{\text{rxn}}^{\circ}$ calculated using free energies of formation taken from literature sources for each of the end members.

Although geothermometry calculations generally assume $\text{Fe}^{2+} = \text{Fe}_{\text{total}}$, limited ferric iron substitution may be relatively common and, as such, would affect any temperature estimates involving iron compositional data. Unfortunately, analytical data regarding the $\text{Fe}^{3+}/\text{Fe}^{2+}$ ratios of various kimberlitic pyroxenes are generally lacking except for four analyses of clinopyroxenes from nodular intergrowths (Bishop, 1977) which

indicated that ferric iron was present as $Fe^{3+} = 0.3 Fe_{total}$. Temperature estimates based on this iron ratio are presented for the four Orapa nodules in Table 17. These data indicate that two effects of this possible substitution are 1) to generally lower all temperatures calculated from iron-bearing mineral equilibria and 2) to diminish the gap between estimates determined using the Bishop (1980) formulation and the others involving various silicate equilibria.

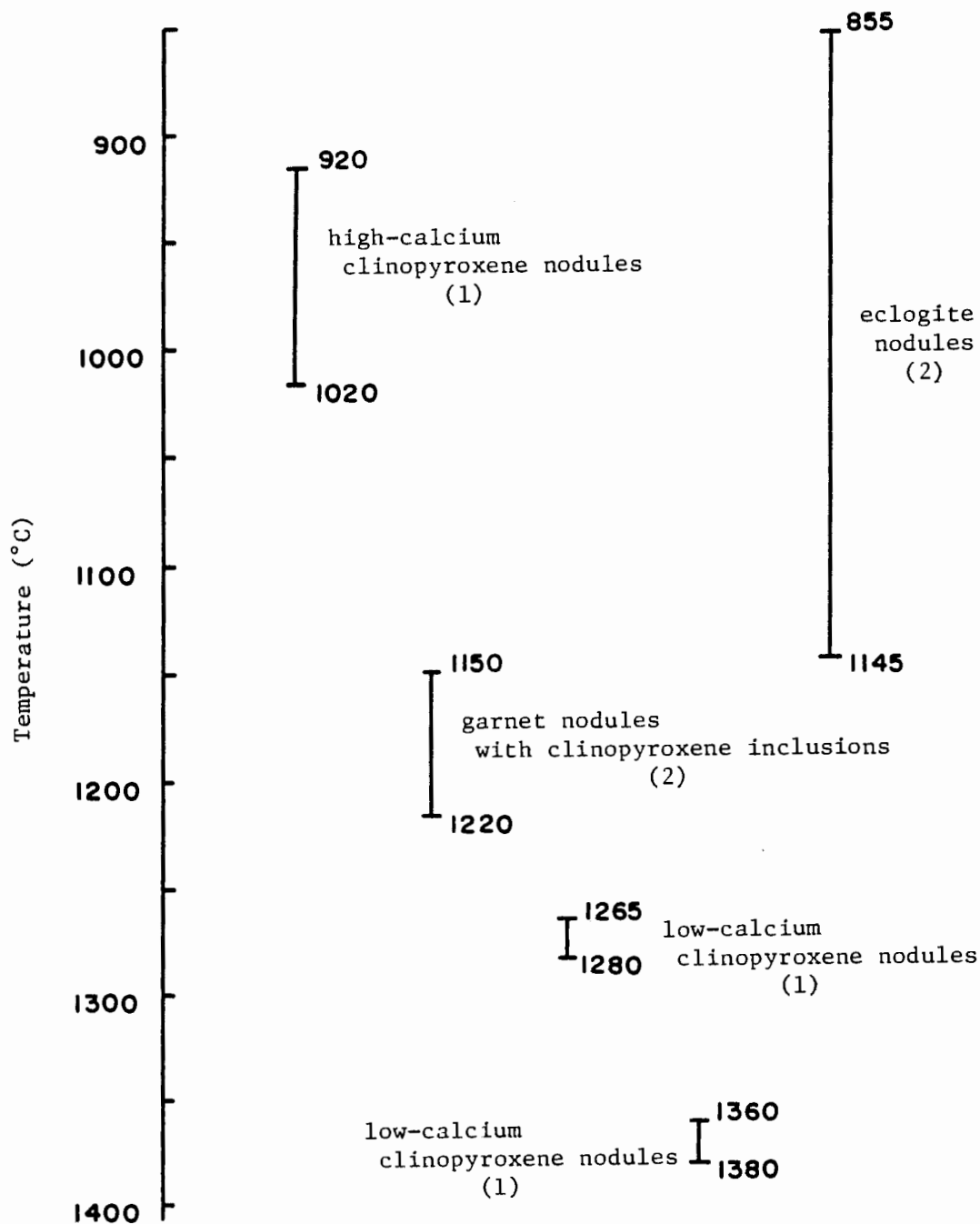
The presence of other non-binary components in clinopyroxene is likely to affect binary-based formulations such as the Bishop (1980) geothermometer because of the large degree to which such substitutions occur in kimberlite and kimberlite-related systems. Although complex thermochemical models can in theory be derived to consider these effects, such tools are generally not available due to the lack of appropriate thermochemical data regarding the numerous possible end members. Nevertheless, the Bishop (1980) solution model can be expanded to consider the pyroxene compositions in terms of seven components (diopside-hedenbergite-enstatite-acmite-jadeite-ureyite-tschermakite), of which only diopside and hedenbergite are considered non-ideal (J.R. Beckett, unpublished data, 1982). As expected, this has the effect of further diluting the contribution of the diopside-hedenbergite binary components and, as shown in Figure 17, results in further lowering of the temperatures calculated through the Bishop (1980) formulation. In addition, as may also be noted from Figure 17, this formulation further reduces the apparent discrepancy between temperatures calculated using the various techniques to an average of less than $10^{\circ}C$ for the eclogites.

These data illustrate the importance of multi-component modelling and, where applicable, the need for accurate determination of $\text{Fe}^{2+}/\text{Fe}^{3+}$ ratios in geothermometry. Modelling of mineralogic equilibria and the calibration of pertinent geothermometers have been greatly advanced in recent years by the application of detailed microprobe data but, as stated above, are presently constrained by the limited availability of appropriate thermochemical measurements. The problem in determining the ferric iron content of the coexisting silicates clearly affects the accuracy of estimations involving iron compositional data and, although accurate wet chemical FeO determinations can be performed routinely on relatively large, clean sample subsplits, it remains difficult to analyze ferric iron in small quantities of intricately intergrown silicates. As a result, the vast majority of kimberlitic silicate data reported in the literature assumes $\text{Fe}^{2+} = \text{Fe}_{\text{total}}$ and thus, for the purposes of comparison, it presently appears best to compute and compare the Orapa data on this basis.

The discrepancy in temperature estimates based on the Bishop (1980) formulation and those obtained using any of the other methods is probably a function of all four of the factors mentioned above and is particularly not surprising in view of the considerable non-binary substitutions characterizing the Orapa clinopyroxenes. The limited applicability of this geothermometer was noted in the initial description of this technique (Bishop, 1980) and is likely to remain a problem until the calibration is extended to include compositions that are removed from the corresponding binary joins. Nonetheless, the clustering of temperature estimates based on silicate equilibria suggests that the ilmenite-bearing

eclogites from Orapa equilibrated within or near the temperature range 900 - 1100°C at a possible pressure of 30 kb. This temperature span encompasses most of the equilibration range indicated by the entire eclogite suite (Figure 31). The temperature estimates based on diopside solvus data (Davis and Boyd, 1966) are probably subject to the greatest error in view of 1) the known pressure effect on the diopside limb (Lindsley and Dixon, 1976), 2) the tentative nature of assumed saturation with an enstatite component, and 3) the extreme sensitivity of this geothermometer to the presence of non-binary components in the pyroxene, as previously discussed. Nevertheless, the agreement between temperatures estimated using the two methods based on Fe/Mg partitioning data and the pyroxene solvus geothermometer (Table 17) is encouraging. Temperature estimates based on the Lindsley and Dixon (1976) solvus data have not been made for the eclogites because the relatively diopside-rich nature of the pyroxenes when projected onto the diopside-enstatite join necessitates undue extrapolation of the original experimental data. An estimate is possible for the ilmenite-clinopyroxene intergrowth, however, and falls at approximately 1040°C. This estimate is 100°C above the corresponding value calculated using the Davis and Boyd (1966) solvus and less than 100°C lower than the value calculated using the seven component ilmenite-clinopyroxene formulation based on Bishop (1980). If this temperature is considered to be representative of equilibration conditions for the Orapa intergrowth, then the estimate falls only slightly below the low temperature range defined by lamellar intergrowths from a variety of worldwide localities (Bishop, 1980).

Figure 31: Comparative geothermometry of five nodule groups from Orapa. All calculations assume a pressure of 30 kb.



(1): temperatures determined using Davis and Boyd (1966)

(2): temperatures determined using Raheim and Green (1974)

Although the two sets of consistent geothermometry data (Tables 16 and 17) are encouraging, accurate temperature-pressure relations cannot be delineated for most of the Orapa nodule suite. A summary of the data that can be generated is presented in Figure 31 which contains the temperature ranges calculated for five groups of nodules at an assumed pressure of 30 kb. The data indicate that these five nodule groups encompass a broad range of possible equilibrium temperatures extending, with minor gaps, from approximately 855°C to at least 1380°C. The highest temperatures are recorded by the two groups of subcalcic diopside discrete nodules (see Figure 17) which are characterized by ranges of 1265-1280°C and 1360-1380°C when plotted on the diopside solvus of Davis and Boyd (1966). Similar temperatures have been determined for diopside nodules from the Monastery pipe in South Africa (Gurney et al., 1979) and from several pipes in Lesotho (Nixon and Boyd, 1973a). The only garnet nodules for which temperature data are available are the three specimens with clinopyroxene inclusions and which, as previously described (Table 16), encompass a possible range of 1150-1220°C. This range is lower than those calculated for similar nodules from the Colorado-Wyoming district (Smith et al., 1976) and from a number of pipes in South Africa and Lesotho (Kresten, 1973; Nixon and Boyd, 1973a; Gurney et al., 1979).

The group of relative Ca-rich diopside discrete nodules from Orapa (see Figure 17) is characterized by temperatures ranging from approximately 920 to 1020°C when plotted on the Davis and Boyd (1966) solvus. Such temperatures are comparable to those calculated for the chrome-rich suite and relatively calcic members of the chrome-poor diopside suite

from Colorado-Wyoming (Eggler et al., 1979). Temperatures in the lower portions of this range and which are not confirmed by some other method, must be interpreted with caution, however, because of the relative insensitivity of the diopside solvus at low temperatures (MacGregor and Basu, 1976; Mori and Green, 1976).

The suite of eclogite nodules from Orapa exhibits the largest range in equilibrium temperatures, extending from approximately 855 to 1145°C using the 30 kb equation of Råheim and Green (1974). This temperature range is nearly coincident with a similar range determined for a suite of comparable eclogites from Angola by Boyd and Danchin (1980). It is interesting to note that this Angolan suite is also characterized by low temperature (800-900°C) and high temperature (1050-1200°C) subgroups which correspond roughly to similar groupings in the data calculated at 30 kb for the Orapa nodules. A similar 30 kb temperature range of 800 to 1200°C, but apparently without subgroups, characterizes a suite of eclogite nodules described by Bishop et al. (1978) from a variety of pipes in southern Africa.

The similarity in temperature calculated for corresponding inclusions from widely separated localities is, of course, encouraging and may be indicative of as yet unspecified, repeatable processes occurring at depth within the lithosphere. Nonetheless, conjecture concerning such processes remains beyond the scope of this project and, in any case, must be preceded by questions of a more fundamental nature concerning the meaning of such temperature estimates. For instance, there is at present no definitive evidence to unequivocally delineate exactly what type of mantle event is represented by the K_D value measured for

coexisting garnet and clinopyroxene. There is little question that K_D values determined for relatively homogeneous phases such as the garnets and clinopyroxenes occurring in the eclogites and garnet discrete nodules with clinopyroxene inclusions from Orapa have probably locked in a record of mineralogic equilibrium. However, the nature of this equilibrium remains unspecified. As reviewed by Boyd and Danchin (1980), K_D values should initially record crystallization temperatures and, as Fe and Mg migrate during subsolidus cooling, should continually change in response to the decreasing temperature. In this way, it may be possible for a set of measured K_D values to record ambient conditions at the site of eclogite residence in the mantle. However, the ability of the assemblage to record this information is a function of the relative rate of atomic migration and the pace of change in the environmental conditions, and it is therefore possible that any temperature between that of crystallization and the ambient may be recorded by individual garnet-clinopyroxene pairs. In a like manner, it is also possible that such mineral assemblages may record any temperature between that ambient in the zone of original crystallization and some other, different ambient to which the assemblage may be subjected as a result of movement due to deep-seated tectonic processes (for example, see Lappin and Dawson, 1975). Thus it is not possible to interpret the Orapa K_D data in terms of specific mantle events other than to infer that, whatever their specific meaning, the temperatures determined from these characteristically homogeneous phases probably represent a record of mineralogic equilibrium.

The interpretation of such xenoliths is further complicated by the uncertain relationship between most nodule suites and the host

kimberlite. Models regarding this relationship have in general varied between two end member hypotheses in which nodules are considered to be either 1) cognate inclusions of materials which form as a by-product of kimberlite magma generation (O'Hara and Yoder, 1967) or 2) accidental inclusions of deep-seated wall rocks incorporated into the kimberlite during its forceful intrusion through the mantle (Barrett, 1975). The former hypothesis has been advanced in conjunction with models primarily concerned with the generation of deep-seated basaltic magmas and involves the production of eclogite cumulates and silica-poor ("kimberlitic") liquids as a result of the fractional crystallization of a picrite parent magma which is itself produced by the fractional melting of garnet lherzolite (O'Hara and Yoder, 1967; O'Hara, 1968). Although this model apparently provides a means to explain the observed association of eclogite and periodotite xenoliths in kimberlite, it has recently fallen into disfavor because it 1) requires the production of enormous volumes of picrite liquid (Pasteris, 1981), 2) is inconsistent with observed concentrations of incompatible elements (Dawson, 1980), and 3) implies a spatial association of various basalts and kimberlite for which there is only limited evidence in the field (Dawson, 1971). On the other hand, recent strontium isotope evidence (Allsopp et al., 1969; Barrett, 1975) strongly suggests that the most common xenoliths have a chemical origin distinct from that of the associated kimberlite. In fact, the limited available data demonstrate marked differences in isotopic concentrations between different members of the nodule suite from one pipe (Barrett, 1975), suggesting specifically that, in the one case studied, clinopyroxene discrete nodules and associated eclogites are characterized by

distinct geochemical origins. The geochemical data (Figures 29a and b) and equilibrium temperatures (Figure 31) obtained from the various garnet, clinopyroxene, and eclogite nodule groups within the Orapa nodule suite are consistent with this latter interpretation.

In this context, however, it should be noted that the temperature data reported in Figures 30 and 31 are presented solely for the purposes of comparison and, in view of the assumptions and limitations inherent in such calculations, no claim can be made for the absolute accuracy of the estimates. A major factor in this regard is the relatively restricted nature of the mineral assemblages that comprise the Orapa nodule suite and which result in the use of temperature indicators that are not truly independent. The case in point for this study is the use of the Akella and Boyd (1974) and Råheim and Green (1974) equations. Although experimentally related to different bulk compositions, these geothermometers are in fact calibrated for what is essentially the same garnet-clinopyroxene partitioning reaction and thus may be expected to yield similar temperatures over a pressure range close to the standard states chosen for the original experiments.

Studies in which various xenoliths have been modelled as accidental inclusions in kimberlite include a wide range of interpretations regarding the significance of such rocks to mantle petrogenesis. A combination of experimental, textural, and geochemical evidence has resulted in models which consider peridotite xenoliths in kimberlite as representative of 1) primary mantle (Kushiro, 1973; O'Hara et al., 1975), 2) residual or depleted mantle (Kushiro, 1973; Gurney et al., 1975; O'Hara et al., 1975), 3) primary ultrabasic magma (O'Hara et al., 1975),

and 4) cumulate aggregates (Gurney et al., 1975). Similarly, a variety of evidence has led to models which consider eclogite xenoliths as possible direct precipitates from mantle liquids (MacGregor and Carter, 1970; O'Hara et al., 1975) and as rocks resulting from complex cumulative processes (MacGregor and Carter, 1970; Hatton and Gurney, 1979). Such studies generally assume that the majority of xenoliths are representative of larger rock bodies at similar stratigraphic levels in the mantle and, indeed, this has been the basis for generating paleogeotherm models (for example: Boyd, 1973). However, as pointed out by Irving (1976), this assumption may not be valid for large portions of the mantle since it is possible that these inclusions are closely linked to the magmatic processes involved in the generation of rocks such as kimberlites, carbonatites, and alkali basalts. The evidence cited by Irving (1976) includes a variety of distinctive textural, mineralogical, and chemical features that are known to characterize xenoliths from different localities and thus may reflect strictly local peculiarities in tectonic and magmatic processes. The possible ramifications of this problem are particularly acute because it may invalidate the generation and interpretation of model geotherms derived from mixed xenolith suites on the basis that such inclusions are genetically related to melting events which may themselves be anomalous phenomena in the upper mantle.

In addition to these concerns, further constraints on the representative nature of kimberlitic xenoliths involve the possible effects of geochemical contamination and the broader based problem of mantle heterogeneity. A variety of detailed geochemical studies have demonstrated that contamination of deep-seated xenoliths may result from

processes such as 1) metasomatism in the mantle (Boettcher et al., 1979), 2) reaction with fluidized kimberlite magma during ascent (Berg, 1968; Lappin and Dawson, 1975), and 3) post-emplacement alteration resulting in elemental migration during the weathering of the kimberlite (Berg, 1968). In general, the latter two processes have been shown to result in an overall enrichment in both K and Cs and are manifested in the production of phlogopite and certain zeolites (Berg, 1968). The effects of mantle metasomatism are more difficult to delineate. However, the oxygen isotope data and detailed geochemical studies of Boettcher et al. (1979) strongly suggest that deep-seated chemical exchange occurs in the presence of aqueous fluids resulting in relative enrichment in H_2O , Ti, K, and Fe. The most obvious effect of such enrichment is usually the stabilization of titaniferous phlogopite and certain amphiboles in both lherzolite and eclogite systems (Boettcher et al., 1979). Evidence for the geochemical heterogeneity of the earth's mantle comes from a variety of sources (see summaries by Ringwood, 1975, 1979), primarily those concerned with the genesis of basalts from various tectonic settings. The available evidence appears to indicate that the degree to which the mantle may be considered geochemically homogeneous is partly a function of the scale at which appropriate phenomena are examined. Although kimberlite xenoliths represent one of the most finely-focussed sources of information in this regard, the difficulties inherent in interpretation are greatly exacerbated by the same processes which make this evidence available.

Kimberlites vary widely in the abundance and variety of deep-seated inclusions brought to the surface. The Monastery pipe in South Africa

is, for example, noted for an abundance of pyroxene-ilmenite intergrowths (Whitelock, 1973), while the Roberts Victor pipe in South Africa and the Zagadochnaya pipe in Yakutia are known for characteristically high proportions of eclogites (Dawson, 1980). Due in part to this variability, there is no evidence to suggest that the xenolith suite from any particular locality represents a complete sampling of that portion of the mantle traversed by the kimberlite. The processes involved in the selective incorporation of xenoliths are difficult to model due to the indirect nature of evidence regarding mantle stratigraphy and the mechanics of kimberlite intrusion. Hypotheses advanced to explain the selective incorporation of eclogites range from mechanical segregation probably related to volatile dynamics in the kimberlite to preferential disaggregation of associated peridotites (Boyd and Danchin, 1980). Although models have been proposed for the mantle that include isolated masses of eclogite surrounded by large volumes of peridotite (O'Hara and Yoder, 1967; Dawson, 1971; Ringwood, 1975, 1979), the Orapa suite cannot at present be considered representative since it would be difficult to envision a mantle composed primarily of eclogite beneath Botswana. However, it should be remembered that the Orapa A/K-1 pipe is still only in the initial stages of exploitation and may, with further mining, yield additional varieties of xenoliths which may be more representative of mantle compositions deduced from geophysical, petrographic, and textural studies of other areas throughout the world. In fact, as digging proceeds, the Orapa site should provide a unique opportunity to refine models regarding the spatial distribution of xenoliths in kimberlites developed from pipes that preserve a less complete diatreme stratigraphy.

Examined with a full realization of the limitations inherent in such samples, kimberlitic nodules such as those described comprising the Orapa suite still represent the most direct evidence available for mantle petrogenesis and it seems certain that the answers to many present questions regarding the mantle will originate from the study of such materials in the future. In view of this promising outlook, efforts should be redoubled to calibrate appropriate experimental equilibria in more chemically complex systems in order to develop more accurate analogues to natural rocks. An important outgrowth of such advances may be the development of additional independent geothermometers and geobarometers which can be used to expand the present data base and to augment interpretation founded in future work. Finally, research must continue to relate textures to chemical characteristics, both for nodules and the host kimberlite, in an attempt to better characterize these materials in terms of mantle stratigraphy and both minor and trace element compositions and isotopic ratios. The rapid proliferation of analytical data in the past twenty years has resulted in major advances in our understanding of processes within the earth's interior. However, all that has been accomplished should only logically serve as the foundation for the future. If this is so, then, with continued effort and a few timely breaks, the future appears quite bright.

C H A P T E R VI
SUMMARY AND CONCLUSIONS

The petrographic and geochemical data presented in this study have demonstrated many similarities between the nodules comprising this Orapa suite and those from previously investigated districts in Africa, Siberia, and the United States. Nevertheless, several striking differences have been noted and new findings observed which together underscore the unique nature of these nodules from Botswana. Although it has not been possible to accurately delineate specific sampling events by which the Orapa kimberlite obtained this suite, it is clear that these nodules represent the end product of a multi-stage process that included two, or possibly three, events for clinopyroxene, at least two for garnet, and a minimum of one each for ilmenite, rutile, and the eclogites. The mineralogically complex mantle section implied by this sampling array may be further complicated by the compositional variations suggested by the niobian rutile and knorringitic garnet intergrowths. In spite of the fact that it appears that further sampling and analysis of nodule suites from the neighboring pipes and from the A/K-1 site itself is needed in the future to formulate a more representative model for the Cretaceous mantle beneath Botswana, the data obtained in this study strongly suggest that any such model will be lithostratigraphically complex and will probably involve significant local variations in geochemical parameters such as Nb, Cr, and fO_2 . The petrographic, geochemical, and experimental data presented in this thesis can be summarized in the following list of observations and conclusions which, for

convenience, are listed according to the appropriate Orapa nodule type:

1. The ilmenite discrete nodule suite:
 - a. contains textural evidence indicative of both intense shearing and thermal re-equilibration experienced during kimberlite ascent through the upper mantle and crust;
 - b. is characterized by distinct kimberlitic compositions which suggest crystallization under deep-seated conditions of relatively low oxygen fugacity;
 - c. contains individual nodules that are characterized by marked increase in MgO content near the peripheries which is probably indicative of reaction with the kimberlitic magma;
 - d. includes nodules that have been fractured at some time after the magnesium zoning trends were established.
2. The rutile discrete nodule suite:
 - a. represents the first reported occurrence of niobian rutile as nodules in kimberlite, including a single homogeneous nodule and, together with similar samples from Jagersfontein, a suite of rutile nodules with intergrown ilmenite lamellae that are characterized by a variety of textural types;

- b. includes host rutile with compositions that are unprecedented in terms of Nb+Cr+Fe substitution in terrestrial and meteoritic environments;
 - c. includes ilmenite lamellae characterized by compositions that are distinct from those of the associated ilmenite discrete nodules;
 - d. contains individual ilmenite-rutile intergrowth nodules characterized by coarse lamellar textures that may have originated by the high pressure breakdown of a trivalent titanium-bearing chromian armalcolite precursor.
3. Silicate discrete nodule suite:
- a. includes diopside discrete nodules that are generally similar in composition to those reported from other districts but which may be subdivided into relatively high-temperature Ca-poor, relatively low temperature Ca-rich, and Na-rich diopside clusters;
 - b. contains a single nodule of intergrown micro-ilmenite and chrome diopside that is texturally similar to a granular type previously described from Lesotho;
 - c. includes garnet discrete nodules that are generally similar in composition to those previously reported from other districts and a separate suite of garnet nodules with

clinopyroxene inclusions which indicate moderate temperatures of equilibration in the range of 1150-1220°C;

- d. contains a single discrete nodule composed of green knorringitic garnet intergrown with both ureyitic diopside and aluminous spinel and which may represent the product of a subsolidus breakdown reaction of an early liquidus chrome-rich garnet.
4. The eclogite nodule suite:
- a. can be divided on a textural basis into foliated and non-foliated, or granular, types;
 - b. includes varieties containing minor amounts of ilmenite, rutile, ilmenite-rutile intergrowths, amphibole, and graphite;
 - c. contains omphacitic pyroxenes showing little variation in composition and which are distinct from the associated clinopyroxene discrete nodules on the basis of chrome content;
 - d. contains pyrope-almandine garnets of variable composition and which are distinct from the associated garnet discrete nodules on the basis of chrome content;
 - e. is estimated on the basis of comparative geothermometry to have equilibrated under upper mantle conditions, possibly in the range

870-1150°C and 35-56 kb, which are consistent with the observed occurrence of both diamond- and graphite-bearing varieties at Orapa.

REFERENCES

- Akella, J. and Boyd, F.R. (1972): Partitioning of Ti and Al Between Pyroxenes, Garnets, and Oxides; Carn. Inst. Wash. Yb.; 71:378.
- Akella, J. and Boyd, F.R. (1974): Petrogenetic Grid for Garnet Peridotites; Carn. Inst. Wash. Yb.; 73:269.
- Albee, A.L. and Ray, L. (1970): Correction Factors for Electron Probe Microanalysis of Silicates, Oxides, Carbonates, Phosphates, and Sulphates; Anal. Chem.; 42:1408.
- Allsopp, H.L., Nicolaysen, L.O., and Hahn-Weinheimer, P. (1969): Rb/K Ratios and Sr-Isotopic Compositions of Minerals in Eclogitic and Peridotitic Rocks; Earth Plan. Sci. Lett.; 5:231.
- Anderson, D.L. (1979): The Upper Mantle Transition Region: Eclogite?; Geophys. Res. Lett.; 6:433.
- Aoki, K. (1974): Phlogopites and Potassic Richterites from Mica Nodules in South African Kimberlites; Con. Min. Pet.; 48:1.
- Aoki, K. (1975): Origin of Phlogopite and Potassic Richterite-Bearing Peridotite Xenoliths from South Africa; Con. Min. Pet.; 53:145.
- Baldock, J.W., Hepworth, J.V., and Marengwa, B.S. (1976): Gold, base metals, and diamonds in Botswana; Econ. Geol.; 71:139.
- Barrett, D.R. (1975): The Genesis of Kimberlites and Associated Rocks: Strontium Isotopic Evidence; in: Physics and Chemistry of the Earth, vol. 9; L.H. Ahrens et al., eds.; Pergamon Press; New York; p. 637.
- Bence, A.E. and Albee, A.L. (1968): Empirical correction factors for the electron microanalysis of silicates and oxides: Jour. Geol.; 76:382.
- Berg, G.W. (1968): Secondary Alteration in Eclogites from Kimberlite Pipes; Am. Min.; 53:1336.
- Berry, L.G. (ed.) (1974): Selected Powder Diffraction Data for Minerals; Joint Committee on Powder Diffraction Standards; Swarthmore, Penn.; 833 p.
- Bishop, F.C. (1977): The Distribution of Fe²⁺ and Mg Between Pyroxene and Ilmenite in Intergrowths from Kimberlites; Abstract, 2nd Int. Kimb. Conf.; Sante Fe, New Mexico; October, 1977.

- Bishop, F.C. (1980): The Distribution of Fe^{2+} and Mg Between Coexisting Ilmenite and Pyroxene with Applications to Geothermometry; *Am. Jour. Sci.*; 280:46.
- Bishop, F.C., Smith, J.V., and Dawson, J.B. (1978): Na, K, P, and Ti in Garnet, Pyroxene and Olivine from Peridotite and Eclogite Xenoliths from African Kimberlites; *Lithos*; 11:155.
- Bloomer, A.G. and Nixon, P.H. (1973): The Geology of the Letseng-la-terae Kimberlite Pipes; in: Lesotho Kimberlites; P.H. Nixon, ed.; Lesotho Nat. Dev. Corp.; p. 20.
- Boctor, N.Z. and Meyer, H.O.A. (1979): Oxide and Sulfide Minerals in Kimberlite from Green Mountain, Colorado; in: Kimberlites, Diatremes, and Diamonds (Proc. 2nd Int. Kimb. Conf., vol. 1); F.R. Boyd and H.O.A. Meyer, eds.; Am. Geophys. Union; Washington, D.C.; p. 217.
- Boctor, N.Z. and Boyd, F.R. (1980): Oxide Minerals in the Liquebong Kimberlite; *Am. Min.*; 65:631.
- Boettcher, A.L., Mysen, B.O., and Modreski, P.J. (1975): Melting in the Mantle: Phase Relationships in Natural and Synthetic Peridotite-H₂O and Peridotite-H₂O-CO₂-C-H-O-S with Application to Kimberlites; in: Physics and Chemistry of the Earth, vol. 9; L.H. Ahrens et al., eds.; Pergamon Press; New York; p. 855.
- Boettcher, A.L., O'Neil, J.R., Windom, K.E., Stewart, D.C., and Wilshire, H.G. (1979): Metasomatism of the Upper Mantle and the Genesis of Kimberlites and Alkali Basalts; in: The Mantle Sample (Proc. 2nd Int. Kimb. Conf., vol. 2); F.R. Boyd and H.O.A. Meyer, eds.; Am. Geophys. Union; Washington, D.C.; p. 173.
- Boullier, A. and Nicolas, A. (1973): Texture and Fabric of Peridotite Nodules from Kimberlite at Mothae, Thaba Putsoa and Kimberley; in: Lesotho Kimberlites; P.H. Nixon, ed.; Lesotho Nat. Dev. Corp.; p. 57.
- Boyd, F.R. (1973): A Pyroxene Geotherm; *Geoch. Cosmoch. Acta*; 37:2533.
- Boyd, F.R. and Danchin, R.V. (1974): Discrete Nodules from the Artur De Paiva Kimberlite, Angola; *Carn. Inst. Wash. Yb.*; 73:278.
- Boyd, F.R. and Danchin, R.V. (1980): Lherzolites, Eclogites, and Megacrysts from Some Kimberlites of Angola; *Am. Jour. Sci.*; 280-A:528.
- Boyd, F.R. and Nixon, P.H. (1973): Origin of the Ilmenite-Silicate Nodules in Kimberlites from Lesotho and South Africa; in: Lesotho Kimberlites; P.H. Nixon, ed.; Lesotho Nat. Dev. Corp.; p. 254.

- Buddington, A.F. and Lindsley, D.H. (1964): Iron-titanium oxide minerals and synthetic equivalents; *Jour. Pet.*; 5:310.
- Cameron, M. and Papike, J.J. (1980): Crystal Chemistry of Silicate Pyroxenes; in: Pyroxenes, Reviews in Mineralogy, vol. 7; C.T. Prewitt, ed.; Min. Soc. of America; p. 5.
- Cameron, M. and Papike, J.J. (1981): Structural and chemical variations in pyroxenes; *Am. Min.*; 66:1.
- Carswell, D.A., Clarke, D.B., and Mitchell, R.H. (1979): The Petrology and Geochemistry of Ultramafic Nodules from Pipe 200, Northern Lesotho; in: The Mantle Sample (Proc. 2nd Int. Kimb. Conf., vol. 2); F.R. Boyd and H.O.A. Meyer, eds.; Am. Geophys. Union; Washington, D.C.; p. 127.
- Carter, D.L. and Okaya, A. (1960): Electron Paramagnetic Resonance of Fe^{3+} in TiO_2 (Rutile); *Phys. Rev.*; 118:1485.
- Cerny, P., Cech, F., and Povondra, P. (1964): Review of ilmenorutile-struverite minerals; *N. Jb. Miner. Abh.*; 101:142.
- Chayes, F. (1956): Petrographic Modal Analysis, John Wiley and Sons, Inc.; New York; 113 p.
- Clark, S.P. Jr. and Ringwood, A.E. (1964): Density Distribution and Constitution of the Mantle; *Rev. Geophys.*; 2:35.
- Clarke, D.B. and Mitchell, R.H. (1975): Mineralogy and Petrology of the Kimberlite from Somerset Island, N.W.T., Canada; in: Physics and Chemistry of the Earth, vol. 9; L.H. Ahrens et al., eds.; Pergamon Press; New York; p. 123.
- Clarke, D.B. and Carswell, D.A. (1977): Green Garnets from the Newlands Kimberlite, Cape Province, South Africa; *Earth Plan. Sci. Lett.*; 34:30.
- Cox, K.G., Gurney, J.J., and Harte, B. (1973): Xenoliths from the Matsoku Pipe; in: Lesotho Kimberlites; P.H. Nixon, ed.; Lesotho Nat. Dev. Corp.; p. 76.
- Danchin, R.V. (1979): Mineral and Bulk Chemistry of Garnet Lherzolite and Garnet Harzburgite Xenoliths from the Premier Mine, South Africa; in: The Mantle Sample (Proc. 2nd Int. Kimb. Conf., vol. 2); F.R. Boyd and H.O.A. Meyer, eds.; Am. Geophys. Union; Washington, D.C.; p. 104.
- Danchin, R.V. and Boyd, F.R. (1976): Ultramafic nodules from the Premier Kimberlite Pipe, South Africa; *Carn. Inst. Wash. Yb.*; 75:531.

- Davis, B.T.C. and Boyd, F.R. (1966): The Join $Mg_2Si_2O_6$ - $CaMgSi_2O_6$ at 30 Kilobars Pressure and Its Applicability to Pyroxenes from Kimberlites; *Jour. Geophys. Res.*; 71:3567.
- Davis, G.L. (1977): The Ages and Uranium Contents of Zircons from Kimberlites and Associated Rocks; Abstract, 2nd Int. Kimb. Conf.; Santa Fe, New Mexico; October, 1977.
- Dawson, J.B. (1962): Basutoland Kimberlites; *Geol. Soc. Am. Bull.*; 73:545.
- Dawson, J.B. (1971): Advances in Kimberlite Geology; *Earth Sci. Rev.*; 7:187.
- Dawson, J.B. (1980): Kimberlites and Their Xenoliths; Springer-Verlag; New York; 252 p.
- Dawson, J.B. and Reid, A.M. (1970): A Pyroxene-Ilmenite Intergrowth from the Monastery Mine, South Africa; *Con. Min. Pet.*; 26:296.
- Dawson, J.B. and Stephens, W.E. (1975): Statistical Classification of Garnets from Kimberlite and Associated Xenoliths; *Jour. Geol.*; 83:589.
- Dawson, J.B. and Stephens, W.E. (1976): Statistical Classification of Garnets from Kimberlite and Associated Xenoliths - Addendum; *Jour. Geol.*; 84:495.
- Dawson, J.B. and Smith, J.V. (1977): The MARID (mica-amphibole-rutile-ilmenite-diopside) suite of xenoliths in kimberlites; *Geoch. Cosmoch. Acta*; 41:309.
- Deer, W.A., Howie, R.A., and Zussman, J. (1963): Rock-Forming Minerals, Vol. 2, Chain Silicates; Longmans, Green, and Co., Ltd.; London; 379 p.
- Eggler, D.H. and Wendlandt, R.F. (1979): Experimental Studies on the Relationship Between Kimberlite Magmas and Partial Melting of Peridotite; in: Kimberlites, Diatremes, and Diamonds (Proc. 2nd Int. Kimb. Conf., vol. 1); F.R. Boyd and H.O.A. Meyer, eds.; Am. Geophys. Union; Washington, D.C., p. 330.
- Eggler, D.H., McCallum, M.E., and Smith, C.B. (1979): Megacryst Assemblages in Kimberlite from Northern Colorado and Southern Wyoming: Petrology, Geothermometry-Geobarometry, and Areal Distribution; in: The Mantle Sample (Proc. 2nd Int. Kimb. Conf., vol. 2); F.R. Boyd and H.O.A. Meyer, eds.; Am. Geoph. Union; Washington, D.C.; p. 213.
- El Goresy, A. (1971): Meteoritic Rutile: A Niobium Bearing Mineral; *Earth Plan. Sci. Lett.*; 11:359.

- Elthon, D. and Ridley, W.I. (1979): The Oxide and Silicate Mineral Chemistry of a Kimberlite from the Premier Mine: Implications for the Evolution of Kimberlitic Magmas; in: The Mantle Sample (Proc. 2nd Int. Kimb. Conf., vol. 2); F.R. Boyd and H.O.A. Meyer, eds.; Am. Geoph. Union; Washington, D.C.; p. 206.
- Erlank, A.J. (1976): Upper Mantle Metasomatism as Revealed by Potassic Richterite-Bearing Peridotite Xenoliths from Kimberlite; EOS (Trans. Am. Geophys. Union); 57:597.
- Erlank, A.J. and Finger, L.W. (1970): The Occurrence of Potassic Richterite in a Mica Nodule from the Wesselton Kimberlite, South Africa; Carn. Inst. Wash. Yb.; 68:320.
- Ferguson, J., Danchin, R.V., and Nixon, P.H. (1973): Petrochemistry of Kimberlite Autoliths; in: Lesotho Kimberlites; P.H. Nixon, ed.; Lesotho Nat. Dev. Corp.; p. 57.
- Finger, L.W. (1972): The Uncertainty in the Calculated Ferric Iron Content of a Microprobe Analysis; Carn. Inst. Wash. Yb.; 71:600.
- Fraser, D.G. and Lawless, P.J. (1978): Paleogeotherms: implications of disequilibrium in garnet lherzolite xenoliths; Nature; 273:220.
- Freer, R. (1981): Diffusion in Silicate Minerals and Glasses: A Data Digest and Guide to the Literature; Con. Min. Pet.; 76:440.
- Frick, C. (1973): Kimberlitic Ilmenites; Geol. Soc. So. Africa Trans.; 76:84.
- Friel, J.J. and Harker, R.I. (1977): Armalcolity stability as a function of pressure and oxygen fugacity; Geoch. Cosmoch. Acta; 41:403.
- Goetze, C. (1975): Sheared lherzolites: from the point of view of rock mechanics; Geology; 3:172.
- Green, D.H. and Ringwood, A.E. (1970): Mineralogy of Peridotitic Compositions Under Upper Mantle Conditions; Phys. Earth. Plan. Int.; 3:359.
- Green, D.H. and Sobolev, N.V. (1975): Coexisting Garnets and Ilmenites Synthesized at High Pressures from Pyrolite and Olivine Basanite and Their Significance for Kimberlitic Assemblages; Con. Min. Pet.; 50:217.
- Green, T. (1981): The World of Diamonds; W. Morrow and Co.; New York; 300 p.
- Griffin, W.L., Jensen, B.B., and Misra, S.N. (1971): Anomalous Elongated Rutile in Eclogite-Facies Pyroxene and Garnet; Norsk Geol. Tidssk; 51:177.

- Gurney, J.J., Fesq, H.W., and Kable, E.J.D. (1973): Clinopyroxene-Ilmenite Intergrowths from Kimberlite: A Re-appraisal; in: Lesotho Kimberlites; P.H. Nixon, ed.; Lesotho Nat. Dev. Corp.; p. 238.
- Gurney, J.J., Harte, B., and Cox, K.G. (1975): Mantle Xenoliths in the Matsoku Kimberlite Pipe; in: Physics and Chemistry of the Earth, vol. 9; L.H. Ahrens et al., eds.; Pergamon Press: New York; p. 507.
- Gurney, J.J., Jakob, W.R.O., and Dawson, J.B. (1979): Megacrysts from the Monastery Kimberlite Pipe, South Africa; in: The Mantle Sample (Proc. 2nd Int. Kimb. Conf., vol. 2); F.R. Boyd and H.O.A. Meyer, eds.; Am. Geophys. Union; Washington, D.C.; p. 227.
- Haggerty, S.E. (1973): Armalcolite and genetically associated opaque minerals in the lunar samples; Proc. 4th Lunar Sci. Conf.; Geoch. Cosmoch. Acta, Suppl. 4; 1:777.
- Haggerty, S.E. (1975): The Chemistry and Genesis of Opaque Minerals in Kimberlites; in: Physics and Chemistry of the Earth, vol. 9; L.H. Ahrens et al., eds.; Pergamon Press; New York; p. 295.
- Haggerty, S.E. (1976): Opaque Mineral Oxides in Terrestrial Igneous Rocks; in: Oxide Minerals, Reviews in Mineralogy, vol. 3; D. Rumble III, ed.; Min. Soc. America; P. Hg-101.
- Haggerty, S.E. (1979a): Spinels in High Pressure Regimes; in: The Mantle Sample (Proc. 2nd Int. Kimb. Conf., vol. 2); F.R. Boyd and H.O.A. Meyer, eds.; Am. Geophys. Union; Washington, D.C.; p. 183.
- Haggerty, S.E. (1979b): The Jagersfontein Kimberlite, South Africa: An Emporium of Exotic Mineral Reactions from the Upper Mantle: abstract, Kimberlite Symposium II; Cambridge, England; July 1979.
- Haggerty, S.E., Hardie III, R.B., and McMahon, B.M. (1979): The Mineral Chemistry of Ilmenite Nodule Associations from the Monastery Diatrema; in: The Mantle Sample (Proc. 2nd Int. Kimb. Conf., vol. 2); F.R. Boyd and H.O.A. Meyer, eds.; Am. Geophys. Union; Washington, D.C.; p. 249.
- Harris, J.W. and Gurney, J.J. (1979): Inclusions in Diamonds; in: The Properties of Diamonds; J.E. Field, ed.; Academic Press; New York; p. 555.
- Hatton, C.J. (1978): Geochemistry and Origin of Eclogite Xenoliths from the Roberts Victor Mine; unpublished Ph.D. thesis; University of Cape Town.

- Hatton, C.J. and Gurney, J.J. (1979): A Diamond-Graphite Eclogite from the Roberts Victor Mine; in: The Mantle Sample (Proc. 2nd Int. Kimb. Conf., vol. 2); F.R. Boyd and H.O.A. Meyer, eds.; Am. Geophys. Union; Washington, D.C.; p. 29.
- Hawthorne, J.B. (1975): Model of a Kimberlite Pipe; in: Physics and Chemistry of the Earth, vol. 9; L.H. Ahrens et al., eds.; Pergamon Press; New York; p. 1.
- Hearn, B.C. and Boyd, F.R. (1975): Garnet Peridotite Xenoliths in a Montana, U.S.A., Kimberlite; in: Physics and Chemistry of the Earth, vol. 9; L.H. Ahrens et al., eds.; Pergamon Press; New York; p. 247.
- Hlava, P.H., Prinz, M., and Keil, K. (1972): Niobian Rutile in an Apollo 14 KREEP Fragment; Meteoritics; 7:479.
- Hornung, G. and Nixon, P.H. (1973): Chemical Variations in the Knorringite-Rich Garnets; in: Lesotho Kimberlites; P.H. Nixon, ed.; Lesotho Nat. Dev. Corp.; p. 122.
- Ilupin, I.P., Kaminskiy, F.V. and Troneva, N.V. (1973): Pyroxene-ilmenite graphic inclusions from the Mir kimberlite pipe (Yakutia) and their origin; Int. Geol. Rev.; 16:1298.
- Irving, A.J. (1976): On the Validity of Paleogeotherms Determined from Xenolith Suites in Basalts and Kimberlites; Am. Min.; 61:638.
- Kennedy, C.S. and Kennedy, G.C. (1976): The Equilibrium Boundary Between Graphite and Diamond; Jour. Geophys. Res.; 81:2467.
- Kesson, S.E. and Lindsley, D.H. (1975): The effects of Al^{3+} , Cr^{3+} , and Ti^{3+} on the stability of armalcolite; Proc. 6th Lunar Sci. Conf.; Geoch. Cosmoch. Acta, Suppl. 6; 1:911.
- Kresten, P. (1973): The Geology of Lemphane Pipes and Neighboring Intrusions; in: Lesotho Kimberlites; P.H. Nixon, ed.; Lesotho Nat. Dev. Corp.; p. 159.
- Kushiro, I. (1973): Partial Melting of Garnet Lherzolites from Kimberlite at High Pressures; in: Lesotho Kimberlites; P.H. Nixon, ed.; Lesotho Nat. Dev. Corp.; p. 294.
- Kushiro, I. and Aoki, K. (1968): Origin of Some Eclogitic Inclusions in Kimberlite; Am. Min.; 53:1347.
- Kushiro, I.K. and Erlank, A.J. (1970): Stability of Potassic Richterites; Carn. Inst. Wash. Yb.; 68:231.
- Lambert, I.B. and Wyllie, P.J. (1968): Stability of Hornblende and a Model for the Low Velocity Zone; Nature; 219:1240.

- Lappin, M.A. (1978): The Evolution of a Grosspydite from the Roberts Victor Mine, South Africa; *Con. Min. Pet.*; 66:229.
- Lappin, M.A. and Dawson, J.B. (1975): Two Roberts Victor Eclogites and Their Re-Equilibrium; in: Physics and Chemistry of the Earth, vol. 9; L.H. Ahrens et al., eds.; Pergamon Press; New York; p. 351.
- Leake, B.E. (1968): A Catalog of Analyzed Calciferous and Subcalciferous Amphiboles Together with Their Nomenclature and Associated Minerals; *Geol. Soc. Amer. Special Paper* 98; 210 p.
- Lindsley, D.H., Kesson, S.E., Hartzman, M.J., and Cushman, M.K. (1974): The stability of armalcolite: Experimental studies in the system MgO-Fe-Ti-O; *Proc. 5th Lunar Sci. Conf.*; *Geoch. Cosmoch. Acta*, Suppl. 5; 1:521.
- Lindsley, D.H. and Dixon, S.A. (1976): Diopside-Enstatite Equilibria at 850°C to 1400°C, 5 to 35 kb; *Am. Jour. Sci.*; 276:1285.
- Lorentz, V. (1975): Formation of Phreatomagmatic Maar-Diatreme Volcanoes and Its Relation to Kimberlite Diatremes; in: Physics and Chemistry of the Earth, vol. 9; L.H. Ahrens et al., eds.; Pergamon Press; New York; p. 17.
- MacGregor, I.D. (1970): The Effect of CaO, Cr₂O₃, Fe₂O₃, and Al₂O₃ on the Stability of Spinel and Garnet Peridotites; *Phys. Earth Planet. Interiors*; 3:372.
- MacGregor, I.D. (1974): The System MgO-Al₂O₃-SiO₂: Solubility of Al₂O₃ in Enstatite for Spinel and Garnet Peridotite Compositions; *Am. Min.*; 59:110.
- MacGregor, I.D. (1979): Mafic and Ultramafic Xenoliths from the Kao Kimberlite Pipe; in: The Mantle Sample (Proc. 2nd Int. Kimb. Conf., vol. 2); F.R. Boyd and H.O.A. Meyer, eds.; Am. Geophys. Union; Washington, D.C.; p. 156.
- MacGregor, I.D. and Carter, J.L. (1970): The Chemistry of Clinopyroxenes and Garnets of Eclogite and Peridotite Xenoliths from the Roberts Victor Mine, South Africa; *Phys. Earth Planet. Interiors*; 3:391.
- MacGregor, I.D. and Basu, A.R. (1974): Thermal Structure of the Lithosphere: A Petrologic Model; *Science*; 185:1007.
- MacGregor, I.D. and Basu, A.R. (1976): Geological problems in estimating mantle geothermal gradients; *Am. Min.*; 61:715.
- Marvin, U. (1971): Lunar Niobian Rutile; *Earth Plan. Sci. Lett.*; 11:7.

- Mercier, J.C. (1979): Xenoliths and the Dynamics of Kimberlite Intrusion; in: The Mantle Sample (Proc. 2nd Int. Kimb. Conf., vol. 2); F.R. Boyd and H.O.A. Meyer, eds.; Am. Geophys. Union; Washington, D.C.; p. 197.
- Mercier, J.C. and Carter, N.L. (1975): Pyroxene Geotherms; Jour. Geophys. Res.; 80:3349.
- Meyer, H.O.A. and Brookins, D.G. (1971): Eclogite Xenoliths from Stockdale Kimberlite, Kansas; Con. Min. Pet.; 34:60.
- Meyer, H.O.A. and Boyd, F.R. (1972): Composition and origin of crystalline inclusions in natural diamonds; Geoch. Cosmoch. Acta; 36:1255.
- Meyer, H.O.A. and Boctor, N.Z. (1975): Sulfide-Oxide Minerals in Eclogite from Stockdale Kimberlite, Kansas; Con. Min. Pet.; 52:57.
- Meyer, H.O.A. and Tsai, H. (1976): The Nature and Significance of Mineral Inclusions in Natural Diamond: A Review; Min. Sci. Engng.; 8:242.
- Mitchell, R.H. (1973): Magnesian Ilmenite and Its Role in Kimberlite Petrogenesis; Jour. Geol.; 81:301.
- Mitchell, R.H. (1977): Geochemistry of magnesium ilmenites from kimberlites in South Africa and Lesotho; Lithos: 10:29.
- Mori, T. and Green, D.H. (1976): Subsolidus equilibria between pyroxenes in the CaO-MgO-SiO₂ system at high pressures and temperatures; Am. Min.; 61:616.
- Nixon, P.H., von Knorring, O., and Rooke, J.M. (1963): Kimberlites and Associated Inclusions of Basutoland: A Mineralogical and Geochemical Study; Am. Min.; 48:1090.
- Nixon, P.H. and Hornung, G. (1968): A New Chromium Garnet End Member, Knorringite, from Kimberlites; Am. Min.; 53:1833.
- Nixon, P.H. and Boyd, F.R. (1973a): The Discrete Nodule Association in Kimberlites from Northern Lesotho; in: Lesotho Kimberlites; P.H. Nixon, ed.; Lesotho Nat. Dev. Corp.; p. 67.
- Nixon, P.H. and Boyd, F.R. (1973b): The Liquobong Intrusions and Kimberlitic Olivine Composition; in: Lesotho Kimberlites; P.H. Nixon, ed.; Lesotho Nat. Dev. Corp.; p. 141.
- Nixon, P.H. and Boyd, F.R. (1973c): Carbonated Ultrabasic Nodules from Sekameng; in: Lesotho Kimberlites; P.H. Nixon, ed.; Lesotho Nat. Dev. Corp.; p. 190.

- Nixon, P.H. and Boyd, F.R. (1973d): Petrogenesis of the Granular and Sheared Ultrabasic Nodule Suite in Kimberlites; in: Lesotho Kimberlites; P.H. Nixon, ed.; Lesotho Nat. Dev. Corp.; p. 48.
- Nixon, P.H. and Boyd, F.R. (1973e): The Geology of the Kao Kimberlite Pipes; in: Lesotho Kimberlites; P.H. Nixon, ed.; Lesotho Nat. Dev. Corp.; p. 106.
- Nixon, P.H. and Kresten, P. (1973): Ilmenite Association Trace Element Studies, Part III: Chromium and Nickel in Kimberlitic Ilmenites; in: Lesotho Kimberlites; P.H. Nixon, ed.; Lesotho Nat. Dev. Corp.; p. 235.
- O'Hara, M.J. (1968): The Bearing of Phase Equilibria Studies in Synthetic and Natural Systems on the Origin and Evolution of Basic and Ultrabasic Rocks; Earth Sci. Rev.; 4:69.
- O'Hara, M.J. and Yoder, Jr., H.S. (1967): Formation and Fractionation of Basic Magmas at High Pressures; Scott. Jour. Geol.; 3:67.
- O'Hara, M.J., Saunders, M.J., and Mercy, E.L.P. (1975): Garnet-Peridotite, Primary Ultrabasic Magma and Eclogite; Interpretation of Upper Mantle Processes in Kimberlite; in: Physics and Chemistry of the Earth, vol. 9; L.H. Ahrens et al., eds.; Pergamon Press: New York; p. 571.
- Palache, C., Berman, H., and Frondel, C. (1944): Dana's System of Mineralogy, 7th edition, vol. I; John Wiley and Sons; New York; 834 p.
- Papike, J.J., Cameron, K.L., and Baldwin, K. (1974): Amphiboles and Pyroxenes: Characterization of *Other* than quadrilateral components and estimates of ferric iron from microprobe data; Geol. Soc. Amer. Abstracts with Programs; 6:1053.
- Pasteris, J.D. (1981): Kimberlites: Strange Bodies?; EOS (Trans. Am. Geophys. Union); 62:713.
- Pasteris, J.D., Boyd, F.R., and Nixon, P.H. (1979): The Ilmenite Association at the Frank Smith Mine, R.S.A.; in: The Mantle Sample (Proc. 2nd Int. Kimb. Conf., vol. 2); F.R. Boyd and H.O.A. Meyer, eds.; Am. Geophys. Union; Washington, D.C.; p. 265.
- Raber, E. (1978): Zircons from Diamond-Bearing Kimberlites: Oxide Reactions, Fission Track Dating, and a Mineral Inclusion Study; unpublished M.S. thesis; University of Massachusetts; 90 p.
- Raber, E. and Haggerty, S.E. (1979): Zircon-Oxide Reactions in Diamond-Bearing Kimberlites; in: Kimberlites, Diatremes, and Diamonds (Proc. 2nd Int. Kimb. Conf., vol. 1); F.R. Boyd and H.O.A. Meyer, eds.; Am. Geophys. Union; Washington, D.C.; p. 229.

- Råheim, A. and Green, D.H. (1974): Experimental Determination of the Temperature and Pressure Dependence of the Fe-Mg Partition Coefficient for Coexisting Garnet and Clinopyroxene; *Con. Min. Pet.*; 48:179.
- Ramdohr, P. (1969): The Ore Minerals and Their Intergrowths; Pergamon Press; New York; 1174 p.
- Rawlinson, P.J. and Dawson, J.B. (1979): A Quench Pyroxene-Ilmenite Xenolith from Kimberlite: Implications for Pyroxene-Ilmenite Intergrowths; in: The Mantle Sample (Proc. 2nd Int. Kimb. Conf., vol. 2); F.R. Boyd and H.O.A. Meyer, eds.; Am. Geophys. Union; Washington, D.C.; p. 292.
- Reid, A.M., Brown, R.W., Dawson, J.B., Whitfield, G.G., and Siebert, J.C. (1976): Garnet and Pyroxene Compositions in Some Diamondiferous Eclogites; *Con. Min. Pet.*; 58:203.
- Rickwood, P.C., Mathias, M., and Siebert, J.C. (1968): A Study of Garnets from Eclogite and Peridotite Xenoliths Found in Kimberlite; *Con. Min. Pet.*; 19:271.
- Ringwood, A.E. (1975): Composition and Petrology of the Earth's Mantle; McGraw-Hill; New York; 618 p.
- Ringwood, A.E. (1979): Origin of the Earth and Moon; Springer-Verlag; New York; 295 p.
- Ringwood, A.E. and Lovering, J.F. (1970): Significance of Pyroxene-Ilmenite Intergrowths Among Kimberlite Xenoliths; *Earth Plan. Sci. Lett.*; 7:371.
- Robinson, D.N. (1979): Diamond and Graphite in Eclogite Xenoliths from Kimberlite; in: The Mantle Sample (Proc. 2nd Int. Kimb. Conf., vol. 2); F.R. Boyd and H.O.A. Meyer, eds.; Am. Geophys. Union; Washington, D.C.; p. 50.
- Robinson, P. (1980): The Composition Space of Terrestrial Pyroxenes - Internal and External Limits; in: Pyroxenes, Reviews in Mineralogy, vol. 7; C.T. Prewitt, ed.; Min. Soc. America; p. 419.
- Sato, M. (1971): Electrochemical Measurements and Control of Oxygen Fugacity and Other Gaseous Fugacities with Solid Electrolyte Systems; in: Research Techniques for High Pressure and High Temperature; G.C. Ulmer, ed.; Spinger-Verlag; New York; p. 43.
- Scott, B.H. and Skinner, E.M.W. (1979): The Premier Kimberlite Pipe, Transvaal, South Africa; abstract, Kimberlite Symposium II; Cambridge, England; July 1979.

- Shannon, R.D. and Prewitt, C.T. (1969): Effective Ionic Radii in Oxides and Fluorides; Acta Cryst.; B25:925.
- Shee, S.R. (1978): The Mineral Chemistry of Xenoliths from the Orapa Kimberlite Pipe, Botswana; unpublished M.S. thesis; University of Cape Town; 148 pages with additional appendices.
- Shee, S.R. (1979): The Opaque Oxides of the Wesselton Mine; abstract, Kimberlite Symposium II; Cambridge, England; July 1979.
- Siivola, J. (1970): Ilmenorutile and Struverite from Penikoja, Somero, SW Finland; Bull. Geol. Soc. Finland; 42:33.
- Smith, C.B., McCallum, M.E., and Egger, D.H. (1976): Clinopyroxene-Ilmenite Intergrowths from the Iron Mountain Kimberlite District, Wyoming; Carn. Inst. Wash. Yb.; 75:542.
- Smith, J.V. and Dawson, J.B. (1975): Chemistry of Ti-Poor Spinel, Ilmenites and Rutiles from Peridotite and Eclogite Xenoliths; in: Physics and Chemistry of the Earth, vol. 9; L.H. Ahrens et al., eds.; Pergamon Press; New York; p. 309.
- Smyth, J.R. and Hatton, C.J. (1977): A Coesite-Sanidine Groszpydite from the Roberts Victor Kimberlite; Earth Plan. Sci. Lett.; 34:284.
- Sobolev, N.V. (1977): Deep-Seated Inclusions in Kimberlites and the Problem of the Composition of the Upper Mantle (English translation); Am. Geophys. Union; Washington, D.C.; 279 p.
- Sobolev, N.V. and Kuznetsova, I.K. (1966): The Mineralogy of Diamond-Bearing Eclogites; Doklady Akad. Nauk. S.S.S.R. (English translation); 167:112.
- Sobolev, N.V., Kuznetsova, I.K., and Zyuzin, N.I. (1968): The Petrology of Groszpydite Xenoliths from the Zagadochnaya Kimberlite Pipe in Yakutia; Jour. Pet.; 9:253.
- Sobolev, N.V., Lavrent'yev, Y.G., Pospelova, L.N., and Sobolev, Y.V. (1969): Chrome Pyrope from Yakutian Diamonds; Doklady Akad. Nauk. S.S.S.R. (English translation); 189:133.
- Sobolev, N.V., Bartoshinskiy, Z.V., Yefimova, E.S., Lavrent'yev, Y.G., and Pospelova, L.N. (1970): Olivine-Garnet-Chrome Diopside Assemblage from Yakutian Diamond; Doklady Akad. Nauk. S.S.S.R. (English translation); 192:134.
- Sobolev, N.V., Lavrent'yev, Y.G., and Usova, L.V. (1972): Minor Elements in Rutiles from Eclogites; Geol. i. Geofiz.; no. 11; p. 108; (in Russian).

- Sobolev, N.V., Lavrent'yev, Y.G. Pokhilenko, N.P., and Usova, L.V. (1973): Chrome-Rich Garnets from the Kimberlites of Yakutia and Their Paragenises; *Con. Min. Pet.*; 40:39.
- Sobolev, V.S., Nai, B.S., Sobolev, N.V., Lavrent'yev, Y.G., and Pospelova, L.N. (1969): Xenoliths of Diamond-Bearing Pyrope Serpentinites from the Aikhal Kimberlite Pipe in Yakutia; *Doklady Akad. Nauk. S.S.S.R. (English translation)*; 188:1141.
- Spry, A. (1969): Metamorphic Textures; Pergamon Press; New York; 350 p.
- Stanton, R.L. (1972): Ore Petrology; McGraw-Hill; New York; 713 p.
- Stephens, W.E. and Dawson, J.B. (1977): Statistical Comparison Between Pyroxenes from Kimberlites and Their Associated Xenoliths; *Jour. Geol.*; 85:433.
- Velde, D. (1975): Armalcolite-Ti Phlogopite-Diopside-Analcite-Bearing Lamproites from Smoky Butte, Garfield County, Montana; *Am. Min.*; 60:566.
- Wager, L.R. (1960): The Major Element Variation of the Layered Series of the Skaergaard Intrusion and a Re-estimation of the Average Composition of the Hidden Series and of the Successive Residual Magmas; *Jour. Pet.*; 1:364.
- Webster, A.H. and Bright, N.F.H. (1961): System Iron-Titanium-Oxygen at 1200°C and Oxygen Partial Pressures Between 1 Atm. and 2×10^{-14} Atm.; *Jour. Am. Cer. Soc.*; 44:110.
- Wechslar, B.A., Prewitt, C.T., and Papike, J.J. (1976): Chemistry and Structure of Lunar and Synthetic Armalcolite; *Earth Plan. Sci. Lett.*; 29:91.
- Whitelock, T.K. (1973): The Monastery Mine Kimberlite Pipe; in: Lesotho Kimberlites; P.H. Nixon, ed.; Lesotho Nat. Dev. Corp.; p. 214.
- Wittke, J. (1967): Solubility of Iron in TiO_2 (Rutile); *Jour. Am. Cer. Soc.*; 50:586.
- Woolsey, T.S., McCallum, M.E., and Schumm, S.A. (1975): Modeling of Diatreme Emplacement by Fluidization; in: Physics and Chemistry of the Earth, vol. 9; L.H. Ahrens et al., eds.; Pergamon Press; New York; p. 29.
- Wyatt, B.A. (1977): The Melting and Crystallization Behavior of a Natural Clinopyroxene-Ilmenite Intergrowth; *Con. Min. Pet.*; 61:1.

- Wyllie, P.J. (1979a): Kimberlite Magmas from the System Peridotite-CO₂-H₂O; in: Kimberlites, Diatremes, and Diamonds (Proc. 2nd Int. Kimb. Conf., vol. 1); F.R. Boyd and H.O.A. Meyer, eds.; Am. Geophys. Union; Washington, D.C.; p. 319.
- Wyllie, P.J. (1979b): Magmas and Volatile Components; Am. Min.; 64:469.
- Wyllie, P.J. and Huang, W.L. (1975): Peridotite, Kimberlite, and Carbonatite Explained in the System CaO-MgO-SiO₂-CO₂; Geology; 3:621.
- Zussman, J. (1977): X-ray Diffraction; in: Physical Methods in Determinative Mineralogy; J. Zussman, ed.; Academic Press; New York; p. 391.

APPENDIX A

LISTING OF THE INDIVIDUAL ELECTRON MICROPROBE ANALYSES
USED IN THE CONSTRUCTION OF FIGURE 7

A series of detailed electron microprobe analyses were performed on discrete nodule #OR-411A to derive a chemical contour map (Figure 7) illustrating the MgO zoning characteristics of the grain. This appendix consists of an index map (Figure 32) on which the locations of all analyses used in the construction of the contour map are plotted and a complete listing (Table 18) of all of the individual analyses.

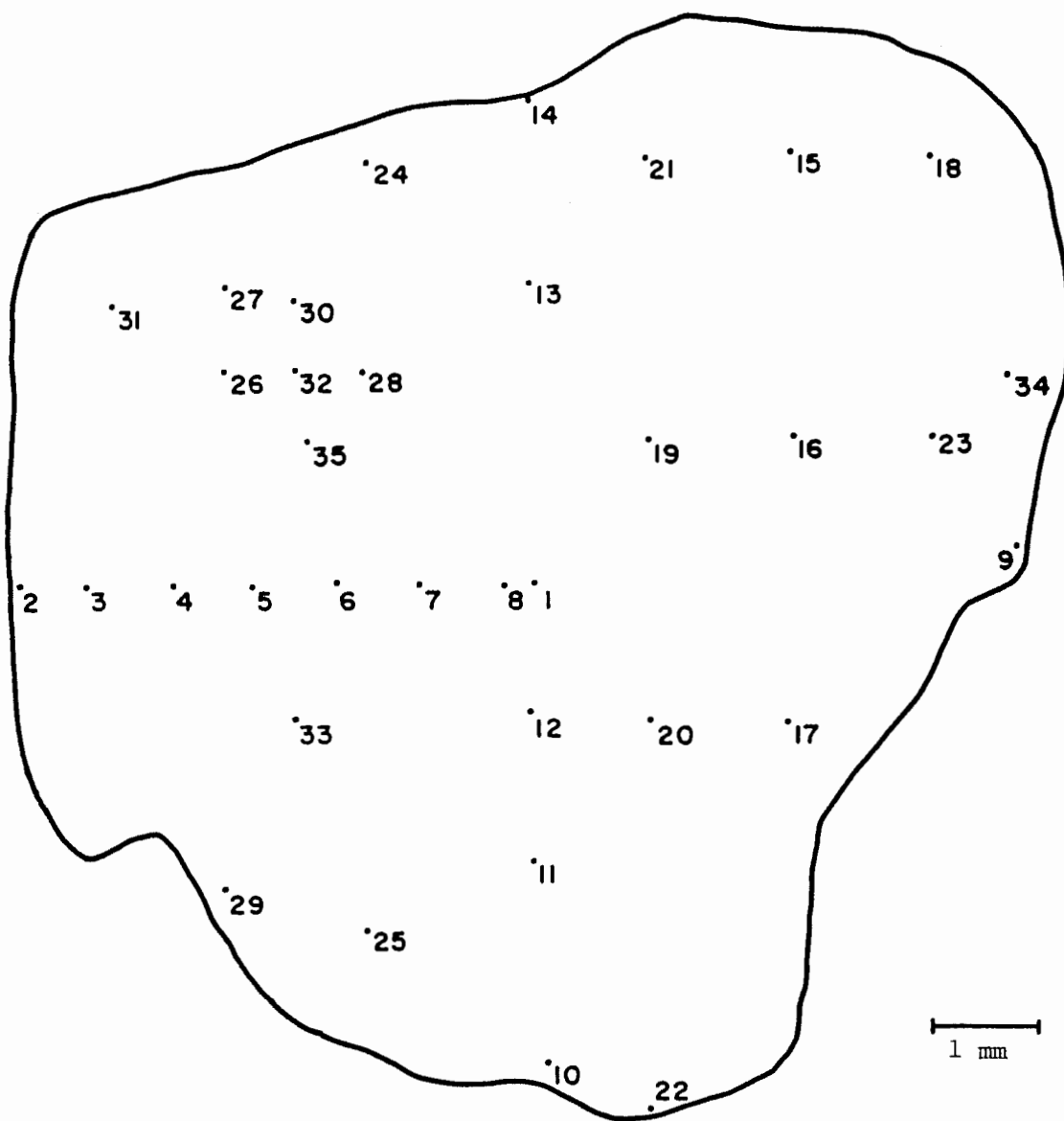


Figure 32: Index map showing the location and number of each microprobe analysis used in the construction of the chemical contour map presented in Figure 7.

Table 18: Individual electron microprobe analyses of ilmenite discrete nodule specimen #411A used in the construction of the chemical contour map presented in Figure 7 of the text. The analysis number at the top of each column refers to the position plotted on Figure 18 of this appendix.

Analysis:	<u>1</u>	<u>2</u>	<u>3</u>	<u>4</u>	<u>5</u>	<u>6</u>	<u>7</u>	<u>8</u>	<u>9</u>
TiO ₂	48.68	49.39	48.72	48.77	47.39	47.87	48.24	48.33	48.56
Cr ₂ O ₃	3.65	3.76	3.73	3.56	3.67	3.62	3.55	3.57	3.43
Al ₂ O ₃	0.17	0.42	0.32	0.31	0.25	0.26	0.23	0.24	0.24
'Fe ₂ O ₃	10.26	11.80	10.35	10.57	12.61	12.32	11.12	11.68	10.89
FeO	28.58	22.23	26.81	27.26	26.24	26.77	27.64	27.42	28.39
MgO	8.56	12.22	9.38	9.21	8.97	8.93	8.67	8.80	8.34
MnO	0.34	0.35	0.24	0.25	0.33	0.33	0.27	0.38	0.36
ZrO ₂	0.26	0.25	0.07	0.24	0.27	0.04	0.24	0.27	0.36
Nb ₂ O ₅	0.32	0.03	0.11	0.09	0.00	0.09	0.05	0.09	0.05
NiO	0.09	0.22	0.19	0.15	0.22	0.13	0.19	0.23	0.31
Total	<u>100.91</u>	<u>100.67</u>	<u>99.92</u>	<u>100.41</u>	<u>99.95</u>	<u>100.36</u>	<u>100.20</u>	<u>101.01</u>	<u>100.93</u>

Cations based on three (3) oxygens

Ti	0.864	0.855	0.866	0.865	0.846	0.851	0.861	0.855	0.863
Cr	0.068	0.068	0.070	0.066	0.069	0.068	0.067	0.066	0.064
Al	0.005	0.011	0.009	0.009	0.007	0.007	0.006	0.007	0.007
'Fe ³⁺	0.182	0.204	0.184	0.187	0.225	0.219	0.199	0.207	0.194
Fe ²⁺	0.564	0.428	0.530	0.538	0.521	0.529	0.549	0.540	0.561
Mg	0.301	0.419	0.331	0.324	0.317	0.315	0.307	0.309	0.294
Mn	0.007	0.007	0.005	0.005	0.007	0.007	0.005	0.008	0.007
Zr	0.003	0.003	0.001	0.003	0.003	0.000	0.003	0.003	0.004
Nb	0.003	0.000	0.001	0.001	0.000	0.001	0.000	0.001	0.000
Ni	0.002	0.004	0.004	0.003	0.004	0.003	0.004	0.004	0.006
Total	<u>1.999</u>	<u>1.999</u>	<u>2.001</u>	<u>2.001</u>	<u>1.999</u>	<u>2.000</u>	<u>2.001</u>	<u>2.000</u>	<u>2.000</u>
Mg/(Mg+Fe ²⁺)	0.348	0.495	0.384	0.376	0.378	0.373	0.359	0.364	0.344

' calculated

Table 18 (con't)

Analysis:	<u>10</u>	<u>11</u>	<u>12</u>	<u>13</u>	<u>14</u>	<u>15</u>	<u>16</u>	<u>17</u>	<u>18</u>
TiO ₂	49.28	48.14	48.36	48.08	48.56	47.74	48.72	48.80	48.52
Cr ₂ O ₃	3.57	3.43	3.59	3.53	3.59	3.48	3.50	3.49	3.58
Al ₂ O ₃	0.25	0.30	0.23	0.26	0.23	0.22	0.23	0.19	0.20
'Fe ₂ O ₃	10.35	10.80	10.91	11.72	11.44	11.78	10.35	10.92	11.45
FeO	27.13	28.31	28.18	27.16	27.56	27.33	28.66	28.80	28.00
MgO	9.44	8.23	8.43	8.80	8.77	8.57	8.23	8.17	8.50
MnO	0.28	0.38	0.28	0.35	0.34	0.30	0.31	0.35	0.33
ZrO ₂	0.19	0.25	0.27	0.20	0.00	0.22	0.05	0.00	0.06
Nb ₂ O ₅	0.00	0.05	0.00	0.04	0.03	0.01	0.00	0.00	0.01
NiO	0.18	0.13	0.15	0.20	0.16	0.15	0.20	0.16	0.18
Total	<u>100.67</u>	<u>100.02</u>	<u>100.40</u>	<u>100.34</u>	<u>100.68</u>	<u>99.80</u>	<u>100.25</u>	<u>100.88</u>	<u>100.83</u>

Cations based on three (3) oxygens

Ti	0.870	0.863	0.863	0.856	0.861	0.856	0.871	0.868	0.861
Cr	0.066	0.066	0.067	0.066	0.067	0.066	0.066	0.065	0.067
Al	0.007	0.008	0.007	0.007	0.007	0.006	0.006	0.005	0.006
'Fe ³⁺	0.183	0.194	0.195	0.209	0.203	0.211	0.185	0.194	0.204
Fe ²⁺	0.533	0.564	0.559	0.538	0.544	0.545	0.570	0.570	0.553
Mg	0.330	0.293	0.298	0.310	0.308	0.305	0.292	0.288	0.299
Mn	0.006	0.008	0.006	0.007	0.007	0.006	0.006	0.007	0.007
Zr	0.002	0.003	0.003	0.002	0.000	0.003	0.001	0.000	0.001
Nb	0.000	0.001	0.000	0.000	0.000	0.000	0.000	0.000	0.000
Ni	0.003	0.002	0.003	0.004	0.003	0.003	0.004	0.003	0.003
Total	<u>2.000</u>	<u>2.001</u>	<u>2.001</u>	<u>1.999</u>	<u>2.000</u>	<u>2.001</u>	<u>2.001</u>	<u>2.000</u>	<u>2.001</u>
Mg/(Mg+Fe ²⁺)	0.382	0.342	0.348	0.366	0.362	0.359	0.339	0.336	0.351

' calculated

Table 18 (con't)

Analysis:	<u>19</u>	<u>20</u>	<u>21</u>	<u>22</u>	<u>23</u>	<u>24</u>	<u>25</u>	<u>26</u>	<u>27</u>
TiO ₂	48.07	48.70	48.08	48.42	48.87	48.75	48.87	48.65	48.45
Cr ₂ O ₃	3.57	3.55	3.59	3.61	3.45	3.47	3.57	3.58	3.67
Al ₂ O ₃	0.21	0.20	0.22	0.26	0.23	0.28	0.24	0.27	0.23
'Fe ₂ O ₃	12.40	10.33	11.88	11.71	10.72	11.33	10.49	9.97	10.70
FeO	27.45	28.40	27.28	27.41	28.96	27.73	27.78	28.23	27.84
MgO	8.61	8.39	8.68	8.81	8.19	8.83	8.90	8.43	8.63
MnO	0.27	0.32	0.31	0.22	0.28	0.23	0.27	0.29	0.26
ZrO ₂	0.02	0.07	0.01	0.01	0.10	0.00	0.18	0.01	0.15
Nb ₂ O ₅	0.00	0.00	0.00	0.00	0.00	0.00	0.03	0.00	0.00
NiO	0.16	0.15	0.16	0.20	0.17	0.12	0.15	0.18	0.18
Total	<u>100.76</u>	<u>100.11</u>	<u>100.21</u>	<u>100.65</u>	<u>100.97</u>	<u>100.74</u>	<u>100.48</u>	<u>99.61</u>	<u>100.11</u>

Cations based on three (3) oxygens

Ti	0.853	0.870	0.857	0.859	0.868	0.863	0.868	0.873	0.865
Cr	0.067	0.067	0.067	0.067	0.064	0.065	0.067	0.068	0.069
Al	0.006	0.006	0.006	0.007	0.006	0.008	0.007	0.008	0.006
'Fe ³⁺	0.220	0.185	0.212	0.208	0.191	0.201	0.186	0.179	0.191
Fe ²⁺	0.542	0.565	0.541	0.541	0.572	0.546	0.549	0.563	0.553
Mg	0.303	0.297	0.307	0.310	0.288	0.310	0.313	0.300	0.305
Mn	0.005	0.007	0.006	0.004	0.006	0.005	0.005	0.006	0.005
Zr	0.000	0.001	0.000	0.000	0.001	0.000	0.002	0.000	0.002
Nb	0.000	0.000	0.000	0.000	0.000	0.000	0.000	0.000	0.000
Ni	<u>0.003</u>	<u>0.003</u>	<u>0.003</u>	<u>0.004</u>	<u>0.003</u>	<u>0.002</u>	<u>0.003</u>	<u>0.004</u>	<u>0.003</u>
Total	1.999	2.001	1.999	2.000	1.999	2.000	2.000	2.001	1.999
Mg/(Mg+Fe ²⁺)	0.359	0.345	0.362	0.364	0.335	0.362	0.363	0.348	0.356

' calculated

Table 18 (con't)

Analysis:	<u>28</u>	<u>29</u>	<u>30</u>	<u>31</u>	<u>32</u>	<u>33</u>	<u>34</u>	<u>35</u>
TiO ₂	48.24	50.26	48.30	49.13	47.89	48.68	48.88	48.28
Cr ₂ O ₃	3.61	3.95	3.56	3.61	3.52	3.60	3.35	3.48
Al ₂ O ₃	0.25	0.52	0.21	0.35	0.26	0.21	0.23	0.28
'Fe ₂ O ₃	10.34	7.33	10.84	11.11	11.70	11.30	10.04	10.97
FeO	28.24	26.10	27.05	26.62	27.65	27.69	27.74	28.13
MgO	8.29	10.50	8.94	9.59	8.41	8.80	8.92	8.39
MnO	0.32	0.28	0.25	0.30	0.28	0.24	0.27	0.25
ZrO ₂	0.18	0.12	0.13	0.00	0.00	0.11	0.04	0.03
Nb ₂ O ₅	0.03	0.00	0.00	0.00	0.00	0.00	0.17	0.02
NiO	<u>0.16</u>	<u>0.17</u>	<u>0.27</u>	<u>0.15</u>	<u>0.13</u>	<u>0.21</u>	<u>0.24</u>	<u>0.12</u>
Total	99.66	99.23	99.55	100.86	99.84	100.84	99.88	99.95

Cations based on three (3) oxygens

Ti	0.867	0.890	0.865	0.864	0.858	0.862	0.872	0.864
Cr	0.068	0.074	0.067	0.067	0.066	0.067	0.063	0.066
Al	0.007	0.014	0.006	0.010	0.007	0.006	0.007	0.008
'Fe ³⁺	0.186	0.130	0.194	0.196	0.210	0.200	0.179	0.197
Fe ²⁺	0.565	0.514	0.539	0.521	0.551	0.545	0.551	0.560
Mg	0.295	0.368	0.317	0.335	0.299	0.309	0.316	0.298
Mn	0.007	0.006	0.005	0.006	0.006	0.005	0.005	0.005
Zr	0.002	0.001	0.002	0.000	0.000	0.001	0.000	0.000
Nb	0.000	0.000	0.000	0.000	0.000	0.000	0.002	0.000
Ni	<u>0.003</u>	<u>0.003</u>	<u>0.005</u>	<u>0.003</u>	<u>0.003</u>	<u>0.004</u>	<u>0.005</u>	<u>0.002</u>
Total	2.000	2.000	2.000	2.002	2.000	1.999	2.000	2.000
Mg/(Mg+Fe ²⁺)	0.343	0.417	0.370	0.391	0.352	0.309	0.343	0.347

' calculated

APPENDIX B

SUMMARY OF THE EXPERIMENTAL CONDITIONS INVOLVED
IN THE ILMENITE-RUTILE SYNTHESIS EXPERIMENTS

This appendix contains a summary (Table 19) of the experimental conditions characterizing each of the individual runs displayed in Figure 16 for the synthesis experiments involving ilmenite-rutile inter-growth nodule #JF-126 from Jagersfontein.

Table 19: Summary of experimental conditions for individual runs involved in the ilmenite-rutile intergrowth experiments.

<u>Run #</u>	<u>Temp (°C)</u>	<u>log fO_2</u>	<u>Run Duration</u>	<u>Remarks</u>
1	1400	- 8.0	24 hrs.	arm + rutile
2	1398	- 8.9	48 hrs.	arm + rutile
3	1400	-10.0	48 hrs.	arm + rutile
4	1401	-11.0	18 hrs.	arm + rutile
5	1485	-10.1	18 hrs.	arm + rutile
6	1490	- 9.1	30 hrs.	arm + rutile
7	1524	- 8.9	10 hrs.	failed quench
8	1451	- 5.7	12 hrs.	arm + rutile
9	1450	- 5.6	22 hrs.	arm + rutile
10	1501	- 5.2	22 hrs.	arm + rutile
11	1351	- 6.8	22 hrs.	arm + rutile
12	1300	- 7.0	23 hrs.	arm + rutile
13	1250	- 7.5	23 hrs.	arm + rutile
14	1200	-10.2	24 hrs.	run aborted
15	1200	- 8.1	44½ hrs.	arm + rutile
16	1151	- 8.7	46½ hrs.	arm + rutile
17	1096	- 9.5	47 hrs.	failed quench
18	1050	-10.1	70½ hrs.	arm + rutile
20	1002	-10.2	70½ hrs.	ilm + rutile
21	952	-11.3	68 hrs.	ilm + rutile
22	1201	-11.0	66 hrs.	arm + rutile
23	1304	-12.8	47 hrs.	arm + rutile

